Università di Padova

Dipartimento di Fisica e Astronomia

Scuola di Dottorato di Ricerca in Fisica

XXV Ciclo

Phenomenology of Compositeness at the LHC

Ph.D. Thesis

Direttore della Scuola:
Ch.mo Prof. ANDREA VITTURI

Dottorando:
ENNIO SALVIONI

Supervisori:
Ch.mo Dr. CHRISTOPHE GROJEAN
Ch.mo Prof. FABIO ZWIRNER

July 30, 2013

Abstract

The hierarchy problem of the weak scale calls for extensions of the Standard Model at the TeV, and thus within the reach of the CERN Large Hadron Collider (LHC). One of the best motivated proposals builds on the idea that the Higgs could be a composite pseudo-Nambu-Goldstone boson. In this thesis we discuss several topics in the phenomenology of composite Higgs models, concentrating mainly on LHC physics.

In Chapter 1 we introduce the hierarchy problem and the essential features of viable theories of compositeness at the TeV scale. Chapter 2 is dedicated to a review of concrete constructions realizing the composite Higgs idea, focusing mostly on models with partial compositeness.

In Chapter 3 we present the effective Lagrangians suited for describing the Higgs boson and the constraints placed by electroweak precision tests on their parameters. Motivated by hints in the experimental results, we also reconsider the possibility of custodial breaking in the couplings of the Higgs to the W and Z.

Chapter 4 is devoted to two different aspects of Higgs physics at the LHC. First we discuss the loop-induced Higgs couplings to photons and gluons in the context of compositeness, focusing on the contribution of fermionic resonances, which are expected to be relatively light ($\lesssim 1 \div 1.5$ TeV) by naturalness arguments. We point out the potentially important role of double Higgs production in providing indirect information on the resonances. Then we turn our attention to the coupling of the Higgs to the top quark, which is currently poorly constrained. We argue that single top and Higgs associated production can be used to probe the *sign* of this coupling.

The phenomenology of fermionic resonances is discussed in Chapter 5. We analyze their impact on electroweak precision data and the constraints from LHC searches for heavy vector-like quarks. The latter give lower bounds in the range $700 \div 800$ GeV, implying that the exploration of the natural region has already started.

Chapter 6 is devoted to the phenomenology of heavy vectors, which are generically subject to a strong constraint ($m_\rho \gtrsim 2 \div 2.5$ TeV) from the S parameter. After a general introduction we study in detail an isospin-singlet W', which, as we will explain, is rather weakly constrained and could thus be lighter than the aforementioned bound. We point out that the subleading decay of the resonance into a W and a photon would constitute a signal of compositeness. Finally, Chapter 7 contains our conclusions.

This thesis is mainly based on the articles [1–4]. Partial results from those works are also contained in the conference proceedings [5, 6].

Abstract

Il problema della gerarchia della scala elettrodebole suggerisce che il Modello Standard (MS) debba essere esteso alla scala del TeV, la quale è in corso di esplorazione al Large Hadron Collider (LHC) del CERN. Una delle estensioni più motivate del MS si basa sull'idea che il bosone di Higgs sia uno stato composto, ed in particolare che sia uno pseudo-bosone di Nambu-Goldstone. Questa tesi affronta vari aspetti della fenomenologia dei modelli di Higgs composto, concentrandosi soprattutto sulla fisica del LHC.

Il Capitolo 1 introduce il problema della gerarchia e le proprietà fondamentali delle teorie che mirano a descrivere in modo realistico fisica fortemente interagente alla scala del TeV. Nel Capitolo 2 vengono presentati i modelli realistici che incarnano l'idea di un Higgs composto, con particolare attenzione alle realizzazioni basate sul meccanismo di *partial compositeness*.

Nel Capitolo 3 vengono introdotte le Lagrangiane effettive che descrivono il bosone di Higgs e i vincoli posti dai test di precisione del MS sui parameteri di tali Lagrangiane. Inoltre, prendendo spunto dai risultati sperimentali, viene riconsiderata la possibilità che la simmetria custodiale sia violata negli accoppiamenti dell'Higgs al W e alla Z.

Il Capitolo 4 analizza due diversi aspetti della fisica dell'Higgs al LHC. In primo luogo vengono discussi gli accoppiamenti radiativi dell'Higgs a fotoni e gluoni nel contesto di una teoria fortemente interagente alla scala del TeV, concentrandosi in particolare sul contributo delle risonanze fermioniche, attese essere relativamente leggere ($\lesssim 1 \div 1.5$ TeV) in base ad argomenti di naturalezza. Viene sottolineata l'importanza del processo di doppia produzione di Higgs, che potrebbe fornire informazioni indirette sulle risonanze. La seconda parte del capitolo si concentra invece sull'accoppiamento dell'Higgs al quark top, accoppiamento che ad oggi è vincolato solo molto debolmente. Si fa notare che il processo di produzione associata di un singolo top e di un Higgs può dare informazioni sul *segno* di questo accoppiamento.

La fenomenologia delle risonanze fermioniche è discussa nel Capitolo 5. Vengono analizzati l'impatto delle risonanze sui test di precisione e i vincoli da ricerche dirette di fermioni pesanti a LHC. Queste ultime costringono le masse delle risonanze ad essere più grandi di $700 \div 800$ GeV, il che implica che l'esplorazione della regione naturale dello spazio dei parametri è già iniziata.

Il Capitolo 6 è dedicato alla fenomenologia dei vettori pesanti, che sono generalmente soggetti a un forte vincolo ($m_\rho \gtrsim 2 \div 2.5$ TeV) dovuto al parametro elettrodebole S. Dopo un'introduzione a carattere generale, l'attenzione viene concentrata su una particolare risonanza, un W' assunto essere un singoletto di isospin. Come verrà discusso in dettaglio, questa risonanza è soggetta a vincoli relativamente deboli e potrebbe quindi essere più leggera del limite inferiore sopra citato. Si fa notare che il decadimento del W' in un W e un fotone costituisce un segnale peculiare di una teoria fortemente interagente. Il Capitolo 7, infine, contiene le conclusioni della tesi.

Questa tesi si basa principalmente sugli articoli [1–4]. Risultati parziali di quei lavori sono contenuti anche negli atti di convegni [5, 6].

Contents

Foreword: the current experimental portrait of the Higgs boson

On July 4, 2012, the ATLAS and CMS Collaborations announced during a joint seminar at CERN[1] the discovery of a resonance of mass ~ 125 GeV , based on data collected in 2011 and 2012 in the $\gamma\gamma$, ZZ^*, WW^*, $\tau\bar{\tau}$ and $b\bar{b}$ final states [7, 8]. ATLAS reported a combined local significance of $5.9\,\sigma$ ($4.9\,\sigma$ were expected for a SM Higgs) whereas CMS reached $5.0\,\sigma$ ($5.8\,\sigma$ expected). The analyses were subsequently updated to the full Run 1 dataset, corresponding roughly to $5\,\text{fb}^{-1}$ at 7 TeV and $20\,\text{fb}^{-1}$ at 8 TeV, for the 2013 winter conferences, where results in other channels were also reported. The current global status of measurements of the properties of the resonance is summarized in Refs. [9, 10], where references to searches in the individual channels can be found. Here we only wish to highlight a few results from those works, while discussions of more specialized topics can be found later in the relevant sections. The mass of the Higgs is measured to be, in GeV

$$125.5 \pm 0.2\,(\text{stat})\,^{+0.5}_{-0.6}\,(\text{sys})\ [\text{ATLAS}], \qquad 125.7 \pm 0.3\,(\text{stat}) \pm 0.3\,(\text{sys})\ [\text{CMS}]\,. \tag{0.1}$$

Experimental results are typically given in terms of the signal strength, defined as the Higgs production cross section times branching ratio, normalized to the Standard Model (SM) prediction

$$\mu \equiv \frac{\sigma_{\text{prod}} \times \text{BR}}{(\sigma_{\text{prod}} \times \text{BR})_{\text{SM}}}\,. \tag{0.2}$$

Figure 1 shows the measured signal strengths in the 5 main channels and their combination, for each experiment. Despite some differences between the results of ATLAS and CMS (notably the signal strength in the $\gamma\gamma$ channel, which is currently 1.6 ± 0.3 for ATLAS and 0.77 ± 0.27 for CMS, *i.e.* a discrepancy of about $2\,\sigma$), the overall picture is very consistent with the predictions of the SM. Several tests of the consistency of the Higgs couplings with the SM can be performed, based on different assumptions. Here we show only the simplest one, which consists in assuming all the $hf\bar{f}$ couplings to be rescaled by a universal factor κ_F, and the hWW, hZZ couplings to be rescaled by a common factor κ_V (as follows from custodial symmetry). In addition, no new physics contributions to the hgg and $h\gamma\gamma$ loops are assumed beyond those following from the rescalings κ_F and κ_V (*i.e.*, no new particles are assumed to contribute to the loop). Finally, no extra contributions to the Higgs total width are considered. With this set of assumptions, a simple 2-parameter fit can be performed, and the resulting likelihoods in the plane (κ_V, κ_F) are shown in Fig. 2.

[1] I would like to thank M. Schmaltz and the students of the BU Particle Theory group for hospitality and company during the late-night live broadcast of the seminar.

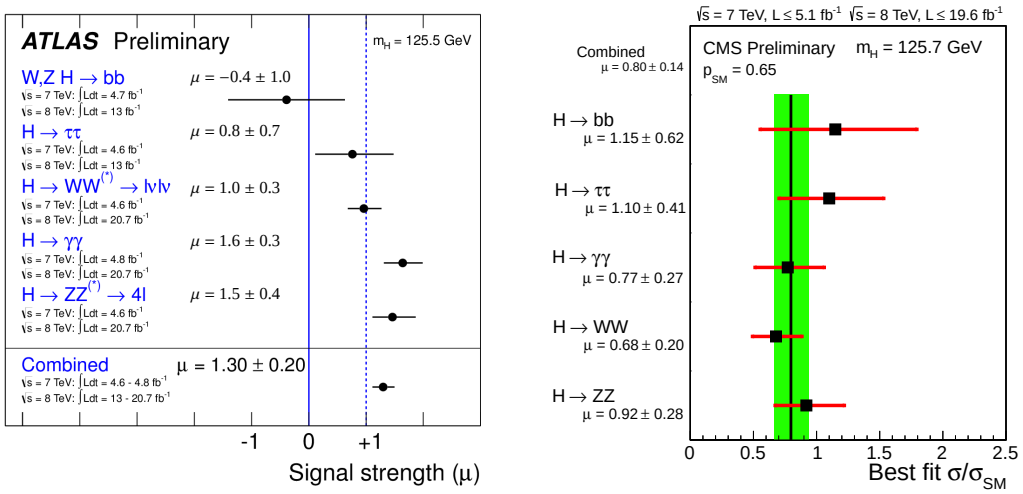

Figure 1: Measurements of the signal strength parameter μ for the individual channels and their combination, for ATLAS (left) and CMS (right). Taken from Refs. [9] and [10], respectively.

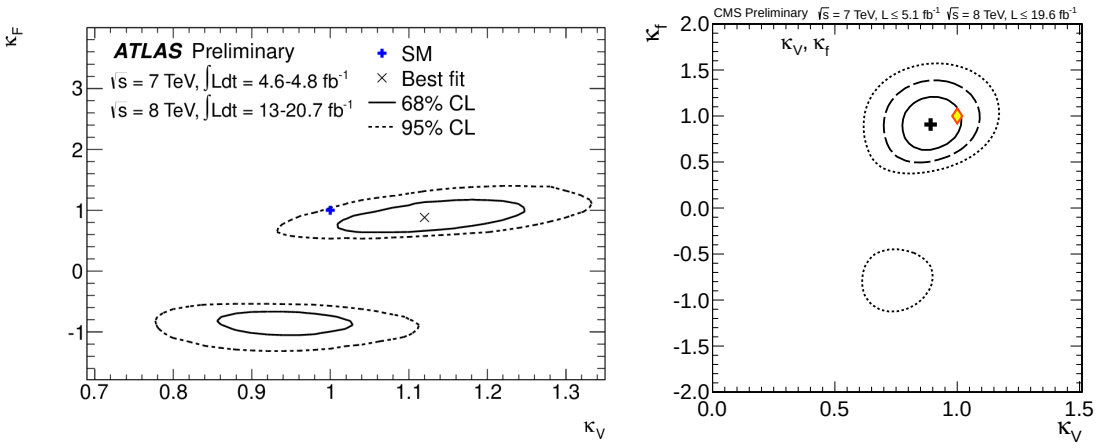

Figure 2: Two-dimensional likelihood for the parameters κ_V and κ_F, for ATLAS (left) and CMS (right). The best-fit and SM points are also indicated. Taken from Refs. [9] and [10], respectively.

Chapter 1

Introduction

As summarized in the foreword, ATLAS and CMS have recently discovered a new particle with mass close to 125 GeV , whose properties are compatible within experimental errors with those of the Standard Model (SM) Higgs boson. It is therefore tempting to say that the last missing ingredient of the SM has finally been found, thus completing a theory that has been proven unprecedentedly successful in explaining a wide range of phenomena.

The SM is a renormalizable theory: in a modern sense, this means that it should be interpreted as an effective theory, valid up to energy scales where new physics enters in play, disrupting the predictions based only on the relevant and marginal interactions contained in the SM Lagrangian. On the one hand, this approach does not seem to provide any hint as to what theory should extend the SM at high energy. On the other hand, it does provide those who adopt it (as we will do in this thesis) with a guideline to identify at least some essential features of the enlarged theory. To understand how this happens, it is useful to recall how Electroweak Symmetry Breaking (EWSB) is achieved in the SM[1]: one complex scalar doublet H is introduced, with a potential

$$V \,=\, m^2 H^\dagger H + \lambda (H^\dagger H)^2 \,. \tag{1.1}$$

For $m^2 < 0$ (and $\lambda > 0$) the potential has a minimum at $v^2/2 \equiv \left\langle H^\dagger H \right\rangle = -m^2/(2\lambda)$, which breaks $SU(2)_L \times U(1)_Y$ down to electromagnetism. Three of the degrees of freedom contained in H are eaten via the Higgs mechanism, and only one real scalar h remains in the spectrum, whose mass reads $m_h^2 = 2\lambda v^2 = -2m^2$. The vacuum expectation value is fixed to be $v \simeq 246$ GeV by the measurement of the Fermi constant, $v^2 = (\sqrt{2} G_F)^{-1}$.

Now as we already mentioned, the above description should be interpreted as effective, valid up to some scale $\Lambda_{\rm NP}$ where the SM is replaced by a new, larger theory. Within the latter, the Higgs mass will generically consist of a sum of many terms, most of which cannot be computed without specifying the ultraviolet theory at hand. However, one unavoidable contribution arises from loops of SM particles, cut off at a scale of the order of $\Lambda_{\rm NP}$. This contribution can be estimated by considering the one-loop effective potential [11] [2] in the SM, which yields

$$\delta m_h^2 = \frac{3\Lambda_{\rm NP}^2}{8\pi^2 v^2} \left(4m_t^2 - m_h^2 - 2m_W^2 - m_Z^2 \right) \,, \tag{1.2}$$

[1] This will also set our conventions, which will be used consistently in the following. In particular, everywhere $v \simeq 246$ GeV.

[2] See Appendix A for the relevant formulas.

where we retained only the leading (quadratic) term in the momentum cutoff. For simplicity, the latter was assumed to be a single scale $\Lambda_{\rm NP}$. Clearly the bigger the new physics scale is, the more we need to fine-tune the contribution in Eq. (1.2) against the remaining ones, to obtain the observed weak-scale mass for the Higgs. For example, if the SM were to be valid up to the Planck scale M_{Pl}, where gravity effects become relevant, then the tuning required to obtain $m_h \sim 100$ GeV would be enormous. This difficulty goes under the name of *hierarchy problem* of the SM.

The amount of fine-tuning in an observable O can be estimated by using the quantity [12]

$$\Delta = \max_i \left| \frac{\partial \log O}{\partial \log x_i} \right| , \tag{1.3}$$

where the x_i are the parameters on which O depends. Applying this definition to $O = m_h^2$ and taking into account that the largest contribution in Eq. (1.2) comes from the top loops, we obtain a relation between the tuning Δ and the scale where the divergence in the Higgs mass is cut off:

$$\Lambda_{\rm NP} \lesssim \sqrt{\frac{2}{3}} \pi v \frac{m_h}{m_t} \sqrt{\Delta} \simeq (450 \text{ GeV}) \sqrt{\Delta} , \tag{1.4}$$

where Δ is the maximum amount of accidental cancellation that we are willing to accept. Setting the bar at $\Delta = 10$ (corresponding to a 10% tuning) we find $\Lambda_{\rm NP} \lesssim 1.5$ TeV. We can so infer one essential property that any *natural* theory of new physics we are after should have: it must be capable to protect the Higgs mass from corrections at large scales, effectively replacing M_{Pl} with a scale of at most a few TeV in Eq. (1.2). The latter scale would be the lowest one at which the protection mechanism is in place. This also implies the generic prediction that *any* theory that solves the hierarchy problem must contain new physics that will be (at least in principle) within the reach of the LHC in its 14 TeV run, which is currently scheduled to start in 2015.

The two most solid proposals that have been built following the naturalness principle are supersymmetry and compositeness, and address the hierarchy problem in radically different ways:

- Supersymmetry extends the Poincaré group and relates bosons and fermions: for each scalar particle a new Weyl fermion is introduced, and similarly for the SM particles with spin 1/2 and 1. Since unbroken supersymmetry (SUSY) predicts that each SM particle and its superpartner have the same mass, the scalar inherits the chiral symmetry protection enjoyed by the fermion, which guarantees that corrections to its mass diverge at most logarithmically, and the hierarchy problem is solved. In addition, if supersymmetry is broken in a soft way (*i.e.* only by mass terms and by couplings with positive mass dimension) the masses of SUSY particles can be made realistic ($M_{\rm SUSY} \sim$ TeV) without spoiling the protection of the Higgs mass. Then $M_{\rm SUSY}$ effectively plays the role of $\Lambda_{\rm NP}$ in Eq. (1.2). In supersymmetry the Higgs is an elementary particle, and the theory can be weakly coupled up to very large scales.

- Composite Higgs theories are based on the idea that the Higgs is not a fundamental scalar, but it is instead a composite state, bound by a new strong interaction with confinement scale Λ of the order of the TeV. In this case the hierarchy problem is solved due to the finite size of the Higgs, which is therefore not sensitive to virtual corrections from scales above Λ: at high energies the Higgs simply 'dissolves' into its fundamental constituents.

The first possibility is very attractive: the hierarchy problem is solved maintaining perturbativity, leading for example to one of the celebrated successes of the Minimal Supersymmetric Standard Model, precision gauge coupling unification. Moreover supersymmetry arises automatically in the context of string theory, making the connection to physics at a more fundamental level natural. It is beyond the scope of this thesis to describe in any detail supersymmetric theories; we simply refer the reader to Ref. [13] for an introduction and a list of references.

The second possibility will be the main subject of this thesis. Notice that this solution is the one adopted by nature for the strong interactions: the mass of the pion, $m_\pi \sim 140\,\mathrm{MeV}$, is certainly not unnatural with respect to M_{Pl}. The radiative corrections to m_π are in fact screened at scales of the order of 1 GeV. Much above this scale physics is described in terms of new degrees of freedom, quarks and gluons, following the rules of Quantum Chromodynamics (QCD), which is a fully natural theory. Once we take this framework seriously, however, we are led to an issue: as we will see, Electroweak Precision Tests (EWPT) require the mass scale m_ρ of the resonances of the strong sector to be heavier than about $2 \div 3$ TeV, which therefore sets roughly the lowest viable scale for the strong sector. But then why is the Higgs so much lighter than the other composite states? A solution is again suggested by the analogy with the QCD pion: if the Higgs were a pseudo-Nambu-Goldstone Boson (pNGB) associated to a spontaneously broken global symmetry of the strong sector, then the 'little hierarchy' $m_h \ll m_\rho$ could be explained. Indeed, this further ingredient is incorporated in all the models of composite Higgs discussed in the thesis.

1.1 Alternatives to naturalness

We should now briefly pause to comment on the robustness of the naturalness arguments we presented above. Are there alternative views on the hierarchy problem, that do not lead to the expectation of New Physics at the TeV scale? Clearly this question has direct relevance to the LHC physics program (and beyond that), therefore we will at least mention two possibilities.

One could argue that perhaps there is no large physical scale, or that any such scale is completely decoupled from the SM. In this case there would be no hierarchy problem, and a weak-scale Higgs mass would be fully natural. However, there is a number of phenomena not described within the SM, which call for new physical scales: in first place and as we already mentioned, gravity is expected to become important at $M_{Pl} \sim 10^{19}$ GeV. Still, one could try and argue that our limited understanding of quantum gravity does not allow us to draw any conclusions about physics at Planckian scales. Even accepting this attitude, many other *observations* suggest the presence of new physics at high scales, at least part of which should be described by the familiar quantum field theory language: dark matter, neutrino masses, the strong CP problem and inflation are prominent examples. One should then imagine that the Higgs is completely decoupled from all the scales involved in the explanation of these phenomena, which does not seem a defendable option.

On the other hand, if new physics at large scales exists and it is coupled to the Higgs (as it seems unavoidable), then one possibility is that the Higgs mass is not protected by any mechanism, but simply fine-tuned to a very large accuracy. The tuning however does not pose a problem, provided there is some anthropic argument that explains why m_h needs to be so light. This is a serious possibility: for example, by means of anthropic reasoning it is possible to justify [14] the tuning of the cosmological constant, which is much larger

than the one needed for the weak scale. If this is the correct point of view, then the LHC could be sitting at the beginning of a vast desert, and hopes to observe new physics in the next years would be dramatically reduced, if not totally erased.[3] In any case, the LHC will contribute to our understanding of this fundamental problem, either by discovering new physics or by establishing a new minimum level of tuning (roughly in the $10^2 \div 10^3$ range) that a would-be natural theory would eventually need to deal with. Whether observing such highly uncomfortable level of tuning would force us to abandon naturalness at all is certainly a difficult question (after all, the dividing line can only be set based on empirical experience), but also one that it is premature to address now. Simply based on 'practical' considerations, at the present time the best attitude we can take is to fully explore, both theoretically and experimentally, the signatures of natural theories, leaving it to the experiment to confirm or disprove them. In the rest of the thesis we will apply this approach to composite Higgs theories.

1.2 A composite Higgs

The original proposal of the Higgs as a composite state dates back to the mid-1980s [15]. Since the very beginning, the lightness of the Higgs was explained by assuming it to be a pNGB associated to the spontaneous breaking of an approximate global symmetry in the strong sector. The original ideas were revived and developed starting in the early 2000s, thanks in particular to the construction of extra-dimensional models, which shed new light on several aspects of the four-dimensional strong dynamics. In fact, the idea of dimensional deconstruction led to the birth of Little Higgs theories [16], and shortly after the first 'holographic Higgs' models, which rely on the use of the AdS/CFT correspondence, were proposed [17, 18].

As already said, one key ingredient of all the above realizations is that the Higgs is a pNGB. Let us consider a symmetry $\mathcal{G}$ spontaneously broken to $\mathcal{H}$ at scale f. To obtain the Higgs as a pNGB, two requirements must be satisfied: on the one hand, the SM group should be contained in $\mathcal{H}$, $SU(2)_L \times U(1)_Y \subset \mathcal{H}$ (otherwise part of the SM gauge symmetry would be broken by the strong sector), and on the other hand $\mathcal{G}/\mathcal{H}$ needs to contain at least one $SU(2)_L$ doublet, which will be identified with the composite Higgs doublet H. At tree level, the shift symmetry forbids a potential for H. The SM fermions and gauge bosons are assumed to be originally external to the strong sector, and we will therefore call them 'elementary fields'. Of course, we need to couple the elementary fields to the strong sector in order to eventually communicate EWSB to them (and in particular, to give them a mass). The elementary/composite couplings must respect the SM gauge symmetry, but in general they will break the global symmetry $\mathcal{G}$. This explicit breaking gives rise to a one-loop potential for H, which in turn realizes the spontaneous breaking of the EW symmetry and thus generates *dynamically* the weak scale v. The Higgs mass arises only at one loop and is therefore naturally smaller than the mass of the other resonances, the latter being $m_\rho \sim g_\rho f$, where g_ρ is the typical coupling in the strong sector.

While the above features are common to all the models that have been put forward, significant differences exist between the modern explicit realizations, which can be essentially classified in two broad classes depending on the form of the Higgs potential they generate.

[3] One could still rely on hints from other open questions in the SM, in particular dark matter, in the light of the so-called 'WIMP miracle' which strikingly suggests a weak-scale mass for dark matter particles. Nevertheless, no robust prediction on the scale of new physics can be made, in contrast to Eq. (1.4).

We postpone a more detailed descriptions of the models to Chapter 2, and summarize here only the essential features:

- The first class is that of 'generic' composite Higgs models, where the potential is entirely generated with 1-loop size, leading to the natural expectation that $v \sim f$, where as already mentioned f is the decay constant associated to the global symmetry breaking $\mathcal{G} \to \mathcal{H}$. A very low f is however forbidden by EWPT and by the S parameter in particular, which requires roughly $\xi \equiv v^2/f^2 \lesssim 0.1$.[4] The hierarchy $f \gg v$ can only be obtained at the price of fine tuning, which scales very roughly as ξ and is thus at least of the order of 10%. This mild tuning is accepted as part of the construction. The most successful models in this class contain an additional ingredient, the so-called *partial compositeness* mechanism [19], which arises from mixing linearly the elementary fermions with operators of the strong sector. Partial compositeness implies that all physical states (except the Higgs) are a mixture of elementary and composite degrees of freedom. As we will see, this mechanism leads to an attractive (although not completely satisfactory) flavor picture, and in addition it has important consequences on the collider phenomenology of the strong sector resonances.

- The second class contains Little Higgs theories, which aim at stabilizing the hierarchy between f and v in a fully natural way. This is achieved by means of the *collective breaking* (CB) mechanism, which is implemented in all sectors of the theory: gauge, fermion and scalar. The form of the potential that follows from CB is peculiar, the Higgs mass term being parameterically smaller than the quartic coupling; the latter is effectively of tree-level size, and arises from the implementation of CB in the scalar sector. This leads to the natural expectation $v^2/f^2 \sim g_\rho^2/(16\pi^2)$, implying that $f \sim$ 1 TeV can be obtained without extra tuning. Little Higgs constructions are thus more ambitious, and as a consequence they contain more ingredients than the generic CH models in the previous class: for example, implementation of CB in the scalar sector automatically requires to enlarge the coset to make room for extra pNGBs beyond the Higgs doublet(s).

From this fleeting overview, it should be clear that so far no single model has been promoted to the status of paradigm for a theory of composite Higgs. This is partly due to the main phenomenological issues these models have to face, and in particular the agreement with EWPT and with flavor observables. Still, in most of the discussion we will make reference to models in the first class, *i.e.* to composite Higgs models with partial compositeness. Their simplicity, together with the calculability that is present not only in holographic models but also in suitable four-dimensional realizations[5], makes these theories a valuable guideline when investigating the LHC phenomenology of compositeness, which is the main subject of this thesis. Nevertheless, we want to emphasize that our approach will be as model-independent as possible, focusing mostly on aspects that are generic to all models, rather than on very specific features of single cases. In this light, the models that we will introduce should be interpreted more as working tools, useful to address a relevant subset of open questions (*e.g.* collider physics, EWPT, and so on), rather than theories capable of describing all aspects of physics at the TeV scale.

[4] In the presence of an extra positive contribution to T, which could come for example from loops of fermionic resonances, the bound can be relaxed to $\xi \lesssim 0.2$.

[5] See for example Refs. [20, 21].

1.3 Phenomenology of compositeness

In this section we are going to depict the broad phenomenological consequences of compositeness at the TeV scale. One generic feature is that the Higgs potential is largely determined by the top sector, which contains the top quark and a set of composite fermions it mixes to, dubbed the *top partners*. In particular, in essentially all cases the fermion loops give the dominant, negative contribution to the Higgs mass, thus triggering EWSB. It is therefore intuitive that the masses of the top partners should control the tuning in the potential, in analogy to the role played by stops in supersymmetry. The connection between the masses of fermionic resonances and naturalness has been made quantitative in models with partial compositeness, as we will briefly review in Chapter 2. The general result [22–26] is that for a level of tuning of 10% (which corresponds very roughly to $f \sim 800$ GeV), at least some of the fermionic resonances should have masses $m_\psi \lesssim 1 \div 1.5$ TeV, which roughly agrees with the naive estimate in Eq. (1.4) if one makes the identification $\Lambda_{\rm NP} = m_\psi$. This is a first crucial piece of information: if EWSB is only mildly tuned, then the LHC should observe colored fermions with masses below 1.5 TeV. In Chapter 5 we will discuss the current limits on top partners coming from searches in a variety of final states, finding that the LHC has already started carving out the natural region: the current limits on m_ψ vary from 700 to 800 GeV, depending on the quantum numbers of the resonance.

As we already mentioned, naturalness of the Higgs potential requires roughly speaking the scale of fermionic resonances m_ψ to be at most 1.5 TeV. On the other hand, the S parameter constrains quite generically vector resonances to $m_\rho \gtrsim 2.5$ TeV. It follows that a separation of the two scales, $m_\psi < m_\rho$, would be welcome in order to limit the tuning to a reasonable amount. Such separation is not expected in a generic strongly coupled theory, and realizing it constitutes an interesting model-building problem. Notably, this issue was recently tackled also in the Little Higgs context [27].

Light top partners can also give important *indirect* effects. In fact, as we will discuss in Section 5.1, the tension with electroweak bounds can be significantly relaxed if the fermionic resonances give a positive contribution to T at 1-loop. Imposing agreement with EWPT strongly constrains the viable resonance spectra [3, 28–32]. Top partners could indirectly manifest their presence also in the loop-mediated couplings of the Higgs to gluons and photons, which have been observed and measured by ATLAS and CMS. It turns out, however, that in most explicit models (both with and without collective breaking) the effects of top partners in the hgg and $h\gamma\gamma$ couplings cancel out exactly [33]: as a consequence, there is no hope to obtain indirect information on the top partners from the analysis of the leading Higgs couplings. This somewhat surprising result has been subject to accurate investigation in the literature [34,35] [6]. In Chapter 4 we review how the exact insensitivity to top partners arises (by applying the so-called Higgs Higgs Low-Energy Theorem [37]), and estimate corrections to it in a model-independent way, finding that they are negligibly small.

Higgs physics is obviously of central importance in the LHC experimental program, and exploiting the full potential of the machine could turn out to be instrumental in understanding the physics underlying EWSB. This implies that subleading processes involving the Higgs should be thoroughly investigated, or revisited in the light of experimental or theoretical progress. The latter is true for double Higgs production, which was originally studied in the SM context as the only handle of the LHC on the Higgs self-coupling, but turns out to be even more interesting in the context of Higgs compositeness. In fact, in the latter case

[6] See also Ref. [36].

the cross section for $pp \to hh$ production can be sizably enhanced due to the presence of a non-renormalizable $t\bar{t}hh$ coupling, ameliorating the prospects of detection at LHC14 [38]. In Chapter 4 we extend the Higgs low-energy theorem to double Higgs production, and include for the first time the effects of top partners in the loops. Contrarily to single Higgs production, we find a non-negligible sensitivity on the masses of the fermionic resonances that run in the loops. We also perform a short analysis of the LHC prospects in $pp \to hh$.

While an open-minded approach is to be preferred whenever possible in phenomenological analyses, it is even more needed in the presence of anomalies in the experiments. In Chapter 3 we illustrate an example of 'data-driven' study in the context of Higgs couplings. In fact, motivated by the results of the 7 TeV run of the LHC, which seemed to point (albeit not in a statistically significant way) to an enhancement of the rate for $h \to ZZ$ with respect to $h \to WW$, in Ref. [2] we reconsidered the possibility of custodial breaking in the couplings of the Higgs. In Chapter 3 we summarize the implications for EWPT and LHC physics, and discuss the latest tests of custodial symmetry performed by ATLAS and CMS.

The top quark plays a special role in composite Higgs theories. In particular, in partial compositeness fermions are coupled to the strong sector with a strength that is proportional to their mass, implying that the top is expected to be the SM particle most sensitive to effects of new physics (besides the Higgs). Interesting observables in top physics that can be measured at the LHC include the $Zt\bar{t}, Wt\bar{b}$ and $ht\bar{t}$ couplings. Let us focus on the last one. Since it is not bounded from EWPT, all the information we currently have on this coupling comes from the fits to Higgs data performed by ATLAS and CMS. The fits however depend on the assumptions made, in particular about possible new physics entering in the loops (*e.g.*, in the fits reported in Fig. 2 the NP contributions are set to zero), and therefore do not allow an unambiguous determination of the $ht\bar{t}$ coupling. A direct measurement is possible in the $pp \to t\bar{t}h$ process, which is experimentally challenging: the current sensitivity is around 5 times the SM cross section [39–41], whereas the ultimate accuracy on the coupling is expected to be $\approx 15\%$ [7]. The measurement of the $ht\bar{t}$ coupling is of high theoretical interest: in fact, as we will see this coupling receives two kinds of corrections, one due to the nonlinearity of the sigma model and the other due to the mixing with top partners (see for example Eq. (4.20)). As we have mentioned, the latter cancels out exactly from the hgg and $h\gamma\gamma$ vertices, singling out $pp \to ht\bar{t}$ [43] as the best process to infer indirect information on the resonances.

Notice that in Fig. 2 two distinct best-fit regions appear, one of them for *negative* values of the $ht\bar{t}$ coupling. As we explain in Sec. 4.4, this discrete ambiguity cannot be lifted in a robust way by 'standard' Higgs analyses. In Sec. 4.5 we argue that another subleading channel, *single* top and Higgs associated production, $pp \to thj$, can efficiently resolve the degeneracy. Following the proposals in Refs. [4, 44], the ATLAS Collaboration is currently investigating the feasibility of an analysis in this channel.

Let us finally turn our attention to vector resonances, which were so far mentioned only in relation to the bound that S sets on their masses, $m_\rho \gtrsim 2.5$ TeV in the absence of cancellations. We will sketch the phenomenology of heavy vectors at the beginning of Chapter 6; a brief summary could go as follows [45]. Heavy spin-1 fields with EW quantum numbers are expected on general grounds, independently of the specific realization. Their couplings to light fermions are suppressed, leading to production cross sections at the LHC that are significantly smaller than those of the 'traditional' Z' and W' (motivated for example by grand unification). On the other hand, the preferred decay patterns depend to some extent on the specific model: in Little Higgs the decay to SM fermions would typically be uni-

[7] At LHC14 with $300\,\text{fb}^{-1}$, see for example Ref. [42].

versal, whereas in partial compositeness the branching ratios into third generation quarks (*e.g.* $Z' \to t\bar{t}\,, W' \to t\bar{b}$) would be larger. In addition, in models with partial compositeness heavy partners for the gluons are present, since the strong sector must carry color charge in order to write down linear mixings with the elementary quarks; these 'heavy gluons' dominantly decay into $t\bar{t}$. The bottom line is that the detection of composite spin-1 resonances at the LHC is challenging, and the reach will strongly depend on the capability to distinguish boosted heavy objects from the QCD background. In the second part of Chapter 6 we will focus on one vector resonance, an $SU(2)_L$-singlet W', which is subject to weaker pre-LHC constraints than the other relevant states. We analyze in detail the W' phenomenology, by adopting a fully model-independent approach [1]. We will point out that if the spin-1 field is not the gauge boson associated with a local symmetry, then a novel decay channel opens up, $W' \to W\gamma$, whose observation would thus be interpreted as a hint of compositeness.

Let us conclude this overview by summarizing our expectations for the spectrum of a very minimal theory of compositeness at the TeV scale. At ~ 100 GeV we find the Higgs, which is entirely composite to solve the hierarchy problem, and the top, which has a sizable degree of compositeness[8]. The properties of these two weak-scale states should deviate from the SM predictions at $\mathcal{O}(\xi)$, *i.e.* at least at $\sim 10\%$ level, if the theory is only mildly tuned. Going to larger scales, we expect at least some of the fermionic resonances to have a mass below 1 or 1.5 TeV and thus to provide the first direct evidence of new physics, while the spin-1 states are heavier than ~ 2.5 TeV. We stress once more, however, that these should be regarded only as guidelines, and that a model-independent, 'open-minded' attitude is the best way to go when studying the phenomenology.

1.4 Outline of the thesis

Before moving on to the core of the discussion, we wish to provide the reader with a 'map' of the remainder of this thesis. To facilitate orientation, only the main topics covered in each chapter are mentioned here, whereas a detailed introduction can be found at the beginning of each chapter. A concise but thorough summary of the results is provided in the Conclusions, Chapter 7, to which the reader interested only in a synthetic overview is referred.

- Chapter 2 contains an introduction to theories that concretely realize the composite Higgs idea. The main focus is on models with partial compositeness, where an efficient suppression mechanism for flavor-violating effects is at work. We discuss in detail the minimal model with custodial symmetry, based on the coset $SO(5)/SO(4)$, and in particular its best-known version, MCHM_5. We quantitatively show that a naturally light Higgs calls for light (roughly $\lesssim 1.5$ TeV) fermionic resonances, known as 'top partners'. Some comments on Little Higgs models and their problems in facing EWPT close the chapter.

- In Chapter 3 we introduce two effective Lagrangians for the Higgs. We start with the electroweak chiral Lagrangian coupled to a scalar h, and apply it to study the constraints from EWPT on generic composite models. Then, motivated by early LHC measurements, we investigate the possibility of extending the chiral Lagrangian to include custodial symmetry violation in the hVV couplings ($V = W, Z$). We discuss the consequences on EWPT and on fits to collider Higgs data. We finally present the Strongly Interacting Light Higgs (SILH) Lagrangian.

[8] Extra light scalars could of course be present, as long as they are pNGBs.

- Chapter 4 is dedicated to the study of Higgs couplings in composite models. We first consider the radiative couplings to gluons and photons, as these can be in principle sizably affected by the light fermionic resonances that make the small Higgs mass natural. This is however known *not* to be the case for the $gg \to h$ and $h \to \gamma\gamma$ amplitudes, where effects of resonances turn out to cancel exactly in the Higgs Low-Energy Theorem (LET) approximation. We review how this result arises, and confirm its robustness by estimating corrections beyond the LET.

  Then we extend the LET to *double* Higgs production, $gg \to hh$, finding that the insensitivity to the top partners holds in this case too. However, in double Higgs production the LET is found to be less accurate[9], so we perform an exact computation of the $gg \to hh$ cross section, including top partners. We find a non-negligible sensitivity on the latter, concluding that double Higgs production can provide relevant indirect information that would complement direct searches and EWPT.

  Finally we focus on the sign degeneracy that plagues the current indirect determination of the $ht\bar{t}$ coupling ($g_{ht\bar{t}}$), see Fig. 2. After discussing why 'standard' Higgs channels cannot robustly resolve this ambiguity, we argue that single top production in association with a Higgs can efficiently serve to that purpose. We show that the cross section for $pp \to thj$ is largely enhanced (up to more than a factor 10) when $g_{ht\bar{t}} < 0$, and proceed to a detailed analysis of signal and backgrounds at the LHC. We focus on the $h \to b\bar{b}$ decay, which leads to final states with 3 and 4 b-jets.

- In Chapter 5 we study the phenomenology of fermionic resonances in partial compositeness, adopting MCHM$_5$ as a benchmark. We discuss EWPT and show that loops of heavy fermions can in some cases provide a very welcome positive ΔT. We identify the two main regions of parameter space that generate this contribution, and for each of the two scenarios we discuss the LHC phenomenology of the lightest resonance, which is in one case an $SO(4)$-singlet state with electric charge $Q = 2/3$, and in the other an exotic quark with $Q = 5/3$.

- In Chapter 6 some aspects of the phenomenology of spin-1 fields are presented. We begin with an introduction to vectors in partial compositeness, by making use of a simple two-sector description that nevertheless captures the main features of the setup. Due to the strong bound from the S parameter and to their peculiar properties, discovering these states at the LHC will be an interesting experimental challenge. Then we focus on one specific example, namely an $SU(2)_L$-singlet W', which is rather weakly constrained (in particular, it does not contribute to the S parameter) and could therefore be lighter than the $2 \div 2.5$ TeV usually quoted as the lower bound on composite vectors. We analyze in detail the phenomenology of the resonance, by means of a fully model-independent approach that only assumes the SM gauge invariance. One parameter (which we call δ_B) in our effective Lagrangian is singled out as especially interesting. Roughly speaking, this parameter measures how much the W' differs from a gauge boson. The width for the decay $W' \to W\gamma$, which is loop-suppressed if the resonance is associated to a spontaneously broken gauge symmetry, is found to be proportional to δ_B^2, leading us to conclude that observation of a resonant signal in the $W\gamma$ channel

[9] Comparison with previous results in MCHM$_5$ [38] show that the LET deviates from the exact result by up to 50% when only top loops are considered. See Sec. 4.3.

would point to compositeness at the TeV scale. We perform an exploratory study of this novel final state at the LHC.

Chapter 2

The Higgs as a composite pseudo-Nambu-Goldstone boson

In this chapter we briefly describe some of the most popular composite Higgs models. As repeatedly said, one central feature is that the Higgs is a pNGB associated to an approximate global symmetry, which is spontaneously broken in the strong sector. In the simplest models, the Higgs potential is entirely generated at 1-loop by the couplings of the elementary (gauge and fermion) fields, which explicitly break the global symmetry. Indeed, a completely analogous mechanism is known to be at work in QCD. Considering the two-flavor case, for $m_{u,d} = 0$ the pions are at tree level the exact GBs of spontaneous chiral symmetry breaking, but they obtain a 1-loop potential from the electromagnetic interactions. This potential contains, in particular, a mass for the π^+, whereas the neutral pion is left massless. Given the close similarity, we find it useful to work out this QCD example explicitly in Sec. 2.1, deriving a celebrated relation between the pion mass difference and the masses of the lightest QCD vector resonances. We introduce composite Higgs models with partial compositeness in Sec. 2.2, and briefly review their flavor structure in Sec. 2.3. The Minimal Composite Higgs model, based on the coset space $SO(5)/SO(4)$, is discussed in detail in Section 2.4, focusing mostly on its best known version, the so-called MCHM_5 where the elementary fermions are embedded in the fundamental representation of the broken symmetry group. We analyze in detail the Higgs potential, and obtain a relation between the Higgs mass and the masses of the lightest *fermionic* resonances that resembles closely the one obtained for the pion mass difference. Finally, Sec. 2.5 is dedicated to Little Higgs models. In particular we will discuss the implementation of the 'collective quartic coupling', through which a parametric separation between the weak and strong sector scales, $v \ll f$, can be naturally obtained. The compatibility of Little Higgs models with EWPT is also briefly addressed.

2.1 A QCD example: the pion potential from electromagnetic interactions

We consider here QCD with two flavors in the chiral limit, $m_{u,d} = 0$. The pattern of symmetry breaking is $SU(2)_L \times SU(2)_R/SU(2)_V$ and the pions are the exact GBs associated to it. We are interested in turning on the electromagnetic interaction, by gauging $U(1)_Q \subset SU(2)_V$. The gauging breaks the global symmetry explicitly, and a potential for the pions is generated by loops involving the photon: in particular, a mass for the charged pion will

be generated, whereas the π^0 remains massless. In the real world, the quark masses are of course non-vanishing, and this explicit breaking of the chiral symmetry generates a tree-level contribution to the mass of both the neutral and charged pion. However, this contribution is the same for π^+ and π^0, so the pion mass difference is essentially of electromagnetic origin even in the realistic theory. The experimental values are

$$m_{\pi^+} = 139.6 \text{ MeV}\,, \quad m_{\pi^0} = 135.0 \text{ MeV}\,, \quad \Delta m_\pi \equiv m_{\pi^+} - m_{\pi^0} = 4.6 \text{ MeV}\,. \tag{2.1}$$

We are going to calculate the splitting Δm_π by considering the effective Lagrangian describing the pions and the photon at low energies, and computing the 1-loop pion potential generated by gauge loops. The pions are described by the field

$$\Sigma = \exp(i\sigma^a\pi^a/f_\pi)\,, \qquad f_\pi \simeq 92\,\text{MeV}\,, \tag{2.2}$$

which transforms as $\Sigma \to U_L \Sigma U_R^\dagger$ under $SU(2)_L \times SU(2)_R$. It is useful to start by assuming that the latter symmetry is fully gauged, and to turn off the unphysical components later. At quadratic order in the gauge fields, the most general Lagrangian reads

$$\mathcal{L} = \frac{1}{2}(P_T)^{\mu\nu}\left[\Pi_L(q^2)\text{Tr}(L_\mu L_\nu) + \Pi_R(q^2)\text{Tr}(R_\mu R_\nu) - \Pi_{LR}(q^2)\text{Tr}(\Sigma^\dagger L_\mu \Sigma R_\nu)\right]\,, \tag{2.3}$$

where $(P_T)^{\mu\nu} = g^{\mu\nu} - q^\mu q^\nu/q^2$ is the projector over the transverse components[1], and Σ is assumed to be a background field, since we are interested in computing only the potential for the pions. The form factors $\Pi_{L,R,LR}(q^2)$ encode the effects of the strong dynamics. The reason why we chose to gauge the full group in Eq. (2.3) is that we can now easily relate the form factors appearing there with the 'physical' ones, corresponding to the vector and axial combinations: by using $\mathcal{V}_\mu, \mathcal{A}_\mu = (R_\mu \pm L_\mu)/\sqrt{2}$ and going to the vacuum $\langle\Sigma\rangle = \mathbb{1}_2$ we obtain

$$\mathcal{L} = \frac{1}{2}(P_T)_{\mu\nu}\left[\Pi_{VV}\text{Tr}(\mathcal{V}^\mu\mathcal{V}^\nu) + \Pi_{AA}\text{Tr}(\mathcal{A}^\mu\mathcal{A}^\nu) + \Pi_{VA}\text{Tr}(\mathcal{V}^\mu\mathcal{A}^\nu + \mathcal{A}^\mu\mathcal{V}^\nu)\right] \tag{2.4}$$

where

$$\Pi_{VV} = \frac{1}{2}(\Pi_L + \Pi_R - \Pi_{LR})\,, \quad \Pi_{AA} = \frac{1}{2}(\Pi_L + \Pi_R + \Pi_{LR})\,, \quad \Pi_{VA} = \frac{1}{2}(\Pi_R - \Pi_L)\,. \tag{2.5}$$

Now let us set the spurions to their physical values,

$$L_\mu, R_\mu \to \frac{\sigma^3}{2}A_\mu \tag{2.6}$$

where A_μ is the photon field: by using the explicit expression of Σ in Eq. (2.2), we obtain the Lagrangian

$$\mathcal{L} = \frac{1}{2}(P_T)_{\mu\nu}A^\mu A^\nu\left[\Pi_{VV}(q^2) + 2\,\Pi_{LR}(q^2)\frac{\pi^+\pi^-}{\pi^2}\sin^2\frac{\pi}{f_\pi}\right]\,, \tag{2.7}$$

where $\pi^\pm \equiv (\pi^1 \mp i\pi^2)/\sqrt{2}$ and $\pi \equiv \sqrt{2\pi^+\pi^- + (\pi^3)^2}$. The photon-photon-$\pi^+$-$\pi^-$ interaction appearing in Eq. (2.7) will generate at one-loop a mass for the charged pion, while such interaction is absent for the π^0, which as expected remains exactly massless. Let us now

[1]The transverse projector is needed to ensure gauge invariance, since the non-homogeneous terms in the gauge transformations of L_μ, R_μ are proportional to q (in momentum space).

have a closer look at the form factor Π_{VV} : we know that the vector current cannot excite the pions (which have the quantum numbers of the broken generators), so its two-point function does not have a pole at $q^2 = 0$. Since

$$\left\langle J_V^\mu J_V^\nu \right\rangle = (P_T)^{\mu\nu} \Pi_{VV}(q^2) \,, \tag{2.8}$$

we conclude that $\Pi_{VV}(0) = 0$. As a consequence, the leading term in an expansion in momenta is $\mathcal{O}(q^2)$,

$$\Pi_{VV}(q^2) \simeq \frac{q^2}{e^2} \,, \tag{2.9}$$

which corresponds to the free-field Lagrangian for the photon. It follows that the Coleman-Weinberg potential can be computed using the standard formula, obtaining

$$V = \frac{3}{2} \int \frac{d^4Q}{(2\pi)^4} \, \log \left(Q^2 + 2e^2 \, \Pi_{LR}(Q^2) \frac{\pi^+\pi^-}{\pi^2} \sin^2 \frac{\pi}{f_\pi} \right) \,, \tag{2.10}$$

where Q is the Euclidean momentum. Dropping field-independent terms and expanding the logarithm at first order, we obtain from Eq. (2.10)

$$V = \frac{3\alpha}{4\pi} \int_0^\infty dQ^2 \, \Pi_{LR}(Q^2) \, \frac{\pi^+\pi^-}{\pi^2} \sin^2 \frac{\pi}{f_\pi} \,, \tag{2.11}$$

leading to a pion mass difference

$$m_{\pi^+}^2 - m_{\pi^0}^2 = \frac{3\alpha}{4\pi f_\pi^2} \int_0^\infty dQ^2 \, \Pi_{LR}(Q^2) \,. \tag{2.12}$$

We see that the integral converges if the LR form factor decreases at least as $\Pi_{LR} \sim 1/Q^4$ at large (Euclidean) momenta. In the specific case at hand, *i.e.* chiral QCD, one can use the operator product expansion for two-point functions of currents to show that this is indeed the case, so the integral is actually convergent [46]. In any case, on general grounds the finiteness of the potential in Eq. (2.11) is equivalent to imposing the two conditions $\lim_{Q^2 \to \infty} Q^n \Pi_{LR}(Q^2) = 0 \;\; (n = 0, 2)$. We will now show that combining these requirements with two approximations, namely the large-N_c limit of QCD and vector meson dominance, allows one to compute the pion mass difference in terms of other measured quantities, obtaining a prediction that we will compare to the experimental value in Eq. (2.1). At the leading order in a $1/N_c$ expansion, the only singularities of a two-point function of a quark bilinear J are one-meson states, *i.e.*

$$\langle JJ \rangle = \sum_n \frac{a_n^2}{Q^2 + m_n^2} \,, \tag{2.13}$$

where the sum runs over an infinite number of meson states, and $a_n = \langle 0|J|n\rangle$ is the matrix element for J to excite the n-th meson from the vacuum [47, 48]. This allows us to write

$$\begin{aligned} \left\langle J_V^\mu J_V^\nu \right\rangle \;&=\; (P_T)^{\mu\nu} \, \Pi_{VV}(Q^2) = (P_T)^{\mu\nu} Q^2 \sum_n \frac{f_{\rho_n}^2}{Q^2 + m_{\rho_n}^2} \,, \\ \left\langle J_A^\mu J_A^\nu \right\rangle \;&=\; (P_T)^{\mu\nu} \, \Pi_{AA}(Q^2) = (P_T)^{\mu\nu} Q^2 \left(\sum_n \frac{f_{a_n}^2}{Q^2 + m_{a_n}^2} + \frac{f_\pi^2}{Q^2} \right) \,, \end{aligned} \tag{2.14}$$

where the ρ_n and a_n are vector and axial resonances respectively. In the expression for the axial current correlator, we have taken into account the fact that in addition to the axial mesons, the pions can also be excited from the vacuum by J_A. We furthermore assume vector meson dominance, which states that the sums in Eq. (2.14) are saturated by the first resonance of each tower, *i.e.* the ρ and a_1 mesons. Recalling that $\Pi_{LR} = \Pi_{AA} - \Pi_{VV}$ (see Eq. (2.5)) and imposing the two constraints on the large-momentum behavior of Π_{LR} discussed above, we obtain two relations between the masses and decay constants of the resonances

$$f_{a_1}^2 + f_\pi^2 - f_\rho^2 = 0\,, \qquad f_\rho^2 m_\rho^2 - f_{a_1}^2 m_{a_1}^2 = 0\,, \tag{2.15}$$

known as first and second Weinberg Sum Rules (WSR) [49]. These relations allow us to eliminate the resonance decay constants $f_{\rho,\,a_1}$, obtaining finally the expression of the LR form factor only in terms of the masses and of the pion decay constant,

$$\Pi_{LR}(Q^2) = f_\pi^2 \frac{m_\rho^2 m_{a_1}^2}{(Q^2 + m_\rho^2)(Q^2 + m_{a_1}^2)}\,. \tag{2.16}$$

Substituting into Eq. (2.12) and performing the integral, we find the result [50]

$$m_{\pi^+}^2 - m_{\pi^0}^2 = \frac{3\alpha}{4\pi} \frac{m_\rho^2 m_{a_1}^2}{m_{a_1}^2 - m_\rho^2} \log \frac{m_{a_1}^2}{m_\rho^2}\,, \tag{2.17}$$

which relates the pion mass splitting with the masses of the lowest-lying vector resonances. Using the experimental values of the π^0 mass in Eq. (2.1), $m_\rho = 770\,\text{MeV}$ and $m_{a_1} = 1260\,\text{MeV}$ we obtain $\Delta m_\pi \simeq 5.9\,\text{MeV}$, which agrees within $\sim 25\%$ with the experimental value of 4.6 MeV. Considering the approximations we made along the way (in particular the large-N_c limit for QCD, which one naively expects to be accurate within $1/N_c \approx 30\,\%$), the agreement with experiment is excellent.

Equation (2.17) relates the mass of the pions, *i.e.* of the GBs of QCD, with the masses of the lowest-lying resonances in the spectrum of the theory. Its analog in the context of strongly coupled EWSB would be a relation connecting the mass of the pNGB Higgs to the masses of the lightest resonances of the TeV-scale strong sector, for example the vector-like composite fermions that are expected to accompany the top. Given our knowledge of the Higgs mass, such a relation could allow us to gain insight into the scale at which the resonances should be observed at the LHC. Indeed, in Section 2.4.1 we will derive one explicit example of the connection between the mass of the composite Higgs and the masses of the first resonances of the strong sector.

2.2 Composite Higgs models with partial compositeness

Let us now go back to the physics of electroweak symmetry breaking, and consider a global symmetry $\mathcal{G}$, spontaneously broken to $\mathcal{H}$ at a scale f. We assume the two necessary conditions for realizing the Higgs as a pNGB to be satisfied, namely (i) it must be that $SU(2)_L \times U(1)_Y \subset \mathcal{H}$ and (ii) $\mathcal{G}/\mathcal{H}$ needs to contain at least one $SU(2)_L$ doublet, which will be identified with the composite Higgs doublet H.

While the Higgs belongs entirely to the strong sector, the SM fermions and gauge bosons are assumed to originate as external, elementary degrees of freedom. The vectors are coupled to the strong sector by gauging the corresponding SM subgroup of $\mathcal{G}$, in complete analogy to

the way the photon was coupled to the QCD pion Lagrangian. This leads to mixing terms of the form

$$\mathcal{L}_g^{UV} = g_{el} W_\mu^{el} J_{cmp}^\mu \tag{2.18}$$

where W^{el} generically denotes the elementary gauge fields, and J_{cmp} the corresponding current operators of the strong sector. At energies below the confinement scale, this results in a *linear* mixing of the elementary states with composite resonances W_{cmp}: once this mixing is rotated away, all the resulting physical states (and in particular the massless ones, which are identified with the SM gauge bosons) turn out to be a linear combination of elementary and composite fields. The choice of the coupling between elementary fermions and the strong sector is instead less obvious, and in fact more than one possibility has been considered in the literature. One way to go would be to write down bilinear couplings to composite operators, of the form

$$\mathcal{L}_f^{UV} = y\, \overline{q}_L t_R \mathcal{O}\,, \tag{2.19}$$

where we considered the top quark as an example. Below the confinement scale, the operator $\mathcal{O}$ maps to a Higgs field, giving rise to the SM Yukawa coupling. This mechanism for fermion mass generation (which was adopted first in the context of Technicolor theories, and also in the first realizations of a composite Higgs), however, typically suffers from a severe flavor problem. See Ref. [51] for a pedagogical discussion, including possible ways to evade this conclusion.

The second possibility, on which we will concentrate in this thesis, is to consider linear couplings of the elementary fermions to the strong sector, somewhat in analogy to what is done for gauge fields, see Eq. (2.18). For example, for the top-bottom doublet we can write

$$\mathcal{L}_f^{UV} = \lambda_L \overline{q}_L \mathcal{O} + \text{h.c.} \tag{2.20}$$

where $\mathcal{O}$ is a fermionic operator in the strong sector which has definite transformation properties under $\mathcal{G}$, since the full global symmetry is restored in the UV. This implies that we can formally uplift q_L to an incomplete representation $\mathcal{Q}_L$ of $\mathcal{G}$ and rewrite the mixing as

$$\mathcal{L}_f^{UV} = \lambda_L (\overline{\mathcal{Q}}_L)_{I_{r_\mathcal{O}}} (\mathcal{O})^{I_{r_\mathcal{O}}} + \text{h.c.} \tag{2.21}$$

where $I_{r_\mathcal{O}}$ is an index in the $\mathcal{G}$-representation $r_\mathcal{O}$ where the composite operator lives. In a similar way, a linear mixing between the elementary t_R and a composite operator $\mathcal{O}' \sim r_{\mathcal{O}'}$ is introduced. Exactly as in the case of vectors, once the linear mixings in the fermion sector are diagonalized, the resulting physical states are a linear combination of elementary and composite degrees of freedom: this picture has therefore been dubbed *partial compositeness* [19]. It is automatically implemented in the 'holographic' composite Higgs theories [52], based on effective field theory in 5-dimensional warped spacetime, related to the 4-dimensional picture we are discussing here via the AdS/CFT correspondence. The fermion masses are given by

$$m_t \sim g_\rho \epsilon_L \epsilon_R \frac{v}{\sqrt{2}}\,, \qquad (\epsilon_{L,R} \equiv \lambda_{L,R}/g_\rho) \tag{2.22}$$

implying that, under the assumption that the strong sector is flavor-anarchic, the light fermions are mostly elementary states ($\epsilon \ll 1$), while the third generation quarks and in particular the top need to have a sizable degree of compositeness. The partial compositeness mechanism significantly improves the compatibility with flavor bounds with respect to the bilinear coupling, and in addition it offers an appealing explanation of the hierarchies in the fermion masses. In fact, assuming the strong sector to be almost conformal above

the confinement scale, the low-energy values of the $\lambda_{L,R}$ are determined by the (constant) anomalous dimension of the CFT operator they mix with. If the UV scale at which the couplings in Eq. (2.21) are generated is large, then $\mathcal{O}(1)$ differences in the anomalous dimensions can generate naturally large hierarchies in the fermion masses via RG running. While the introduction of partial compositeness greatly ameliorated the flavor problem of the original composite Higgs models, nevertheless it did not solve the issue completely, at least in the case where the strong sector is assumed to be flavor-anarchic. Before discussing this important point, however, we want to have a first look at the Higgs potential in order to complete the sketch of the construction.

So far we have kept the analysis general, and in particular we did not specify the global symmetry breaking pattern. Several possibilities have been considered in the literature, leading either to the standard or to extended scalar spectra. In the former case the minimal choice would be $\mathcal{G} = SU(3)$ and $\mathcal{H} = SU(2) \times U(1)$, which however does not incorporate custodial symmetry, implying that the T parameter receives large tree-level corrections. The issue is solved by requiring that $SO(4) \subset \mathcal{H}$, which naturally leads to consider $SO(5)/SO(4)$: this coset contains exactly four Goldstones transforming as a $\mathbf{4}$ of $SO(4)$, or equivalently as a $(\mathbf{2},\mathbf{2})$ under $SU(2)_L \times SU(2)_R$. This is the 'Minimal' Composite Higgs Model (MCHM), which has been the subject of extensive study, and on which we will focus in the rest of the discussion. It is important to mention, however, that several other symmetry breaking patterns have been considered, including cosets that lead to two Higgs doublet models [53] or to extra scalars in representations of $SU(2)_L \times SU(2)_R$ different from the $(\mathbf{2},\mathbf{2})$ [54, 55].

Let us now focus on $SO(5)/SO(4)$. Even after the global symmetries are fixed, there still remains an ambiguity in the embeddings of the elementary fermions, which are to some extent arbitrary. In fact, several possibilities have been studied in the literature: for example $q_L \sim r_{\mathcal{O}} = \mathbf{4},\mathbf{5},\mathbf{10},\mathbf{14}$, whereas for t_R the embeddings $r_{\mathcal{O}'} = \mathbf{1},\mathbf{4},\mathbf{5},\mathbf{10},\mathbf{14}$ have been considered. One important consequence of the choice of embedding is the structure of the Higgs potential (by assumption, the latter is generated only via loops of the elementary states, and the fermionic contribution is typically dominant), which is dictated by the global symmetry. We will summarize the detailed structure of the MCHM momentarily, however for the purpose of estimating the Higgs potential we need to anticipate the power-counting rule we adopt [56, 57],

$$\mathcal{L} = \sum f^2 m_\rho^2 \left(\frac{\lambda_L q_L}{m_\rho^{3/2}}\right)^{N_q} \left(\frac{\lambda_R t_R}{m_\rho^{3/2}}\right)^{N_t} \left(\frac{\partial}{m_\rho}\right)^{N_\partial} \left(\frac{g_{\rm SM} W_\mu}{m_\rho}\right)^{N_W} \left(\frac{\mathbf{\Pi}}{f}\right)^{N_\Pi} \left(\frac{g^2}{16\pi^2}\right)^{\eta} \tag{2.23}$$

where $\mathbf{\Pi}$ indicates the four Goldstones, W_μ collectively indicates the SM gauge fields, and $g_{\rm SM}$ stands for the corresponding coupling (g, g' or g_s). In the last term, the exponent satisfies $\eta \geq 0$, however in some cases and in particular in the presence of symmetries, the minimum value of η for an operator can be larger than zero, thus implying an extra loop suppression. The symbol g denotes in this case the relevant coupling, which can be any of the couplings of the theory. We will see several examples of this extra suppression in the following. Indeed, for the Higgs potential we find $\eta = 1$: $V(H)$ is entirely generated at 1-loop due to the pNGB nature of the Higgs. The leading contribution to the potential arises from top loops, and is

suppressed by $\lambda_{L,R}^2/(16\pi^2)$.[2] One finds

$$V(H) = m_\rho^4 N_c \frac{\epsilon^2}{16\pi^2}\left[\alpha \sin^2(H/f) + \beta \sin^4(H/f)\right] , \tag{2.24}$$

where we assumed for simplicity $\lambda_L \simeq \lambda_R \simeq \lambda$ and defined $\epsilon \equiv \lambda/g_\rho$. α and β are numbers of $\mathcal{O}(1)$. We wrote down the structure of H-dependent invariants appearing in MCHM_{14} , where q_L and t_R are embedded into a **14** of $SO(5)$. As we will see, this model realizes the 'most generic' situation, and is therefore well suited for our current purpose, which is just to illustrate the essential features. The gauge contribution to the potential is [18]

$$\sim m_\rho^4 \, \frac{g^2/g_\rho^2}{16\pi^2} \sin^2(H/f) \, , \tag{2.25}$$

which is parametrically suppressed with respect to the top contribution in Eq. (2.24) by $\sim g^2/(g_\rho y_t)$. Therefore we will neglect the gauge term in the following. Also notice that the gauge term is always positive, and cannot trigger EWSB by itself. The minimization condition of the potential in Eq. (2.24) reads

$$\sin^2 \frac{\langle H \rangle}{f} = -\frac{\alpha}{2\beta} \, , \tag{2.26}$$

which implies that the natural expectation is $v \sim f$. Obtaining $v \ll f$, as required phenomenologically (in particular due to the bound on the S parameter), requires some degree of tuning, which scales like $\xi \equiv v^2/f^2$. A mild tuning of the order of 10% ($\xi \simeq 0.1$) is typically enough to comply with EWPT. This is an important point: in the class of models we are considering, the entire Higgs potential is generated at one loop, therefore the separation between v and f can only be obtained at a price of a (mild) tuning, which we accept as part of the construction. This marks a difference with respect to the other well-known class of composite Higgs models, the Little Higgses (LH), which realize a parametric hierarchy between the quartic and mass through the collective symmetry breaking mechanism. In fact in LH the quartic is a tree-level effect, leading to a potential

$$V(H) \simeq \frac{g_{\rm SM}^2}{16\pi^2} m_\rho^2 H^2 + g_{\rm SM}^2 H^4 \, , \tag{2.27}$$

where $g_{\rm SM}$ generically denotes the SM couplings. The minimization condition now reads $v^2/f^2 \sim g_\rho^2/(16\pi^2)$, therefore v is formally loop suppressed with respect to f . This is the major achievement of the Little Higgs constructions.

Going back to the partial compositeness potential in Eq. (2.24), what is the estimate for the Higgs mass? We find

$$m_h^2 \simeq \frac{N_c}{2\pi^2} g_\rho^3 y_t v^2 \, , \tag{2.28}$$

where we made use of $y_t \sim \lambda^2/g_\rho$. It follows that the limit $f \to \infty$ ($\xi \to 0$) is a true decoupling limit: all the resonances of the strong sector become heavy except the Higgs, which remains light. Equation (2.28) predicts a quite heavy Higgs, $m_h \simeq (g_\rho/5)^{3/2}$ TeV [26]. The observed value of the Higgs mass then forces one to go to small values of g_ρ , in which

[2] As it will be discussed in the following, the leading contributions to $V(H)$ arise from the H-dependent corrections to the kinetic terms of the top, which scale like $\sim \lambda_{L,R}^2/g_\rho^2$. This explains why the loop suppression is $\sim \lambda_{L,R}^2/(16\pi^2)$.

case the expansion in ϵ we performed to obtain Eq. (2.24) breaks down, and so does the estimate for m_h in Eq. (2.28). The conclusion is that this model can be viable for small g_ρ, which in turn implies that all the resonances in the fermionic sector (the ones most relevant for the Higgs potential) need to be quite light, not much above f.[3] We conclude our first overwiew of the models by briefly commenting on the generality of the structure of the potential in Eq. (2.24), in which two distinct invariants (that can be tuned to achieve EWSB) arise at order ϵ^2. While this would be indeed the most naive expectation, it turns out that in some of the most studied models (such as MCHM$_5$, which we will discuss at length in the following) the situation is different, and only one H-dependent invariant is generated at $\mathcal{O}(\epsilon^2)$. Then to obtain realistic EWSB one needs to consider terms at the order ϵ^4, where additional invariants arise: therefore a second tuning is needed (beyond the one $\sim \xi$), to reduce the size of the leading $\mathcal{O}(\epsilon^2)$ term. Together with this extra tuning comes, however, a bonus: the Higgs mass can be made light enough even for $g_\rho \gg 1$, provided there is at least one 'anomalously' light top partner (see Sec. 2.4.1). We postpone a careful analysis of the potential for MCHM$_5$ to a later stage, and conclude by stressing that a detailed analysis of the tuning and Higgs mass necessarily depends on the model at hand. Nevertheless, the general feature remains that in models with partial compositeness some degree of tuning in $V(H)$ is accepted as unavoidable, since no mechanism is known, other than collective breaking, that can make the quartic coupling parametrically larger than the mass.

2.3 Flavor

We now briefly discuss the flavor structure of composite Higgs models with partial compositeness. As we already mentioned, an attractive possibility is that the strong sector has no flavor structure, and that the hierarchies in the quark masses follow from hierarchical mixings λ. Despite the many new flavor-violating structures and CP-breaking present in the strong sector, an effective protection against flavor violation is in place, because effects from light generations are suppressed by the correspondingly small mixings. This mechanism, which in the dual five-dimensional picture is based on the small overlap between the wavefunctions of elementary fermions (localized near the UV brane) and those of the KK modes (localized near the IR brane), goes under the name of 'RS-GIM'. For example, for a four-fermion $LRLR$ operator generated by the exchange of a resonance with mass m_ρ one finds

$$\epsilon_L^i \epsilon_R^j \epsilon_L^k \epsilon_R^l \frac{g_\rho^2}{m_\rho^2} \left(\overline{f}_L^i f_R^j \overline{f}_L^k f_R^l \right) , \tag{2.29}$$

where i, j, k, l are flavor indexes. For the operator relevant to Kaon mixing, this leads to a suppression

$$\sim \frac{2 m_d m_s}{v^2 m_\rho^2} , \tag{2.30}$$

which is in some tension with the CP-violating observable ϵ_K: the corresponding bound is roughly $m_\rho \gtrsim 10$ TeV [58,59], which is clearly inacceptable from the naturalness standpoint[4]. On the other hand, it is not totally unconceivable that some accidental suppression in the

[3] Also notice that when $g_\rho \sim 1$ in the fermionic sector, the gauge contribution to the potential can become important and should be included.

[4] Other dangerous observables are $b \to s\gamma$ and EDMs [59]. If the lepton sector is included the situation is much worse, in particular due to the constraints on $\mu \to e\gamma$ and on the electron EDM [60].

values of the parameters can relax this tension. We also note that depending on the choice of embeddings for the elementary fermions, Higgs-mediated FCNC can be present at tree-level. The flavor-changing Higgs interactions are $\sim g_\rho \epsilon_L^i \epsilon_R^j \xi$ (the misalignment between the mass matrices and the couplings to h can only be at order v^2/f^2, since it arises from non-renormalizable interactions), leading to a contribution to the operator in Eq. (2.29)

$$\epsilon_L^i \epsilon_R^j \epsilon_L^k \epsilon_R^l \frac{g_\rho^2 \xi^2}{m_h^2} \left(\overline{f}_L^i f_R^j \overline{f}_L^k f_R^l \right) , \tag{2.31}$$

which is larger than the one in Eq. (2.29) by $m_\rho^2 \xi^2 / m_h^2 \sim 6$ for $\xi = 0.1$ and $m_\rho = 3$ TeV. As a consequence, in models where tree-level Higgs-mediated FCNC appear the tension with flavor observables is more severe. One example of such a model is MCHM$_{14}$, whereas in MCHM$_5$ this problem is avoided, because the symmetry structure implies alignment of the couplings to the Higgs with the fermion mass matrices[5].

To ameliorate the residual tension with flavor bounds, one can consider the possibility that the strong sector is flavor symmetric, and the SM flavor structure arises from the mixings [59]. In this case MFV can be implemented, automatically solving the flavor problem. Depending on the specific realization, either the left mixings $(\lambda_L^{u,d})_{ij}$ or the right mixings $(\lambda_R^{u,d})_{ij}$ are taken to be proportional to the identity in flavor space; this implies that one of the chiralities of the light up quarks are sizably composite, in order to obtain the physical top mass. It follows that the collider phenomenology of the MFV models is very different from the anarchic case: the strong sector resonances have a significant coupling to light quarks, therefore their production cross sections at the LHC are not suppressed as it happens in the anarchic realization. The sizable compositeness of light quarks also leads to bounds from flavor-conserving observables, notably dijet searches. For example, the exchange of a heavy gluon leads to the following four-fermion operator

$$-\frac{g_\rho^2}{2m_\rho^2} \sin^4 \phi_L (\overline{q}_L \gamma^\mu T^A q_L)^2 \tag{2.32}$$

where $q_L = (u_L, d_L)^T$, and $\sin \phi_L$ measures the degree of left-handed compositeness. The CMS search for quark compositeness [62] constrains the coefficient suppressing this operator to be larger than 3.4 TeV [63], leading to

$$\sin^2 \phi_L \leq \frac{f}{2.4 \text{ TeV}} , \tag{2.33}$$

i.e., for example, $\sin \phi_L \lesssim 0.6$ for $\xi = 0.1$. Analogous bounds apply to right-handed compositeness. Furthermore, the case of large left-handed compositeness is strongly constrained by EWPT, in particular by the modified couplings to the Z [59]. The latter constraints are milder in the case of RH compositeness, which is thus favored phenomenologically. Composite models with MFV, or more in general models where the light quarks are significantly composite, will not be discussed in this thesis. We refer the reader to Refs. [64] for detailed studies.

[5]The presence of Higgs FCNC at tree level depends on the number of $SO(4)$ invariants contained in the product of the embeddings $\mathcal{Q}_L$ and $\mathcal{T}_R$: if this number is exactly one, the Higgs FCNC do not arise. Naively, there would be 3 invariants in MCHM$_{14}$ (because $\mathbf{14} \sim \mathbf{9} \oplus \mathbf{4} \oplus \mathbf{1}$) and 2 in MCHM$_5$. However, one invariant is trivial and vanishing in both cases, leading to the conclusion in the text above [53]. According to the same argument, tree-level Higgs FCNC are absent if $\mathcal{Q}_L \sim \mathbf{14}$ and $\mathcal{T}_R \sim \mathbf{1}$, as in the model of Ref. [61].

Finally, it has been pointed out [65] that it is also possible to treat the top differently from the light quarks, thus deviating from MFV. Flavor bounds are still satisfied, but since the first two generations are mostly elementary the constraints from EWPT and from searches for compositeness are relaxed. In this setup left-handed and right-handed top compositeness are both viable, and the phenomenology is expected to be analogous to the case where the strong sector is flavor-anarchic, given that the light generations are mostly elementary.

2.4 The Minimal Composite Higgs model

We now proceed to describe in detail the minimal realization of a composite Higgs, which is based on the coset $SO(5)/SO(4)$ [18, 66]. In order to correctly reproduce the hypercharges of SM fermions, one is actually forced to extend the global symmetry to include an extra $U(1)_X$ factor, leading effectively to the symmetry breaking pattern $SO(5)\times U(1)_X/SO(4)\times U(1)_X$. The SM electroweak group $SU(2)_L\times U(1)_Y$ is embedded into $SO(4)\times U(1)_X$ and the hypercharge Y is then given by $Y=T^3_R+X$. The GBs are introduced in terms of the Σ field, constructed acting with the Goldstone matrix $U(\mathbf{\Pi})$ on the vacuum Σ_0:

$$\Sigma=\Sigma_0 U(\mathbf{\Pi})\,,\qquad U(\mathbf{\Pi})=\exp\left(-i\frac{\sqrt{2}}{f}T^{\hat{a}}\Pi_{\hat{a}}\right)\,,\qquad \Sigma_0=\,(\,0\,,\,0\,,\,0\,,\,0\,,\,1\,)\,. \tag{2.34}$$

The $T^{\hat{a}}$ ($\hat{a}=1,\dots,4$) are the generators of $SO(5)/SO(4)$, and $\Pi_{\hat{a}}$ are the 4 real GBs. Using the explicit expressions of the $SO(4)$ and $SO(5)/SO(4)$ generators ($i,j=1,...,5$)

$$\begin{aligned}T^{a_{L,R}}_{ij}&=-\frac{i}{2}\left[\frac{1}{2}\epsilon^{abc}(\delta^b_i\delta^c_j-\delta^b_j\delta^c_i)\pm(\delta^a_i\delta^4_j-\delta^a_j\delta^4_i)\right]\quad(a_{L,R}=1,2,3\;;\;a,b,c=1,2,3)\,,\\ T^{\hat{a}}_{ij}&=-\frac{i}{\sqrt{2}}(\delta^{\hat{a}}_i\delta^5_j-\delta^{\hat{a}}_j\delta^5_i)\,,\quad\hat{a}=1,\dots,4\end{aligned} \tag{2.35}$$

one obtains

$$\Sigma=\frac{\sin(\Pi/f)}{\Pi}\left(\Pi_1,\;\;\Pi_2,\;\;\Pi_3,\;\;\Pi_4,\;\;\Pi\cot(\Pi/f)\right)\,,\qquad \Pi=\sqrt{\sum_{\hat{a}}\Pi^2_{\hat{a}}}\,. \tag{2.36}$$

The two-derivative Lagrangian reads

$$\mathcal{L}_{(2)}=\frac{f^2}{2}(D_\mu\Sigma)(D^\mu\Sigma)^T\,,\qquad D_\mu\Sigma=\partial_\mu\Sigma+ig\,W^a_\mu\Sigma T^a_L+ig'\,B_\mu\Sigma T^3_R\,. \tag{2.37}$$

By performing an $SO(4)$ rotation, it is always possible to align the Higgs VEV to the Π_3 direction, thus identifying $H=\Pi_3$, where H is the Higgs field (with $\langle H\rangle\neq 0$). Then in the unitary gauge

$$U=\begin{pmatrix}1&&&&\\&1&&&\\&&\cos(H/f)&&-\sin(H/f)\\&&&1&\\&&\sin(H/f)&&\cos(H/f)\end{pmatrix}\,,\qquad \Sigma=\,(\,0\,,\,0\,,\,s_H\,,\,0\,,\,c_H\,)\,, \tag{2.38}$$

where we defined $s_H\equiv\sin(H/f)$ and analogously for c_H. Therefore

$$\mathcal{L}_{\rm kin}=\frac{1}{2}\partial_\mu H\partial^\mu H+\frac{g^2f^2}{4}s^2_H\left[W^+_\mu W^{-\,\mu}+\frac{1}{2\cos^2\theta_W}Z_\mu Z^\mu\right] \tag{2.39}$$

which fixes $f^2 \sin^2(\langle H \rangle / f) = v^2 \simeq (246\,\mathrm{GeV})^2$.

According to partial compositeness, the elementary fermions are coupled *linearly* to the strong sector. We will focus only on the quarks of the third generation, because the light fermions are expected to be coupled very weakly to the strong sector. Thus we need to specify the $SO(5)$ representations in which q_L and t_R are embedded. The most minimal choice would be the spinorial, $q_L, t_R \sim \mathbf{4}_{2/3}$ under $SO(5) \times U(1)_X$. This representation has, however, the phenomenological problem that tree-level corrections to the Z-b_L-$\bar{b}_L$ coupling, which is strongly constrained by LEP data, arise. As pointed out in Ref. [67], such large corrections can be avoided (at zero momentum) by embedding the elementary doublet q_L into an $SO(4)$ representation that is an eigenstate of a discrete parity P_{LR} which exchanges $L \leftrightarrow R$. The simplest choice is a $\mathbf{4}_{2/3} \sim (\mathbf{2},\mathbf{2})_{2/3}$, and the minimal $SO(5)$ representation containing it is the fundamental $\mathbf{5}_{2/3} \sim \mathbf{4}_{2/3} \oplus \mathbf{1}_{2/3}$ (where we wrote the decomposition under the $SO(4) \times U(1)_X$ unbroken subgroup). We thus choose to embed both q_L and t_R into a $\mathbf{5}_{2/3}$: this model goes under the name of MCHM$_5$, and will be used as a useful reference in various parts of the thesis. While MCHM$_5$ is the best known example, several other choices of embeddings have been considered in the literature, for example the $\mathbf{10} \sim \mathbf{4} \oplus \mathbf{6}$ (MCHM$_{10}$) and the $\mathbf{14} \sim \mathbf{9} \oplus \mathbf{4} \oplus \mathbf{1}$ (MCHM$_{14}$). We will highlight some features of these representations in the following, but we discuss first and in greater detail the MCHM$_5$.

We introduce a vector-like multiplet of composite fermions $\psi \sim \mathbf{5}_{2/3}$, which can be written as

$$\psi = \frac{1}{\sqrt{2}} \begin{pmatrix} B - X_{5/3} \\ -i(B + X_{5/3}) \\ T + iX_{2/3} \\ X_{2/3} + iT \\ \sqrt{2}\tilde{T} \end{pmatrix} . \tag{2.40}$$

The $SU(2)_L$ doublets $Q = (T, B)^T$ and $X = (X_{5/3}, X_{2/3})^T$ form a bidoublet $(\mathbf{2},\mathbf{2})$ under $SU(2)_L \times SU(2)_R$, while $\tilde{T}$ is a singlet $(\mathbf{1},\mathbf{1})$. The SM quantum numbers of the composite fields are summarized in Table 2.1. Note that Q has the same SM quantum numbers as the

field	T_L^3	T_R^3	Y	$Q = T_L^3 + Y$
T	$+1/2$	$-1/2$	$1/6$	$+2/3$
B	$-1/2$	$-1/2$	$1/6$	$-1/3$
$X_{5/3}$	$+1/2$	$+1/2$	$7/6$	$+5/3$
$X_{2/3}$	$-1/2$	$+1/2$	$7/6$	$+2/3$
$\tilde{T}$	0	0	$2/3$	$+2/3$

Table 2.1: SM quantum numbers of the fermionic resonances in ψ. The last column denotes the electric charge.

elementary doublet $q_L = (t_L, b_L)^T$, therefore a linear mixing between Q and q_L respects the SM symmetry. Similarly, $\tilde{T}$ has the right quantum numbers to mix with t_R. The presence of the 'exotic' doublet X, which is contained in the fundamental but not in the spinorial representation of $SO(5)$, is a prediction that follows from the protection of the Z-b_L-$\bar{b}_L$ vertex and leads to an interesting phenomenology, because X contains a heavy colored fermion with electric charge $5/3$. An additional feature of the fundamental is that the t_R is embedded into a singlet of custodial symmetry, which implies that no corrections to T are generated from loops involving this field. Introducing only one complete $SO(5)$ multiplet of resonances

(this corresponds loosely speaking to a '2-site' model, see later discussion), the Lagrangian for the fermion sector reads

$$\begin{aligned}\mathcal{L} =& i\bar{q}_L \not{D} q_L + i\bar{t}_R \not{D} t_R \\ &+ i\overline{\psi}_L \not{D} \psi_L + i\overline{\psi}_R \not{D} \psi_R - (M\overline{\psi}_L \psi_R + h.c.) \\ &- yf(\overline{\psi}_L \Sigma^T)(\Sigma \psi_R) + \text{h.c.} + iy'_L(\overline{\psi}_L \Sigma^T)\not{D}(\Sigma \psi_L) + (L \to R) \\ &- \lambda_q \overline{\mathcal{Q}}_L \psi_R - \lambda_u \overline{\psi}_L \mathcal{T}_R + h.c.\end{aligned} \tag{2.41}$$

where the embeddings of q_L and t_R are

$$\mathcal{Q}_L = \frac{1}{\sqrt{2}} \begin{pmatrix} b_L & -ib_L & t_L & it_L & 0 \end{pmatrix}^T , \qquad \mathcal{T}_R = \begin{pmatrix} 0 & 0 & 0 & 0 & t_R \end{pmatrix}^T \tag{2.42}$$

and the covariant derivative acting on ψ is given by

$$D_\mu \psi = \left[\partial_\mu - ig\, W^a_\mu T^a_L - ig'\, B_\mu (T^3_R + X) \right] \psi , \qquad X = (2/3)\mathbb{1}_5 . \tag{2.43}$$

It will also be useful to define the spurions corresponding to the embeddings of t_L and t_R,

$$\hat{\lambda}_{t_L} = \frac{\lambda_q}{\sqrt{2}} \begin{pmatrix} 0 & 0 & 1 & i & 0 \end{pmatrix}^T , \qquad \hat{\lambda}_{t_R} = \lambda_u \begin{pmatrix} 0 & 0 & 0 & 0 & 1 \end{pmatrix}^T \tag{2.44}$$

and similarly for b_L. Integrating out the fermionic resonances in ψ we obtain the following effective Lagrangian

$$\begin{aligned}\mathcal{L}_{\text{eff}} =& \; \bar{b}_L \not{p}\, \Pi_0^{q_L}(p)\, b_L + \bar{t}_L \not{p} \left(\Pi_0^{q_L}(p) + \frac{1}{2} s_H^2 \Pi_1^{t_L}(p) \right) t_L + \bar{t}_R \not{p} \left(\Pi_0^{t_R}(p) + c_H^2 \Pi_1^{t_R}(p) \right) t_R \\ &+ \frac{s_H c_H}{\sqrt{2}} M_1^t(p) \bar{t}_L t_R + \text{h.c.} ,\end{aligned} \tag{2.45}$$

whose structure is dictated by the global symmetry: for example, the only nontrivial invariant in the LL sector is $(\hat{\lambda}^\dagger_{t_L} \Sigma^T)(\Sigma \hat{\lambda}_{t_L}) \propto s_H^2/2$, and similarly for the RR and LR terms. The form factors read (in Euclidean space)

$$\begin{aligned}&\Pi_0^{q_L}(p) = 1 + \Pi_4^L(p) , \qquad \Pi_1^{t_L}(p) = \Pi_1^L(p) - \Pi_4^L(p) \\ &\Pi_0^{t_R}(p) = 1 + \Pi_4^R(p) , \qquad \Pi_1^{t_R}(p) = \Pi_1^R(p) - \Pi_4^R(p) \\ &M_1^t(p) = M_1(p) - M_4(p)\end{aligned} \tag{2.46}$$

with the definitions

$$\begin{aligned}\Pi_4^{L,R}(p) &= \frac{|\lambda_{q,u}|^2}{p^2 + m_4^2} , \qquad \Pi_1^{L,R}(p) = \frac{|\lambda'_{q,u}|^2}{p^2 + m_1^2} \\ M_1(p) &= \frac{\lambda'^*_q \lambda'_u m_1}{p^2 + m_1^2} , \qquad M_4(p) = \frac{\lambda^*_q \lambda_u m_4}{p^2 + m_4^2} .\end{aligned} \tag{2.47}$$

The masses and mixings appearing in Eqs. (2.47) are related to the parameters in the Lagrangian as

$$m_4 = M , \qquad m_1 = \frac{M + yf}{\sqrt{1 + y'_L}\sqrt{1 + y'_R}} , \qquad \lambda'_{q,u} = \frac{\lambda_{q,u}}{\sqrt{1 + y'_{R,L}}} . \tag{2.48}$$

From the effective Lagrangian we derive the Coleman-Weinberg potential

$$V(H) = -2N_c \int \frac{d^4p}{(2\pi)^4} \left[\log \Pi_{b_L} + \log\left(p^2 \Pi_{t_L} \Pi_{t_R} + |\Pi_{t_L t_R}|^2\right)\right] \tag{2.49}$$

where p is the Euclidean momentum, and

$$\Pi_{b_L} = \Pi_0^{q_L}\,, \quad \Pi_{t_L} = \Pi_0^{q_L} + \frac{s_H^2}{2}\Pi_1^{t_L}\,, \quad \Pi_{t_R} = \Pi_0^{t_R} + c_H^2 \Pi_1^{t_R}\,, \quad \Pi_{t_L t_R} = \frac{s_H c_H}{\sqrt{2}} M_1^t\,. \tag{2.50}$$

Notice that the Higgs potential can also be obtained from the formula

$$V(H) = -2N_c \int \frac{d^4p}{(2\pi)^4} \log\left[\det\left(p^2 \delta_{ij} + (\mathcal{M}^\dagger \mathcal{M})_{ij}\right)\right]\,, \tag{2.51}$$

where $\mathcal{M}$ is the full fermion mass matrix, including all $Q = 2/3$ and $Q = -1/3$ states[6]. From Eq. (2.45) we read that the bottom sector is decoupled from the Higgs, so there is no contribution to the Higgs potential from b_L loops, and as we will see there is no contribution to the hgg coupling from bottom partners as well. This is peculiar of the **5**, and does not apply for other representations, for example the **10** or the **14**.

Performing an expansion in the linear mixings $\epsilon = \lambda/m$, we find that at $\mathcal{O}(\epsilon^2)$ only one invariant is present in the potential: $V_{\epsilon^2} \sim \sin^2(H/f)$, which does not allow for a realistic EWSB. We thus need to go to $\mathcal{O}(\epsilon^4)$, where we find

$$V(H) = \alpha \sin^2(H/f) + \beta \sin^4(H/f) \tag{2.52}$$

with[7]

$$\begin{aligned}
\alpha &= N_c \int \frac{d^4p}{(2\pi)^4} \left[-\frac{\Pi_1^{t_L}}{\Pi_0^{q_L}} + \frac{2\Pi_1^{t_R}}{\Pi_0^{t_R} + \Pi_1^{t_R}} - \frac{\left|M_1^t\right|^2}{p^2}\right]\,, \\
\beta &= N_c \int \frac{d^4p}{(2\pi)^4} \left[\left(\frac{\Pi_1^{t_L}}{2}\right)^2 + \left(\Pi_1^{t_R}\right)^2 + \frac{\left|M_1^t\right|^2}{p^2}\right]\,.
\end{aligned} \tag{2.53}$$

As we already mentioned, $\alpha \sim \mathcal{O}(\epsilon^2)$ and $\beta \sim \mathcal{O}(\epsilon^4)$. The potential in Eq. (2.52) yields a VEV and Higgs mass

$$\sin^2 \frac{\langle H \rangle}{f} = \xi = -\frac{\alpha}{2\beta}\,, \qquad m_h^2 = \left(\frac{\partial^2 V}{\partial H^2}\right)_{\langle H \rangle} = \frac{8\beta}{f^2} \xi\,(1-\xi)\,. \tag{2.54}$$

Expanding the potential around the vacuum, we also obtain the values of the coefficients d_3, d_4 which parameterize the deviation of the Higgs self-interactions from the SM predictions. The values of the coefficients of the chiral Lagrangian for MCHM$_5$ are listed in Table 3.1.

Inspecting Eqs. (2.46–2.48) we see that for $y'_{L,R} \neq 0$ the form factors $\Pi_1^{t_L, t_R}$ go like $\sim 1/p^2$ at large values of the momentum. This would make the Higgs mass term α in Eq. (2.53)

[6] Fermions with 'exotic' electric charges (such as for example the $X_{5/3}$ in MCHM$_5$) do not contribute to the Higgs potential, because since they do not mix with the elementary fermions, they do not feel any explicit breaking of the $SO(5)$ symmetry; as a consequence, loops involving only the exotic states cannot generate any effects that break the shift symmetry protecting the Higgs, including a potential for the Higgs and a $hG^A_{\mu\nu} G^{\mu\nu\,A}$ (or $hF_{\mu\nu}F^{\mu\nu}$) coupling.

[7] Notice that the power-counting in Eq. (2.23) suggests $\alpha \sim m_\rho^4 N_c \epsilon^2/(16\pi^2)$ and $\beta \sim m_\rho^4 N_c \epsilon^4/(16\pi^2)$.

quadratically divergent, and the quartic β logarithmically divergent. Therefore for the sake of calculability we set $y'_{L,R} = 0$ in the Lagrangian (2.41), in which case the form factors have the asymptotic behavior $\Pi_1^{t_L,t_R} \sim 1/p^4$.[8] This turns the quadratic divergence in the Higgs mass term into a logarithmic one, whereas the quartic is now finite. As a consequence, one can regularize the logarithmic divergence in α by a single counterterm, whose coefficient is fixed by v (in practice, one can treat α as a free parameter), and still have a prediction for the Higgs mass [22]. Also, we remark that setting $y'_{L,R} = 0$ is equivalent to imposing two pairs of Weinberg sum rules, $\lim_{p\to\infty} p^n \Pi_1^{t_L,t_R}(p) = 0$ $(n = 0, 2)$: the conditions for $n = 0$ are trivially satisfied, while those for $n = 2$ give $y'_{L,R} = 0$. To obtain an entirely finite potential, we would need to introduce additional structure, for example by considering the 5-dimensional realization of the model, or a deconstructed version with three rather than two sites [20].

From the Lagrangian in Eq. (2.41), with $y'_{L,R} = 0$, we obtain the mass matrix for top-like states

$$-\mathcal{L}_m = \overline{\Psi}_L \mathcal{M} \Psi_R + \text{h.c.}\,, \qquad \mathcal{M} = \begin{pmatrix} 0 & \lambda_q & 0 & 0 \\ 0 & M + \frac{fys_H^2}{2} & \frac{iyfs_H^2}{2} & \frac{yfs_Hc_H}{\sqrt{2}} \\ 0 & -\frac{iyfs_H^2}{2} & M + \frac{fys_H^2}{2} & -i\frac{yfs_Hc_H}{\sqrt{2}} \\ \lambda_u & \frac{yfs_Hc_H}{\sqrt{2}} & \frac{iyfs_Hc_H}{\sqrt{2}} & M + yfc_H^2 \end{pmatrix} , \quad (2.55)$$

where we defined $\Psi \equiv (\, t,\, T,\, X_{2/3},\, \tilde{T}\,)^T$. The diagonalization of the matrix, which mixes elementary fields and composite states, is immediate in the limit of unbroken electroweak symmetry, *i.e.* for $v = 0$. Then the mass terms become diagonal after the rotations

$$\begin{aligned} \begin{pmatrix} q_L \\ Q_L \end{pmatrix} &\to \begin{pmatrix} \cos\phi_L & \sin\phi_L \\ -\sin\phi_L & \cos\phi_L \end{pmatrix} \begin{pmatrix} q_L \\ Q_L \end{pmatrix} , \qquad \tan\phi_L = \frac{\lambda_q}{M} \\ \begin{pmatrix} t_R \\ \tilde{T}_R \end{pmatrix} &\to \begin{pmatrix} \cos\phi_R & \sin\phi_R \\ -\sin\phi_R & \cos\phi_R \end{pmatrix} \begin{pmatrix} t_R \\ \tilde{T}_R \end{pmatrix} , \qquad \tan\phi_R = \frac{\lambda_u}{M + yf}\,. \end{aligned} \quad (2.56)$$

In this limit the top is massless, whereas the masses of the composite states are

$$M_Q = \frac{M}{c_L}\,, \qquad M_X = M\,, \qquad M_{\tilde{T}} = \frac{yf + M}{c_R}\,. \quad (2.57)$$

We see that the doublet Q is always heavier than the 'exotic' doublet X, with mass splitting $M_Q^2 - M_X^2 = \lambda_q^2$. On the other hand, the mass of the singlet $\tilde{T}$ is determined by the relative sign of the composite Yukawa coupling y and the $SO(5)$-preserving mass M. Electroweak symmetry breaking effects generate additional mixings, which also involve t_L and t_R. Thus the top becomes massive due to its mixing with composite states: at the leading order in $\xi \equiv v^2/f^2$ we have

$$m_t = y \sin\phi_L \sin\phi_R \frac{v}{\sqrt{2}}\,, \quad (2.58)$$

which is the exact version of Eq. (2.22). In addition, the masses of the composite fermions in Eq. (2.57) receive corrections, in particular the components of the X and Q doublets are split by terms of $\mathcal{O}(v)$.

[8] This can also be understood by noticing that $y'_{L,R}$ generate interactions in the strong sector that carry an extra power of the momentum compared to the 'composite Yukawa' y.

We should comment here on the relation between the Lagrangian in Eq. (2.41) and similar constructions studied in the literature. After setting $y'_{L,R} = 0$, Eq. (2.41) agrees exactly with Refs. [31, 32]. On the other hand, by performing a field redefinition on the composite multiplet, $\psi \to U^T \psi$, the Lagrangian assumes the form (omitting kinetic terms of elementary fields and gauge interactions)

$$\begin{aligned}\mathcal{L} = & \, i\overline{\psi}_L \not{\partial} \psi_L + i\overline{\psi}_L \gamma^\mu U(\partial_\mu U^T)\psi_L + (L \to R) \\ & - yf(\overline{\psi}_L \Sigma_0^T)(\Sigma_0 \psi_R) - M\overline{\psi}_L \psi_R + \text{h.c.} \\ & - \lambda_q \overline{\mathcal{Q}}_L U^T \psi_R - \lambda_u \overline{\psi}_L U \, \mathcal{T}_R + \text{h.c.}\,, \end{aligned} \tag{2.59}$$

where we set again $y'_{L,R} = 0$. In this field basis, the pNGB nature of the Higgs is manifest: when setting to zero the parameters that break explicitly the global symmetry, *i.e.* $\lambda_{q,u}$, the shift symmetry is preserved and the Higgs has only derivative interactions. Equation (2.59) and the fermionic sector of the 2-site model in Ref. [20] (written in the so-called 'holographic gauge') differ by the Higgs derivative interactions in the first line of Eq. (2.59), which have a coefficient equal to zero in the 2-site case[9]. The Higgs derivative interactions, however, are not relevant when computing the Higgs potential via the Coleman-Weinberg technique, which assumes the Higgs to be a background field. Indeed, our expression for the Higgs potential agrees with the one given in Ref. [22].

2.4.1 The light resonance connection

We start by noticing that the quartic coupling β in Eq. (2.53) is a sum of positive terms. This allows us to obtain a lower bound on the Higgs mass as a function of the masses of resonances in a simple way: keeping only the last term in β we can write

$$m_h^2 \geq \frac{N_c}{\pi^2} \frac{\xi(1-\xi)}{f^2} \int_0^\infty dp\, p \left| M_1^t(p) \right|^2 \tag{2.60}$$

and recalling that the top mass is given by $m_t \simeq \langle s_H c_H \rangle \left| M_1^t(0) \right| / \sqrt{2}$, we obtain

$$m_h^2 \geq \frac{2N_c}{\pi^2} \frac{m_t^2}{f^2} \int_0^\infty dp\, p \left| \frac{M_1^t(p)}{M_1^t(0)} \right|^2 . \tag{2.61}$$

Performing the integration we find

$$m_h^2 \geq \frac{2N_c}{\pi^2} \frac{m_t^2}{f^2} \frac{m_1^2 m_4^2}{m_1^2 - m_4^2} \frac{m_1^2 - m_4^2 - m_1 m_4 \log(m_1^2/m_4^2)}{(m_1 - m_4)^2}\,, \tag{2.62}$$

which in the limit where one of the two $SO(4)$ multiplets is much heavier than the other, simplifies to

$$m_h^2 \geq \frac{2N_c}{\pi^2} \frac{m_t^2}{f^2} m^2_{\text{lightest}} \tag{2.63}$$

where m_{lightest} is the mass of the lightest multiplet. Under the assumption of a sizable hierarchy between m_4 and m_1, we have thus obtained an upper bound on the mass of the lightest resonance

$$m_{\text{lightest}} \lesssim 1.1 \left(\frac{m_h}{125 \text{ GeV}} \right) f \simeq 530 \text{ GeV} \left(\frac{m_h}{125 \text{ GeV}} \right) \left(\frac{f}{500 \text{ GeV}} \right) . \tag{2.64}$$

[9] Notice that all the models mentioned here can be obtained as particular limits of the CCWZ construction [68] for $SO(5)/SO(4)$. See for example Refs. [36, 69].

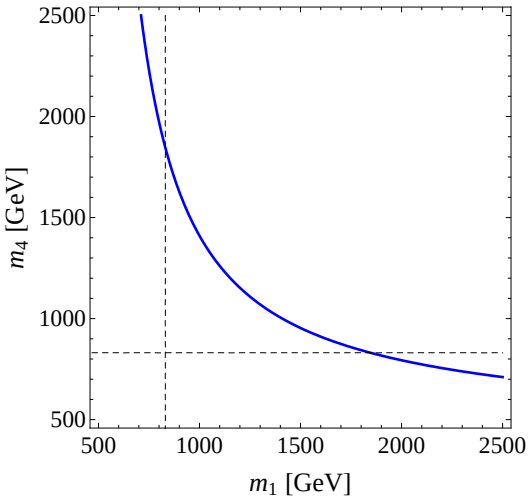

Figure 2.1: Relation between the resonance masses in MCHM$_5$, Eq. (2.66), for $m_h = 125$ GeV and $\xi = 0.1$ (solid line). The dashed lines correspond to the bound in Eq. (2.64), which was derived assuming one of the resonances to be much lighter than the other.

This equation expresses in a quantitative way, although in a simple approximation, the 'light resonance connection': accommodating a Higgs as light as the one observed by the LHC experiments in a natural (or only mildly tuned) theory of compositeness requires the presence of light fermionic resonances [22–26]. [10]

The expression of the quartic β in Eqs. (2.53) is simple enough that the integral over momenta can be performed analytically, obtaining

$$\beta = \frac{N_c}{8\pi^2}\frac{1}{m_4^2-m_1^2}\left\{\lambda_q^2\lambda_u^2(m_1-m_4)^2\log\frac{m_4}{m_1}+\frac{(\lambda_q^2-2\lambda_u^2)^2}{4}\left[m_1^2-m_4^2+(m_1^2+m_4^2)\log\frac{m_4}{m_1}\right]\right\}. \tag{2.65}$$

Notice that the $\mathcal{O}(\epsilon^2)$ terms in α generated by top loops are proportional to $\lambda_q^2 - 2\lambda_u^2$, see Eq. (2.53), so one could argue that this latter quantity needs to be small in order to make α and β of the same order, as required to obtain realistic EWSB. However, as pointed out in Ref. [22], the tuning of α could entirely come from the (already mentioned) counterterm that we need to add to regularize the logarithmic divergence. Nevertheless, even if we do not assume $\lambda_q^2 - 2\lambda_u^2$ to be small, the second term in Eq. (2.65) is numerically subleading. Dropping it and recalling the approximate expression for the top mass, we find

$$m_h^2 \simeq \frac{N_c}{\pi^2}\frac{m_t^2}{f^2}\frac{m_1^2 m_4^2}{m_4^2-m_1^2}\log\frac{m_4^2}{m_1^2}\,, \tag{2.66}$$

which links in a simple way the Higgs mass and the masses of the resonances. Notice that Eq. (2.66) resembles very closely the expression for the electromagnetic mass difference of pions, see Eq. (2.17), with the fermionic resonances playing here a role analogous to that of the spin-1 states in the QCD case. The relation between m_1 and m_4, for $m_h = 125$ GeV

[10] Notice that the bound in Eq. (2.64) is a factor $\sqrt{2}$ stronger than the one reported by Ref. [25], where employing the WSR approach, only one resonance was introduced to perform the integral in Eq. (2.61).

and $\xi = 0.1$, is displayed in Fig. 2.1: we see that there is always at least one resonance[11] lighter than about 1.2 TeV. The bound of Eq. (2.64), which was derived assuming a sizable hierarchy between the masses of the two multiplets, reads in this case $m_{\rm lightest} \lesssim 800$ GeV.

Recently, the authors of Ref. [26] pointed out that a simple correlation between the Higgs mass and the masses of the lightest resonances, such as Eq. (2.66), does not hold in general, but is rather typical of models with 'double tuning' such as MCHM$_5$, where one of the two invariants in the potential has a lower degree of divergence: for example, in MHCM$_5$ β is finite already in the 2-site picture, which allowed us to derive Eq. (2.66). On the other hand, the finiteness of α requires at least two composite multiplets, but this has no effect on the Higgs mass, because α can be effectively traded for the Higgs VEV. In general, however, finiteness of each invariant appearing in the potential will require at least two composite multiplets, thus a simple relation between m_h and the masses of the lightest resonances does not need to hold.

2.5 Little Higgses

Let us now briefly turn our attention to Little Higgs models. It is beyond our purposes to describe them in detail (see Refs. [70] for excellent reviews), and we will limit ourselves to some considerations on the mechanism that leads to a collective quartic, which is crucial to achieve a natural separation $f \gg v$. As an example, let us consider the Littlest Higgs model [71], which is based on the coset $SU(5)/SO(5)$. The sigma field is given by

$$\Sigma(x) = e^{2i\Pi/f}\Sigma_0\,, \qquad \Pi = \begin{pmatrix} 0 & H/\sqrt{2} & \varphi \\ H^\dagger/\sqrt{2} & 0 & H^T/\sqrt{2} \\ \varphi^\dagger & H^*/\sqrt{2} & 0 \end{pmatrix}, \qquad \Sigma_0 = \begin{pmatrix} & & \mathbb{1}_2 \\ & 1 & \\ \mathbb{1}_2 & & \end{pmatrix}, \tag{2.67}$$

where H is the Higgs doublet and φ is a complex triplet. An $[SU(2)\times U(1)]^2$ subgroup of the global symmetry is gauged[12] and is spontaneously broken at the scale f to the diagonal, identified with the $SU(2)_L \times U(1)_Y$ of the SM. In Eq. (2.67) we omitted the GBs that get eaten by the heavy vectors. The two-derivative Lagrangian reads

$$\mathcal{L} = \frac{f^2}{8}\mathrm{Tr}\left[(D_\mu\Sigma)^\dagger D^\mu\Sigma\right], \qquad D_\mu\Sigma = \partial_\mu\Sigma - i\sum_{j=1,2}\left[g_j W_j^a(Q_j^a\Sigma + \Sigma Q_j^{a\,T}) + g'_j B_j(Y_j\Sigma + \Sigma Y_j)\right], \tag{2.68}$$

with the gauged generators given by

$$Q_1^a = \begin{pmatrix} \sigma^a/2 & & \\ & & \\ & & \end{pmatrix}, \qquad Q_2^a = \begin{pmatrix} & & \\ & & \\ & & -\sigma^{a\,*}/2 \end{pmatrix} \tag{2.69}$$

and $Y_1 = \mathrm{diag}\left(3,3,-2,-2,-2\right)/10$, $Y_2 = \mathrm{diag}\left(2,2,2,-3,-3\right)/10$. Now let us set $g_1 = g'_1 = 0$. Then the $SU(5)$ global symmetry is explicit broken to[13] $SU(3)_{\rm ULC}\times SU(2)_2\times U(1)_2$, which

[11] Notice that since we performed an expansion in ϵ, the resonance masses in Eq. (2.66) do not include the contributions coming from the mixing with elementary states. However, it can be shown that by avoiding the expansion in ϵ, one simply obtains the same expression with $m_{1,4}$ the physical masses [22].

[12] In App. D we collect all the relevant formulas, and compute the SILH coefficients, for the variation of the Littlest Higgs in which only one $U(1)$ is gauged. This modification eliminates the $U(1)$ Z' from the spectrum.

[13] ULC stands for 'upper left corner'.

is in turn spontaneously broken down to $SU(2)_L \times U(1)_Y$. The corresponding 8 Goldstones are the four eaten by the heavy gauge vectors, plus the Higgs doublet H. We can see this explicitly: under the $SU(3)_{\rm ULC}$ transformation

$$U = e^{\,i(\epsilon_1 T_4 + \epsilon_2 T_6)}\,, \qquad T_4 = \frac{1}{2}\begin{pmatrix} & & 1 \\ & & \\ 1 & & \end{pmatrix}\,, \qquad T_6 = \frac{1}{2}\begin{pmatrix} & & \\ & & 1 \\ & 1 & \end{pmatrix} \tag{2.70}$$

we find $(i, j = 1, 2)$

$$H_i \to H_i + \frac{\epsilon_i f}{2\sqrt{2}}\,, \qquad \varphi_{ij} \to \varphi_{ij} + \frac{i}{4\sqrt{2}}(\epsilon_i H_j + \epsilon_j H_i)\,. \tag{2.71}$$

We see that H shifts at zeroth order in the fields, and so cannot acquire a potential. A similar argument holds when $g_2 = g_2' = 0$: in this case the $SU(3)$ living in the lower right corner protects H. So at least two gauge couplings (*e.g.*, g_1 and g_2) are needed to generate a potential for H, and the well-known conclusion is that no quadratically divergent contribution to the Higgs mass can arise at 1 loop.

But what about the quartic? Let us keep $g_1 = g_1' = 0$ and compute the leading, quadratically divergent part of the Coleman-Weinberg potential from gauge loops: for example for g_2 we find

$$\frac{\Lambda^2}{32\pi^2}{\rm Tr} M^2_{(2)}(\Sigma) \sim g_2^2 f^4\, {\rm Tr}\left[Q_2^a \Sigma (Q_2^a \Sigma)^*\right]\,, \tag{2.72}$$

where $M^2_{(2)}(\Sigma)$ is the squared mass matrix of the W_2 fields in the Σ background, and in the last step we used $\Lambda \sim 4\pi f$. Notice that this potential is effectively of tree-level size. The explicit form of V_- is simply dictated by Eq. 2.71, the leading terms being

$$V_- \sim \lambda_- f^2 \left|\varphi_{ij} - \frac{i}{4f}(H_i H_j + H_j H_i)\right|^2 + \dots\,, \tag{2.73}$$

where in $\lambda_- \sim g_2^2 + g_2'^2$ we included also the effect of g_2'. The potential contains a mass term for φ. This is no suprise, since the triplet is not protected by the shift symmetry contained in $SU(3)_{\rm ULC}$. On the other hand, naively it seems we have also a quartic coupling for H; but this cannot be, because the Higgs is an exact Goldstone for $g_1 = g_1' = 0$. In fact the quartic is fake: once we integrate out φ, the potential for H vanishes entirely[14].

However, let us write down the leading contribution to the potential coming from g_1:

$$\frac{\Lambda^2}{32\pi^2}{\rm Tr} M^2_{(1)}(\Sigma) \sim g_1^2 f^4\, {\rm Tr}\left[Q_1^a \Sigma (Q_1^a \Sigma)^*\right]\,, \tag{2.74}$$

which leads to

$$V_+ \sim \lambda_+ f^2 \left|\varphi_{ij} + \frac{i}{4f}(H_i H_j + H_j H_i)\right|^2 + \dots \tag{2.75}$$

with $\lambda_+ \sim g_1^2 + g_1'^2$. Now we consider the full potential $V = V_+ + V_-$: when both λ_+ and λ_- are turned on, all global symmetries protecting the Higgs are broken, so now H can get a potential. Indeed integrating out φ we obtain

$$V_{\rm eff} = \lambda (H^\dagger H)^2\,, \qquad \lambda = \frac{\lambda_+ \lambda_-}{\lambda_+ + \lambda_-}\,. \tag{2.76}$$

[14] Equivalently, one can eliminate the quartic by a field redefinition, leaving only a mass for the triplet.

Thus individually each of the operators in Eqs. (2.73) and (2.75) cannot generate a potential for H, but collectively they give rise to a tree-level quartic, and no mass term. Furthermore, and importantly, these operators do not generate radiatively a quadratically divergent contribution to the Higgs mass, but only one of the form

$$\frac{\lambda}{16\pi^2} m_\varphi^2 \log \frac{\Lambda^2}{m_\varphi^2} \,. \tag{2.77}$$

In this way (provided that we implement collective breaking also in the fermion sector, see App. D) a parametric separation between f and v is obtained. This constitutes the remarkable success of Littlest Higgs constructions.

Notice that the form of V_+ and V_- is generic in Little Higgs: one always finds schematically

$$V_\pm \sim \lambda_\pm f^2 \left|\phi \pm H^2/f\right|^2 + \dots \,, \tag{2.78}$$

where ϕ indicates a pNGB with suitable quantum numbers. The Littlest Higgs model however is special, in the sense that these interactions are *automatically* generated by gauge loops, whereas in general one would need to introduce them 'by hand', by adding to the Lagrangian operators analogous to those in the right-hand sides of Eqs. (2.72) and (2.74), with coefficients of $\mathcal{O}(1)$.

The Littlest Higgs model suffers from quite strong constraints from EWPT. One reason is the heavy $U(1)$ gauge boson, which is accidentally quite light and leads to a sizable violation of custodial symmetry unless $f \sim$ few TeV (thus reintroducing fine-tuning, due to the large mass of the top partner T). This issue can be eliminated by gauging only $U(1)_Y$ (see App. D), in which case the constraints are mainly due to the triplet VEV and $f \sim 1.2$ TeV can be obtained in a small region of parameter space [72]. One can actually show [73] that in LH models with one Higgs doublet, the presence of a scalar triplet is *unavoidable*. Let us see quickly why this happens. Given the generic form in Eq. (2.78), the quantum numbers of ϕ can be classified by analyzing those of H^2, which can be in one of the following $SU(2)_L$ representations: $\mathbf{2} \otimes \mathbf{2} = \mathbf{3}_S \oplus \mathbf{1}_A$ or $\mathbf{2} \otimes \overline{\mathbf{2}} = \mathbf{3} \oplus \mathbf{1}$. For one doublet H the antisymmetric $\mathbf{1}_A$ vanishes, $\epsilon^{ij} H_i H_j = 0$; on the other hand, for a real singlet $\eta \sim \mathbf{1}$ (with hypercharge $Y = 0$) the operators $V_\pm$ read simply $\lambda_\pm f^2 \left(\eta \pm H^\dagger H/f\right)^2$. One can then see that the Lagrangian $V = V_+ + V_-$ generates a *quadratically* divergent tadpole for η and mass term for H, of the form [73]

$$\frac{\lambda_+ f \Lambda^2}{16\pi^2} \left(\eta + \frac{H^\dagger H}{f}\right) - \frac{\lambda_- f \Lambda^2}{16\pi^2} \left(\eta - \frac{H^\dagger H}{f}\right) . \tag{2.79}$$

(notice that one cannot take $\lambda_+ = -\lambda_-$ to cancel the unwanted Higgs mass term, since in this case no quartic is generated). This tadpole is allowed by the shift symmetry, and not forbidden by other symmetries since η is a complete singlet.

One is thus led to the conclusion that a viable LH model with one Higgs doublet necessarily contains an $SU(2)_L$-triplet. This is rather problematic, since in general triplets get a VEV which is strongly constrained by EWPT. Ways out include for example imposing T-parity[15], which forbids the triplet tadpole, or going to two-Higgs doublet models. In the latter case, a successful collective quartic can be obtained even via a real singlet: for example, in the model of Ref. [27] the structure is

$$\lambda_+ f \left(\sigma + \frac{h_1^T h_2}{\sqrt{2} f}\right)^2 + \lambda_- f \left(\sigma - \frac{h_1^T h_2}{\sqrt{2} f}\right)^2 \tag{2.80}$$

[15] The phenomenology of Little Higgs models with T-parity is significantly different, and will not be discussed in this thesis.

(h_i indicates the Higgs doublets in $SO(4)$ notation) and a discrete symmetry under which $\sigma \to -\sigma$, $h_2 \to -h_2$, $h_1 \to h_1$ forbids the dangerous tadpole. Clearly, such a discrete symmetry cannot be enforced in the presence of only one Higgs doublet H.

To summarize, in this section we sketched some of the basic features of Little Higgs models. It is apparent (and obvious) that these models need some amount of complication in order to achieve their ambitious goal. From the analysis of Ref. [73], it also turns out that in order to generate a collective quartic, one Higgs doublet LH models must contain an $SU(2)_L$ scalar triplet in their spectrum, which can be in general problematic for EWPT. Considering two-Higgs doublet models improves the situation, at the price of enlarging significantly the particle spectrum. Importantly, from the phenomenological point of view there are several similarities with the 'generic' composite Higgs models previously discussed: for example, the presence of relatively light fermionic partners for the top[16], as well as an extended EW gauge spectrum (see for comparison Chapter 6). The extra scalars (beyond the Higgs doublet(s)) that participate in the collective generation of the quartic are instead rather peculiar of LH models, but their mass is of order f, which makes their detection challenging [74].

[16]For example, the heavy T in the Littlest Higgs model has a phenomenology very similar to the $\tilde{T}$ in the MCHM$_5$.

Chapter 3

Effective Lagrangians for a composite Higgs

The first run of the LHC has proved the existence of a scalar with mass close to 125 GeV , and whose properties resemble those of the SM Higgs particle within the experimental errors. On the other hand, no hint pointing to the presence of other states beyond the SM has emerged, implying that no indication as to how the SM should be completed in the UV is available. It follows that at the present time, our best description of the new particle has to rely on effective Lagrangians, based on the assumption that the new, unknown states have masses much larger than m_h. Effects of new physics are then accounted for by performing in the Lagrangian an expansion in mass dimension and in derivatives. In this chapter we introduce two different parameterizations of this kind, which will be employed repeatedly in the rest of the thesis and in particular in Chapter 4, where Higgs couplings are analyzed. The first parameterization, presented in Sec. 3.1, is based on the electroweak chiral Lagrangian [75], where the SM gauge symmetry is non-linearly realized. The chiral Lagrangian is coupled to a CP-even real scalar h , assumed to be a singlet under custodial symmetry. This approach, which relies on an expansion in derivatives, is completely general, and applies in fact also to the case where h plays no role in EWSB. In Sec. 3.2 we discuss the constraints placed by EWPT on the parameters of the effective Lagrangian. Then, following Ref. [2], in Sec. 3.3 we introduce explicit custodial breaking in the couplings of the Higgs to the W and Z. This was originally motivated by early LHC results, which seemed to point to an enhancement of the ZZ signal over the WW one, although not in a statistically significant way. First we discuss the implications on EWPT. Then we present our methodology for taking into account custodial breaking when fitting to Higgs data, and discuss the tests of custodial symmetry performed directly by ATLAS and CMS on their full datasets. In Sec. 3.4 a different parameterization is presented, namely the so-called 'SILH Lagrangian' [57], which is based on the assumption that the Higgs forms an $SU(2)_L$ doublet together with the longitudinal polarizations of the W and Z . In this case the SM symmetry is linearly realized above the weak scale, and the Lagrangian is written as an expansion in the mass dimension of the operators. The SILH power-counting rule takes into account the Goldstone nature of the Higgs, and was given in Eq. (2.23) for the case of partial compositeness. As a useful exercise, we apply Eq. (2.23) to derive the coefficients of each of the dimension-6 operators in the SILH Lagrangian. The latter is valid only in the limit $\xi = v^2/f^2 \ll 1$, where f denotes the decay constant of the global symmetry breaking.

3.1 The electroweak chiral Lagrangian

To describe the spontaneous breaking of the electroweak symmetry, we can introduce the longitudinal components of the massive W and Z, $\pi^a\,(a=1,2,3)$, via the chiral field ($v\simeq 246$ GeV)

$$\Sigma(x)=\exp(i\sigma^a\pi^a(x)/v)\,, \tag{3.1}$$

in terms of which the mass terms for gauge and fermion fields can be written in $SU(2)_L\times U(1)_Y$ invariant form as

$$\mathcal{L}_\chi^{(2)}=\frac{v^2}{4}\mathrm{Tr}\left[(D_\mu\Sigma)^\dagger\,(D^\mu\Sigma)\right]-\frac{v}{\sqrt{2}}\sum_{i,j}\left(\bar{u}_L^i\bar{d}_L^i\right)\Sigma\begin{pmatrix}y_{ij}^u\,u_R^j\\ y_{ij}^d\,d_R^j\end{pmatrix}+\mathrm{h.c.}\,, \tag{3.2}$$

where

$$D_\mu\Sigma=\partial_\mu\Sigma-ig\frac{\sigma^a}{2}\Sigma W_\mu^a+ig'\Sigma\frac{\sigma^3}{2}B_\mu\,. \tag{3.3}$$

Equation (3.2) is the electroweak chiral Lagrangian at $\mathcal{O}(p^2)$. It is approximately invariant under the global symmetry $SU(2)_L\times SU(2)_R$, under which the chiral field transforms linearly, $\Sigma\to U_L\,\Sigma\,U_R^\dagger$. This symmetry is spontaneously broken by the vacuum $\langle\Sigma\rangle=1$ to the diagonal subgroup $SU(2)_c$, known as 'custodial symmetry'. The latter invariance guarantees that at tree level, $m_W=m_Z$ for $g'\to 0$ and

$$\rho\equiv\frac{m_W^2}{m_Z^2\cos^2\theta_W}=1 \tag{3.4}$$

for generic g'. The relation (3.4) has been experimentally verified to high accuracy by electroweak precision tests (EWPT). At one loop, small corrections to $\rho=1$ arise, proportional to g' and y_u-y_d, *i.e.* to the parameters that break $SU(2)_L\times SU(2)_R$ explicitly. In principle the Lagrangian (3.2) should contain an additional operator,

$$\mathcal{L}_{cb}=-t_{cb}\frac{v^2}{8}\left(\mathrm{Tr}\left[\Sigma^\dagger D_\mu\Sigma\,\sigma^3\right]\right)^2\,, \tag{3.5}$$

which respects the gauge symmetry. This term, however, breaks $SU(2)_L\times SU(2)_R$ and thus generates a tree-level correction to the ρ parameter, $\rho=1-t_{cb}$. Therefore EWPT imply that the coefficient t_{cb} must be very small, $\mathcal{O}(10^{-3})$, which provides a phenomenological rationale for discarding the operator in Eq. (3.5).

As it is well known, the description in Eq. (3.2) leads to amplitudes for longitudinal gauge boson scattering that grow with energy, and as a consequence to a loss of perturbative unitarity at a scale $4\pi v\sim 3$ TeV. After the first run of the LHC, we know that the growth of scattering amplitudes is moderated, at least partially, by a new scalar resonance h of mass $\sim 125\,\mathrm{GeV}$. Assuming the resonance to be a singlet under custodial symmetry to prevent large corrections to the ρ parameter, the Lagrangian coupling h to the SM fields reads, up to the two-derivative order [75]

$$\begin{aligned}\mathcal{L}^{(2)} &= \frac{1}{2}(\partial_\mu h)^2-V(h)+\frac{v^2}{4}\mathrm{Tr}\left[(D_\mu\Sigma)^\dagger\,D^\mu\Sigma\right]\left(1+2\,a\,\frac{h}{v}+b\,\frac{h^2}{v^2}+b_3\,\frac{h^3}{v^3}+\cdots\right)\\ &\quad-\frac{v}{\sqrt{2}}\left(\bar{u}_L^i\bar{d}_L^i\right)\Sigma\left[1+c\,\frac{h}{v}+c_2\,\frac{h^2}{v^2}+\cdots\right]\begin{pmatrix}y_{ij}^u\,u_R^j\\ y_{ij}^d\,d_R^j\end{pmatrix}+\mathrm{h.c.}\,,\quad\text{with}\\ V(h) &= \frac{1}{2}\,m_h^2\,h^2+d_3\left(\frac{m_h^2}{2v}\right)h^3+d_4\left(\frac{m_h^2}{8v^2}\right)h^4+\cdots\,,\end{aligned} \tag{3.6}$$

Chiral Lagrangian	SILH	MCHM$_5$, pure Higgs nonlinearities
a	$1-(c_H-c_r/2)\,\xi/2$	$\sqrt{1-\xi}$
b	$1+(c_r-2c_H)\,\xi$	$1-2\xi$
b_3	$(c_r-2c_H)2\,\xi/3$	$-\frac{4}{3}\xi\sqrt{1-\xi}$
c	$1-(c_H/2+c_y)\,\xi$	$\frac{1-2\xi}{\sqrt{1-\xi}}$
c_2	$-(c_H+3c_y+c_r/4)\,\xi/2$	-2ξ
d_3	$1+(c_6-c_r/4-3c_H/2)\,\xi$	$\frac{1-2\xi}{\sqrt{1-\xi}}$
d_4	$1+(6c_6-25c_H/3-11c_r/6)\,\xi$	$\frac{1-28\xi(1-\xi)/3}{1-\xi}$
$k_g=k_{2g}$	$3c_g(y_t^2/g_\rho^2)\xi$	0
k_γ	$2c_\gamma(g^2/g_\rho^2)\xi$	0

Table 3.1: Values of the couplings of the effective Lagrangian in Eqs. (3.6–3.7) in the SILH framework (with $c_T=0$) and for MCHM$_5$ considering only Higgs nonlinearities (*i.e.* neglecting the effects of resonances). The values of the SILH parameters in MCHM$_5$ are, in the 'natural' basis for the nonlinear σ-model where $c_r=-4\,c_H,\ c_H=1/3$, $c_r=-4/3$, $c_y=4/3$, $c_6=-4/3$.

where we also introduced a potential for h. The Higgs couplings to fermions $c, c_2, ...$ are in general matrices in flavor space. For simplicity we assume them to be flavor-diagonal, so that MFV is realized. In addition, we introduce a subset of the four-derivative operators, which will be most relevant in the discussion of the Higgs phenomenology (for a complete list, see Refs. [75, 76]): the full Lagrangian reads $\mathcal{L}=\mathcal{L}^{(2)}+\mathcal{L}^{(4)}$, where

$$\mathcal{L}^{(4)}=\frac{g_s^2}{48\pi^2}G^{\mu\nu\,a}G^a_{\mu\nu}\left(k_g\frac{h}{v}+\frac{1}{2}k_{2g}\frac{h^2}{v^2}+\dots\right)+\frac{e^2}{32\pi^2}F_{\mu\nu}F^{\mu\nu}\left(k_\gamma\frac{h}{v}+\dots\right). \tag{3.7}$$

The couplings k_g, k_{2g}, k_γ arise at one-loop, mediated by heavy particles. The SM with an elementary Higgs boson corresponds to the point $a=b=c=d_3=d_4=1$, $c_2=b_3=k_g=k_{2g}=k_\gamma=0$ and vanishing higher order terms in h.

3.2 Electroweak precision tests

We wish now to discuss the compatibility of the Lagrangian in Eq. (3.6) with the EWPT. As we already mentioned, one crucial quantity is the ρ parameter, which measures the amount of breaking of custodial symmetry. As pointed out for the first time in Ref. [77], a logarithmically divergent contribution to $T\equiv(\rho-1)/\alpha$ arises when $a\neq 1$. This contribution can be computed in the low-energy theory, without specifying the UV completion for the chiral Lagrangian. In the SM, the logarithmically divergent contribution to T coming from loops of the Goldstones π^a is exactly cancelled by the loop involving the Higgs, see Fig. (3.1). This is ultimately due to the renormalizability of the SM: since T is associated with a dimension-6 operator, which

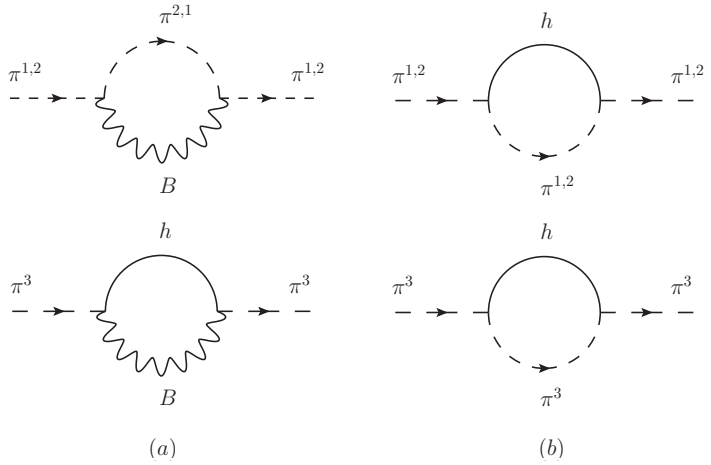

Figure 3.1: (a) Diagrams giving a logarithmic divergence in T when $a \neq 1$. This is the leading correction in the custodial-preserving case. (b) Diagrams giving a quadratic divergence in T when $a_{cb} \neq 0$, see Eq. (3.21).

can be written in terms of the Higgs doublet H as

$$\mathcal{O}_T = \frac{c_T}{2f^2}\left(H^\dagger D_\mu H - (D_\mu H)^\dagger H\right)^2 , \tag{3.8}$$

a divergent contribution to T cannot be absorbed by any counterterm. As a consequence, the logarithmic divergences must cancel exactly, and T is finite in the SM. Away from the SM point, however, the renormalizability argument does not hold, and the cancellation of the log divergences is not exact. The leading contribution to the T parameter[1] can be computed via the formula [78]

$$\Delta\hat{T} = (\delta Z_+ - \delta Z_3)_{\text{Landau gauge}} \tag{3.9}$$

where $\delta Z_{+,3}$ are corrections to the charged and neutral Goldstone wavefunction renormalizations, respectively. The reason why the computation needs to be carried out in Landau gauge is that in this gauge the kinetic B-π^3 mixing vanishes, and the only diagrams contributing to T are indeed those corresponding to Goldstone wavefunction renormalizations. In a generic gauge, other diagrams should be taken into account, see for example Ref. [79].

The contribution of the Goldstones to Eq. (3.9) is given by the top left diagram in Fig. 3.1, which we need to compute for vanishing external momentum, $p \to 0$. By explicit computation, we find

$$\Delta\hat{T} = \delta Z_+ = -\frac{3g'^2}{32\pi^2}\log\frac{\Lambda}{m_Z} \quad \text{(Goldstones)} . \tag{3.10}$$

The Higgs contribution corresponds to the bottom left diagram in Fig. 3.1, again for $p \to 0$. We obtain

$$\Delta\hat{T} = -\delta Z_3 = a^2\frac{3g'^2}{32\pi^2}\log\frac{\Lambda}{m_h} \quad \text{(Higgs)} , \tag{3.11}$$

[1] In this thesis we will always refer to the parameters $\hat{T} = \alpha T$ and $\hat{S} = (\alpha/4\sin^2\theta_w)S$.

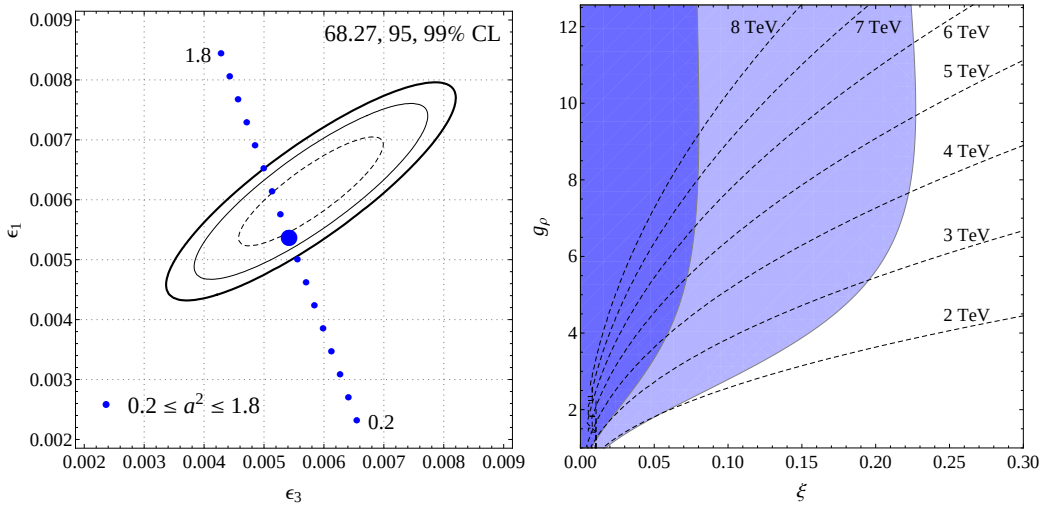

Figure 3.2: (*Left panel*) The contours show the region of the (ϵ_3, ϵ_1) plane preferred by EWPT, obtained setting $\epsilon_{2,b}$ to their SM values. The ellipses correspond to 68.27, 95 and 99% CL. The big dot is the SM prediction, whereas the small dots are obtained including the IR contributions in Eqs. (3.14), varying a^2 in the range indicated. (*Right panel*) In dark blue, the region of the plane (ξ, g_ρ) allowed by EWPT at 99% CL, assuming the IR contributions to $\hat{T}$ and $\hat{S}$ in Eqs. (3.14) with $a = \sqrt{1-\xi}$ and $\Lambda = m_\rho$, and the UV contribution to $\hat{S}$ in Eq. (5.3). We set $m_\rho = g_\rho v/\sqrt{\xi}$. The light blue region is obtained assuming an extra contribution $\Delta\hat{T} = +10^{-3}$ to be present. $\epsilon_{2,b}$ have been set to their SM values. Isocontours of m_ρ are also shown as dashed lines.

and summing up Eqs. (3.10) and (3.11), we arrive to

$$\Delta\hat{T} = -\frac{3g'^2}{32\pi^2}\log\frac{m_h}{m_Z} - \frac{3g'^2}{32\pi^2}(1-a^2)\log\frac{\Lambda}{m_h} \quad \text{(Higgs + Goldstones)}, \tag{3.12}$$

where the first piece is the finite SM contribution, whereas the second piece is logarithmically sensitive to the cutoff and arises for a nonstandard Higgs coupling to gauge fields. A similar reasoning applies to the S parameter, which is also logarithmically divergent for $a \neq 1$. Summing the Goldstone and Higgs one-loop diagrams one finds

$$\Delta\hat{S} = \frac{g^2}{96\pi^2}\log\frac{m_h}{m_Z} + \frac{g^2}{96\pi^2}(1-a^2)\log\frac{\Lambda}{m_h} \tag{3.13}$$

Notice that in Eqs. (3.12) and (3.13) terms of $\mathcal{O}(m_Z^2/m_h^2)$ are neglected. These subleading terms are responsible for the well-known, slight bending for a light Higgs, $m_h \lesssim 200$ GeV, of the curve tracing the SM prediction in the (S,T) plane [78].

Summarizing, the BSM contributions to T and S arising due to the modified Higgs coupling to gauge bosons read

$$\begin{aligned}\Delta\hat{S}_{\rm IR} &= +\frac{\alpha}{24\pi s_W^2}(1-a^2)\log\frac{\Lambda}{m_h}\,.\\ \Delta\hat{T}_{\rm IR} &= -\frac{3\alpha}{8\pi c_W^2}(1-a^2)\log\frac{\Lambda}{m_h}\,,\end{aligned} \tag{3.14}$$

These equations imply that a is constrained by EWPT, as it is illustrated for example in the left panel of Fig. 3.2, where we set to zero the UV contributions to $(\hat{S}, \hat{T})$ and assume only the IR terms in Eqs. (3.14) beyond the SM. Setting $\Lambda = 3$ TeV, roughly corresponding to the scale of the vector resonances, we find the bound $0.9 \lesssim a^2 \lesssim 1.3$ at 99% CL. Quite in general, for a composite Higgs $a < 1$ is expected: in fact, $a > 1$ can only be obtained in the presence of an isospin-2 scalar multiplet [80]. For a pNGB Higgs belonging to a composite doublet H, one can relate the coefficient a to the SILH coefficient c_H as[2]

$$a = 1 - \frac{c_H}{2}\xi \,. \tag{3.15}$$

The contribution to c_H from the nonlinear σ-model is necessarily positive, provided one considers symmetry breaking patterns $\mathcal{G}/\mathcal{H}$ with $\mathcal{G}$ a *compact* group. The contribution to c_H obtained integrating out heavy vectors is still positive, whereas by integrating out a scalar multiplet containing a doubly-charged scalar a negative c_H is generated. Indeed, the complex scalar triplets that appear in several Little Higgs constructions do contain a doubly-charged scalar; nevertheless, the *total* contribution to c_H is positive even in LH theories [81].

In addition, in a realistic theory of compositeness a UV, positive contribution to S should be present, due to the tree-level exchange of spin-1 resonances. The size of the latter contribution is, barring cancellations (an explicit computation can be found in Chapter 6),

$$\hat{S}_{\rm UV} = \frac{m_W^2}{m_\rho^2} \,, \tag{3.16}$$

where m_ρ is the mass of the spin-1 states. These two facts, $a < 1$ and $\hat{S}_{\rm UV} > 0$, imply that an extra *positive* contribution to T would improve the agreement with EWPT. This is shown in the right panel of Fig. (3.2), which was obtained by making the following assumptions:

- in Eqs. (3.14) we set a to the expression it has in the MCHM, $a = \sqrt{1-\xi}$ with $\xi = v^2/f^2$ (see Table 3.1);
- in Eq. (3.16) we made use of the relation $m_\rho = g_\rho f = g_\rho v/\sqrt{\xi}$.

In this way, the BSM contribution to EWPT is parameterized only by ξ and g_ρ . As can be clearly seen from the figure, without any extra contribution to T the bound on ξ is very stringent, $\xi \lesssim 0.08$, whereas an even moderate $\Delta T > 0$ relaxes the constraint significantly: assuming $\Delta\hat{T} = +10^{-3}$ we find $\xi \lesssim 0.2$. A positive contribution to T can arise due to loops of heavy fermions, which are typically present in composite Higgs theories, and in fact the requirement of a positive ΔT from fermion loops could be seen as an additional constraint on models that aim at being fully realistic. This will be discussed in Chapter 5.

We also note that EWPT are not sensitive to c , which parameterizes the $ht\bar{t}$ coupling: while in the SM there is an important one loop contribution to T due to the top, this is proportional to the coupling of the latter with the Goldstones, and not with the Higgs. This contribution can be obtained, again via Eq. (3.9), by computing the wavefunction renormalization of π^+ due to a top-bottom loop, and of π^3 due to a top loop. Each wavefunction renormalization constant is UV divergent, but their difference is finite as it must be, and reads

$$\Delta\hat{T} = \frac{3y_t^2}{32\pi^2} \quad (\text{top}) \,. \tag{3.17}$$

[2]This relation holds in the 'SILH basis' where $c_r = 0$, see Table 3.1.

3.3 A custodial-breaking Higgs

Motivated by early results of LHC searches for a Higgs boson, which hinted at an enhancement of the $h \to ZZ$ signal with respect to $h \to WW$, we investigated in Ref. [2] the consequences of relaxing the assumption of custodial symmetry in Higgs couplings. In fact, custodial symmetry predicts $\mu_{WW} = \mu_{ZZ}$, where μ was defined in Eq. (0.2), as it is immediately read from Eq. (3.6): the hWW and hZZ couplings are both simply rescaled by a with respect to their SM values[3]. Since we are interested in custodial-breaking effects, we add to the two-derivative Lagrangian (3.6) the following terms

$$\mathcal{L}_{cb} = -\frac{v^2}{8}\left(\mathrm{Tr}\left[\Sigma^\dagger D_\mu \Sigma\, \sigma^3\right]\right)^2 \left(t_{cb} + 2a_{cb}\frac{h}{v} + \cdots\right), \tag{3.18}$$

where t_{cb} and a_{cb} are free parameters[4] and the overall normalization has been chosen for later convenience. If we consider a SILH-type Lagrangian, where the SM gauge symmetries are linearly realized in the strong sector, custodial breaking is associated with the dimension-6 operator of Eq. (3.8), where H is the composite Higgs doublet emerging as a pseudo-Nambu-Goldstone boson from the strong sector. The corresponding values of the parameters in Eq. (3.18) are

$$t_{cb} = -c_T\xi\,, \qquad a_{cb} = -2c_T\xi\,, \qquad \left(\xi \equiv v^2/f^2\right), \tag{3.19}$$

i.e. in this case t_{cb} and a_{cb} are of the same order.

As we already mentioned, t_{cb} contributes to T at tree level, $\Delta\hat{T} = -t_{cb}$. On the other hand, the consequences of a non-vanishing a_{cb} can be seen by going to the unitary gauge, $\Sigma = 1$: the interactions of the Higgs with vector bosons are now given by

$$\mathcal{L}_{hVV} = \left[a\; m_W^2 W_\mu^+ W^{-\mu} + \frac{1}{2}(a + a_{cb})\; m_Z^2 Z_\mu Z^\mu\right]\left(2\frac{h}{v}\right). \tag{3.20}$$

The ratio between the hWW and hZZ couplings differs from the usual custodial-preserving value $g_{hWW}/g_{hZZ} = \cos^2\theta_W$. A non-vanishing a_{cb} has an important consequence on EWPT: in fact, even if we set $t_{cb} = 0$ in Eq. (3.18), a large UV sensitivity appears in T due to the one-loop diagrams involving the Higgs shown in Fig. 3.1(b). These diagrams give a *quadratically* divergent contribution

$$\Delta\hat{T}^{UV} = \left(a^2 - (a + a_{cb})^2\right)\frac{\Lambda^2}{16\pi^2 v^2}\,, \tag{3.21}$$

where Λ is the cutoff. In a concrete model, new degrees of freedom below the cutoff would need to conspire to make the total contribution to T compatible with EWPT. This will require in general a certain amount of tuning, which we quantify in Fig. 3.3 by showing isocontours of $|\Delta\hat{T}^{UV}/\epsilon_1^{exp}|^{-1}$ (we set $\Lambda = 4\pi v$ in $\Delta\hat{T}^{UV}$), where the experimental value of the ϵ_1 parameter is $\epsilon_1^{exp} = (5.4 \pm 1.0) \times 10^{-3}$, see Appendix B. In the same figure we also show isocontours of $|\Delta\hat{T}^{TL}/\epsilon_1^{exp}|^{-1}$, where

$$\Delta\hat{T}^{TL} = -\frac{a_{cb}}{2} \tag{3.22}$$

is the tree-level contribution that arises when the full gauge invariant operator $\mathcal{O}_T$ is considered. We see that the level of tuning is roughly similar in the two cases. A full computation of T requires choosing a complete model, see Refs. [83–85] and references therein for examples.

[3] At $\mathcal{O}(p^4)$, the equality $\mu_{WW} = \mu_{ZZ}$ can receive corrections even under the assumption of custodial invariance [82].

[4] Higher orders in the Higgs are negligible for our purposes.

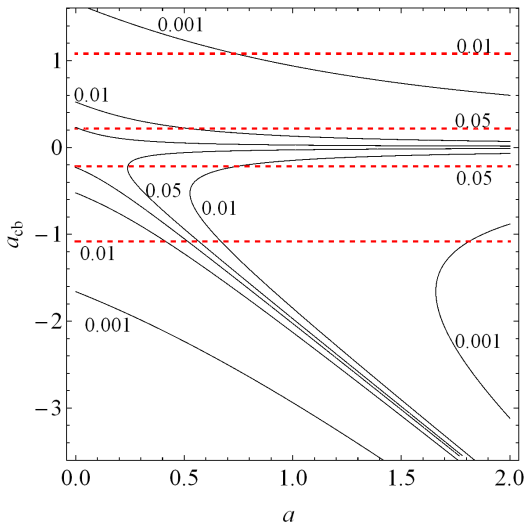

Figure 3.3: Isocontours in the (a, a_{cb}) plane of $|\Delta\hat{T}^{UV}/\epsilon_1^{exp}|^{-1}$ (solid, black) and of $|\Delta\hat{T}^{TL}/\epsilon_1^{exp}|^{-1}$ (red, dashed), roughly representing the amount of tuning needed to satisfy EWPT.

3.3.1 Testing custodial symmetry at the LHC

If we allow for explicit violation of custodial symmetry as in Eq. (3.20), and assume for simplicity that a single factor c rescales the Higgs couplings to all fermions, then the Higgs signal strengths can be predicted in terms of three parameters, namely a, a_{cb} and c. The scaling of the main channels with these parameters is reported in Table 3.2. The functions r_{VBF} and r_{Vh} are defined as

$$r_{VBF}(a, a_{cb}) = \frac{a^2 + R_{VBF}(a + a_{cb})^2}{1 + R_{VBF}} \qquad r_{Vh}(a, a_{cb}) = \frac{a^2 + R_{Vh}(a + a_{cb})^2}{1 + R_{Vh}}\,, \tag{3.23}$$

where R_{VBF} is the ratio of the SM ZZ and WW fusion production cross sections and R_{Vh} is the ratio of Zh and Wh production in the SM. Furthermore we defined the function $r_{\gamma\gamma}$, which controls the rescaling of the partial width for Higgs decay into photons, as

$$r_{\gamma\gamma}(a, c) = (1.26\, a - 0.26\, c)^2\,. \tag{3.24}$$

In Ref. [2] we performed a fit to LHC (and Tevatron) data as of April 2012, with (a, a_{cb}, c) as free parameters. Since our interest is in custodial breaking effects, we chose to marginalize the χ^2 over c, thus treating the latter as a nuisance parameter. The result of the fit is summarized in Fig. 3.4. The best fit points are respectively $(a, a_{cb}) = (0.93, 0.25)$ and $(0.93, -2.11)$, both corresponding to $\chi^2 = 9.2$ with 13 d.o.f. As a consequence of a slight enhancement of the ZZ signal with respect to the WW one in 7 TeV LHC data, the best fit points are 'Zphilic' (or equivalently, Wphobic): $\mu_{ZZ}/\mu_{WW} = (a + a_{cb})^2/a^2 \approx 1.6$.

Notice that all the observables involved in Higgs searches are insensitive to the sign of $a + a_{cb}$, as such combination always appears squared, implying the symmetry of the constant-χ^2 contours under $(a, a_{cb}) \to (a, -(2a + a_{cb}))$. In the best-fit region where $a + a_{cb} < 0$, the Higgs is actually 'dys$Z$philic', since the sign of the hZZ coupling is opposite with respect to

channel	$\sigma_{\rm prod} \times \Gamma \sim$
$gg \to h \to \gamma\gamma$	$c^2\, r_{\gamma\gamma}(a,c)$
$qq' \to hjj \to \gamma\gamma jj$	$r_{VBF}(a,a_{cb})\, r_{\gamma\gamma}(a,c)$
$gg \to h \to ZZ^*$	$c^2\,(a+a_{cb})^2$
$qq' \to hjj \to ZZ^* jj$	$r_{VBF}(a,a_{cb})(a+a_{cb})^2$
$gg \to h \to WW^*$	$c^2\, a^2$
$qq' \to hjj \to WW^* jj$	$r_{VBF}(a,a_{cb})\, a^2$
$gg \to h \to \tau\bar{\tau}$	c^4
$qq' \to hjj \to \tau\bar{\tau} jj$	$r_{VBF}(a,a_{cb})\, c^2$
$qq' \to hV \to b\bar{b}V$	$r_{Vh}(a,a_{cb})\, c^2$

Table 3.2: Leading dependence of the main Higgs production cross sections and decay widths on the parameters (a, a_{cb}, c) , under the assumptions of explicit custodial breaking in the hVV couplings and universal rescaling of $hf\bar{f}$ couplings.

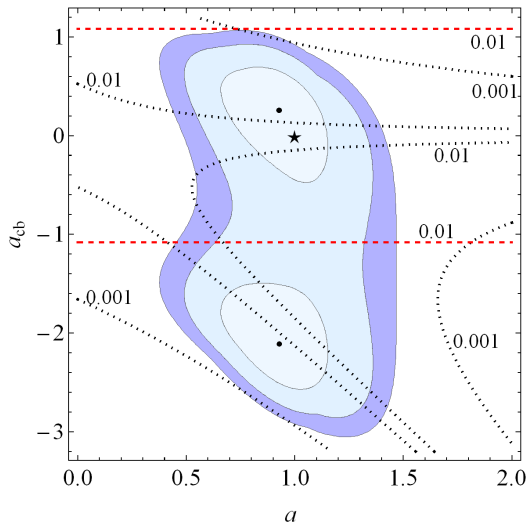

Figure 3.4: Best-fit region in the (a, a_{cb}) plane from LHC7 and Tevatron results, at $68, 95, 99\%$ C.L., after marginalization over c. The two best fit points are shown as black dots, while the star is the SM point corresponding to $(a, a_{cb}) = (1, 0)$. All the observables involved are insensitive to the sign of $a + a_{cb}$, implying the symmetry under $(a, a_{cb}) \to (a, -(2a + a_{cb}))$. Isocontours of $|\Delta\hat{T}^{UV}/\epsilon_1^{exp}|^{-1}$ (dotted, black) and of $|\Delta\hat{T}^{TL}/\epsilon_1^{exp}|^{-1}$ (red, dashed), indicating the level of tuning needed to satisfy EWPT, are superimposed to the LHC best fit region.

the standard case. In Section 3 of Ref. [2] we presented some future measurements at e^+e^- linear colliders that may lift the degeneracy between a Zphlic and a dys$Z$phlic Higgs.

The same test of custodial symmetry has been performed directly by ATLAS and CMS on their full $7 + 8$ TeV data set, assuming as independent parameters $\lambda_{WZ} \equiv a/(a + a_{cb})$, a and c (or combinations of them). We show in Fig. 3.5 the one-dimensional likelihoods in λ_{WZ} they obtained, after profiling on the other two parameters. The best fit is for both

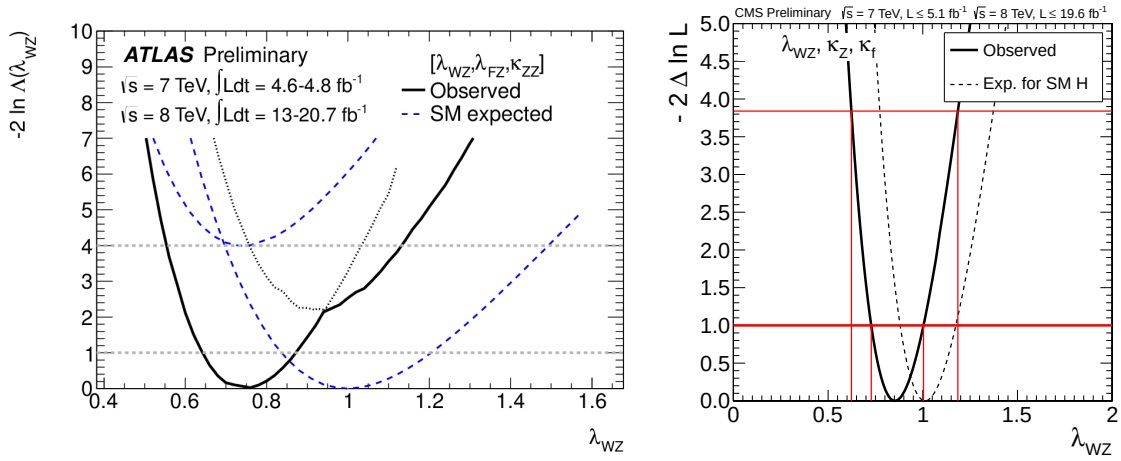

Figure 3.5: (*Left panel*) Likelihood distribution for the custodial-testing parameter λ_{WZ} from ATLAS data. The dashed curves show the expectation for a SM Higgs, the two curves correspond to regions with different sign of c. The thin dotted lines indicate the continuation of the likelihood curve when restricting the parameters to either the positive or negative branch of c. From Ref. [9]. (*Right panel*) The same likelihood distribution, from CMS data. The dashed curve shows the expectation for a SM Higgs. From Ref. [10].

experiments $\lambda_{WZ} \approx 0.8$, with the 95% CL intervals being

$$0.56 < \lambda_{WZ} < 1.13 \quad [\text{ATLAS}]\,, \qquad 0.62 < \lambda_{WZ} < 1.19 \quad [\text{CMS}]\,. \tag{3.25}$$

Intriguingly, data still prefer a Higgs coupling more strongly to ZZ than to WW, although the result is not statistically significant (the custodial-preserving point $\lambda_{WZ} = 1$ is within the 95% CL measured region for both experiments). The future run of the LHC will tell if this is merely a fluctuation, or rather custodial symmetry is violated in the couplings of the Higgs. If the latter turned out to be true, the consequences on the theory would be dramatic: as we have already mentioned, new light degrees of freedom are required in order to make a sizeable a_{cb} compatible with EWPT. In the absence of a symmetry a significant tuning is generically needed, as it is also shown in Fig 3.4. However, it is important to keep in mind that the presence of such new light degrees of freedom could in principle alter the interpretation of results of Higgs searches.

3.4 The SILH Lagrangian

As we discussed at length, an interesting solution to the hierarchy problem is given by the Higgs boson being a composite bound state emerging from a new strongly-interacting sector, broadly characterized by a mass scale m_ρ and a coupling g_ρ. If in addition the Higgs emerges as a pseudo-Nambu-Goldstone boson of a spontaneous symmetry breaking $\mathcal{G}/\mathcal{H}$ at the scale $f = m_\rho/g_\rho$, then it can be naturally lighter than the other resonances of the strong sector and $v^2/f^2 \ll 1$ can be accommodated. A low-energy, model-independent description of this idea is given by the strongly-interacting light Higgs (SILH) Lagrangian [57], which applies to the general scenario where the Higgs is a light pseudo-Nambu-Goldstone boson, including Little Higgs and composite Higgs models with partial compositeness. At scales much smaller than

m_ρ, deviations from the SM are parameterized in terms of a set of dimension-six operators. Most relevant to our discussion will be the subset of operators containing the (composite) Higgs doublet H,

$$\begin{aligned}\mathcal{L}_{\rm SILH} &= \frac{c_H}{2f^2}\partial^\mu(H^\dagger H)\partial_\mu(H^\dagger H) + \frac{c_r}{2f^2}H^\dagger H(D_\mu H)^\dagger(D^\mu H) - \frac{c_6\lambda}{f^2}(H^\dagger H)^3 \\ &+ \left(\frac{c_y y_f}{f^2}H^\dagger H\bar{f}_L H f_R + \text{h.c.}\right) + \frac{c_T}{2f^2}\left(H^\dagger\overleftrightarrow{D^\mu}H\right)^2 \\ &+ \frac{c_g g_s^2}{16\pi^2 f^2}\frac{y_t^2}{g_\rho^2}H^\dagger H G^a_{\mu\nu}G^{a\,\mu\nu} + \frac{c_\gamma g'^2}{16\pi^2 f^2}\frac{g^2}{g_\rho^2}H^\dagger H B_{\mu\nu}B^{\mu\nu} \\ &+ \frac{ic_W g}{2m_\rho^2}\left(H^\dagger\sigma^a\overleftrightarrow{D^\mu}H\right)(D^\nu W_{\mu\nu})^a + \frac{ic_B g'}{2m_\rho^2}\left(H^\dagger\overleftrightarrow{D^\mu}H\right)(\partial^\nu B_{\mu\nu}) \\ &+ \frac{ic_{HW}g}{16\pi^2 f^2}(D^\mu H)^\dagger\sigma^a(D^\nu H)W^a_{\mu\nu} + \frac{ic_{HB}g'}{16\pi^2 f^2}(D^\mu H)^\dagger(D^\nu H)B_{\mu\nu} \end{aligned} \tag{3.26}$$

where g_s, g, g' are the SM $SU(3)_c \times SU(2)_L \times U(1)_Y$ gauge couplings, whereas λ and y_f are the Higgs quartic and Yukawa[5] coupling appearing in the SM Lagrangian, respectively. We made the definitions $H^\dagger\overleftrightarrow{D^\mu}H \equiv H^\dagger(D^\mu H) - (D^\mu H)^\dagger H$, and so on. In Eq. (3.26) we have kept explicitly the operator proportional to c_r, which can be eliminated at $\mathcal{O}(1/f^2)$ by a field redefinition

$$H \to H + a(H^\dagger H)H/f^2\,, \tag{3.27}$$

under which

$$c_H \to c_H + 2a\,, \qquad c_r \to c_r + 4a\,, \qquad c_6 \to c_6 + 4a\,, \qquad c_y \to c_y - a\,, \tag{3.28}$$

while the remaining coefficients do not change under this transformation. The choice $c_r = 0$ corresponds to the 'SILH basis', which can be reached starting from a generic basis where $c_r \neq 0$ by applying the transformation in Eq. (3.27) with $a = -c_r/4$. We choose to keep explicitly the operator proportional to c_r as the 'natural' basis for nonlinear σ-models actually corresponds to a non-vanishing c_r : in fact, in a nlσm the relation $c_H = -4c_r$ holds [34]. Furthermore, since physical amplitudes have to be invariant under field redefinitions, Eqs. (3.27) and (3.28) can be used to check the consistency of our results.

We now briefly discuss each term in the SILH Lagrangian, and in particular we will derive the coefficients of the operators listed in Eq. (3.26) by employing the power-counting rule that applies to models with partial compositeness, Eq. (2.23). Nevertheless we remark that the SILH approach applies to a wide class of theories, well beyond those with partial compositeness.

The operators in the first two lines are genuinely sensitive to the nonlinearity of the Higgs sector, being suppressed by $1/f^2 = g_\rho^2/m_\rho^2$. The coefficients of the operators with two derivatives and four Higgses ($\mathcal{O}_H, \mathcal{O}_r$ and $\mathcal{O}_T$) are straightforwardly obtained by the rules in Eq. (2.23). The operator $\mathcal{O}_T$ stands alone: it breaks custodial symmetry and thus gives a tree-level contribution to the T parameter, $\Delta\hat{T} = c_T v^2/f^2$, which is strongly constrained by electroweak data. If the strong sector is invariant under custodial symmetry, as it is the case for example in composite Higgs models based on the coset $SO(5)/SO(4)$, then c_T vanishes

[5]In the expression for the operator $\mathcal{O}_y$, $\bar{f}_L H f_R$ is understood to be a shorthand for the gauge-invariant expression involving the appropriate $SU(2)$ fermion doublet, and H or $\widetilde{H}$ for down and up type quarks respectively.

at tree-level. As for the operator $\mathcal{O}_y$, in partial compositeness its coefficient is estimated to be $\sim \lambda_L \lambda_R/(g_\rho f^2)$, which is indeed equal to y_f/f^2. On the other hand, $\mathcal{O}_6$ is generated at one loop, its coefficient will be for example

$$\sim \frac{g_\rho^2 \lambda_L^2}{16\pi^2 f^2} \,. \tag{3.29}$$

Since the corresponding expression for the quartic coupling reads $\lambda = g_\rho^2 \lambda_L^2/(16\pi^2)$, we obtain the coefficient given in Eq. (3.26).[6]

The operators in the third line parameterize the effective couplings of the Higgs to gluons and to photons, respectively. These couplings arise at one-loop in theories satisfying reasonable assumptions[7] (indeed, this is another example of $\eta > 0$ in Eq. (2.23)). Furthermore, since these operators do not respect the shift symmetry protecting the Higgs (they can be thought as Higgs mass terms with extra insertions of gauge field-strengths), to generate them one actually needs a loop involving the couplings that break this symmetry. For $\mathcal{O}_g$ we find

$$\frac{y_t^2}{16\pi^2}\frac{g_s^2}{m_\rho^2} \,, \tag{3.30}$$

where we assumed that the coupling providing the breaking of the shift symmetry is y_t. The coefficient of $\mathcal{O}_\gamma$ is obtained in the same way, by assuming that the relevant breaking comes from g. These operators are important in the presence of relatively light resonances, *i.e.* when $g_\rho \sim 1$. As we discussed, in the context of composite models the observed value of the Higgs mass implies that light ($\lesssim$ TeV) fermionic resonances are expected. The contribution of these light states to c_g and c_γ could thus be sizable.

The operators parameterized by $c_{W,\,B}$ can arise due to the tree-level exchange of vector resonances (see for example the discussion at the beginning of Chapter 6, where we compute c_W for an $SU(2)_L$-triplet spin-1 resonance); their naive coefficients are computed straightforwardly. These operators give a contribution to the electroweak S parameter[8]

$$\Delta\hat{S} = (c_W + c_B)\frac{m_W^2}{m_\rho^2} \,. \tag{3.31}$$

Finally, the operators parameterized by c_{HW} and c_{HB} arise only at one-loop level in 'reasonable' theories. This can be explained by noticing that these operators give a correction to the gyromagnetic ratio of the W, whereas in a minimally coupled theory where all vectors are associated to gauge symmetries all g's are equal to 2 at tree level [86]. This implies that the coefficient of, *e.g.*, $\mathcal{O}_{HW}$ is

$$\frac{g_\rho^2}{16\pi^2}\frac{g}{m_\rho^2} \,. \tag{3.32}$$

This is yet another example where a symmetry implies $\eta > 0$ in Eq. (2.23); in this case the coupling associated to the extra suppression is g_ρ. We point out that in Chapter 6 we discuss

[6] Notice that the coefficients of $\mathcal{O}_y$ and $\mathcal{O}_6$ can also be obtained by using the field redefinition in Eq. (3.27).

[7] Specifically, we consider minimally coupled field theories where all states have spin ≤ 1, and all vectors are associated to (spontaneously broken) gauge symmetries [57].

[8] Notice that the dimension-6 operator usually associated to S is $\mathcal{O}_{WB} = g g' H^\dagger \sigma^a H W^a_{\mu\nu} B^{\mu\nu}/(4m_\rho^2)$, which gives $\Delta\hat{S} = c_{WB}(m_W^2/m_\rho^2)$. This operator is not independent from those appearing in Eq. (3.26): in fact one can easily derive the relation $O_{WB} = O_B - (16\pi^2/g_\rho^2)O_{HB} - (4\pi^2/g^2)O_\gamma$, by integrating by parts and making use of the identity $D^\mu D^\nu H - D^\nu D^\mu H = (-i/2)(g\,\sigma^a W^{\mu\nu\,a} + g' B^{\mu\nu})H$.

an effective Lagrangian for a W', where we do not assume the heavy vector to be a gauge boson, but only require invariance under the SM gauge symmetry. In this case $g_{W'} \neq 2$ at tree level, see Eq. (6.38), and the operators $\mathcal{O}_{HW,HB}$ will be generated with tree-level (rather than one-loop) suppression.

Chapter 4

Phenomenology of spin 0: Higgs couplings

ATLAS and CMS have already measured the Higgs mass with an accuracy better than 1 GeV, see Eq. (0.1), and strongly disfavored (although not completely excluded) quantum numbers different from $J^{CP} = 0^+$. A more complex and ambitious experimental task, which will require a long-term effort, is that of determining the couplings of the Higgs to the other SM fields with the best precision possible at the LHC, which with $300\,\text{fb}^{-1}$ at 14 TeV is expected to be roughly of order $5 \div 10\%$ depending on the coupling (for a very recent appraisal, see Ref. [42]).

A precise knowledge of the Higgs couplings is important because the properties of a naturally light Higgs are expected to deviate from those of the SM Higgs, which is extremely fine-tuned. This is especially true for the loop-induced couplings to gluons and photons, because any state that radiatively contributes to the Higgs mass will also contribute to these vertexes. In addition, these couplings play a crucial role phenomenologically, in particular all inclusive Higgs rates are proportional to the hgg vertex. Sections 4.1 and 4.2 are dedicated to a study of the loop-induced Higgs couplings in composite models [3]. Using the background-field method known as Higgs low-energy theorem (LET) [37,87] we derive general expressions of the amplitudes in terms of the parameters of the effective Lagrangians introduced in Chapter 3. Importantly, we include the contribution of fermionic resonances, which are expected to be light by naturalness considerations (see Sec. 2.4.1 for a quantitative expression of this fact). One singular feature of composite Higgs models is that the amplitudes for $gg \to h$ and $h \to \gamma\gamma$ are not sensitive to light fermionic resonances running in the loops, as first noticed in Ref. [33]. We review the symmetry reason behind this cancellation, which holds exactly in the LET approximation, and verify that no dependence on the resonances is hidden in the subleading terms in the inverse mass expansion.

In Sec. 4.3 we turn to *double* Higgs production, an a priori subleading channel which can however give valuable information in the context of composite models [38]. We extend the LET to $gg \to hh$, again in a model-independent way, and find that the cancellation of the effects of resonances is in place even in this case. However, by comparison with a previous computation where only the top loops were considered [38] we find that the LET approximation fails by up to 50%. This motivates an exact computation of $gg \to hh$, which we perform in MCHM_5. Our results show that there is indeed a dependence on the spectrum of resonances, so double Higgs production could usefully complement the information coming from direct searches for vector-like quarks. We also analyze the phenomenology of $pp \to hh$

at LHC14.

In Sec. 4.4 we focus our attention on the $ht\bar{t}$ coupling, which has not been directly measured yet by ATLAS and CMS, due to the limited sensitivity of the $pp \to t\bar{t}h$ process [39–41]. An indirect determination of the coupling is currently possible by means of fits to Higgs data, thanks to the sizable contribution of the top to the radiative hgg and $h\gamma\gamma$ couplings. Clearly, this indirect method requires to make assumptions on new states possibly running in the loops. Assuming no new states beyond the SM ones the likelihoods in Fig. 2 are obtained, which display an ambiguity in the *sign* of the $ht\bar{t}$ coupling. We review how this ambiguity arises and why Higgs fits in 'standard' channels cannot robustly exclude the negative sign hypothesis. In Sec. 4.5 we argue that single top production in association with a Higgs can efficiently remove the degeneracy [4]. We perform a detailed phenomenological study of this process at the LHC, focusing on the decay of the Higgs into b quarks. We finally estimate the impact on the parameter space of Higgs couplings, finding that already LHC8 could exclude part of the 'negative sign' region.

4.1 One-loop couplings via the Higgs Low Energy Theorem

Here we discuss applications of the Higgs Low-Energy Theorem [37,87] in composite models. The LET allows one to obtain the leading interactions of the Higgs boson with gluons and photons arising from loops of heavy particles. By heavy particles we mean here both SM states (in particular, W and top) and new states belonging to the putative TeV scale theory, such as for example fermionic resonances in composite Higgs models. The couplings of the Higgs to gluons and photons are needed in the computation of the cross sections for single and double Higgs production via gluon fusion at the LHC, as well as of the partial width of the decay $h \to \gamma\gamma$. These couplings are especially interesting because they are related to the tuning of the EW scale: the new degrees of freedom that cancel the quadratic divergence in the Higgs mass necessarily affect also the hgg and $h\gamma\gamma$ couplings, therefore we expect the latter to differ from the standard values for a natural Higgs (see for example Ref. [88]). Conversely, the more standard the Higgs couplings are, the more the theory will be tuned, *i.e.*

$$\frac{\sigma(gg \to h)}{\sigma(gg \to h)_{\rm SM}} \sim 1 + (\text{tuning})\,, \tag{4.1}$$

and similarly for the $h \to \gamma\gamma$ partial width.[1] We will adopt a model-independent approach and compute the couplings of the Higgs to gluons and photons in terms of the parameters of the effective Lagrangians defined in Eqs. (3.6–3.7) and (3.26). Therefore, given a specific model, one only needs to perform the matching to one of the two parameterizations; once that is done, our results apply straightforwardly and without further computations. The analysis that follows, presented for the first time in Ref. [3], extends the results of Refs. [34, 81] to Higgs pair production in gluon fusion, and also includes a discussion of corrections to the LET approximation arising from higher order terms in the $1/M$ expansion, where M is the mass of the generic heavy particle running in the loops. Notice that the LET can be extended to 2-loop order to include the leading QCD corrections, see for example Ref. [87] for applications

[1] Equations (4.17) and (4.22) in the following are concrete examples of this broad statement, the first in the context of compositeness and the second in SUSY. Notice, however, that in the composite case the cancellation of the effects of resonances modifies the interpretation in terms of tuning. Nevertheless, even in the presence of the cancellation, the correction to the hgg coupling is $\propto \xi$ (see Eq. (4.17)), which is a rough measure of tuning.

in the SM. However, our discussion will be mainly limited to couplings at the leading 1-loop order.

4.1.1 Couplings to gluons

According to the LET the interactions of the physical Higgs boson with gluons, mediated by loops of a heavy colored particle which gets some of its mass from EWSB, can be obtained by treating the Higgs H as a background field and taking the field-dependent mass $M(H)$ of the heavy particle as a threshold for the running of the QCD gauge coupling.[2] The coupling of the low-energy theory is given by

$$\frac{1}{g^2_{s\,\mathrm{eff}}(\mu, H)} = \frac{1}{g_s^2(\mu)} - \delta b\, \frac{C(r)}{8\pi^2} \log \frac{M(H)}{\mu}\,, \tag{4.2}$$

where g_s is the coupling of the UV theory[3]. Here $C(r)$ is the Dynkin index of the representation where the heavy particle lives, whereas $\delta b = 2/3$ for a Dirac fermion and $\delta b = 1/6$ for a complex scalar. The effective Lagrangian is simply given by the kinetic term

$$-\frac{1}{4g^2_{s\,\mathrm{eff}}(\mu, H)}\, G^A_{\mu\nu} G^{A\,\mu\nu}\,. \tag{4.3}$$

This yields, assuming the presence of a set of heavy particles p_i transforming in the fundamental representation of $SU(3)_c$ $(C(r) = 1/2)$

$$\mathcal{L}_{\mathrm{eff}} = \frac{g_s^2}{64\pi^2} G^A_{\mu\nu} G^{A\,\mu\nu} \sum_{p_i} \delta b_{p_i} \log M^2_{p_i}(H)\,. \tag{4.4}$$

Here we will focus only on the effects of the heavy fermion sector, which in composite Higgs models typically includes new states beyond the top quark. By expanding the field-dependent masses of the heavy particles around the VEV $\langle H \rangle$ we obtain the couplings of the Higgs boson to gluons mediated by loops of heavy fermions

$$\mathcal{L}_{gg} = \frac{g_s^2}{48\pi^2} G^A_{\mu\nu} G^{A\,\mu\nu} \sum_{n=1}^{\infty} \frac{1}{n!} A_n h^n\,, \tag{4.5}$$

with the definition

$$A_n \equiv \left(\frac{\partial^n}{\partial H^n} \log |\det \mathcal{M}(H)| \right)_{\langle H \rangle}\,, \tag{4.6}$$

where $\mathcal{M}$ is the heavy fermion mass matrix. In the SM only the top quark contributes[4] with $m_t(H) = y_t H/\sqrt{2}$, yielding $A_n = (-1)^{n+1}(n-1)!\, v^{-n}$, which allows to resum the series in

[2] Throughout the discussion, we will denote by H both the Higgs doublet and the scalar field with $\langle H \rangle \neq 0$, as it will always be clear from the context which one we are referring to. On the other hand, h denotes the physical Higgs scalar.

[3] One has $1/g_s^2(\mu) = 1/g_s^2(\Lambda) + b_{UV} \log(\Lambda/\mu)/(8\pi^2)$, where $\Lambda > M$ is a UV scale, and $b_{UV} = b_{IR} + \delta b$ (our conventions are such that b is negative, $b = -11 + 4C(r_f)n_f/3 + C(r_s)n_s/3$).

[4] In the SM, the bottom contribution to the hgg amplitude (which of course cannot be computed using the LET, since $m_b \ll m_h$) is not negligible: at LO, including the b loop decreases the rate by approximately 10%. This is because the fermion form factor scales in the limit $m_b \to 0$ as $\sim x \log^2 x$, $x \equiv m_b^2/m_h^2$. Since we are interested in the effects of heavy fermions, unless otherwise specified we will neglect the bottom loop. Its inclusion would nevertheless be straightforward.

Eq. (4.5) (see for example Refs. [87, 89])

$$\mathcal{L}_{gg}^{\rm SM} = \frac{g_s^2}{48\pi^2} G^A_{\mu\nu} G^{A\,\mu\nu} \, \log\left(1+\frac{h}{v}\right) . \tag{4.7}$$

The corresponding gauge invariant operator is $\log(H^\dagger H) G^a_{\mu\nu} G^{a\,\mu\nu}$, which is associated with a chiral fermion (the singularity of the operator for $H \to 0$ signals the presence of a massless state in that limit, which cannot be integrated out). The lowest-order operator arising from vector-like fermions is instead $H^\dagger H G^a_{\mu\nu} G^{a\,\mu\nu}$. The effects of these two operators on double Higgs production were discussed in Ref. [90].

Using Eq. (4.5) it is straightforward to derive the expression of the hgg and $hhgg$ couplings in the SILH formalism. We refer the interested reader to App. C for a detailed derivation, and report here only the results. We remark that from now on we will work in the unitary gauge, where the Higgs doublet reads $(0\,,\, H/\sqrt{2})^T$. The effective coupling of the Higgs boson to two gluons reads (see App. C)

$$\mathcal{L}_{hgg} = \frac{g_s^2}{48\pi^2} G^A_{\mu\nu} G^{A\,\mu\nu} \frac{h}{v} \left[\left(\frac{\partial}{\partial \log H} \log |\det \mathcal{M}(H)| \right)_{H=v} - \frac{c_H}{2} \xi \right] . \tag{4.8}$$

This coupling governs the rate of single Higgs production via gluon fusion, and its expression was already obtained in Refs. [34, 81]. The production rate normalized to the SM one is given by the square of the expression in square brackets in Eq. (4.8). On the other hand the effective coupling of two Higgs bosons to two gluons, which contributes to Higgs pair production via gluon fusion, has the following expression

$$\mathcal{L}_{hhgg} = \frac{g_s^2}{96\pi^2} G^A_{\mu\nu} G^{A\,\mu\nu} \frac{h^2}{v^2} \left[\left(\left(\frac{\partial^2}{\partial (\log H)^2} - \frac{\partial}{\partial \log H} \right) \log |\det \mathcal{M}(H)| \right)_{H=v} - \frac{c_r}{4} \xi \right] . \tag{4.9}$$

In terms of the effective Lagrangian in Eqs. (3.6–3.7), the couplings read

$$\mathcal{L}_{hgg} = \frac{g_s^2}{48\pi^2} G^A_{\mu\nu} G^{A\,\mu\nu} \frac{h}{v} \left(c + k_g\right) , \qquad \mathcal{L}_{hhgg} = \frac{g_s^2}{96\pi^2} G^A_{\mu\nu} G^{A\,\mu\nu} \frac{h^2}{v^2} \left(2c_2 - c^2 + k_{2g}\right) . \tag{4.10}$$

In the expression of the $hhgg$ coupling in Eq. (4.10), the first term comes from the triangle top loop involving the $t\bar{t}hh$ vertex, whereas the second is the contribution of top box diagrams, see Fig. 4.2. On the other hand, k_g and k_{2g} are parameterizing the contributions from integrated-out heavy particles.

4.1.2 Coupling to photons

Another loop process of crucial relevance for Higgs phenomenology at the LHC is the decay of a Higgs into two photons. The coupling receives contributions both from loops of fermions and vectors. Here we will neglect the effect of spin-1 resonances, whose contribution is typically suppressed since they need to be relatively heavy to comply with EWPT. Application of the LET leads to the following effective Lagrangian [87]

$$\mathcal{L}_{eff} = \frac{e^2}{16\pi^2} F_{\mu\nu} F^{\mu\nu} \Big(\sum_f Q_f^2 \log m_f^2(H) - \frac{7}{4} \log m_W^2(H) \Big) , \tag{4.11}$$

which is valid for $m_h \lesssim 2m_W, 2m_f$, and where we have assumed that the heavy fermions transform in the fundamental representation of $SU(3)_c$. Expanding around the VEV we obtain the $h\gamma\gamma$ interaction

$$\mathcal{L}_{h\gamma\gamma} = \frac{e^2}{8\pi^2} F_{\mu\nu}F^{\mu\nu} h \left(Q_t^2 A_1 - \frac{7}{8}\left(\frac{\partial}{\partial H}\log m_W^2(H)\right)_{\langle H\rangle}\right), \tag{4.12}$$

where we have assumed that all fermions have electric charge equal to that of the top quark[5], $Q_f = Q_t = 2/3$, and A_1 was defined in Eq. (4.6). By performing simple manipulations we obtain (see App. C)

$$\begin{aligned}\mathcal{L}_{h\gamma\gamma} = \frac{e^2}{32\pi^2} F_{\mu\nu}F^{\mu\nu}\frac{h}{v}\Bigg[4Q_t^2\Bigg(\left(\frac{\partial}{\partial \log H}\log|\det \mathcal{M}(H)|\right)_{H=v} - \frac{c_H}{2}\xi\Bigg) \\ - A_1(\tau_W)\left(1+\xi\left(\frac{c_r}{4}-\frac{c_H}{2}\right)\right)\Bigg],\end{aligned} \tag{4.13}$$

where $\tau_W \equiv m_h^2/(4m_W^2)$ and we have replaced the LET approximation for the W loop with the full result encoded by the function

$$A_1(\tau) = \frac{1}{\tau^2}\left[2\tau^2 + 3\tau + 3(2\tau-1)f(\tau)\right], \qquad f(\tau) = \arcsin^2\sqrt{\tau}, \tag{4.14}$$

which tends for $\tau \to 0$ to $A_1(0) = 7 = 22/3 - 1/3$, where the first term comes from the transverse polarizations of the W and is equal to the gauge contribution to the β function of the $SU(2)_L$ coupling, while the second term arises from the eaten Goldstone bosons. The use of the full expression for the W loop implies that the validity of Eq. (4.13) is extended to $m_h \lesssim 2m_f$, which is a reliable approximation. The rescaling of the decay width $\Gamma(h\to\gamma\gamma)/\Gamma(h\to\gamma\gamma)_{\rm SM}$ is obtained by comparing the square of the expression multiplying $hF^{\mu\nu}F_{\mu\nu}$ in Eq. (4.13) in the two cases. In terms of the parameters of the effective Lagrangian in Eqs. (3.6–3.7) the coupling reads

$$\mathcal{L}_{h\gamma\gamma} = \frac{e^2}{32\pi^2} F^{\mu\nu}F_{\mu\nu}\frac{h}{v}\Big(4Q_t^2 c + k_\gamma - aA_1(\tau_W)\Big). \tag{4.15}$$

4.2 Single Higgs production via gluon fusion

Let us now apply the general formula for the hgg coupling, Eq. (4.8), to our benchmark model MCHM$_5$: from the mass matrix in Eq. (2.55) we find

$$\det\mathcal{M} = \frac{\lambda_q\lambda_u M y f}{2\sqrt{2}}\sin\frac{2H}{f} \qquad \Longrightarrow \qquad \left(\frac{\partial}{\partial\log H}\log|\det\mathcal{M}(H)|\right)_{H=v} = 1 - \frac{4}{3}\xi \tag{4.16}$$

which together with $c_H = 1/3$ (see Table 3.1) leads to

$$\frac{\Gamma(h\to gg)}{\Gamma(h\to gg)_{\rm SM}} = 1 - 3\xi \qquad (\text{MCHM}_5). \tag{4.17}$$

[5]The extension to heavy states with different electric charge is straightforward.

Actually, because our construction of MCHM$_5$ does not contain heavy vectors or scalars [6], we can easily go further and obtain a result at all orders in ξ: since the Higgs is canonically normalized in the nonlinear σ-model (see Eq. (2.39)), we can directly apply Eq. (4.5). We find

$$\frac{\Gamma(h \to gg)}{\Gamma(h \to gg)_{\rm SM}} = \left(\frac{1-2\xi}{\sqrt{1-\xi}}\right)^2 , \tag{4.18}$$

where we used $\sin^2(\langle H \rangle / f) = \xi$. An important observation is that Eq. (4.17) does not depend on the details of the spectrum of the colored resonances which contribute to the coupling, *i.e.* it does not depend on the couplings and masses of composite states, but it is a simple function of only the overall scale of the strong sector f. This somewhat surprising insensitivity of the hgg coupling (computed in the LET approximation) to resonances has been shown to hold in several explicit realizations of the composite Higgs idea [33–35], including both models with partial compositeness and Little Higgs theories. As another example, in the Littlest Higgs model one finds

$$\frac{\Gamma(h \to gg)}{\Gamma(h \to gg)_{\rm SM}} = 1 - \frac{7}{4}\xi \qquad ({\rm LH}) , \tag{4.19}$$

where we included also the effect of heavy vectors and scalars on c_H .

Let us now focus on MCHM$_5$ and analyze how the result in Eq. (4.17) arises. It is important to note that while the hgg coupling is insensitive to resonances, the $ht\bar{t}$ coupling does receive a correction which depends on composite couplings, as a consequence of the mixing of the top with resonances. In the amplitude for hgg, however, the BSM contribution arising from such modification of the top Yukawa is exactly canceled by the loops of extra fermions, leading to a dependence of the $gg \to h$ rate only on ξ . This also implies that the cross section $\sigma(gg \to h)$ can be obtained by simply multiplying the SM one by c^2, where c is the rescaling of the $ht\bar{t}$ coupling coming only from the nonlinearity of the σ-model, and neglecting corrections due to fermionic resonances. To make this point more transparent, we can compute the value of the $ht\bar{t}$ coupling in MCHM$_5$,

$$c = \frac{g_{ht\bar{t}}}{g^{\rm SM}_{ht\bar{t}}} = \frac{v}{m_t}\left.\frac{\partial m_t(H)}{\partial H}\right|_{\langle H \rangle} = \frac{1}{\sqrt{1-\xi}}\left[1 - 2\xi + \xi(1-\xi)\left(\frac{1}{m_1^2} - \frac{1}{m_4^2}\right)\left(\lambda_u^2 - \frac{\lambda_q^2}{2}\right) + \mathcal{O}(\epsilon^4)\right] \tag{4.20}$$

as can be easily obtained from Eq. (2.45) by means of an expansion in ϵ. Eq. (4.20) makes manifest the two distinct corrections to the coupling that are in general expected: one following from the nonlinearity of the σ-model, and the other due to the mixing with resonances. As we already remarked, the latter contribution cancels exactly in hgg, leading to the expression in Eq. (4.17).

It is worth pausing to note that the insensitivity of the hgg coupling to heavy states is peculiar of composite Higgs models, and does not take place for example in SUSY, where there is a dependence on the stop masses. Let us consider for example the MSSM: working in the decoupling limit and neglecting stop mixing, the field-dependent stop mass matrix reads

$$\mathcal{M}_t^2(H) = \begin{pmatrix} m_{Q_3}^2 + m_t^2(H) & 0 \\ 0 & m_{U_3}^2 + m_t^2(H) \end{pmatrix} , \qquad m_t(H) = \frac{y_t \sin\beta}{\sqrt{2}} H , \tag{4.21}$$

[6] Additional scalars could be below the cutoff only if they were Goldstones, which is forbidden by construction by our choice of the coset $SO(5)/SO(4)$. Instead vector resonances should in general be included, we neglect them here for simplicity.

where we have also neglected the small D-term contributions to the diagonal entries. $m^2_{Q_3,U_3}$ are soft-SUSY breaking masses. Considering both the top and stop contributions in Eq. (4.4) and expanding around $\langle H\rangle = v$ we immediately obtain the hgg coupling

$$\mathcal{L}^{\rm MSSM}_{hgg} = \frac{g_s^2}{48\pi^2}\frac{h}{v}\left[1+\frac{1}{4}\left(\frac{m_t^2}{m^2_{\tilde{t}_L}}+\frac{m_t^2}{m^2_{\tilde{t}_R}}\right)\right] \tag{4.22}$$

with $m^2_{\tilde{t}_{L,R}} = m^2_{Q_3,\,U_3} + m_t^2$ the physical stop masses. We see that Eq. (4.22) depends on the masses of the heavy particles running in the loops. Notice [81] that the positive sign of the field-dependent terms in Eq. (4.21), and as a consequence of the BSM correction in Eq. (4.22), is fixed by the cancellation of the quadratic divergence in the Higgs mass, which requires the absence of the $\mathcal{O}(H^2)$ term in

$$\mathrm{STr}\,\mathcal{M}^\dagger\mathcal{M} = -2m_t^2(H) + \mathrm{Tr}\,\mathcal{M}_{\tilde{t}}^2(H)\,. \tag{4.23}$$

It is however important to mention that while Eq. (4.22) predicts an enhancement of the coupling, this is not necessarily the case in general, *i.e.* when stop mixing is considered. See Ref. [88] and references therein.

Let us now go back to a composite Higgs, and review how the cancellation of top partner effects arises. It is due to the fact that the determinant of the heavy fermion mass matrix takes the form

$$\det\mathcal{M}(H) \;=\; F(H/f)\times P(\lambda_i, M_i, f)\,, \tag{4.24}$$

where F is a function satisfying $F(0) = 0$ since the top becomes massless in the limit of unbroken electroweak symmetry, and P is a function of the composite couplings λ_i and masses M_i, but independent of H. It is then immediate to see that the hgg coupling in Eq. (4.8) does not depend on the masses and couplings of the fermionic resonances.[7] The origin of the factorization in Eq. (4.24) was explained in the context of partial compositeness in Ref. [35], by means of a spurion analysis: the key observation is that by promoting the linear mixings $\lambda_{q,u}$ to spurions, see Eq. (2.44), one can make the Lagrangian Eq. (2.41) formally $SO(5)$ invariant. In particular, the determinant of the fermion mass matrix will also be formally invariant. On the other hand, it is easy to read from Eq. (2.55) that the dependence of $\det\mathcal{M}$ on the mixings reads simply $\det\mathcal{M}\propto\lambda_q^*\lambda_u$. We thus conclude, based purely on symmetry arguments, that

$$\det\mathcal{M}\propto(\hat{\lambda}^\dagger_{t_L}\Sigma^T)(\Sigma\hat{\lambda}_{t_R}) = \frac{\lambda_q^*\lambda_u}{2\sqrt{2}}\sin\left(\frac{2H}{f}\right) \tag{4.25}$$

i.e. the mass matrix has the factorized form of Eq. (4.24). This result follows from the fact that when embedding the fermions in a **5**, there is only one $SO(5)$ invariant $\propto\lambda_q^*\lambda_u$ that can be built out of the spurions. In general, however, there can be more than one invariant: for example, assuming to mix both q_L and t_R with a **14** (symmetric traceless), $\hat{\lambda}_{t_L,t_R}\sim\mathbf{14}$, one finds two distinct structures and the determinant of the fermion mass matrix has the form

$$\det\mathcal{M} = (\Sigma\hat{\lambda}^\dagger_{t_L}\Sigma^T)(\Sigma\hat{\lambda}_{t_R}\Sigma^T)\times P_1(\lambda_i,M_i,f) + \Sigma\hat{\lambda}^\dagger_{t_L}\hat{\lambda}_{t_R}\Sigma^T\times P_2(\lambda_i,M_i,f) \tag{4.26}$$

where

$$(\Sigma\hat{\lambda}^\dagger_{t_L}\Sigma^T)(\Sigma\hat{\lambda}_{t_R}\Sigma^T) = \frac{\lambda_q^*\lambda_u}{2\sqrt{5}}s_Hc_H(4c_H^2-s_H^2)\,,\qquad \Sigma\hat{\lambda}^\dagger_{t_L}\hat{\lambda}_{t_R}\Sigma^T = \frac{3\lambda_q^*\lambda_u}{4\sqrt{5}}s_Hc_H\,. \tag{4.27}$$

In this case the hgg coupling will depend on the masses and couplings of resonances.

[7] The coefficient c_H does not receive contributions from the heavy fermion sector.

4.2.1 Corrections to the LET

Although exceptions such as MCHM$_{14}$ exist, in a wide class of models (including Little Higgses) the factorization in Eq. (4.24) takes place, and consequently the hgg vertex is insensitive to the composite couplings (collectively denoted by λ_i). This result, however, holds exactly only in the LET approximation, and corrections due to finite fermion mass effects are expected. We can estimate the residual dependence on the λ_i due to subleading terms in the fermion mass expansion in a simple way. Assuming for simplicity the presence of only one top partner T, the mass eigenvalues can be written at $\mathcal{O}(1/f^2)$ as

$$m_t(H) = \frac{y_t H}{\sqrt{2}}\left(1 - \frac{c_y^{(t)}}{2}\frac{H^2}{f^2}\right), \qquad m_T(H) = \lambda_T f\left(1 + a_T\frac{H^2}{f^2}\right), \tag{4.28}$$

where a_T is a parameter dependent on the couplings $\lambda_i = \{y_t, \lambda_T\}$ as $a_T = \mathcal{O}(y_t^2/\lambda_T^2)$.[8] On the other hand, we can write $c_y^{(t)} = c_y^{(\sigma)} + \mathcal{O}(y_t^2/\lambda_T^2)$, where $c_y^{(\sigma)}$ is a pure number arising from the nonlinearity of the σ-model. The LET result for the hgg coupling reads, taking the effect of c_H into account,

$$\mathcal{L}_{hgg} = \frac{g_s^2}{48\pi^2}G^a_{\mu\nu}G^{a\,\mu\nu}\frac{h}{v}\left(1 - \left(c_y^{(t)} - 2a_T + \frac{c_H}{2}\right)\xi\right). \tag{4.29}$$

Notice that in the limit where T is heavy, corresponding to large λ_T, the effects of the heavy resonance on the hgg coupling vanish. In fact, a_T goes to zero, whereas $c_y^{(t)} \to c_y^{(\sigma)}$, implying that only the nonlinearity in the top Yukawa arising from the σ-model is relevant.

By using the expression of the top Yukawa coupling $(m_t/v)(1 - (c_y^{(t)} + c_H/2)\xi)$ we can compute explicitly the top loop diagram, retaining the first subleading term in the $1/m_t^2$ expansion. This is the leading correction to the LET coupling, given that $m_T \gg m_t$. Thus Eq. (4.29) is improved to

$$\mathcal{L}_{hgg} = \frac{g_s^2}{48\pi^2}G^a_{\mu\nu}G^{a\,\mu\nu}\frac{h}{v}\left[1 - \left(c_y^{(t)} - 2a_T + \frac{c_H}{2}\right)\xi + \frac{7}{120}\frac{m_h^2}{m_t^2}\left(1 - \xi(c_y^{(t)} + c_H/2)\right) + \ldots\right], \tag{4.30}$$

where we have used $\hat{s} = m_h^2$ and the ellipses stand for subleading corrections, including terms of order $1/m_T^2$. The independence of the LET hgg vertex of the composite couplings λ_i is equivalent to the statement that $c_y^{(t)} - 2a_T$ is a pure number (independent of couplings), $c_y^{(t)} - 2a_T = c_y^{(\sigma)}$.[9] If this is the case then the dependence on the λ_i of Eq. (4.30) is due to the last term, and we can estimate the sensitivity of the cross section to the λ_i to be, for a light top partner $\lambda_T \sim y_t$,

$$\frac{\delta\sigma(gg \to h)}{\sigma(gg \to h)_{\rm SM}} \sim \frac{7}{60}\frac{m_h^2}{m_t^2}\,\xi \simeq 0.06\,\xi\,. \tag{4.31}$$

Thus corrections are expected to be very small even for large ξ.

[8] If the quadratic divergence in the Higgs mass due to the top is cancelled by T, then the absence of an $\mathcal{O}(H^2)$ term in $\mathrm{Tr}\,\mathcal{M}^2(H) = m_t^2(H) + m_T^2(H)$ implies $a_T = -y_t^2/(4\lambda_T^2)$. See for example the explicit values of $c_y^{(t)}$ and a_T in the Littlest Higgs model, reported in App. D, Eq. (D.18).

[9] Notice that by using Eq. (4.28) one finds $\det\mathcal{M}^2 = y_t^2\lambda_T^2 f^2 H^2(1 - (c_y^{(t)} - 2a_T)H^2/f^2)/2$. So if the factorization in Eq. (4.24) holds then $c_y^{(t)} - 2a_T$ is a pure number.

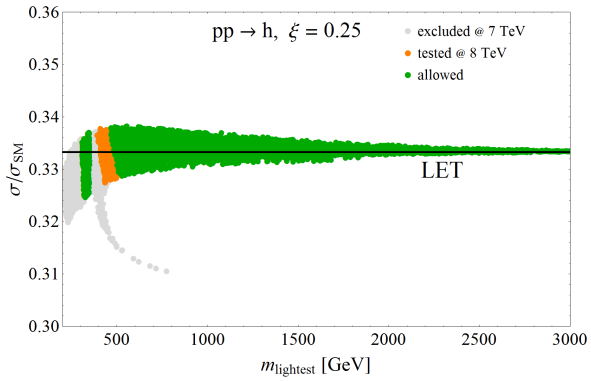

Figure 4.1: The MCHM$_5$ cross section for single Higgs production via gluon fusion (including the exact dependence on top and heavy fermion masses), normalized to the SM cross section computed retaining the m_t dependence, as a function of the mass of the lightest fermion resonance m_{lightest} . We set $m_h = 125\,\text{GeV}$ and $\xi = 0.25$. Green points are currently allowed by both EWPT and collider searches, gray points are excluded by current collider constraints, whereas orange points have been tested by LHC8 in 2012 (see Section 5.1 for details). For comparison, the cross section ratio computed with the LET, Eq. (4.18), is shown as a black line.

4.2.2 Comparison with exact cross section in MCHM$_5$

We will now check our estimate of the expected corrections to the LET, Eq. (4.31), by computing the full $pp \to h$ cross section (where we retain the dependence on the masses of the particles in the loop) in MCHM$_5$ and comparing it to the LET cross section.

Figure 4.1 shows the cross section for single Higgs production via gluon fusion including the fermionic resonances, normalized to the SM cross section computed with finite m_t, as a function of the mass of the lightest resonance[10]. The agreement with the prediction of the LET in Eq. (4.18), shown as a black line, confirms that the cross section is to an excellent approximation independent of the details of the spectrum, and is fixed only by ξ. The sensitivity to the composite couplings is at most $2\% \times \sigma_{SM}$ for light top partners, in agreement with our estimate in Eq. (4.31).

From our detailed analysis of MCHM$_5$, we thus conclude that the LET provides a very accurate single Higgs production cross section for any spectrum of the fermionic resonances, including the realistic case where at least one multiplet of top partners is light. The same conclusion applies also to the fermionic contribution to the $h\gamma\gamma$ coupling.

4.3 Double Higgs production via gluon fusion

Within the SM, double Higgs production via gluon fusion received interest mainly because it is sensitive to the trilinear Higgs self-coupling[11], see the first diagram in Fig. 4.2. In composite Higgs models, the process $gg \to hh$ is affected essentially in two main ways. Firstly, the

[10] Note that the QCD K-factors cancel out under the assumption that the higher order corrections are the same in both cases. This is exactly true only at NLO in QCD; however, it was found to hold within a few percent even at NNLO [91].

[11] See *e.g.* Ref. [92].

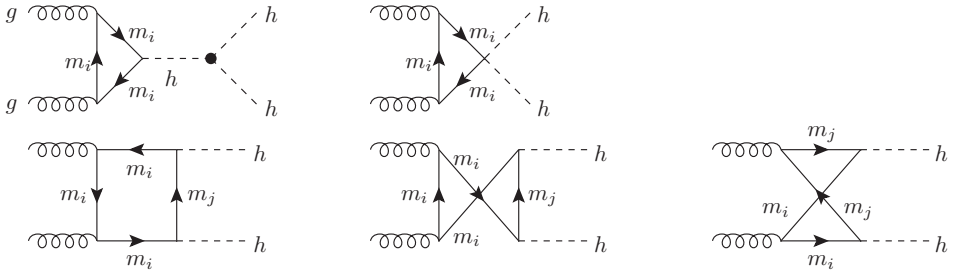

Figure 4.2: Generic diagrams contributing to double Higgs production via gluon fusion in composite Higgs models. The indices i, j run over the heavy fermions, including the top.

nonlinearity of the strong sector gives rise to a $f\bar{f}hh$ coupling (which vanishes in the SM) and thus to a genuinely new contribution to the amplitude, see the second diagram in Fig. 4.2. Secondly, one should take into account the effects of top partners, which include also new box diagrams involving off-diagonal Yukawa couplings (shown in the second line of Fig. 4.2). A first study of $gg \to hh$ in composite Higgs models, neglecting top partners, was performed in Ref. [38], where it was found that a large enhancement of the cross section is possible due to the new $t\bar{t}hh$ coupling. For example, in MCHM$_5$ with $\xi = 0.25$, which corresponds to $f \simeq 500\,\text{GeV}$, the cross section was found to be about 3.6 times larger than in the SM. Recently, Ref. [93] performed a model-independent study of the process, making reference to the effective Lagrangian in Eq. (3.6) and again neglecting the effects of top partners, and found a large sensitivity of the cross section to the c_2 coefficient parameterizing the $t\bar{t}hh$ coupling.

In Ref. [3] we included for the first time the effects of top partners in double Higgs production via gluon fusion. This is especially interesting in the light of the correlation between a light Higgs and light top partners, since the latter can in principle affect the $gg \to hh$ cross section in a sizeable way. Our analysis will confirm that this is indeed the case.

We start by discussing the cross section in the LET approximation, which greatly simplifies the computation and allows us to obtain a general result, applicable to any model via the matching to the coefficients of the SILH or chiral Lagrangian. In the LET limit, the amplitude for $gg \to hh$ is simply the sum of two diagrams, one with the effective hgg coupling followed by a trilinear Higgs coupling and the other involving the effective $hhgg$ coupling. Adopting the SILH formalism, and recalling the expressions of the relevant Feynman rules

$$\begin{aligned}
hgg \quad &: i\,\tfrac{\alpha_s}{3\pi v}\delta^{AB}(p_1^\nu p_2^\mu - p_1\cdot p_2\, g^{\mu\nu})\left[\left(\tfrac{\partial}{\partial \log H}\log|\det \mathcal{M}(H)|\right)_{H=v} - \tfrac{c_H}{2}\xi\right], \\
hhgg \quad &: i\,\tfrac{\alpha_s}{3\pi v^2}\delta^{AB}(p_1^\nu p_2^\mu - p_1\cdot p_2\, g^{\mu\nu})\left[\left(\left(\tfrac{\partial^2}{\partial(\log H)^2} - \tfrac{\partial}{\partial \log H}\right)\log|\det \mathcal{M}(H)|\right)_{H=v} - \tfrac{c_r}{4}\xi\right], \\
hhh \quad &: -i\,3\tfrac{m_h^2}{v}\left[1 + \xi\left(c_6 - \tfrac{3}{2}c_H - \tfrac{1}{4}c_r\right)\right]
\end{aligned} \tag{4.32}$$

(where $p_{1,2}$ denote the momenta of the incoming gluons), we can write the amplitude as

$$\mathcal{A}_{\text{LET}}\,(gg \to hh) = \frac{\alpha_s}{3\pi v^2}\delta^{AB}(p_1^\nu p_2^\mu - p_1\cdot p_2\, g^{\mu\nu})\, C_{\text{LET}}(\hat{s})\,, \tag{4.33}$$

where

$$C_{\rm LET}(\hat{s}) = \frac{3m_h^2}{\hat{s}-m_h^2}\left[\left(\frac{\partial}{\partial \log H}\log|\det \mathcal{M}(H)|\right)_{H=v} + \xi\,(c_6 - 2c_H - \frac{c_r}{4})\right] \\ + \left(\left(\frac{\partial^2}{\partial(\log H)^2} - \frac{\partial}{\partial \log H}\right)\log|\det \mathcal{M}(H)|\right)_{H=v} - \frac{c_r}{4}\xi \qquad (4.34) \\ = \frac{3m_h^2}{\hat{s}-m_h^2}\left(1 - \xi(c_y^{(t)} - c_6 + 2c_H + \frac{c_r}{4} - 3c_g\frac{y_t^2}{g_\rho^2})\right) - \left(1 + \xi(c_y^{(t)} + \frac{c_r}{4} - 3c_g\frac{y_t^2}{g_\rho^2})\right)\,,$$

with $\hat{s} \equiv (p_1+p_2)^2$ denoting the partonic center-of-mass (c.m.) energy. To obtain the second equality in Eq. (4.34) we used Eqs. (C.3) and (C.4) contained in App. C. It is immediate to check that the combinations $c_y^{(t)} - c_6 + 2c_H + c_r/4$ and $c_y^{(t)} + c_r/4$ are invariant under the reparameterization in Eq. (3.27). For completeness, we also give the result in terms of the coefficients of the chiral Lagrangian in Eq. (3.6):

$$C_{\rm LET}(\hat{s}) = \frac{3m_h^2}{\hat{s}-m_h^2}\,(c+k_g)\,d_3 + 2c_2 - c^2 + k_{2g}\,. \qquad (4.35)$$

The partonic cross section reads

$$\hat{\sigma}_{gg\to hh}(\hat{s},\mu) = \frac{G_F^2\alpha_s^2(\mu)\hat{s}}{128(2\pi)^3}\,\frac{1}{9}\sqrt{1-\frac{4m_h^2}{\hat{s}}}\,C_{\rm LET}^2(\hat{s})\,. \qquad (4.36)$$

The hadronic cross section is obtained by convolution with the parton distribution function $f_{g/P}$ of the gluon in the proton,

$$\sigma = \int_{4m_h^2/s}^1 d\tau \int_\tau^1 \frac{dx}{x} f_{g/P}(x,Q)\,f_{g/P}(\tau/x,Q)\,\hat{\sigma}_{gg\to hh}(\tau s,\mu)\,, \qquad (4.37)$$

with the collider c.m. energy s related to $\hat{s}$ by $\hat{s} = \tau s$. The renormalization scale μ and the factorization scale Q are chosen equal to the invariant mass of the Higgs boson pair, $\mu = Q = \sqrt{\hat{s}}$. The parton distribution functions of MSTW2008 [94] are employed. For $\xi \to 0$, Eq. (4.34) correctly reproduces the SM result in the limit of large top mass [95, 96]

$$C_{\rm LET}^{\rm SM}(\hat{s}) = \frac{3m_h^2}{\hat{s}-m_h^2} - 1\,. \qquad (4.38)$$

In the SM the $m_t \to \infty$ limit gives a total cross section in agreement with the full result only within 20% for $m_h \lesssim 200\,\text{GeV}$ (for $m_h = 125\,\text{GeV}$ we find $\sigma_{\rm LET}^{SM} = 14.6\,\text{fb}$ and $\sigma_{\rm full}^{SM} = 17.9\,\text{fb}$) and moreover it produces incorrect kinematic distributions, as noticed in Ref. [97]. Thus we expect the LET to be in general less accurate in $gg \to hh$ than in single Higgs production.

From Eq. (4.34) we read that in models where the factorization of $\det\mathcal{M}$ in Eq. (4.24) holds, the $gg \to hh$ LET cross section is insensitive to composite couplings, due to a cancellation completely analogous to the one that we discussed for single Higgs production. Let us consider our benchmark model, MCHM_5: using the determinant of the fermion mass matrix in Eq. (4.16) and the expressions of the SILH coefficients reported in Table 3.1 we arrive to the result

$$C_{\rm LET}^{\rm MCHM_5}(\hat{s}) = \frac{3m_h^2}{\hat{s}-m_h^2}\,(1-3\xi) - 1 - \xi\,, \qquad (4.39)$$

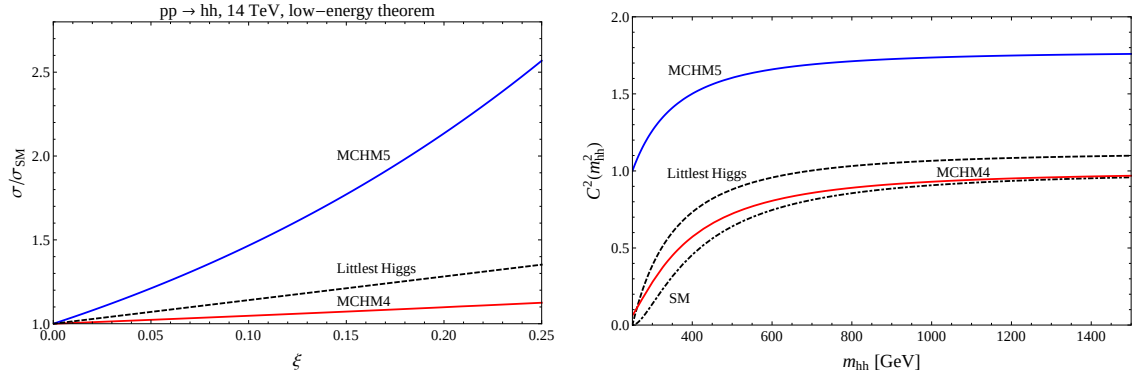

Figure 4.3: (*Left panel*) The $pp \to hh$ cross section for $m_h = 125$ GeV at LHC14, computed using the LET, normalized to the SM cross section also computed in the $m_t \to \infty$ limit. MHCM$_5$ is discussed in detail in the text, whereas the $gg \to hh$ amplitude for the Littlest Higgs model is given in App. D. (*Right panel*) Square of the function $C(m_{hh}^2)$, which was defined in Eq. (4.34) and is proportional to the LET $gg \to hh$ amplitude, in the three models under consideration (for $\xi = 0.25$) and in the SM, as a function of $m_{hh} = \sqrt{\hat{s}}$.

which depends only on ξ as a consequence of the factorization of $\det \mathcal{M}$. In the left panel of Fig. 4.3 we show for $m_h = 125$ GeV and a c.m. energy of 14 TeV the $pp \to hh$ cross section normalized to the SM cross section (both were computed applying the LET) as a function of ξ for some well-known models, in all of which the factorization holds. We note that in MCHM$_5$ the enhancement of the cross section is striking. This can be traced back to the behavior of the function $C_{\rm LET}(\hat{s})$, which is proportional to the LET amplitude and is shown in the right panel of Fig. 4.3 for the three models under consideration and for the SM. The enhancement for MCHM$_5$ is evident. As pointed out for the first time in Ref. [38], where the $gg \to hh$ process was studied in MCHM$_5$ considering only Higgs nonlinearities but keeping the full dependence on m_t, the dramatic increase of the $gg \to hh$ cross section compared to the SM is mostly due to the presence of a new $t\bar{t}hh$ coupling. The large enhancement of $gg \to hh$ in MCHM$_5$ is in contrast with the sizable suppression in the same model of the single Higgs production cross section, see Eq. (4.17).

By comparison with Ref. [38] we find that when fermionic resonances are above the cutoff, the LET underestimates the ratio $\sigma^{\rm MCHM_5}/\sigma^{\rm SM}$ by about 30%: for example for $\xi = 0.25$, application of the LET gives a cross section of 2.6 times the SM, whereas Ref. [38] found an enhancement factor of 3.6. This difference is due to the fact that in the former case $m_h \ll m_t$ is assumed, whereas in the latter the full m_t dependence was retained. Notice that the best estimate of the cross section that can be obtained using the LET is $\sigma^{\rm MCHM_5} = (\sigma^{\rm MCHM_5}_{\rm LET}/\sigma^{\rm SM}_{\rm LET}) \times \sigma^{\rm SM}_{full}$, because part of the corrections due to the finite top mass should cancel in the ratio of LET cross sections. In fact, in terms of cross sections the disagreement between the LET and the result obtained taking into account only Higgs nonlinearities is larger. For $\xi = 0.25$ we obtain $\sigma^{\rm MCHM_5}_{\rm LET} = 37\,{\rm fb}$, whereas Ref. [38] found $\sigma^{\rm MCHM_5} = 64\,{\rm fb}$, *i.e.* the difference is of order 50%.

4.3.1 Comparison with exact cross section in MCHM$_5$

In the LET approximation, the cross section for $gg \to hh$ in MCHM$_5$ depends only on ξ, see Eq. (4.39). However, as already mentioned, corrections from finite mass effects are

expected to be sizable in double Higgs production. This motivated a full computation of the $gg \to hh$ cross section in MCHM$_5$, including resonances, which was presented in Ref. [3]. We summarize here the main results, referring the reader to that work for the details. We remark that while we focused on MCHM$_5$ as a concrete example, the results of Ref. [3] can be straightforwardly applied to other models.

In the triangle diagrams which contribute to double Higgs production, the gluons couple to the total spin $S_z = 0$ along the z-axis, whereas the box diagrams involve $S_z = 0$ and $S_z = 2$ couplings. The amplitude for the process can hence be expressed in terms of independent form factors $F_\triangle$, $F_\square$, $F_{\square,5}$ associated with spin 0 and $G_\square$, $G_{\square,5}$ associated with spin 2. The total partonic cross section is given by

$$\hat{\sigma}_{gg\to hh}(\hat{s},\mu) = \frac{\alpha_s^2(\mu)}{1024(2\pi)^3}\frac{1}{\hat{s}^2}\int_{\hat{t}_-}^{\hat{t}_+} d\hat{t}\left[\left|\sum_{i=1}^{4}\sum_{j=1}^{4}\left(g^2_{h\bar{q}_i q_j}G_\square(m_i,m_j) + g^2_{h\bar{q}_i q_j,5}G_{\square,5}(m_i,m_j)\right)\right|^2 + \left|\sum_{i=1}^{4}\left(C_{i,\triangle}F_\triangle(m_i) + \sum_{j=1}^{4}\left(g^2_{h\bar{q}_i q_j}F_\square(m_i,m_j) + g^2_{h\bar{q}_i q_j,5}F_{\square,5}(m_i,m_j)\right)\right)\right|^2\right], \tag{4.40}$$

with the integration limits

$$\hat{t}_\pm = -\frac{\hat{s}}{2}\left(1 - 2\frac{m_h^2}{\hat{s}} \mp \sqrt{1 - \frac{4m_h^2}{\hat{s}}}\right), \tag{4.41}$$

where $\hat{s}$ denotes the partonic c.m. energy. The triangle and box form factors are given in App. E of Ref. [3]. The various couplings appearing in Eq. (4.40) are also defined there. We have explicitely verified that in the SM limit our result agrees with Ref. [96]. The hadronic cross section is obtained by convolution with the parton distribution function of the gluon in the proton, see Eq. (4.37).

In Fig. 4.4 we show the double Higgs production cross section (normalized to the SM) as a function of the lightest top partner mass, for a set of points passing EWPT with $\xi = 0.25$ (see Section 5.1 for details). The dependence on the masses of the loop particles has been fully taken into account. The black solid line shows the result in the limit of heavy partners, keeping only the top contribution (with full mass dependence) in the loop, while the black dashed line corresponds to the LET result in Fig. 4.3.

Some comments are in order. First of all, we find a sizeable dependence of the cross section on the spectrum of the heavy fermions with $2.7 \lesssim \sigma/\sigma_{SM} \lesssim 3.7$. We recall that both the LET cross section and the cross section in the limit of heavy partners only depend on ξ. The LET approximation, however, underestimates the ratio σ/σ_{SM}, and this effect is even worse if we refer directly to the cross section, since we are consistently normalizing the LET cross section for MCHM5 to $\sigma_{SM}(m_t \to \infty)$, which is $\sim 20\%$ smaller than the full result. On the other hand, the result obtained in the limit of heavy partners, while keeping the full top mass dependence [38], overestimates the cross section in the region $m_{\text{lightest}} \lesssim 1\,\text{TeV}$. The latter is the region compatible with the 125 GeV Higgs, see Eq. (2.66). For large values of the resonance masses, of course, the cross section tends to the value obtained including only top loops (with top couplings following the 'trigonometric' rescalings given in Table 3.1).

It should be noted that we have not taken into account higher-order QCD corrections. They have been calculated at NLO for SM and MSSM Higgs pair production in Ref. [98] in

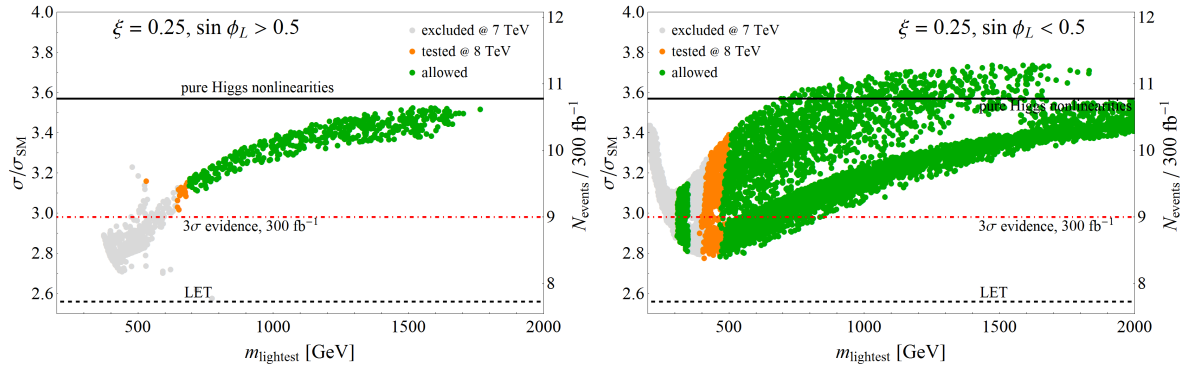

Figure 4.4: The cross section for double Higgs production through gluon fusion normalized to the SM as function of the mass of the lightest resonance of the heavy top sector, for $m_h = 125$ GeV. We have set $\xi = 0.25$. Green (gray) dots denote points which pass (do not pass) all current constraints, whereas orange dots correspond to points that have been tested by LHC8, see Sec. 5.1 for details. The left panel shows points for which $X_{2/3}$ is the lightest top partner (as a consequence of t_L being largely composite), whereas for points in the right panel the lightest top partner is typically the singlet $\tilde{T}$. The black solid (dashed) line corresponds to the result in the limit of heavy top partners keeping the full top mass dependence (to the LET result as in Fig. 4.3). The expected number of events in the $hh \to b\bar{b}\gamma\gamma$ final state after all cuts at LHC14 with $L = 300\,\text{fb}^{-1}$ is also shown, along with the 3σ evidence threshold (dot-dashed line), see text for details.

the heavy top mass limit. However, they cannot be taken over here as we have the additional diagram with the two-Higgs two-fermion coupling and more seriously box diagrams with different loop particle masses. For heavy loop particle masses we do not expect the corrections to be too different from the SM case, so that they approximately cancel out in the ratio of the two cross sections.

In Fig. 4.5 we show results for a lower value of $\xi = 0.1$, which corresponds to $f \simeq 800\,\text{GeV}$. Due to the larger value of f, the cross section is less enhanced compared to the SM. Similarly to the case $\xi = 0.25$ the LET underestimates the cross section, although in a milder way than in the previous case.

4.3.2 LHC prospects on double Higgs production

To estimate the reach of the 14 TeV run of the LHC on double Higgs production, we focus on the final state $hh \to b\bar{b}\gamma\gamma$, which was shown to be the most promising for a light Higgs boson [97, 99–101]. Reference [101] found that assuming a luminosity $L = 600\,\text{fb}^{-1}$, 6 signal events could be obtained after all cuts, with a background of 11 events. We estimate the expected number of signal events for MCHM$_5$ by computing $\sigma(pp \to hh) \times \text{BR}(hh \to b\bar{b}\gamma\gamma)$ for each point in the parameter space (taking into account the QCD production K-factor[12] of 1.9 and the non-standard Higgs branching ratios) and multiplying it times the acceptance for all

[12] As stated above the SM QCD corrections to double Higgs production cannot be translated trivially to the composite Higgs case. Assuming the top partners to be heavy we expect, however, the error not to be too large by applying the SM K-factor to MCHM$_5$ double Higgs production. Concerning the diagram involving the two-Higgs two-fermion coupling we explicitly verified that it hardly changes the QCD corrections compared to the SM ones.

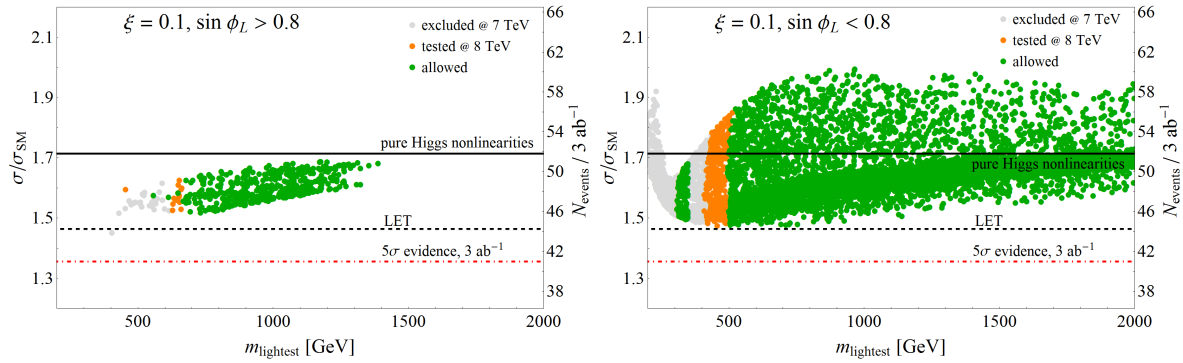

Figure 4.5: Cross section for double Higgs production via gluon fusion normalized to the SM as function of the mass of the lightest resonance of the heavy top sector, for $\xi = 0.1$ and $m_h = 125$ GeV. Points are split in the two panels depending on the degree of compositeness of t_L. The meaning of the dots and lines is the same as in Fig. 4.4, except that we assumed an integrated luminosity $L = 3\,\text{ab}^{-1}$ at LHC14. The dot-dashed line corresponds to the 5σ discovery threshold, see text for details.

cuts as computed in Ref. [101] for the SM. This rough approximation cannot of course replace a full analysis of the effects of cuts in the MCHM$_5$ case, which however goes beyond the scope of our analysis. We therefore apply the simplified procedure for an illustratory purpose. We also quote the number of events needed for $3\,(5)\sigma$ evidence with $L = 300\,(3000)\,\text{fb}^{-1}$, based on the background estimate of Ref. [101] with the requirement of one b-tagged jet. Notice that this is likely conservative, because the analysis of reducible backgrounds (whose sum is larger than the irreducible $b\bar{b}\gamma\gamma$) performed in Ref. [101] made use of efficiencies and misidentification probabilities, in particular for b-jets, that have since then been improved by ATLAS and CMS. We find that a 3σ excess can be obtained already with $300\,\text{fb}^{-1}$ if $\xi = 0.25$, except perhaps in some regions of the parameter space with a very light top partner (in this case, however, a direct observation of the resonance would be guaranteed). A 5σ discovery would be possible at the LHC luminosity upgrade for a more moderate value $\xi = 0.1$.

We note that in Ref. [93] two b-tagged jets were required, and the efficiency and rejection probabilities for b-tagging were updated to current values. However, since we are only interested in a rough estimate of the LHC reach, we conservatively adopt the numbers of Ref. [101]. Furthermore, a realistic analysis of the instrumental backgrounds relevant to $b\bar{b}\gamma\gamma$ would require a detailed knowledge of the detector properties, which is out of the reach of a theoretical analysis. Recently, the LHC prospects for detecting double Higgs production have been explored or re-analyzed in a variety of channels, partly due to the results of studies in the context of composite Higgs models which, as we discussed, found the cross section to be potentially enhanced compared to the SM. See for example Ref. [102] for a study of the $b\bar{b}\tau\tau$ final state, Ref. [103] for an analysis of the $b\bar{b}WW \to b\bar{b}\ell\nu jj$ channel, and Ref. [104] for the $4b$ final state. See also Ref. [105] for a recent study of Higgs pair production in several new physics models.

Additionally, we studied if applying a cut on the invariant mass m_{hh} could be useful to measure deviations from the SM cross section. Therefore, in Fig. 4.6 we show the same as Fig. 4.4 but after an invariant mass cut of $m_{hh} \geq 600$ GeV has been applied. As can be inferred from the plot the composite cross section is more enhanced compared to the SM than without application of a cut, see also Fig. 4.4. On the other hand the absolute

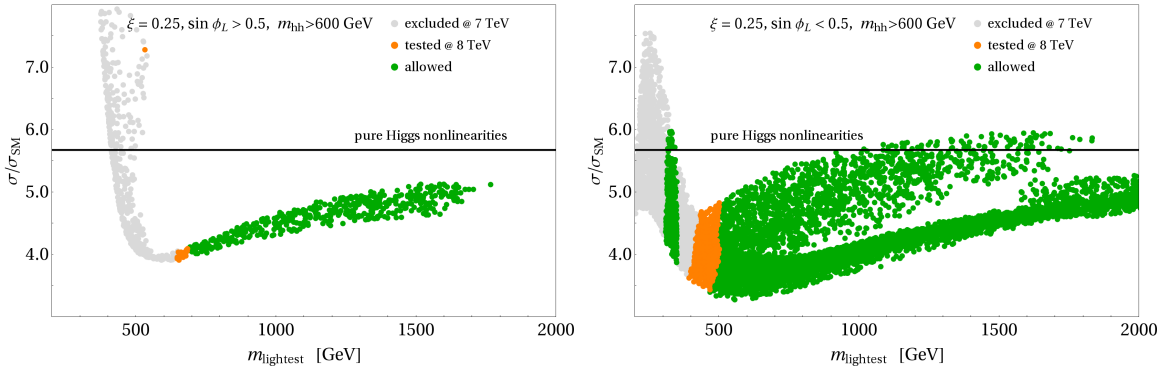

Figure 4.6: The cross section for double Higgs production through gluon fusion after an invariant mass cut $m_{hh} \geq 600\,\text{GeV}$, normalized to the SM for $m_h = 125$ GeV, as function of the mass of the lightest resonance of the heavy top sector. The compositeness parameter has been set to $\xi = 0.25$. Green/dark gray (gray) dots denote points which pass (do not pass) all current constraints, whereas orange/fair gray dots correspond to points that have been tested by LHC8. The left panel shows points for which $X_{2/3}$ is the lightest top partner, whereas for the points in the right panel the lightest top partner is typically the singlet $\tilde{T}$. The black solid line corresponds to the result obtained considering only Higgs nonlinearities, *i.e.* in the limit of heavy top partners and keeping the full top mass dependence.

value of the cross section after cuts becomes very small. The plots reveal, however, another interesting feature. While for masses of the lightest top partner above 2 TeV the total cross section is reasonably well approximated by the cross section where only Higgs nonlinearities are considered, see Fig. 4.4, this is not the case any more after application of cuts. This can be inferred from Fig. 4.6 by comparing the full result, given by the points, to the black line, which is the ratio of the double Higgs production cross section considering only Higgs nonlinearities to the SM cross section (the full top dependence has been included in both cases). So we conclude that not only the heavy top partner limit in the total cross section of double Higgs production is a rather bad approximation unless the top partners are really heavy, but this approximation becomes even worse when a cut on m_{hh} is applied. The latter, however, may be relevant in the experimental analyses to enhance the signal to background ratio and to extract information on the couplings involved in the process.

4.4 Probing the sign of the $ht\bar{t}$ coupling at the LHC

As we discussed in the Foreword, current Higgs data leave open the possibility that the $ht\bar{t}$ coupling has negative sign[13]. Assuming a universal rescaling c_F of the $h\bar{f}f$ couplings, this corresponds to $c_F < 0$. The exact degeneracy under $c_F \to -c_F$ is broken mainly by the $h\gamma\gamma$ coupling, where the top and W loops interfere. Let us first analyze [106] how a degeneracy arises in the $h \to \gamma\gamma$ channel alone: recalling that

$$\frac{\Gamma(h \to \gamma\gamma)}{\Gamma(h \to \gamma\gamma)_{\text{SM}}} \simeq (1.26\, c_V - 0.26\, c_F)^2\,, \tag{4.42}$$

[13]The sign of the $ht\bar{t}$ coupling is not physical by itself, but the relative sign compared to the Higgs coupling to gauge bosons (we take the latter to be positive) is physical.

(c_V denotes the rescaling of the hWW and hZZ couplings, and is simply a different name for the parameter a in Eq. (3.6)) we have for inclusive, VBF and associated production

$$\mu_{incl} \sim (1.26\, c_V - 0.26\, c_F)^2\,, \qquad \mu_{VBF} \sim \mu_{Vh} \sim c_V^2\, \frac{(1.26\, c_V - 0.26\, c_F)^2}{c_F^2}\,. \tag{4.43}$$

Assuming a 'true' signal (c_V^t, c_F^t), it is easy to show that in addition to $(c_V, c_F) = (c_V^t, c_F^t)$ there is another point giving the same event yields, which will therefore also be a local maximum of the experimental likelihood. The coordinates of the second solution are given by

$$c_V = c_V^t \left|\frac{1.26\, c_V^t - 0.26\, c_F^t}{1.26\, c_V^t + 0.26\, c_F^t}\right|\,, \qquad c_F = -c_F^t \left|\frac{1.26\, c_V^t - 0.26\, c_F^t}{1.26\, c_V^t + 0.26\, c_F^t}\right|\,. \tag{4.44}$$

Assuming the SM to be the true signal, we find for this second solution $(c_V, c_F) \simeq (0.66, -0.66)$. Looking at the plots in Fig. 2, where the ATLAS and CMS likelihoods (including all Higgs decay channels) are shown, we see that the minima with negative c_F are not located exactly at this point: this is of course a consequence of the combination of all channels. Nevertheless, the preferred regions with negative c_F are indeed located at a smaller c_V compared to the preferred regions with positive c_F, as our simple analysis of $\gamma\gamma$ alone suggested.

How can the degeneracy in the sign of the $ht\bar{t}$ coupling be lifted? The authors of Ref. [106] proposed to combine the two most precise channels, $\gamma\gamma$ and ZZ^*, the latter being sensitive essentially only to $|c_V|$. However, they found that assuming the SM to be the true signal, the data collected by ATLAS and CMS together in Run 1 of the LHC will not be sufficient to exclude the hypothesis $c_F < 0$. Reference [107] also reached the conclusion that the degeneracy cannot be completely lifted by Higgs fits in 'standard' channels alone. On the other hand, one may argue that the current results by CMS already strongly disfavor the 'wrong sign' solution. We note, however, that this is due to $\mu_{\gamma\gamma}^{\rm CMS} = 0.8 < 1$, while if the signal strength were close to 1 (*i.e.*, only very slightly higher, well within the 1σ experimental uncertainty), the CMS plot would look different, and the conclusions of Ref. [106] would apply. In other words, Higgs fits that consider 'standard' channels show a sizable dependence on statistical fluctuations, which does not allow us to draw a robust conclusion about the fate of the $c_F < 0$ region. It would be therefore desirable to find a measurement that can lift the degeneracy in a direct and robust way. In Ref. [4], whose findings are reported below, we argued that the associated production of single top and Higgs, $pp \to thj$, is suitable for this purpose.

Before discussing the proposed solution for the degeneracy in the sign of c_F, it is worth mentioning how a negative $ht\bar{t}$ coupling can arise: adding to the SM the operator

$$\frac{c_y y_t}{\Lambda^2} H^\dagger H \bar{q}_L \widetilde{H} t_R + \text{h.c.}\,, \tag{4.45}$$

we find

$$\mathcal{L} = -m_t \bar{t}t - \frac{m_t}{v}\left(1 - c_y \frac{v^2}{\Lambda^2}\right) ht\bar{t} \quad \Longrightarrow \quad c_t = 1 - c_y \frac{v^2}{\Lambda^2}\,, \tag{4.46}$$

which implies that for $\mathcal{O}(1)$ values of c_y, a negative c_t requires the scale suppressing the dimension-6 operator to be $\Lambda \approx v$. While this is a very low scale, we remark that no bound from EWPT exists on the operator in Eq. (4.45), as already mentioned. Actually, we have already encountered a model where a negative c_t arises: this is the case in MCHM$_5$ for $\xi > 0.5$ ($f \lesssim 350\,\text{GeV}$), see Table 3.1. A minimal composite Higgs model with such low f is certainly ruled out, being in conflict with the measured values of other observables (notably

the S parameter), which suggests that building a viable model where $c_t < 0$ would be very challenging. However, current experimental data alone do not forbid this possibility, and it is therefore relevant to devise a strategy to rule out directly the 'wrong sign' option.

The leading process involving the Higgs coupling to real top quarks is $t\bar{t}h$ production, see for example Ref. [43] for a study in the BSM context. However, this process can be simply seen as QCD $t\bar{t}$ production with emission of a Higgs from one of the top legs, therefore we have

$$\sigma(pp \to t\bar{t}h) = c_t^2\, \sigma(pp \to t\bar{t}h)_{\rm SM}\,, \tag{4.47}$$

which holds also at NLO in QCD. Therefore top pair production in association with a Higgs is not sensitive to the *sign* of the $ht\bar{t}$ coupling. In Ref. [4] we argued that, even though subleading, Higgs boson production in association with a single top quark can also bring valuable information, in particular regarding the sign of the Higgs coupling to the top quark. This is because an almost totally destructive interference between two large contributions, one where the Higgs couples to a space-like W boson and the other where it couples to the top, takes place in the SM. This fact can be exploited to probe deviations in the Higgs coupling structure, which will inevitably jeopardize perturbative unitarity at high energy and lead to a striking enhancement of the cross section compared to the SM. We discuss below how this enhancement can be used to extract information on the sign of the $ht\bar{t}$ coupling, and show that th production can be used to lift the degeneracy plaguing the Higgs coupling fit of the LHC data. While a moderate integrated luminosity at 14 TeV should allow us to make a conclusive statement, we point out that already with the full Run 1 luminosity, corresponding to $\sim 25\,\text{fb}^{-1}$ per experiment, an interesting sensitivity on the sign of the $ht\bar{t}$ coupling could be reached.

In our study we focused on the decay of the Higgs into $b\bar{b}$, updating the early analysis of Ref. [108] (see also Refs. [109, 110]). This choice leads to an experimental signature (lepton + missing energy + multijets, among which ≥ 3 are b-jets) which is very similar to the one ATLAS and CMS have already analyzed in their searches for $t\bar{t}h$ production [39, 111]. In this respect we believe that the experimental collaborations could easily perform the analysis we present here in the very near future, thus adding new important information to the challenge of identifying the true nature of the recently discovered particle.

The large enhancement of the th cross section for nonstandard Higgs couplings is associated to the growth of the scattering amplitude at high energy, which in turn implies that perturbative unitarity is lost at some UV scale Λ. We estimate Λ, which acts as the cutoff of our effective theory, to be at least of $\mathcal{O}(10)$ TeV and thus above the energy scales that the LHC will be able to probe. In fact, the th invariant mass distribution in LHC collisions essentially vanishes above 1 TeV, therefore we can safely conclude that our analysis remains insensitive to UV physics above the cutoff scale.

4.5 Single top and Higgs production at the LHC

In this section we summarize the main findings of Ref. [4], to which the reader is referred for additional details.

4.5.1 The hard-scattering process

The Feynman diagrams contributing to the core process $Wb \to th$ are shown in Fig. 4.7. The diagram where the Higgs is emitted from a b leg is suppressed by the bottom Yukawa,

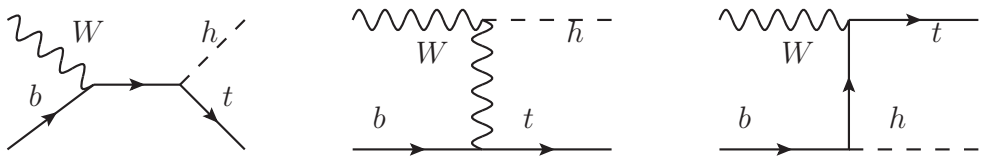

Figure 4.7: Feynman diagrams contributing to the partonic process $Wb \to th$.

and will be consistently neglected in our study. In the th production process at the LHC the initial W is radiated from a quark in the proton, and is thus spacelike. However, at high energy the effective W approximation [112] holds, which allows us to factorize the process into the emission of an approximately on-shell W from the quark times its hard scattering with a bottom. Thus it makes sense to discuss the amplitude for $Wb \to th$ at high energies assuming the initial W to be on-shell, in order to gain an approximate understanding of the full picture.

In the high-energy, hard-scattering regime, where $s, -t, -u \gg m_t^2, m_W^2, m_h^2$, the amplitude for $W_L b \to th$ (the longitudinal polarization dominates at large s) reads[14]

$$\mathcal{A} = \frac{g}{\sqrt{2}}\left[(c_F - c_V)\frac{m_t\sqrt{s}}{m_W v}\,A\left(\frac{t}{s},\varphi;\xi_t,\xi_b\right) + \left(c_V\,\frac{2m_W}{v}\frac{s}{t} + (2c_F - c_V)\,\frac{m_t^2}{m_W v}\right)\,B\left(\frac{t}{s},\varphi;\xi_t,\xi_b\right)\right], \tag{4.48}$$

where we have omitted terms that vanish in the high-energy limit and, for simplicity, also neglected the Higgs mass in addition to setting $m_b = 0$. The functions A, B are given by

$$A\left(t/s,\varphi;\xi_t,\xi_b\right) = \xi_t^\dagger \begin{pmatrix} -t/s & 0 \\ -e^{i\varphi}\sqrt{-\frac{t}{s}\left(1+\frac{t}{s}\right)} & 0 \end{pmatrix} \xi_b \quad \longrightarrow \quad \begin{pmatrix} 0 & 0 \\ -e^{i\varphi}\sqrt{-t/s} & 0 \end{pmatrix}, \tag{4.49}$$

$$B\left(t/s,\varphi;\xi_t,\xi_b\right) = \xi_t^\dagger \begin{pmatrix} 1+t/s & 0 \\ e^{i\varphi}\sqrt{-\frac{t}{s}\left(1+\frac{t}{s}\right)} & 0 \end{pmatrix} \xi_b \quad \longrightarrow \quad \begin{pmatrix} e^{i\varphi}\sqrt{1+t/s} & 0 \\ 0 & 0 \end{pmatrix}, \tag{4.50}$$

where in the rightmost term of each line we have chosen a specific basis for the spinors, namely

$$\xi_b^L = \begin{pmatrix} 1 \\ 0 \end{pmatrix}, \quad \xi_b^R = \begin{pmatrix} 0 \\ 1 \end{pmatrix}; \qquad \xi_t^L = \begin{pmatrix} e^{-i\varphi}\sqrt{1+t/s} \\ \sqrt{-t/s} \end{pmatrix}, \quad \xi_t^R = \begin{pmatrix} -e^{-i\varphi}\sqrt{-t/s} \\ \sqrt{1+t/s} \end{pmatrix}, \tag{4.51}$$

which correspond to the chiral states $\{F_L, F_R\}$ $(F = b, t)$ in the $m_F \to 0$ limit[15]. The amplitudes involving the helicity state ξ_b^R, which is identified with a right-handed bottom since we are assuming $m_b = 0$, exactly vanish due to the $V - A$ structure of the couplings of the W to fermions. From Eq. (4.48) we see that when $c_V \neq c_F$ the amplitude grows with energy like $\sqrt{s}$ and is enhanced compared to the case $c_V = c_F$ (which includes the SM), where the amplitude is constant in the large s limit. The non-cancellation of the terms in the amplitude growing with energy is at the origin of the striking enhancement of the cross section when $c_V \neq c_F$.

[14] We take final momenta outgoing, and define $s = (p_W + p_b)^2$, $t = (p_W - p_h)^2$. φ is the azimuthal angle around the z axis, which is taken parallel to the direction of motion of the incoming W.

[15] However, note that the limit $m_t \to 0$ does not interest us here.

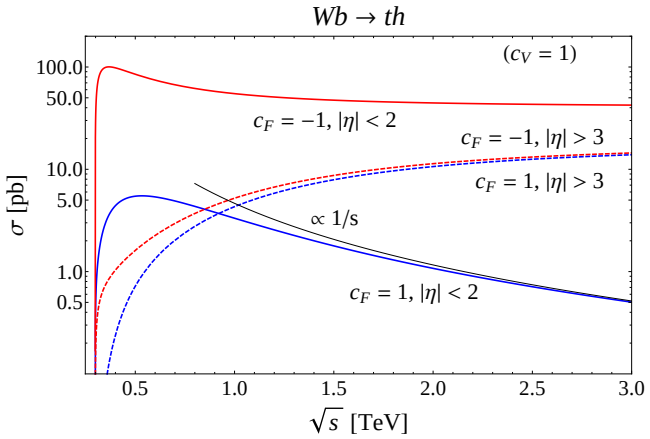

Figure 4.8: Partonic cross sections for the process $Wb \to th$ as a function of the center of mass energy $\sqrt{s}$. The parameter c_V is set to 1. The hard scattering cross section is defined by a cut $|\eta| < 2$: the large enhancement obtained for $c_F = -c_V$ with respect to the SM case is evident. The forward cross section, defined by a cut $|\eta| > 3$, is also shown (dashed curves).

The cross section for $Wb \to th$ is shown as a function of the center of mass energy in Fig. 4.8. The large enhancement of the hard scattering cross section (defined by a centrality cut $|\eta| < 2$) for $c_F = -c_V$ is evident.[16] At large energies, the amplitude is constant for $c_V = c_F$ and thus the cross section vanishes as $\sim 1/s$. On the other hand, when $c_F \neq c_V$ the amplitude grows with energy like $\sqrt{s}$ and as a consequence the cross section tends to a constant for large s. It is easy to compute this asymptotic value of the cross section: squaring the leading term of the amplitude in Eq. (4.48), summing and averaging over polarizations and integrating over t we find

$$\sigma(|\eta| < \tilde{\eta}, s \to \infty) \simeq \frac{g^2 (c_F - c_V)^2 m_t^2}{384\pi\, m_W^2 v^2} \tanh\tilde{\eta}\,. \tag{4.52}$$

This simple formula gives accurate results: for example for $\sqrt{s} = 5\,\text{TeV}$, $c_V = -c_F = 1$ and a centrality cut[17] $|\eta| < 2$ we find that the cross section computed without any approximations is $\sigma_{\text{full}}(|\eta| < 2) = 41.3\,\text{pb}$, whereas $\sigma(|\eta| < 2, s \to \infty) = 40.7\,\text{pb}$.

Since for $c_V \neq c_F$ the hard scattering amplitude grows with energy, perturbative unitarity will be lost at some cutoff scale Λ, which we now estimate. In the spinor basis of Eq. (4.51), only one s-wave amplitude is non-vanishing

$$a_0 = \frac{1}{16\pi\sqrt{2}\sqrt{s}}(c_F - c_V)\frac{g m_t}{m_W v}\int_{-s}^{0} A(t/s, \varphi; \xi_t^R, \xi_b^L) = -\frac{1}{24\sqrt{2}\pi}(c_F - c_V)\frac{g m_t \sqrt{s}}{m_W v} e^{i\varphi} \tag{4.53}$$

from which, imposing the condition $|a_0| < 1$, we find that perturbative unitarity is violated

[16] Incidentally, we note that the cross section shows another feature, a Coulomb enhancement at small $|t|$ due to the diagram with a W exchange in the t-channel. As can be read off Fig. 4.8 the forward cross section tends to a constant limit for large s, which can be computed in a simple way in terms of the parameter c_V alone and is insensitive to the value of c_F. See Appendix A of Ref. [4].

[17] Note that for the expression in Eq. (4.52) to be reliable, $\tilde{\eta}$ cannot be too large. In fact, as already mentioned, in the forward region the cross section has a Coulomb enhancement which is not captured by the approximations we made here.

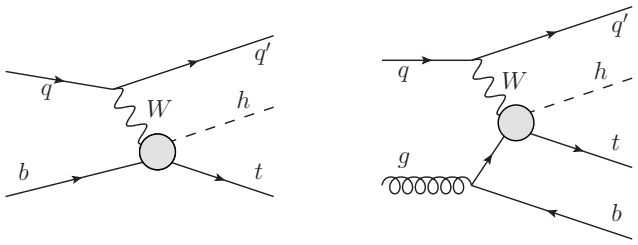

Figure 4.9: Feynman diagrams for the processes $pp \to thj$ and $pp \to thjb$.

at a scale $\sqrt{s} \simeq \Lambda$ with

$$\Lambda = 12\sqrt{2}\pi \frac{v^2}{m_t\,|c_F - c_V|}\,. \tag{4.54}$$

For example, for $c_V = -c_F = 1$ the cutoff is $\Lambda \simeq 9.3\,\text{TeV}$. One may worry about other processes involving top quarks, in which perturbative unitarity could be lost at a scale lower than the one in Eq. (4.54) for $c_F < 0$. A relevant and often mentioned process is $W_L^+ W_L^- \to t\bar{t}$. Using the chiral Lagrangian in Eq. (3.6) and applying the Goldstone equivalence theorem, we find two relevant diagrams: one with a $\pi^+\pi^- t\bar{t}$ contact interaction, and one with Higgs exchange in the s-channel [51]. From the expression of the amplitude, which grows with energy as $\sim \sqrt{s}$, we obtain

$$\Lambda = 16\pi \frac{v^2}{m_t\,|1 - c_V c_F|}\,.$$

For $c_V = -c_F = 1$ this formula yields 8.8 TeV, essentially the same cutoff scale we found for $W_L b \to th$. For previous discussions of perturbative unitarity breakdown in processes with external fermions, see Refs. [113, 114].

4.5.2 LHC cross sections

Having analyzed the behavior of the partonic cross section, we can now turn our attention to single top and Higgs associated production in hadron collisions. At the LHC, t-channel single top production goes through an initial-state gluon splitting into a $b\bar{b}$ pair. Such a process can be efficiently described in a 5-flavor scheme where b's are in the initial state and described by a perturbative b PDF, Fig. 4.9(a). In this scheme, the non-collinearly enhanced contribution, where the spectator b (*i.e.* the one not struck by the W boson) is central and at high p_T (see Fig. 4.9(b)), is moved to the next-to-leading order term. This contribution, which we indicate with $pp \to thjb$, is finite and can be easily calculated at tree-level, contributing to a final state signature with an extra b-jet, a useful handle to suppress the background. In Table 4.1 we present the rates for th production in the 5-flavor scheme, fully inclusive as well as with the requirement of the extra b to be in the tagging region, for 8 and 14 TeV, in the $c_V = 1, c_F \pm 1$ cases. Our analysis will consider both processes, which lead to final states containing 3 and 4 b-jets respectively, once the decay of the Higgs to $b\bar{b}$ is taken into account. The cross sections in Table 4.1 were computed using MadGraph 5 [115] with CTEQ6L1 PDFs [116], setting the factorization and renormalization scales to the default event-by-event MadGraph 5 value. As an estimate of the theoretical uncertainty on the signal, we have computed the fully inclusive cross sections at NLO in QCD, in the 5-flavor scheme, using the code aMC@NLO [117–119] and CTEQ6M PDFs [116]. The results are

	$\sigma^{\rm LO}(pp \to thj)$ [fb]		$\sigma^{\rm LO}(pp \to thjb)$ [fb]	
	$c_F = 1$	$c_F = -1$	$c_F = 1$	$c_F = -1$
8 TeV	17.4	252.7	5.4	79.2
14 TeV	80.4	1042	26.9	363.5

Table 4.1: Leading-order cross sections for the processes $pp \to thj$ and $pp \to thjb$ (with $p_T^b > 25$ GeV and $|\eta^b| < 2.5$) at the LHC. The parameter c_V has been set to 1.

	$\sigma^{\rm NLO}(pp \to thj)$ [fb]	
	$c_F = 1$	$c_F = -1$
8 TeV	$18.28^{+0.42}_{-0.38}$	$233.8^{+4.6}_{-0.}$
14 TeV	$88.2^{+1.7}_{-0.}$	982^{+28}_{-0}

Table 4.2: Cross sections at NLO in QCD for the process $pp \to thj$ at the LHC. The parameter c_V has been set to 1.

reported in Table 4.2, where the uncertainties correspond to variations of the factorization and renormalization scales with $\mu_F = \mu_R$ around $\mu = (m_t + m_h)/2$ from $\mu/2$ to 2μ. The NLO cross sections appear to be extremely stable under radiative corrections and therefore we deem the theory uncertainty of the signal rates in our analysis negligible.

The striking enhancement of the hadronic cross section for $c_F \neq c_V$ is shown in Fig. 4.10, where $\sigma(pp \to thj)$ for an LHC energy of 14 TeV, normalized to its SM value, is displayed as a function of c_F for three different choices of c_V (very similar plots are obtained considering 8 TeV and/or the $pp \to thjb$ process). For example, for a standard hWW coupling, *i.e.* $c_V = 1$, a $ht\bar{t}$ coupling with equal magnitude and opposite sign with respect to the standard one ($c_F = -1$) yields an enhancement of the cross section of more than a factor 10.

As noted above, perturbative unitarity in $Wb \to th$ scattering is lost at a scale $\Lambda \gtrsim 10$ TeV for $c_V, c_F \sim \mathcal{O}(1)$. The right panel of Fig. 4.10 clearly shows that after convolution with the PDFs the contribution of the region $\sqrt{\hat{s}} \gtrsim 1$ TeV, where $\sqrt{\hat{s}}$ is the center of mass energy of the th system, to the hadronic cross section is negligible. This implies that our perturbative computations can be fully trusted. Indeed Fig. 4.10 demonstrates that the relative contribution to the cross section from large values of $\sqrt{\hat{s}}$ is more sizable in the SM than for $c_F \neq c_V$. This is compatible with the different behaviors of the partonic cross section in the two cases, shown in Fig. 4.8.

4.5.3 Signal and background study

Signal and background events were generated at the parton level using MadGraph 5 with CTEQ6L1 PDFs, setting the factorization and renormalization scales to the default event-by-event MadGraph 5 value. Jets are defined at the parton level. In order to take showering, hadronization, detector and reconstruction effects minimally into account, we smear the p_T

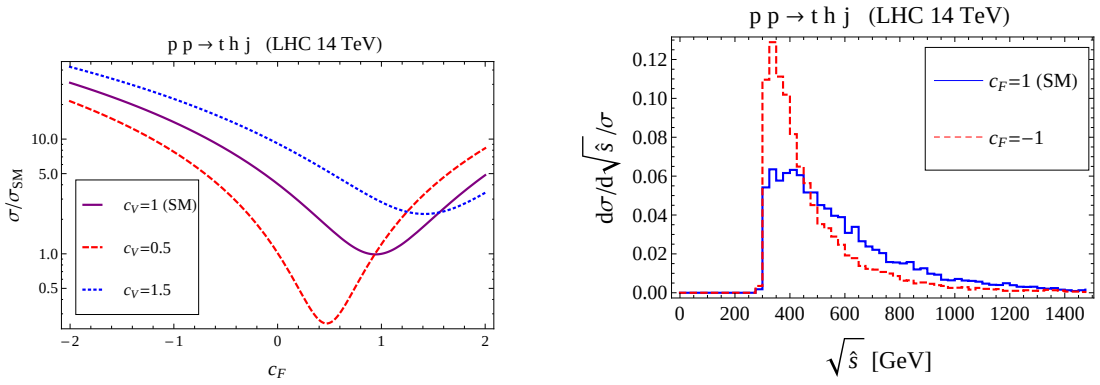

Figure 4.10: (*Left panel*) Cross section for $pp \to thj$ at 14 TeV normalized to the SM one, as a function of c_F for three choices of c_V. Solid, dashed and dotted lines correspond to $c_V = 1$, 0.5 and 1.5 respectively. (*Right panel*) Histogram of normalized $pp \to thj$ cross section as a function of the center of mass energy of the hard scattering process $Wb \to th$, at 14 TeV.

of the jets uniformly in η using a jet energy resolution defined by

$$\frac{\sigma(p_T)}{p_T} = \frac{a}{p_T} \oplus \frac{b}{\sqrt{p_T}} \oplus c\,, \tag{4.55}$$

where the parameters are taken to be $a = 2$, $b = 0.7$ and $c = 0.06$. With these choices, Eq. (4.55) is compatible with the results of the ATLAS jet energy resolution study of Ref. [120] (see Fig. 9 there). The jet 4-momentum is then rescaled by a factor $p_T^{smeared}/p_T$. The acceptance cuts reported in Table 4.3, chosen following the ATLAS $t\bar{t}h$ analysis [39], are applied on the physical objects. We do not require any acceptance cut on the missing transverse energy.

Cut	$p_T^b >$	$p_T^\ell >$	$p_T^j >$	$\lvert\eta^{b,\ell}\rvert <$	$\lvert\eta^j\rvert <$	$\Delta R_{ij} >$
Value	25 GeV	25 GeV	30 GeV	2.5	5	0.4

Table 4.3: Acceptance cuts applied to the signal and backgrounds at the reconstructed level. The ΔR requirement applies to all objects.

An object is considered to be missed if it does not pass one of the acceptance cuts. If, in particular, two jets are collinear with $\Delta R < 0.4$ we merge them by summing their 4-momenta and we consider them as a single jet when applying further cuts.[18] Additionally we require the lepton to be isolated from any jet in the event, including those that do not pass acceptance cuts and therefore are missed.

In all the signal and background processes we consider in the analysis, a semileptonically decaying top is present. We assume a 100% efficiency for the reconstruction of this top, which

[18] The exception to this procedure is the case where the b coming from a semileptonic top decay is collinear to another jet. Since we are assuming ideal semileptonic top reconstruction (see below), we simply reject the event in this case.

implies an unambiguous identification of the b originating from its decay. This assumption is of course idealized, however the use of a more realistic semileptonic top reconstruction efficiency will only affect the overall normalization of both signal and background, and not their relative values.

Concerning b-tagging, we assume the following performance: efficiency $\epsilon_b = 0.7$, charm mistag probability $\epsilon_c = 0.2$ and light jet mistag probability $\epsilon_j \approx 0.008$ [39]. Finally we assume a lepton reconstruction efficiency $\epsilon_\ell = 0.9$.

Final state with 3 b-tags

We start by discussing the 3 b-jet final state, which arises from $pp \to thj$ after selecting the Higgs decay into $b\bar{b}$. Requiring the top to decay semileptonically ($t \to b\ell^+\nu$) gives the signature

$$3\,b + 1\,\text{forward jet} + \ell^\pm + E_T^{miss}. \tag{4.56}$$

We can now turn our attention to the most relevant backgrounds:[19]

- tZj, $Z \to b\bar{b}$: an irreducible background where a Z boson mimics the Higgs in decaying to $b\bar{b}$.
- $tb\bar{b}j$: an irreducible QCD background.
- $t\bar{t}$, $\bar{t} \to \bar{b}\bar{c}s$: a reducible background where either the c or s are mistagged.
- $t\bar{t}j$, $\bar{t} \to \bar{b}\bar{c}s$: also in this case, either the c or s are mistagged while the other is missed.

As can be seen in Table 4.4 for 8 TeV [20], after acceptance cuts and efficiencies the last two backgrounds are extremely large. In particular, their values are larger than those quoted in Ref. [108], mainly due to a larger charm mistag rate considered here (we use $\epsilon_c = 0.2$, whereas Ref. [108] adopted $\epsilon_c = 0.1$) and to the fact that we increased the p_T threshold for jets, which results in a larger probability of missing a jet from $t\bar{t}j$. The dominance of backgrounds where a c is mistagged suggests that it may be sensible to prefer a b-tagging performance with smaller efficiency but higher rejection against charm. However, for definiteness we stick to the numbers reported above, taken from Ref. [39].

After acceptance cuts and efficiencies, the signal is overwhelmed by the $t\bar{t}$ background not only for the standard case $c_F = 1$, but even considering the enhanced case $c_F = -1$ (we set $c_V = 1$). Thus, we require a set of additional cuts in order to isolate the signal. These cuts are listed in Table 4.4, together with the cross sections obtained after their application. The value of each cut is chosen by optimizing the Poisson exclusion limit in the $c_F = -1$ case. We remark that since we are assuming ideal top reconstruction, the b coming from the semileptonic top is always assumed to be unambiguously identified, therefore no cut on it is applied beyond the acceptance ones, neither for the signal nor for the backgrounds.

The first cut we apply requires the $b\bar{b}$ pair to have an invariant mass around m_h, which of course helps to eliminate the tZj background. The second cut selects large values for the bbj invariant mass and is effective against the reducible backgrounds, in particular it suppresses enormously $t\bar{t}$, where the jet and 2 b's are decay products of a top and therefore we expect their invariant mass to be close to m_t. The last cut singles out a forward jet,

[19] For the sake of readability we do not write the top decay $t \to bl^+\nu$ explicitly, as it is the same for all processes.

[20] The tables for 14 TeV can be found in Ref. [4].

	Signal		Backgrounds				
Cuts	$c_F = 1$	$c_F = -1$	Total	tZj	$tb\bar{b}j$	$t\bar{t}$	$t\bar{t}j$
Acceptance Cuts + ϵ	0.18	2.88	600.81	0.61	1.01	456.40	142.80
$\lvert m_{bb} - m_h \rvert < 15$ GeV	0.15	2.55	245.95	0.02	0.11	184.2	61.65
$m_{bbj} > 270$ GeV	0.10	2.02	31.78	0.01	0.08	0.	30.68
$\lvert \eta^j \rvert > 1.7$	0.08	1.70	17.98	0.01	0.06	0.	17.24
Events at $25\,\text{fb}^{-1}$	1.9	42.5	449.4				

Table 4.4: Cross sections in fb for the 3 b-tag case at 8 TeV. In the event line backgrounds are summed.

which is a distinctive feature of the signal. However, after all cuts the background cross section, completely dominated by $t\bar{t}j$, is still one order of magnitude larger than the signal for $c_F = -1$.

In the last line of Table 4.4, we present the number of signal and total background events expected after $25\,\text{fb}^{-1}$ of integrated luminosity. At 8 TeV, the Poisson exclusion is at 97.4% CL or $2.2\,\sigma$ (by abuse of notation, we are expressing the probability in terms of number of σ's, *e.g.* $2\,\sigma$ approximately corresponds to the 95% CL), while at 14 TeV it reaches $\sim 4\,\sigma$.

Final state with 4 b-tags

As suggested in Ref. [108], a way to enhance the sensitivity on the th signal is to require an extra b, coming from the splitting of an initial gluon: the process of interest is thus $pp \to thjb$. Requiring a semileptonic top and the decay $h \to b\bar{b}$ leads to the signature

$$4\,b + 1\,\text{forward jet} + \ell^{\pm} + E_T^{miss}. \tag{4.57}$$

Here the main backgrounds are:

- $tZ\bar{b}j$, $Z \to b\bar{b}$: an irreducible background where the Z mimics the Higgs.
- $t\bar{b}b\bar{b}j$: similarly to the 3 b case, an irreducible QCD background.
- $t\bar{t}b\bar{b}$, $\bar{t} \to \bar{b}jj$: a reducible background where one of the two jets, originating from a hadronically decaying W, is missed.
- $t\bar{t}b\bar{b}$, $\bar{t} \to \bar{b}\bar{c}s$ (one mistag): here the c or the s is mistagged, while either the other one is missed (and one b is not tagged) or one of the b's is missed.
- $t\bar{t}j$, $\bar{t} \to \bar{b}\bar{c}s$ (two mistags): in this case both c and s are mistagged.

Looking at Table 4.5, we see that requiring 4 b-jets allows us to obtain a much larger signal to background ratio after acceptance cuts compared to the 3 b case. On the other hand, the overall rates are obviously smaller. Analogously to what was done in the 3 b case, a set of additional cuts are imposed to enhance the signal. The cuts are listed in Table 4.5, together with the cross sections obtained after their application. The value of each cut is again chosen by optimizing the Poisson exclusion limit in the $c_F = -1$ case.

The first cut requires the invariant mass of one of the 3 bb pairs (we recall that ideal reconstruction of the semileptonic top is assumed) to be inside a window around m_h. This

	Signal		Backgrounds					
Cuts	$c_F = 1$	$c_F = -1$	Total	$tZ\bar{b}j$	$tb\bar{b}\bar{b}j$	$t\bar{t}b\bar{b}$	$t\bar{t}b\bar{b}$ (mis)	$t\bar{t}j$
Acceptance Cuts + ϵ	0.043	0.63	7.81	0.11	0.26	2.66 (0.48)	2.25	2.54
$\lvert m_{bb} - m_h \rvert < 15$ GeV	0.039	0.58	4.06	0.03	0.08	0.94 (0.40)	1.29	1.71
min $m_{bb} > 110$ GeV	0.023	0.30	0.67	0.002	0.015	0.20 (0.18)	0.44	0.
min $m_{bj} > 180$ GeV	0.008	0.15	0.014	0.	0.007	0.002 (0.001)	0.004	0.
Events at $25\,\text{fb}^{-1}$	0.2	3.8	0.4					

Table 4.5: Cross sections in fb for the 4 b-tag case at 8 TeV. In the event line backgrounds are summed. For $t\bar{t}b\bar{b}$, the contribution of $t\bar{t}h$ is shown in parentheses.

helps again to eliminate the $tZ\bar{b}j$ background. The second cut demands all bb invariant masses to be higher than about 100 GeV, and is most effective on $t\bar{t}j$, where the mistagged c and s, coming from a W decay, have an invariant mass around m_W. The last cut requires all 3 bj pairs to have a large invariant mass. This efficiently suppresses the $t\bar{t}b\bar{b}$ backgrounds, for which in most cases at least one bj pair comes from a top decay and thus has an invariant mass $m_{bj} \lesssim \sqrt{m_t^2 - m_W^2} \sim 150\,\text{GeV}$.

The exclusion limits obtained for $c_F = -1$, assuming $25\,\text{fb}^{-1}$ of data, are $2.4\,\sigma$ and $\sim 6\,\sigma$ at 8 and 14 TeV respectively. The sensitivity at 8 TeV is comparable to the one obtained in the 3 b case, while at 14 TeV requiring an extra b-jet improves the result significantly.

Before discussing the implications of our results, we wish to comment here on the sensitivity of the proposed analysis to the $t\bar{t}h$ process. As can be read from Table 4.5, this process makes up a sizable fraction of the $t\bar{t}b\bar{b}$ cross section after the cuts. Moreover, after the first three cuts, the rate for $t\bar{t}h$ is comparable to the th signal for $c_F = -1$. Being insensitive to the sign of $g_{t\bar{t}h}$, $t\bar{t}h$ production can be considered as a background process in our analysis. It is, however, quite useful to observe that the simple search strategy we propose in the $4b$ channel would be sensitive to both single and pair top production in association with a Higgs boson. In this respect, a key role is played by the cut on m_{bj} that was designed to suppress processes with a $t\bar{t}$ pair in the final state, as discussed above. The relative contribution of $t\bar{t}h$ to the $t\bar{t}b\bar{b}$ background with one mistag, on the other hand, is small, approximately 5%.

4.5.4 Implications on Higgs couplings

We are now able to study the implications of our results on the general parameter space of Higgs couplings. To do so we combine the two analyses we performed, *i.e.* 3 and 4 b-tags, in order to exploit the full LHC sensitivity in $th \to tb\bar{b}$ production. Note that in the combination we consider the $3b$ and $4b$ samples as independent. While this is an approximation (which can be easily lifted in a more realistic analysis by defining fully exclusive samples), in practice it has a small effect as the $4b$ sample is significantly smaller than the $3b$ one. In Fig. 4.11 we present the results of our analysis in the (c_V, c_F) plane, where a universal rescaling of the Higgs couplings to fermions $c_t = c_b = c_\tau = c_c = c_F$ is assumed. The regions that can be excluded (at 95% CL) by th production with an integrated luminosity of 25 and $50\,\text{fb}^{-1}$ are presented, along with the regions currently favored by a fit to Higgs data[21]. As can be seen,

[21] The Higgs coupling fit displayed in Figs. 4.11 and 4.12 is out-of-date, being based on the data reported by ATLAS, CMS and Tevatron after ICHEP 2012 and collected in Ref. [121]. It is used only for illustrative

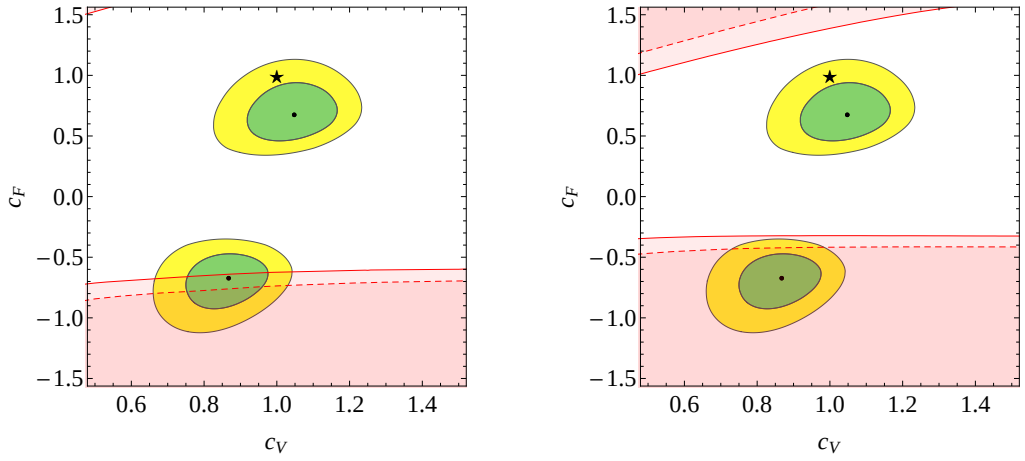

Figure 4.11: Regions of the (c_V, c_F) plane excluded at 95% CL by our analysis of $th \to hb\bar{b}$ (3 and 4 b final states combined), at 8 TeV (left) and 14 TeV (right), assuming an integrated luminosity of $25\,\text{fb}^{-1}$ and $50\,\text{fb}^{-1}$ (dashed and solid respectively). The 68% and 95% CL contours of a fit to current Higgs data are also shown, in green and yellow respectively. A universal rescaling by c_F of the Higgs coupling to fermions is assumed.

already at 8 TeV parts of the preferred region with $c_F < 0$ can be excluded. The current best fit point with $c_F < 0$ is excluded at $2.1\,\sigma$ with $50\,\text{fb}^{-1}$. On the other hand, a moderate luminosity at 14 TeV can conclusively remove the degeneracy between the two regions that are at the present time preferred by Higgs data, for example reaching a $5.8\,\sigma$ exclusion of the best fit point with $c_F < 0$ after $50\,\text{fb}^{-1}$. Notice that in addition to the th production cross section (recall Fig. 4.10), also the branching ratio of the Higgs into $b\bar{b}$ depends on the parameters (c_V, c_F). In particular, for $|c_F| \ll 1$ the branching ratio becomes very small and thus makes the $h \to b\bar{b}$ channel ineffective, as can be clearly seen in Fig. 4.11.

It is also possible to relax the assumption of universal couplings of the Higgs to fermions and consider the case where only the $ht\bar{t}$ coupling c_t has a rescaled value compared to the SM while $c_b = c_\tau = c_c = 1$, so in particular $\Gamma(h \to b\bar{b})$ is equal to its SM value. In this case, the $th \to tb\bar{b}$ rate is essentially fixed by the dependence on c_V, c_t of the production cross section (a mild sensitivity to c_V, c_t through the Higgs total width is also present). The results are shown in the (c_V, c_t) plane in Fig. 4.12. Excluded regions at 95% C.L. are displayed for 25 fb^{-1} and 50 fb^{-1} integrated luminosity. Superimposed are the regions currently favored by Higgs data. The most striking feature is, that the best fit region with $c_t < 0$ can already be completely excluded at 8 TeV with 25 fb^{-1} (reaching a $4.0\,\sigma$ exclusion of the best fit point with negative c_t).

Comparison with studies in other Higgs decay channels

Single top and Higgs associated production was studied also in Refs. [44,122], but focusing on different decay channels of the Higgs, namely $\gamma\gamma, WW^*$ and $\tau\bar{\tau}$. It is interesting to note that the results obtained in those papers are partly complementary to ours: as we have discussed, under the universal rescaling hypothesis the $b\bar{b}$ channel is not effective for $|c_F| \ll 1$, because the branching ratio is suppressed. On the other hand, in this region the bosonic decays $\gamma\gamma$

purpose.

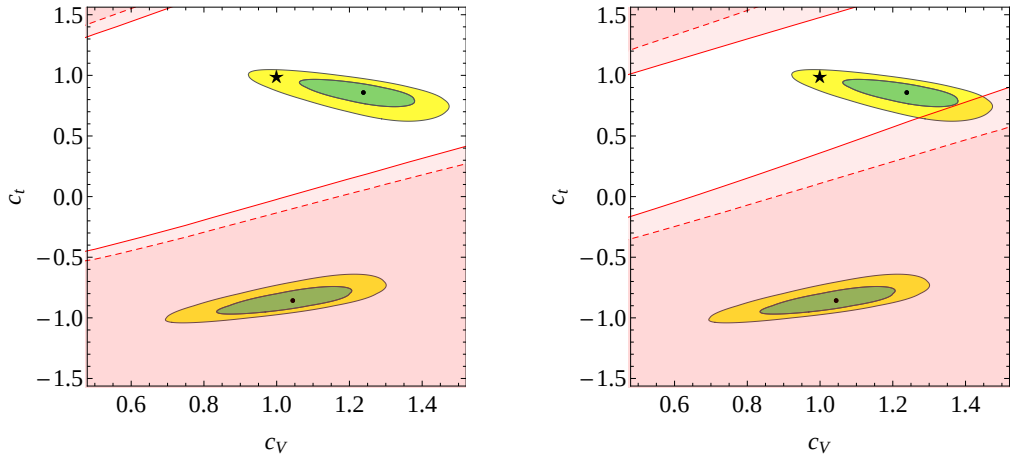

Figure 4.12: Regions of the (c_V, c_t) plane excluded at 95% CL by our analysis of $th \to hb\bar{b}$ (3 and 4 b final states combined), at 8 TeV (left) and 14 TeV (right), assuming an integrated luminosity of $25\,\text{fb}^{-1}$ and $50\,\text{fb}^{-1}$ (dashed and solid respectively). The 68% and 95% CL contours of a fit to current Higgs data are also shown, in green and yellow respectively. The top Yukawa is assumed to be rescaled by c_t, while we have set $c_b = c_\tau = c_c = 1$.

and WW^* are effective, see Ref. [122]. Combining the constraints obtained in all final states would allow to exclude the $c_t < 0$ hypothesis in a reliable way already with 8 TeV data.

Chapter 5

Phenomenology of spin $1/2$: the 'top partners'

As it was discussed in Chapter 2, one of the key ideas of 'modern' realizations of the composite Higgs idea is partial compositeness, which arises from the choice of writing down linear mixings between the elementary states and composite operators. In the fermionic sector, these couplings have the form (taking for example the top-bottom doublet q_L)

$$\mathcal{L}_f^{UV} = \lambda_q \bar{q}_L \mathcal{O} + \text{h.c.} \tag{5.1}$$

where $\mathcal{O}$ is a fermionic operator in the strong sector which has definite transformation properties under the full global symmetry $SO(5)$,[1] since the latter is restored in the UV. It follows that we can formally uplift q_L to an incomplete representation of $SO(5)$ (the so-called embedding), $q_L \to \mathcal{Q}_L \sim r_\mathcal{O}$, where $r_\mathcal{O}$ is the $SO(5)$ representation where the composite operator lives. This raises the question of what embeddings should be chosen: limiting the analysis to the top quark, one needs to specify those of q_L and t_R.

In Section 2.4 we worked out the details of the choice $q_L, t_R \sim \mathbf{5}_{2/3}$, and mentioned that several other choices have been considered, for example $q_L, t_R \sim \mathbf{10}_{2/3}, \mathbf{14}_{2/3}$. The choice of embedding has several consequences: most importantly, it fixes the structure of the Higgs potential, which by assumption is generated only via loops of the elementary states, and dominated by the fermionic contribution. Furthermore, the embedding also determines which composite resonances are expected to be low-lying: for example, in MCHM_5 we expect two $SO(4)$ multiplets of resonances to be present, $\mathbf{4}_{2/3}$ and $\mathbf{1}_{2/3}$, which amounts to three states with electric charge equal to $2/3$, one bottom-like state and one 'exotic' fermion with charge $Q = 5/3$. In MCHM_{14} we expect in addition a $\mathbf{9}_{2/3}$, which contains among others one exotic fermion with electric charge $8/3$ and one with $Q = -4/3$. The spectrum of resonances is important not only for the study of their on-shell production at the LHC, but also for assessing the compatibility of the theory with EWPT, since loops of the new fermions contribute to the electroweak observables, in particular to the T parameter and to the Z-b-$\bar{b}$ coupling.

In addition, the relatively small value of the Higgs mass implies that at least some of the fermionic resonances should be light, roughly below $1 \div 1.5$ TeV for a strong sector scale $f \lesssim 800$ GeV, which corresponds to a naive fine-tuning of $\sim 10\%$. This 'light resonance connection' was quantitatively established for MCHM_5 in Section 2.4.1, see Eq. 2.66: for $f = 800$ GeV, at least one $SO(4)$ multiplet of resonances must be ligher than 1.2 TeV.

[1] We concentrate on the minimal coset $SO(5)/SO(4)$ in this chapter.

It follows that the LHC has the potential to fully explore the region of masses where the heavy fermions should be found, thus confirming or confuting in a robust way the idea of compositeness as a natural solution to the hierarchy problem. Therefore LHC searches for heavy vector-like fermions should be regarded as crucial: in this sense, light fermionic resonances in composite Higgs play a role not dissimilar to that of light stops in the context of natural SUSY. Heavy vector-like quarks are a generic prediction of composite models, and their LHC phenomenology has been subject to thorough studies in the literature [123–128], also including the effects of the heavy partner for the gluon [129], which is expected in theories with partial compositeness (see Chapter 6).

In the following we will focus on the fermionic resonances that appear in MCHM$_5$, as described by Eq. (2.41) (with $y'_{L,R} = 0$). We will discuss first the bounds from EW precision measurements[2], and subsequently the LHC phenomenology.

5.1 Constraints from EWPT

The strongest experimental constraints on composite Higgs models still come from the electroweak precision measurements at the Z pole mass at LEP. A convenient description of LEP precision data is given in terms of the parameters ϵ_1, ϵ_2, ϵ_3 and ϵ_b [130]. In MCHM$_5$, three BSM contributions to the ϵ parameters arise. The first effect is due to the modified hVV coupling ($V = W, Z$), which in the MCHM is rescaled by $a = \sqrt{1-\xi}$. This induces a logarithmically divergent contribution to the oblique parameters T and S, or equivalently to ϵ_1 and ϵ_3, see Eq. (3.14). We assume the divergence to be cut off by the mass m_ρ of the first composite vector resonance, obtaining

$$\Delta\epsilon_1^{\rm IR} = \hat{T}^{\rm IR} = -\frac{3\alpha}{8\pi c_W^2}\xi \log\frac{m_\rho}{m_h}\,, \qquad \Delta\epsilon_3^{\rm IR} = \hat{S}^{\rm IR} = +\frac{\alpha}{24\pi s_W^2}\xi \log\frac{m_\rho}{m_h}\,. \tag{5.2}$$

The second effect is the tree-level contribution of spin-1 resonances to the S parameter. Assuming for definiteness that the leading contribution comes from one vector ρ and one axial-vector a_1 resonance, we find

$$\Delta\epsilon_3^{\rm UV} = \frac{m_W^2}{m_\rho^2}\left(1+\frac{m_\rho^2}{m_{a_1}^2}\right) \cong 1.36\,\frac{m_W^2}{m_\rho^2}\,. \tag{5.3}$$

where in the second equality we have used the relation $m_{a_1}/m_\rho \cong 5/3$, which holds in the five-dimensional realization of the model [18]. The third and last contribution to EW precision parameters comes from the top partners, which contribute at one loop both to T and to the Z-$\bar{b}$-b vertex, *i.e.* respectively to ϵ_1 and ϵ_b [30–32, 131]. Computing the precise value of these contributions requires the numerical diagonalization of the mass matrix of the top quark and its partners, which depends on the parameters λ_q, λ_u, M, y and f. The constraint that the top mass matches the measured value $m_t = 173.3$ GeV allows, however, to express the corrections to ϵ_1 and ϵ_b in terms of four dimensionless parameters,

$$\Delta\epsilon_1^{\rm fermions} = f_1\left(\xi, \phi_L, \phi_R, R\right), \qquad \Delta\epsilon_b^{\rm fermions} = f_b\left(\xi, \phi_L, \phi_R, R\right), \tag{5.4}$$

where ξ, ϕ_L, ϕ_R were defined previously, and $R \equiv (M + yf)/M = m_1/m_4$ is the ratio of the composite masses (before mixing with elementary states). The function f_1 is computed

[2] See also Ref. [69] for a very recent discussion of EWPT in the MCHM$_5$.

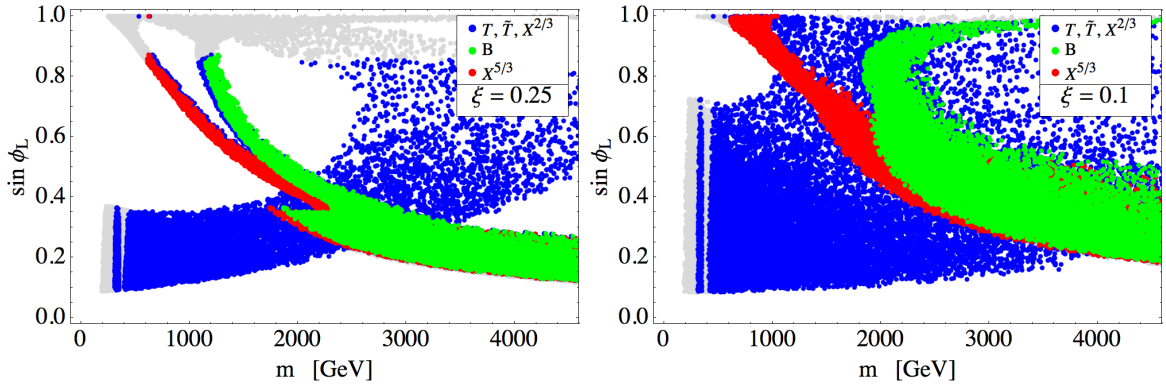

Figure 5.1: Physical mass spectrum of the resonances for a sample of points passing the electroweak precision tests, as a function of the left-handed top compositeness for $\xi = 0.25$ (left) and $\xi = 0.1$ (right). The blue points are top-like fermions (charge $+2/3$), the green points are bottom-like (charge $-1/3$), and the red ones correspond to the exotic X (charge $+5/3$). Gray points are excluded by present collider constraints.

exactly at one loop, while for f_b only the longitudinal polarizations of the gauge bosons are taken into account in the loop. The values obtained in this way are consistent with the full one-loop result of Ref. [32]. The agreement of the model with experimental data is then assessed through a χ^2 test, described in detail in App. B. The latest electroweak precision data are used, including the 2012 update of the W mass. Fixing the Higgs mass to $m_h = 125$ GeV, the model is completely determined by the five parameters ξ, ϕ_L, ϕ_R, R and m_ρ. After setting ξ to one of the two benchmark values we chose, namely $\xi = 0.1$ or 0.25 , we performed a scan in the parameter set (ϕ_L, ϕ_R, R) and retained only the points which fulfill the constraints from EWPT. By this we mean that there exists a value of $m_\rho \in [1.5\,\text{TeV}, 4\pi f]$ such that the configuration $(\xi, \phi_L, \phi_R, R, m_\rho)$ passes EWPT at 99% CL.

In Fig. 5.1, the spectrum of resonances is shown for a sample of points passing the EWPT. The green points correspond to B, the red ones to $X_{5/3}$, and the blue points for each set of parameters denote the top partners T, $X^{2/3}$ and $\tilde{T}$, which cannot be properly distinguished one from another once the rotation to the physical basis is performed. At leading order in v/f, however, composite fermions within an electroweak doublet have the same mass, so the green points describe approximately the mass of the (T, B) doublet and the red ones the mass of the $(X_{5/3}, X_{2/3})$ doublet. The blue points far from the red and green regions in Fig. 5.1 can therefore be interpreted as singlets $\tilde{T}$. As can be seen clearly in the case of $\xi = 0.25$, there are two distinct regions of the parameter space compatible with EWPT where in addition at least one multiplet of resonances is light, as it is needed in order to have a light enough Higgs (see Fig. 2.1):

1. The first region corresponds to low values of the left-handed top compositeness parameter $\sin\phi_L$ [3]. In this region the lightest top partner is typically the singlet $\tilde{T}$, whereas the states in the $\mathbf{4}_{2/3} \sim (\mathbf{2}, \mathbf{2})_{2/3}$ are heavier than 1.5 TeV and essentially decoupled. As discussed in Refs. [31, 32], in this case the behavior of the EW observables is relatively easy to understand: the light singlet contributes positively to T [28, 29], thus helping to compensate the IR and UV contributions of Eqs. (5.2, 5.3). However, the contribu-

[3] Note that t_R must then be largely composite in order to yield the correct top mass.

tion to T is strongly correlated to the (also positive) contribution to ϵ_b, resulting in a delicate compromise between the two constraints.

2. The second region corresponds to large values of $\sin\phi_L$, for which the top-bottom left-handed doublet becomes fully composite. In this second region, the 'custodian' doublet X is very light, having a mass below a TeV, and the 'exotic' $X_{5/3}$ turns out to be the lightest new fermion in the theory. In this case, agreement with EWPT is achieved through a rather involved interplay of different contributions, we refer the reader to Refs. [31, 32] for a discussion.

5.2 Collider phenomenology of top partners

Since the resonances have masses much larger than the weak scale, $M_\psi \gg m_W$, when describing their on-shell interactions it is convenient to apply the Goldstone Equivalence Theorem, which is valid at energies $E \gg m_W$. Making use of the expression of the Σ field in the R_ξ gauge,

$$\Sigma \simeq \frac{1}{f}\begin{pmatrix} \frac{\pi^+ + \pi^-}{\sqrt{2}} & \frac{\pi^- - \pi^+}{i\sqrt{2}} & H & \pi^0 & f \end{pmatrix}, \tag{5.5}$$

where we kept only the leading terms in the $1/f$ expansion, we extract from the 'composite Yukawa' coupling the interactions between one heavy fermion and two SM particles,

$$\begin{aligned}\mathcal{L}_{\rm Y} =& y s_L c_R \left(\bar{b}_L \pi^- + \frac{\bar{t}_L}{\sqrt{2}}(h - i\pi^0)\right)\tilde{T}_R + y\frac{s_R}{\sqrt{2}}\overline{X}_{2/3L}\left(\pi^0 - i\,h\right)t_R + \text{h.c.} \\ &+ \frac{y}{\sqrt{2}} s_R c_L \overline{T}_L \left(h - i\pi^0\right) t_R + y s_R c_L \overline{B}_L t_R \pi^- - y s_R \overline{X}_{5/3L} t_R \pi^+ + \text{h.c.}\,,\end{aligned} \tag{5.6}$$

where we have already performed the rotations $\propto \phi_{L,R}$ that diagonalize the mass matrix in the top sector for $v \to 0$. In particular, from Eq. (5.6) we can read the leading order branching ratios of the heavy fermions

$$\begin{aligned} \text{BR}(\tilde{T} \to Wb) =& \frac{1}{2}, \qquad \text{BR}(\tilde{T} \to Zt) = \text{BR}(\tilde{T} \to ht) = \frac{1}{4}; \\ \text{BR}(X_{2/3} \to Zt) =& \text{BR}(X_{2/3} \to ht) = \frac{1}{2}; \qquad \text{BR}(X_{5/3} \to Wt) = 1; \\ \text{BR}(T \to Zt) =& \text{BR}(T \to ht) = \frac{1}{2}; \qquad \text{BR}(B \to Wt) = 1, \end{aligned} \tag{5.7}$$

valid in the limit $M_\psi \gg m_{W,Z}, m_h$. Looking first at top-like states, we see that $\tilde{T}$ (which transforms as a $\mathbf{1}_{2/3}$ under the unbroken $SO(4) \times U(1)_X$) decays 'democratically' into all three allowed final states, namely Wb, Zt and ht, whereas T, $X_{2/3} \in \mathbf{4}_{2/3}$ do not decay (at leading order in v/f) into Wb. The exotic $X_{5/3}$ and heavy bottom B decay instead into Wt with branching ratio equal to one.

Let us now turn our attention to the production of the resonances at hadron colliders. Firstly, being colored, the heavy fermions are produced in pairs via QCD interactions. The cross section for the process $\sigma(pp,\, p\bar{p} \to \psi\overline{\psi})$, where ψ stands for any of the heavy fermions, only depends on the mass of ψ. In order to make contact with the experimental searches, we obtained the cross sections for QCD pair-production at approximate NNLO [132] at the TeVatron and at the LHC at 7, 8 and 14 TeV, see Fig. 5.2.

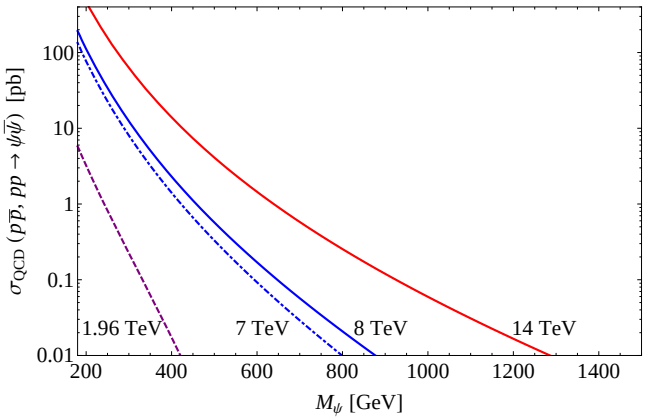

Figure 5.2: Cross sections for QCD pair production of heavy fermions at approximate NNLO, at the Tevatron and at the LHC at 7, 8 and 14 TeV energy. The cross sections were computed using HATHOR [132] and MSTW2008 PDFs. [94]

In addition, the top partners can be singly produced through the electroweak interactions, via the process $qg \to j\psi\bar{f}$, where ψ is a resonance, j indicates a jet, and $f = b, t$: an EW gauge boson V, emitted from the initial quark, scatters with either a bottom or a top coming from the splitting of the initial gluon to form the resonance ψ. Because of the lower kinematic threshold, single production is expected to be relevant for intermediate and large resonance masses [125]. Single production of a charge-2/3 resonance in association with a b quark is especially large, due to the contribution from the collinear region in the gluon splitting. Looking at Eq. (5.6) we see that neglecting small effects due to EWSB, the only state which couples to Wb is the singlet $\tilde{T}$. In Ref. [128] it was shown that for typical values of the parameters, the single production process $qg \to j\tilde{T}b$ dominates over pair production even when the resonance is relatively light. However, current LHC searches are tailored to pair production and turn out to be insensitive to single production in association with a b [128]. The ATLAS and CMS Collaborations will hopefully fill this gap in the very near future, by performing searches for singly produced top partners. However for the purpose of estimating the current bounds on the resonances, which is our next subject, it is sufficient to consider pair production.

5.2.1 Constraints from TeVatron and LHC direct searches

As we already discussed, combining constraints from EWPT with the requirement of at least one light multiplet of resonances (as it follows from the lightness of the Higgs) selects two distinct regions of the parameter space of MCHM$_5$, with very different features. Here we analyze the constraints that can be derived in each case from searches for vector-like quarks at the TeVatron and at the LHC:

1. In the first region (small $\sin\phi_L$) the lightest top partner is typically the singlet $\tilde{T}$, whereas the states in the $\mathbf{4}_{2/3}$ are heavier than 1.5 TeV and thus essentially irrelevant for LHC phenomenology, at least in first approximation. As we already discussed, the singlet $\tilde{T}$ decays with sizable branching ratio into three different final states, namely

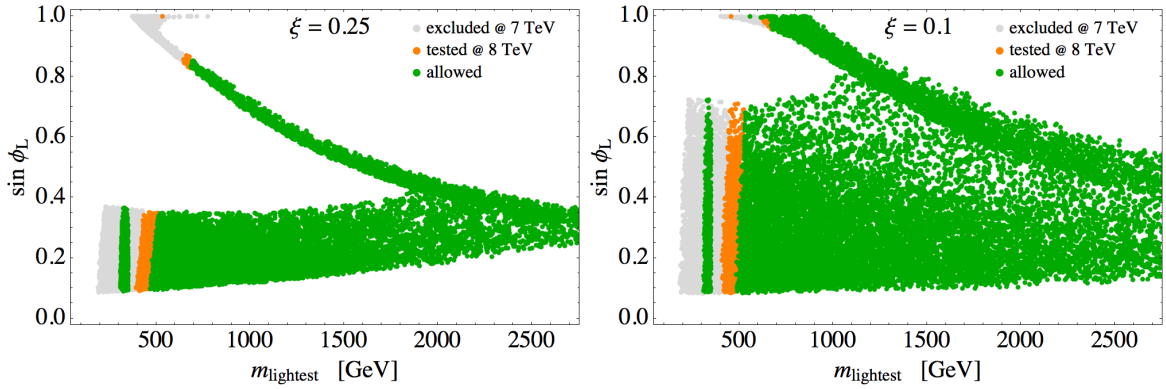

Figure 5.3: A sample of parameters passing the χ^2-test of electroweak precision observables, displaying the compositeness of the left-handed top versus the mass of the lightest top partner, for $\xi = 0.25$ (left) and $\xi = 0.1$ (right). The points in gray do not pass the direct collider constraints. Points in orange pass the present constraints but have been tested by the LHC in the 8 TeV run.

Wb, Zt and ht. The most constraining LHC search is in the $\tilde{T}\overline{\tilde{T}} \to WbWb$ final state (1 or 2 leptons), which gives a bound[4] $m_{\tilde{T}} \gtrsim 400$ GeV with 7 TeV data, see Fig. 5.1 [5].

2. The second region corresponds to large values of $\sin\phi_L$, for which the left-handed doublet q_L becomes fully composite. In this second region, the 'custodian' doublet X is typically below a TeV, and the exotic state $X_{5/3}$ is the lightest new fermion. As a consequence, the most relevant LHC search is the one for $X_{5/3}\overline{X}_{5/3} \to WtWt$. We note that the analysis of the $WtWt$ final state, although intended by the experiments to be a search for heavy charge $-1/3$ quarks such as the B, applies straightforwardly also to the $X_{5/3}$, which decays into the same final state[6]. The bound obtained is $m_{X_{5/3}} \gtrsim 610$ GeV, significantly stronger than the one on the singlet $\tilde{T}$. This is partly due to the fact that the $X_{5/3}$ decays into Wt with unity branching ratio, while $\mathrm{BR}(\tilde{T} \to Wb) \simeq 1/2$.

The bounds quoted so far were obtained from LHC data at 7 TeV. In Fig. 5.3 we show instead an estimate of the reach of the LHC with the full 8 TeV luminosity. Our estimate, which is based only on pair production, was derived as follows. The increase in energy enhances significantly the production cross section of heavy fermion pairs (see Fig. 5.2); on the other hand, the present exclusion limits quoted by ATLAS and CMS will be modified due to the changes in the background and to the additional integrated luminosity. Backgrounds in searches for top partners are dominated by $t\bar{t}$ production, which is increased by 42%

[4]The bounds quoted in this section were obtained in Ref. [3] by combining the results of a number of searches in various final states, performed by CDF, ATLAS and CMS. For brevity, in each case we only mention the most relevant channel.

[5]In Fig. 5.1 a thin region of parameter space in the range $m_{\tilde{T}} \in [300, 350]$ GeV is present, which is not directly excluded. This happens because the TeVatron only has enough sensitivity to exclude top partners below 300 GeV, while the most stringent LHC constraints start at 350 GeV.

[6]Note that the decay products of $B\overline{B}$ and $X_{5/3}\overline{X}_{5/3}$ would have different spatial configurations. For example, same-sign leptons necessarily stem either from $X_{5/3}$ or from its antiparticle, while in the case of $B\overline{B}$ production each of the same-sign leptons arises from a different heavy particle. However, since in the current searches only basic cuts on single objects are applied, this kind of kinematic differences is expected to give negligible effects on the exclusion limits. This was confirmed by Ref. [128].

when going from 7 to 8 TeV. The search strategies typically rely on a cut on the $t\bar{t}$ invariant mass, whose distribution is not significantly affected by the increase in energy, as we explicitly checked using MadGraph 5 [115]. The upper limit on the top partner production cross section is therefore softened in the Gaussian approximation by a factor $\sqrt{1.42} \cong 1.19$. The larger luminosity collected at 8 TeV is nevertheless tightening the limit on the cross section, lowering it by a square root factor of the luminosity in every channel [7]. The resulting constraints are $m_{\tilde{T}} \gtrsim 450 \div 500$ GeV and $m_{X_{5/3}} \gtrsim 700$ GeV for cases 1 and 2 discussed above, respectively.

At the time of completing this thesis, the ATLAS and CMS Collaborations have performed several searches for heavy vector-like quarks based on the full 8 TeV luminosity. An inclusive CMS search for pair-produced top-like resonances [133], where the Wb, Zt and ht final states were all considered, yields for the singlet (whose branching ratios are approximately $\mathrm{BR}(Wb) \simeq 2\,\mathrm{BR}(Zt) \simeq 2\,\mathrm{BR}(ht) \simeq 1/2$, see Eq. (5.7)) the bound $m_{\tilde{T}} \gtrsim 700$ GeV. Because all the relevant final states were considered in Ref. [133], this bound is significantly stronger than our naive estimate, which was essentially based on a projection of the sensitivity in the $\tilde{T}\bar{\tilde{T}} \to WbWb$ channel only. On the other hand, a CMS search dedicated to the $X_{5/3}$ [134] yields the constraint $m_{X_{5/3}} > 770$ GeV, in reasonable agreement with our simple estimate. Thanks to the significantly higher energy, the next run of the LHC will fully explore the natural region for the top partners.

[7] In the estimate of Fig. 5.3, taken from Ref. [3], we assumed 15 fb^{-1} as an educated guess of the size of the 2012 dataset for each experiment.

Chapter 6

Phenomenology of spin 1: heavy vectors

This chapter is devoted to the phenomenology of spin-1 fields. In Section 6.1 we sketch the main features of heavy vectors in the context of partial compositeness: in a nutshell, detecting these states constitutes a serious challenge for the LHC experiments, for two reasons. On the one hand, EWPT suggest that they should be rather heavy (above $2 \div 2.5$ TeV). On the other hand, they couple weakly to light fermions, and furthermore they typically decay into heavy SM states, such as W, Z and top.

Subsequently, following Ref. [1] we focus on one case, an $SU(2)_L$-singlet W'. As we explain in Sec. 6.2, a resonance with these quantum numbers is weakly constrained, and could thus be relatively light. In Sec. 6.3 we present our model-independent parameterization, based on an effective Lagrangian where no assumptions are made on the theoretical origin of the heavy particle, and in particular no underlying BSM gauge symmetry is imposed. In Sections 6.4 and 6.5 several aspects of the W' phenomenology are studied, including EWPT, low-energy observables, and Tevatron and LHC searches. We identify one parameter in our effective Lagrangian, labeled δ_B, which plays a particularly interesting role. In fact this parameter vanishes at tree level if the W' is associated to a spontaneously broken gauge symmetry, but can be nonzero for a generic composite vector. Since the partial decay width for the decay $W' \to W\gamma$ is $\propto \delta_B^2$, we conclude that observation of this decay at the LHC would constitute a signal of compositeness, and perform an estimate of the reach in this channel.

6.1 Spin-1 resonances in partial compositeness

The key features of the physics of resonances in partial compositeness can be understood by introducing a simplified 'two-sector' picture [45], which describes the SM fields along with their first composite partners (or KK excitations, in the warped picture). This simple setup has some limitations, in particular the Higgs is not explicitly introduced as a pNGB, but as an ordinary scalar. As a consequence, the properties that follow from its Goldstone nature are hidden [20]; however, this fact has no consequence on the broad characterization we aim to perform here. The elementary vector fields are assumed to gauge an 'elementary' copy of the symmetry $G_{\rm SM} = SU(3)_c \times SU(2)_L \times U(1)_Y$, labeled $[G_{\rm SM}]_{el}$. Since all the elementary gauge bosons need to mix with a composite partner, we are forced to introduce in the theory at least a set of heavy spin-1 fields transforming in the adjoint representation of

a $G_{\rm SM}$ group. However, in order to protect the T parameter the symmetry of the composite sector needs to be enlarged to include custodial symmetry, the minimal choice being $G \equiv SU(3)_c \times SU(2)_L \times SU(2)_R \times U(1)_X$, which we assume here. The spin-1 resonances are taken to be the gauge bosons associated to the 'composite' symmetry group $[G]_{cmp}$. Notice that the heavy vectors need not be associated with gauge symmetries. Relaxing this assumption leads to a faster growth of scattering amplitudes at energies above the mass of the resonances, but can also have interesting phenomenological consequences. We will discuss this point in detail in Sec. 6.5.2, in the concrete example of a W' that we will not assume to be a gauge boson. Here for simplicity we assume the heavy vectors to gauge $[G]_{cmp}$. The Higgs field transforms as a bi-doublet under $[SU(2)_L \times SU(2)_R]_{cmp}$.

In order to gain some insight on the properties of the vector resonances, it is useful to consider a simple toy model describing one up-type quark, by introducing only $q_L = (u_L, d_L)^T$ and u_R as elementary fermions, and one multiplet of elementary gauge fields W_μ^{el} (for definiteness, we will assume they are associated to the $SU(2)_L$ gauge group), plus the composite states they mix with. The Lagrangian reads

$$\begin{aligned}\mathcal{L}_{\rm pc} \,=\, & - M_Q \overline{Q} Q - M_{\tilde U} \overline{\tilde U} \tilde U + \Big(\lambda_q \overline{q}_L Q_R + \lambda_u \overline{\tilde U}_L u_R + \text{h.c.} \Big) \\ & - Y \overline{Q}_L \widetilde{H} \tilde U_R + \text{h.c.} + \frac{1}{2} m_{\tilde\rho}^2 \left(\tilde\rho_\mu^a - \frac{g_{el}}{g_\rho} W_\mu^{el\,a} \right)^2 + |D_\mu H|^2 \end{aligned} \tag{6.1}$$

where $Q = (U, D)^T$ and $\tilde U$ are vector-like composite fermions, and $\tilde\rho_\mu^a$ denotes the multiplet of gauge bosons associated to $[SU(2)_L]_{cmp}$. The composite gauge coupling is denoted g_ρ , while the elementary one is g_{el} ; by assumption $g_\rho \gg g_{el}$.[1] Kinetic terms for fermion and gauge fields are understood. The Higgs doublet H only couples to other composites, and its tree-level potential is assumed to vanish as a consequence of the Goldstone symmetry. As already remarked, the Goldstone nature of the Higgs is 'hidden' in this description, and in particular the nonlinearities due to the sigma model are absent. The 'composite Yukawa' coupling Y is of the same order of g_ρ , $Y \sim g_\rho \gg g_{el}$.[2]

The Lagrangian in Eq. (6.1) respects a gauge symmetry, which will be identified with the SM one. The corresponding (massless) gauge bosons, denoted simply by W_μ^a , are found by diagonalizing the mixing between $\tilde\rho_\mu$ and W_μ^{el}

$$\begin{pmatrix} W_\mu \\ \rho_\mu \end{pmatrix} = \begin{pmatrix} \cos\theta & \sin\theta \\ -\sin\theta & \cos\theta \end{pmatrix} \begin{pmatrix} W_\mu^{el} \\ \tilde\rho_\mu \end{pmatrix} , \qquad \tan\theta \equiv \frac{g_{el}}{g_\rho} , \tag{6.2}$$

which also gives $m_\rho^2 = m_{\tilde\rho}^2 / \cos^2\theta$. The SM gauge coupling is identified with $g = g_\rho g_{el} / \sqrt{g_\rho^2 + g_{el}^2}$. The mixings in the fermionic sector are diagonalized by means of the rotations

$$\begin{pmatrix} q_L \\ Q_L \end{pmatrix} \to \begin{pmatrix} \cos\phi_L & -\sin\phi_L \\ \sin\phi_L & \cos\phi_L \end{pmatrix} \begin{pmatrix} q_L^{\rm SM} \\ Q'_L \end{pmatrix} , \qquad \begin{pmatrix} u_R \\ \tilde U_R \end{pmatrix} \to \begin{pmatrix} \cos\phi_R & -\sin\phi_R \\ \sin\phi_R & \cos\phi_R \end{pmatrix} \begin{pmatrix} u_R^{\rm SM} \\ \tilde U'_R \end{pmatrix} , \tag{6.3}$$

with mixing angles defined by $\tan\phi_L = \lambda_q / M_Q$ and $\tan\phi_R = \lambda_u / M_{\tilde U}$. We have now all the ingredients needed to write down the couplings of the physical ρ resonances to the SM

[1] The mass terms for the gauge fields might look unfamiliar, however it is easy to realize that this is the form one obtains if the $[SU(2)_L]_{el} \times [SU(2)_L]_{cmp}$ is broken down to the diagonal at scale $f \equiv m_\rho / g_\rho$.

[2] Notice that for simplicity we assumed the composite sector Lagrangian to be invariant under parity.

fermions, which play a crucial role in the phenomenology: the fermion kinetic terms in the original Lagrangian contained interactions of the form

$$\sim \quad g_{el}\bar{q}_L\gamma^\mu\sigma^a q_L W_\mu^{el\,a} + g_\rho\overline{Q}_L\gamma^\mu\sigma^a Q_L\,\tilde{\rho}_\mu^a\,, \tag{6.4}$$

because, as we already stated, the elementary fermions were taken to transform under an 'elementary' $SU(2)_L$, whereas the composite fermions transform under a 'composite' copy of the same group. In the physical basis, these interactions can be rewritten as

$$g\,(\mathrm{cotan}\,\theta\sin\phi_L^2 - \tan\theta\cos\phi_L^2)\,\rho_\mu^a\,\bar{q}_L^{\rm SM}\gamma^\mu\sigma^a q_L^{\rm SM}\,. \tag{6.5}$$

The first term in Eq. (6.5) is proportional to the degree of compositeness of the fermion, whereas the second term arises from the W^{el}-$\tilde{\rho}$ mixing. In addition, the mass of the SM fermion reads

$$m_u = Y\sin\phi_L\sin\phi_R\frac{v}{\sqrt{2}}\,, \tag{6.6}$$

with $v \simeq 246$ GeV. From Eq. (6.6) we read that the degree of compositeness of light fermions is very small: it follows that the coupling of the ρ to light generations in Eq. (6.5) is $\sim g\tan\theta \simeq g^2/g_\rho$, which is parametrically smaller than the SM coupling by a factor g/g_ρ. As a consequence, the Drell-Yan process $q\bar{q}\to\rho$, which is the main production mechanism for vectors at hadron colliders, is suppressed. On the other hand, the coupling of the resonances to third-generation quarks, which have a sizable degree of compositeness, is $\sim g\,\mathrm{cotan}\,\theta\,\sin^2\phi_L \simeq g_\rho\sin^2\phi_L$ and dominates over the coupling to light fermions. In addition, the ρ couples strongly to the components of the Higgs doublet, *i.e.* to the longitudinal polarizations of W and Z and the physical Higgs boson: the kinetic term of the Higgs contains a coupling

$$g_\rho\tilde{\rho}_\mu^a iH^\dagger\frac{\sigma^a}{2}\overleftrightarrow{\partial^\mu}H \qquad\Longrightarrow\qquad g\,\mathrm{cotan}\,\theta\,\rho_\mu^a iH^\dagger\frac{\sigma^a}{2}\overleftrightarrow{\partial^\mu}H\,, \tag{6.7}$$

where the second expression is written in the physical basis. Using the Goldstone Equivalence Theorem we thus obtain that the resonance couples with strength $g\,\mathrm{cotan}\,\theta\simeq g_\rho$ to $W_L^\pm, Z_L$ and h. We conclude that the main decay channels of the vector resonances are to scalars and heavy fermions. For example, the electrically neutral ρ^0 will decay to $W_L^+W_L^-$, Z_Lh, $t\bar{t}$, whereas the largest branching fractions of the electrically charged ρ^+ are expected to be into $W_L^+Z_L$, W_L^+h, $t\bar{b}$. The large coupling of the resonances to W_L and Z_L, together with the suppression of DY, suggests that production of the resonances via vector boson fusion could become important. The production cross sections of the ρ at the LHC are shown in Fig. 6.1, taken from Ref. [135]. Indeed we see that in the high mass region $m_\rho \gtrsim 2$ TeV, which as we will see is favored by EWPT, DY is comparable to vector boson fusion[3]. In summary, the spin-1 resonances that appear in partial compositeness have relatively small production cross sections and decay mostly to heavy SM particles.

Another crucial piece of information comes from EWPT, which constrain the resonances to be heavier than approximately 2.5 TeV. This is mostly due to the tree-level corrections to the S parameter generated by heavy vectors. Generically, the T parameter is also affected at tree-level by spin-1 states, however if a custodial symmetry is imposed on the strong sector, as we assumed, then the total tree-level contribution to T exactly vanishes. By contrast, no

[3]Notice, however, that in Ref. [136] the vector boson fusion cross section is found to be much smaller than the DY one, see their Fig. 4(b). The reason for this difference needs to be investigated.

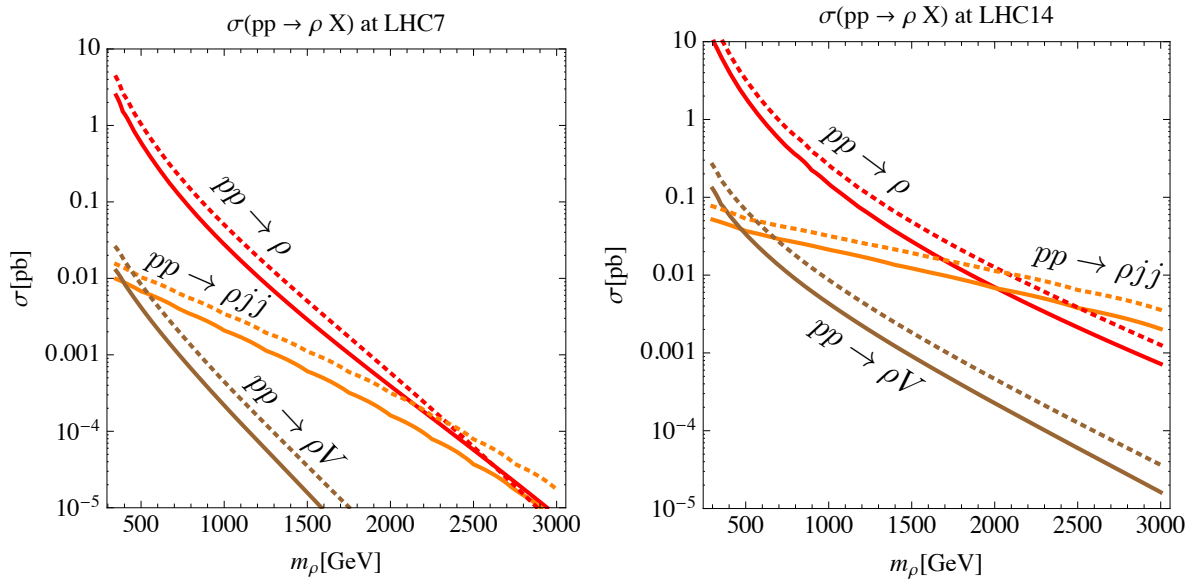

Figure 6.1: Production cross sections for the ρ vectors at the LHC7 (left) and LHC14 (right). $pp \to \rho$ indicates Drell-Yan production, whereas $pp \to \rho jj$ corresponds to vector boson fusion and $pp \to \rho V$ to production in association with a $V = W, Z$. Solid (dashed) lines correpond to the neutral (charged) resonance. Taken from Ref. [135].

symmetry is known that can protect S. It is instructive to compute explicitly the contribution to S given by the ρ resonance we considered above. The relevant terms in the Lagrangian are, in the original basis of Eq. (6.1), [4]

$$\mathcal{L}_{\tilde{\rho}} = -\frac{1}{4}\tilde{\rho}^a_{\mu\nu}\tilde{\rho}^{\mu\nu\,a} + \frac{1}{2}m^2_{\tilde{\rho}}\left(\tilde{\rho}^a_\mu - \frac{g_{el}}{g_\rho}W^{el\,a}_\mu\right)^2 + ig_\rho\tilde{\rho}^a_\mu H^\dagger\frac{\sigma^a}{2}\overleftrightarrow{\partial^\mu}H \tag{6.8}$$

which we rewrite as

$$\mathcal{L}_{\tilde{\rho}} = -\frac{1}{4}\tilde{\rho}^a_{\mu\nu}\tilde{\rho}^{\mu\nu\,a} + \frac{1}{2}m^2_{\tilde{\rho}}\,\tilde{\rho}^a_\mu\tilde{\rho}^{\mu\,a} + \tilde{\rho}^a_\mu J^{\mu\,a} + \frac{1}{2}m^2_{\tilde{\rho}}\frac{g^2_{el}}{g^2_\rho}\,W^{el\,a}_\mu W^{\mu\,a}_{el}\,, \tag{6.9}$$

$$J^a_\mu = g_\rho J^a_{H\,\mu} - m^2_{\tilde{\rho}}\,\frac{g_{el}}{g_\rho}\,W^{el\,a}_\mu\,, \qquad J^a_{H\,\mu} = iH^\dagger\frac{\sigma^a}{2}\overleftrightarrow{\partial^\mu}H\,.$$

We now proceed to integrate out the resonance. The equations of motion for $\tilde{\rho}$ derived from Eq. (6.9) can be readily solved, obtaining (in momentum space)[5]

$$\tilde{\rho}^a_\mu = \frac{1}{q^2 - m^2_{\tilde{\rho}}}\left(g_{\mu\nu} - \frac{q_\mu q_\nu}{m^2_{\tilde{\rho}}}\right)J^{\nu\,a} \simeq \left(-\frac{g_{\mu\nu}}{m^2_{\tilde{\rho}}} + \frac{1}{m^4_{\tilde{\rho}}}(q_\mu q_\nu - q^2 g_{\mu\nu})\right)J^{\nu\,a}\,, \tag{6.10}$$

where in the last expression we retained only the first two terms in an expansion in $q^2/m^2_{\tilde{\rho}}$.

[4] To simplify the computation, in the expression of the coupling of the $\tilde{\rho}$ to the Higgs current we simply take the ∂_μ part instead of the full covariant derivative. We will restore explicit gauge invariance at the end.

[5] We neglected nonlinear terms in $\tilde{\rho}$ in the equations of motion.

Substituting back, we obtain the effective Lagrangian

$$\begin{aligned}\mathcal{L}_{\rm eff} &= -\frac{1}{2m_{\tilde\rho}^2}J_\mu^a J^{\mu\,a}+\frac{1}{2m_{\tilde\rho}^4}J_\nu^a(q^\mu q^\nu-q^2g^{\mu\nu})J_\mu^a+\frac{1}{2}m_{\tilde\rho}^2\,\frac{g_{el}^2}{g_\rho^2}\,W_\mu^{el\,a}W_{el}^{\mu\,a}\\ &= \frac{1}{2}\frac{g_{el}^2}{g_\rho^2}W_{el}^{\nu\,a}(q_\mu q_\nu-q^2g_{\mu\nu})W_{el}^{\mu\,a}+g_{el}W_\mu^{el\,a}J_H^{\mu\,a}-\frac{1}{m_{\tilde\rho}^2}g_{el}J_{H\,\nu}^a(q^\mu q^\nu-q^2g^{\mu\nu})W_\mu^{el\,a}+\dots\end{aligned} \tag{6.11}$$

where in the second line the dots stand for terms of dimension 6 or higher that are not relevant for the current discussion. The first term in the second line of Eq. (6.11) is a correction to the kinetic term of W_{el}, and it adds to the canonical term that was already present in the Lagrangian of the elementary sector. It follows that W_{el} is made canonical by the redefinition

$$W_{el}^\mu\to\frac{g_\rho}{\sqrt{g_\rho^2+g_{el}^2}}\,W^\mu=\cos\theta\,W^\mu\,. \tag{6.12}$$

Applying this transformation to Eq. (6.11) and going back to position space, we find (recall that $g_{el}\cos\theta=g$)

$$\mathcal{L}_{\rm eff}=-\frac{1}{4}W^{\mu\nu\,a}W_{\mu\nu}^a+gW_\mu^a iH^\dagger\frac{\sigma^a}{2}\overleftrightarrow{\partial^\mu}H+\frac{i\,g}{2m_{\tilde\rho}^2}\left(H^\dagger\sigma^a\overleftrightarrow{\partial^\mu}H\right)\partial_\nu W^{\mu\nu\,a}+\dots\,, \tag{6.13}$$

where $W^{\mu\nu\,a}$ contains only the terms linear in W^μ. At this point we can use the fact that the effective Lagrangian must respect the SM gauge symmetry, and make the replacement $\partial_\mu\to D_\mu$ everywhere. The second term in Eq. (6.13) is of dimension 4, it couples the SM gauge field W_μ to the corresponding Higgs current, and is part of the kinetic term of H in the low-energy theory, $|D_\mu H|^2$, where the covariant derivative is now defined with respect to the SM gauge group. The third term is the one relevant for S: in the SILH basis [57] it corresponds to the operator $\mathcal{O}_W$, with coefficient $c_W=1$ (see Sec. 3.4). Using $m_{\tilde\rho}^2=m_\rho^2\cos^2\theta\simeq m_\rho^2$, we find from Eq. (3.31)

$$\hat S_\rho=\frac{m_W^2}{m_\rho^2}\,, \tag{6.14}$$

which is our desired result. In a complete model, an analogous contribution will come from the resonances associated to the $[SU(2)_R\times U(1)_X]_{cmp}$ invariance of the strong sector, which is necessary to guarantee custodial protection. Assuming all resonances to have roughly the same mass, the total contribution to $\hat S$ is simply given by twice Eq. (6.14) [45]. Requiring that $\hat S\lesssim 2.3\times10^{-3}$ (as demanded by LEP data at 99% CL) we find $m_\rho\gtrsim 2.3$ TeV.

The lower bound from the S parameter, combined with the small production cross sections and the preferred decay into heavy SM states, makes the discovery of spin-1 resonances challenging: detailed studies have shown that the composite (or KK) vectors with EW quantum numbers can be discovered at the LHC if their mass is smaller than about 3 TeV [136, 137]. The prospects are slightly better for the partners of the gluons, which have larger couplings to light fermions compared to the partners of EW gauge bosons, if a common mass scale for the resonances is assumed (this is simply due to $g_s\gg g$). It has been shown that the decay of KK gluons into $t\bar t$ can be discovered at the LHC for resonance masses up to approximately 4 TeV [138]. In all cases the decay products of resonances are expected to be highly boosted

and thus difficult to separate from the QCD background. The application of jet substructure techniques is therefore of crucial importance, and could allow the LHC experiments to improve significantly the reach on spin-1 vectors in partial compositeness. For a review of recent developments in the field of jet substructure, see Ref. [139].

So far we have described the general features that spin-1 resonances are expected to display in models with partial compositeness (or equivalently in warped compactifications, according to AdS/CFT). However, when studying the phenomenology it is very useful to take an approach as model-independent as possible, and leave open the possibility of deviations from the expected patterns. The most convenient way to proceed is to write down the most general effective Lagrangian describing interactions of the new state with the SM fields and invariant under the SM gauge symmetry (see, *e.g.*, Refs. [140,141]). Once the representation in which the extra state transforms is specified, the Lagrangian is fully determined by a set of free parameters, namely the mass of the heavy state and its couplings to the SM particles. A specific gauge model, in which the vector is the gauge boson associated with an extra symmetry, can then be recovered by taking some special values of these free parameters. In Ref. [1] we applied this model-independent approach to a color-neutral resonance with electric charge $Q = 1$, commonly called a W'. In the rest of this chapter we summarize and partially update the results of that work.

6.2 A weakly constrained W': motivations and introduction

We apply an effective approach to study the LHC phenomenology of a W' transforming in the representation

$$(\mathbf{1},\mathbf{1})_1 \tag{6.15}$$

under the SM gauge symmetry $G_{\rm SM}$, where the notation $(SU(3)_c, SU(2)_L)_Y$ has been adopted. Our approach is similar to that of Ref. [141], where however the focus was on computing constraints from electroweak data. In Ref. [141], bounds from EWPT were discussed for all the irreducible representations of $G_{\rm SM}$ which can have linear and renormalizable couplings to SM fields. There it was shown that the only such representations containing a color-singlet W' coupled to the SM fermions, in addition to that in Eq. (6.15), are $(\mathbf{1},\mathbf{3})_0$ and $(\mathbf{1},\mathbf{2})_{-3/2}$. The $(\mathbf{1},\mathbf{2})_{-3/2}$ multiplet does not have any renormalizable coupling to quarks or gluons, and as a consequence its production at the LHC would be very suppressed: therefore, we do not discuss it any further. The two remaining representations, $(\mathbf{1},\mathbf{1})_1$ and $(\mathbf{1},\mathbf{3})_0$, are both present in many explicit models, and in particular they both appear in the partial compositeness picture that was discussed in the previous section. Our choice to discuss the $(\mathbf{1},\mathbf{1})_1$ is motivated by the fact that in this case we can add to the SM only a charged resonance, without any associated neutral state. This is in contrast with the $SU(2)_L$ triplet $(\mathbf{1},\mathbf{3})_0$: in the latter case the W' and Z' masses are degenerate, apart from corrections proportional to v, and as a result the strong bounds from neutral currents (including LEP2 data on four-fermion operators) apply also to the W', pushing its mass well into the TeV range unless its couplings to leptons are very small. On the other hand the isospin-singlet W', because its only couplings to leptons arise through W-W' mixing and are therefore strongly suppressed[6], is only constrained by hadronic processes (except for the oblique T parameter), making this type of resonance relatively *weakly constrained*.

[6]Since we only consider the SM field content, we do not include right-handed neutrinos; or, equivalently for our purposes, we assume them to be heavier than the W', so that the decay $W' \to \ell_R \nu_R^\ell$ is forbidden.

We note that the isospin-singlet W' also appears in 'left-right' (LR) extensions of the SM [142], based on the $SU(2)_L \times SU(2)_R \times U(1)_X$ gauge symmetry, together with a neutral Z' which is a complete singlet under $G_{\rm SM}$. The mass splitting between the W' and Z' can be large, without violating EWPT constraints, if one takes $g_X \gg g_R$, where g_X and g_R are the couplings of $U(1)_X$ and of $SU(2)_R$, respectively [143, 144]. If $m_{W'} \ll m_{Z'}$, constraints from the Z' become negligible and in first approximation one can study the phenomenology of the W' only, by using an effective theory for a $(\mathbf{1},\mathbf{1})_1$ state. While the partial compositeness picture and LR models provide specific examples of W' that are described by the effective theory we consider, we stress that our approach is completely general and encompasses any composite state, whose properties could depart significantly from those of a gauge boson.

The outline of our discussion is as follows. After introducing the effective Lagrangian in Sec. 6.3, we briefly review in Sec. 6.4 the pre-LHC constraints on the parameter space of the model. Then we move to an analysis of the LHC phenomenology, which is the subject of Sec. 6.5. We discuss first the prospects to discover the W' in the dijet channel, which, together with the tb final state, is the main avenue to look for the 'leptophobic' W' we are studying. Then we point out that the subleading decay $W' \to W\gamma$ is particularly interesting, since it is extremely suppressed if the W' is a gauge boson. This implies that observation of resonant production of a W and a photon at the LHC would point to a composite resonance. In this light, we discuss the LHC reach in the $W' \to W\gamma$ final state. We also present the prospects for observing $W' \to WZ$ at the early LHC, and compare the reach in this channel to that in the $W\gamma$ final state. For other related work on the phenomenology of a W' at the LHC, see Refs. [145–147].

6.3 Effective Lagrangian

We consider, in addition to the SM field content, a complex spin-1 state transforming as a singlet under color and weak isospin, and with hypercharge equal to unity, according to Eq. (6.15). The resonance is therefore electrically charged, with unit charge. We do not make any assumption on the theoretical origin of the extra state, and in particular we do not assume it to be a gauge boson associated with an extended gauge symmetry. Taking a model-independent approach, we write down all the renormalizable interactions between the new vector and the SM fields which are allowed by the $SU(3)_c \times SU(2)_L \times U(1)_Y$ gauge symmetry. Higher-dimensional operators would be suppressed with respect to renormalizable ones by the cut-off of the theory; we neglect them in our analysis. Within this framework, we write down the Lagrangian

$$\mathcal{L} = \mathcal{L}_{SM} + \mathcal{L}_V + \mathcal{L}_{V-SM}\,, \tag{6.16}$$

where $\mathcal{L}_{SM}$ is the SM Lagrangian, and[7]

$$\begin{aligned}\mathcal{L}_V =& D_\mu V_\nu^- D^\nu V^{+\mu} - D_\mu V_\nu^- D^\mu V^{+\nu} + \tilde{M}^2 V^{+\mu} V_\mu^- \\ &+ \frac{g_4^2}{2}|H|^2 V^{+\mu} V_\mu^- + ig'(1-\delta_B) B^{\mu\nu} V_\mu^+ V_\nu^-\,, \end{aligned} \tag{6.17}$$

$$\mathcal{L}_{V-SM} = V^{+\mu}\left(ig_H H^\dagger (D_\mu \tilde{H}) + \frac{g_q}{\sqrt{2}} (V_R)_{ij} \overline{u_R^i} \gamma_\mu d_R^j \right) + \text{h.c.}\,, \tag{6.18}$$

[7] To be general, we should also include the operators $V_\mu^+ V^{+\mu} V_\nu^- V^{-\nu}$ and $V_\mu^+ V^{-\mu} V_\nu^+ V^{-\nu}$; however, these operators only contribute to quartic interactions of vectors and can thus be neglected for the scope of this study. On the other hand, a cubic self-interaction of V_μ is forbidden by gauge invariance.

where we have denoted the extra state with $V_\mu^\pm$, and defined $\tilde{H} \equiv i\sigma_2 H^*$. We remark that we have not introduced right-handed neutrinos, in order to avoid making any further assumptions about the underlying model. The coupling of V_μ to left-handed fermionic currents is forbidden by gauge invariance. The covariant derivative is referred to the SM gauge group: for a generic field $\mathcal{X}$, neglecting color we simply have

$$D_\mu \mathcal{X} = \partial_\mu \mathcal{X} - igT^a \hat{W}_\mu^a \mathcal{X} - ig' Y B_\mu \mathcal{X} \,, \tag{6.19}$$

where T^a are the generators of the $SU(2)_L$ representation where $\mathcal{X}$ lives, and we have denoted the $SU(2)_L$ gauge bosons with a hat, to make explicit that they are gauge (and not mass) eigenstates. In fact, upon electroweak symmetry breaking the coupling g_H generates a mass mixing between $\hat{W}_\mu^\pm$ and $V_\mu^\pm$. This mixing is rotated away by introducing the mass eigenstates

$$\begin{pmatrix} W_\mu^+ \\ W_\mu'^+ \end{pmatrix} = \begin{pmatrix} \cos\hat{\theta} & \sin\hat{\theta} \\ -\sin\hat{\theta} & \cos\hat{\theta} \end{pmatrix} \begin{pmatrix} \hat{W}_\mu^+ \\ V_\mu^+ \end{pmatrix} . \tag{6.20}$$

The expression of the mixing angle is

$$\tan(2\hat{\theta}) = \frac{2\Delta^2}{m_{\hat{W}}^2 - M^2} \,, \tag{6.21}$$

where

$$m_{\hat{W}}^2 = \frac{g^2 v^2}{4}, \quad \Delta^2 = \frac{g_H g v^2}{2\sqrt{2}}, \quad M^2 = \tilde{M}^2 + \frac{g_4^2 v^2}{4} \,. \tag{6.22}$$

We assume that Eq. (6.16) is written in the mass eigenstate basis for fermions. We have written the heavy vector mass explicitly: the details of the mass generation mechanism will not affect our phenomenological study, as long as additional degrees of freedom possibly associated with such mechanism are heavy enough. We assume that the standard redefinition of the phases of the quark fields has already been done in $\mathcal{L}_{SM}$, thus leaving only one CP-violating phase in the Cabibbo–Kobayashi–Maskawa (CKM) mixing matrix V_{CKM}. The right-handed mixing matrix V_R does not need to be unitary in the framework we adopt here: it is in general a complex 3×3 matrix. This is a relevant difference with respect to LR models, where V_R must be unitary as a consequence of the gauging of $SU(2)_R$. We normalize g_q in such a way that $|\det(V_R)| = 1$ (a generalization of this condition can be applied if V_R has determinant zero).

In the mass eigenstate basis both for spin-1/2 and spin-1 fields, the charged current interactions for quarks read:

$$\mathcal{L}_{cc}^q = W_\mu^+ \, \overline{u}^i \left(\gamma^\mu v_{ij} + \gamma^\mu \gamma_5 a_{ij}\right) d^j + W_\mu'^+ \, \overline{u}^i \left(\gamma^\mu v'_{ij} + \gamma^\mu \gamma_5 a'_{ij}\right) d^j + \text{h.c.} \,, \tag{6.23}$$

where u^i, d^j are Dirac fermions, and the couplings have the expressions

$$\begin{aligned}
v_{ij} =& \frac{1}{2\sqrt{2}} \left(g_q \sin\hat{\theta} (V_R)_{ij} + g \cos\hat{\theta} (V_{CKM})_{ij} \right) , \\
a_{ij} =& \frac{1}{2\sqrt{2}} \left(g_q \sin\hat{\theta} (V_R)_{ij} - g \cos\hat{\theta} (V_{CKM})_{ij} \right) , \\
v'_{ij} =& \frac{1}{2\sqrt{2}} \left(g_q \cos\hat{\theta} (V_R)_{ij} - g \sin\hat{\theta} (V_{CKM})_{ij} \right) , \\
a'_{ij} =& \frac{1}{2\sqrt{2}} \left(g_q \cos\hat{\theta} (V_R)_{ij} + g \sin\hat{\theta} (V_{CKM})_{ij} \right) .
\end{aligned}$$

We note that in general, g_H is a complex parameter: for example, it is complex in LR models, see Eq. (6.26). However, the transformation $g_H \to g_H e^{-i\alpha}$ (with α an arbitrary phase) on the Lagrangian (6.16) only results, after diagonalization of W-W' mixing, in $V_R \to e^{i\alpha} V_R$, therefore its effects are negligible for our scopes. Thus for simplicity we take g_H to be real. The charged current interactions for leptons have the form

$$\mathcal{L}^{\ell}_{cc} = W^+_\mu \cos\hat{\theta}\frac{g}{\sqrt{2}}\overline{\nu}^i_L\gamma^\mu e^i_L - W'^+_\mu \sin\hat{\theta}\frac{g}{\sqrt{2}}\overline{\nu}^i_L\gamma^\mu e^i_L\,. \tag{6.24}$$

The trilinear couplings involving the W', the W and the Higgs and the W' and two SM gauge bosons read

$$\begin{aligned}
\mathcal{L}_{W'Wh} &= \Big[-\frac{1}{2}g^2\sin\hat{\theta}\cos\hat{\theta} + \frac{g_H g}{\sqrt{2}}(\cos^2\hat{\theta}-\sin^2\hat{\theta}) + \frac{g_4^2}{2}\sin\hat{\theta}\cos\hat{\theta}\Big] \\
&\quad \times vh\,(W^{+\mu}W'^{-}_{\mu} + W^{-\mu}W'^{+}_{\mu})\,, &\text{(6.25a)}\\
\mathcal{L}_{W'W\gamma} &= -i\,e\,\delta_B\sin\hat{\theta}\cos\hat{\theta}F_{\mu\nu}(W^{+\mu}W'^{-\nu} + W'^{+\mu}W^{-\nu})\,, &\text{(6.25b)}\\
\mathcal{L}_{W'WZ} &= i\sin\hat{\theta}\cos\hat{\theta}\Big[(g\cos\theta_w + g'\sin\theta_w)(W^{-\mu}W'^{+}_{\nu\mu} + W'^{-\mu}W^{+}_{\nu\mu} - W'^{+\mu}W^{-}_{\nu\mu} \\
&\quad - W^{+\mu}W'^{-}_{\nu\mu})Z^\nu - (g\cos\theta_w + g'\sin\theta_w(1-\delta_B))\left(W^{+\mu}W'^{-\nu} + W'^{+\mu}W^{-\nu}\right)Z_{\mu\nu}\Big]\,, &\text{(6.25c)}
\end{aligned}$$

where θ_w is the weak mixing angle. Partial widths for decays into two-body final states are collected in App. A of Ref. [1] [8]. In summary, in addition to the W' mass, four couplings appear in our phenomenological Lagrangian: g_q, g_H (or equivalently the W-W' mixing angle $\hat{\theta}$), δ_B and g_4.

We conclude this section by commenting on the expected size of the couplings in concrete realizations of our effective theory. In partial compositeness the coupling of spin-1 resonances to light quarks (in our language this is given, for example, by $(V_R)_{11}\times g_q$) is expected to be small, because the latter are mostly elementary states[9]. Nevertheless, in models where the strong sector is assumed to be flavor-symmetric, so that MFV can be implemented [59], one of the chiralities of all SM quarks needs to be sizably composite and thus significantly coupled to the resonances. On the other hand, regardless of the flavor structure the coupling of the W' to heavy SM fermions ($(V_R)_{33}\times g_q$) and to longitudinal W, Z and to the Higgs (g_H) is expected to be large, typically leading to sizable branching ratios for the decays $W' \to tb, WZ, Wh$.

Our framework also describes the low energy limit of a LR model[10], provided the following identifications are made (see App. C of Ref. [1] for the notation)

$$\begin{gathered}
g = g_L\,, \qquad g' = \frac{g_X g_R}{\sqrt{g_X^2+g_R^2}}\,, \qquad g_q = g_R\,, \qquad g_H = -2\sqrt{2}g_R\frac{kk'e^{-i\alpha_1}}{v^2}\,, \\
\delta_B = 0\,, \qquad g_4^2 = g_R^2\,, \qquad \tilde{M}^2 = \frac{g_R^2 v_R^2}{4}\,, \qquad v^2 = 2(k^2+k'^2)\,.
\end{gathered} \tag{6.26}$$

[8] The correspondence with the notation of Ref. [1] is $\delta_B \equiv 1 + c_B$.

[9] Notice that because the SM does not contain any gauge boson with the quantum numbers of the iso-singlet W', in partial compositeness the latter does not mix with any elementary state in the limit of unbroken EW symmetry. It follows that the coupling of the resonance to light fermions is entirely proportional to their degree of compositeness. In other words, the analog of the second term in Eq. (6.5) is absent.

[10] Here we are assuming the Z' to be sufficiently heavier than the W', and neglecting effects coming from the different scalar spectrum.

Notice that $\delta_B = 0$ is not special of LR models, but rather holds at tree level in *any* theory where the W' is a gauge boson. This makes the W'-W-γ coupling in Eq. (6.25b) especially interesting, as we will discuss below.

Finally, we wish to mention that t-channel exchange of a W' was proposed [148] as an explanation of the anomaly in the forward-backward asymmetry of $t\bar{t}$ pairs ($A_{FB}^{t\bar{t}}$) observed by the Tevatron experiments. To solve the puzzle, the W' should couple only to t and d quarks: for example, in Refs. [149] it was shown that the observed asymmetry can be reproduced with the introduction of a right-handed W' with mass in the range $200 \div 600$ GeV, and coupling W'-t-d of magnitude $0.85 \div 2.1$. Such W' is described by our framework, where the right-handed mixing matrix does not need to be unitary, and as a consequence it can accommodate a large W'-t-d coupling, while having the remaining entries tuned to evade, *e.g.*, the strong bounds coming from meson mixing.

6.4 Pre-LHC bounds

6.4.1 Indirect bounds

The indirect bounds on the couplings that appear in our Lagrangian can be summarized as follows:

- The main indirect constraints on g_q come from $\Delta F = 2$ transitions. K-meson mixing gives the strongest bound, which however is very sensitive to the assumed form for the right-handed quark mixing matrix V_R (we remark that V_R does not need to be unitary in our effective approach). It was shown in Ref. [150] that for some special choices of V_R the constraint from K mixing is weakened significantly. We choose for our phenomenological analysis the least constrained of these special forms, namely

$$|V_R| = \mathbb{1}_3 \,, \tag{6.27}$$

  for which the bound reads at 90% CL [150]

$$M_{W'} > \frac{g_q}{g}\, 300 \text{ GeV} \,. \tag{6.28}$$

  We note that in specific models, the bound can be much stronger: for example, if a discrete symmetry (P or C) relating the left and right sectors is imposed in LR models, then the bound reads approximately $M_{W'} > (2-3)\,\text{TeV}$ [151]. This happens because the discrete symmetry forces V_R to be close to V_{CKM}, implying a mixing of the order of the Cabibbo angle between the first two generations. The bound in Eq. (6.28) is negligible with respect to the constraints coming from Tevatron direct searches (see the next paragraph). Also notice that, as discussed in Ref. [150], this bound still holds if each $(V_R)_{ij}$ is varied of $\epsilon = 0.01$ from its central value, so that extreme fine tuning is avoided. In addition, the form in Eq. (6.27) automatically satisfies constraints from B mixing.

- $\hat{\theta}$ is constrained by the electroweak T parameter and by $u \to d, s$ transitions. The W-W' mixing generated by Eq. (6.18) breaks custodial symmetry and gives rise to a tree-level, negative contribution to T. We find

$$\hat{T}_V = -\frac{\Delta^4}{M^2 m_{\hat{W}}^2} \qquad \Longrightarrow \qquad \left|\frac{g_H}{M}\right| < 0.17\,\text{TeV}^{-1} \tag{6.29}$$

at 95% CL[11]. We can translate the constraint on $|g_H/M|$ into an upper bound on $\hat{\theta}$: the resulting limit becomes stronger when the mass of the W' is increased, and varies from $|\hat{\theta}| \lesssim 8 \times 10^{-3}$ for $M_{W'} = 300\,\text{GeV}$ to $|\hat{\theta}| \lesssim 1 \times 10^{-3}$ for $M_{W'} = 2$ TeV. An independent bound on the mixing angle $\hat{\theta}$ comes from the precise low-energy measurement of $u \to d$ and $u \to s$ transitions (*i.e.* from the measurements of the corresponding entries of the CKM matrix). Integrating out both the W and the W', we obtain a four-fermion effective Lagrangian that can be used to compute constraints from such measurements. The operators relevant to semileptonic processes, which give the strongest bounds, are

$$\mathcal{L}_{\text{eff}} = -\frac{4G_F}{\sqrt{2}}\,\overline{u}\,\gamma^\mu\Big[(1+\epsilon_L)V_{CKM}P_L + \epsilon_R V_R P_R\Big]d\,(\overline{\ell}_L\gamma_\mu\nu_L^\ell) + \text{h.c.}\,, \tag{6.30}$$

where, neglecting $O(v^4/M_{W'}^4)$ terms, $\epsilon_L = 0$ and $\epsilon_R = g_q\,\hat{\theta}/g$. In Ref. [152] the bound $\epsilon_R\,\text{Re}(V_R^{ud}) = (0.1 \pm 1.3) \times 10^{-3}$ was obtained, which assuming small CP phases implies at 95% CL

$$-\,2 \times 10^{-3} \lesssim \epsilon_R V_R^{ud} \lesssim 3 \times 10^{-3}\,. \tag{6.31}$$

On the other hand, such bound is strongly relaxed if CP phases in V_R are large: in the limit where the phases are maximal, only a milder second-order constraint survives, leading (assuming $V_R^{ud} \approx 1$) roughly to $|\epsilon_R| < 10^{-(2\,\div\,1)}$, as discussed in Ref. [150].

- The parameter δ_B is weakly constrained by Trilinear Gauge Couplings (TGC). The WWV_0 vertex ($V_0 = \gamma, Z$) can be described, assuming C and P conservation, by an effective Lagrangian containing 6 parameters (see for example Ref. [153]):

$$\mathcal{L}_{\text{eff}}^{WWV_0} = i g_{WWV_0}\Big[g_1^{V_0}V_0^\mu(W^-_{\mu\nu}W^{+\nu} - W^+_{\mu\nu}W^{-\nu}) + k_{V_0}W^+_\mu W^-_\nu V_0^{\mu\nu} + \frac{\lambda_{V_0}}{m_W^2}V_0^{\mu\nu}W^{+\rho}_\nu W^-_{\rho\mu}\Big]$$

where $g_{WW\gamma} = e$, $g_{WWZ} = g\cos\theta_w$, and the SM values of the parameters are given by $g_1^{\gamma,Z} = \kappa_{\gamma,Z} = 1$ and $\lambda_{\gamma,Z} = 0$. Assuming $SU(2)_L \times U(1)_Y$ gauge invariance reduces the number of independent parameters to three, which can be taken to be $\Delta g_1^Z \equiv g_1^Z - 1$, $\Delta k_\gamma \equiv k_\gamma - 1$, and λ_γ. In the case under discussion, the expressions of these parameters read

$$\Delta g_1^Z = -\sin^2\hat{\theta}(1 + \tan^2\theta_w)\,, \qquad \Delta k_\gamma = -\sin^2\hat{\theta}\,\delta_B\,, \qquad \lambda_\gamma = 0\,. \tag{6.32}$$

Thus we can use the fits to LEP2 data, performed by the LEP experiments letting $\Delta g_1^Z, \Delta k_\gamma$ free to vary while keeping fixed $\lambda_\gamma = 0$, to constrain the values of our model parameters $(\delta_B, \hat{\theta})$. By combining this limit with the upper bound on the mixing angle $\hat{\theta}$ presented in the previous subsection, we can in principle constrain δ_B. However, since as discussed above the mixing angle is required to be very small, in practice TGC constrain only extremely weakly the value of δ_B. For example, using the analysis performed by the DELPHI Collaboration [154], we find that even considering a very large mixing angle $|\hat{\theta}| \sim 10^{-1}$, the wide range $-19 < \delta_B < 12$ is allowed by TGC measurements at 95% CL.

- g_4 is essentially unconstrained, and it plays a marginal role in our analysis: it only affects (in a subleading way) the partial width for the decay $W' \to Wh$, see Eq. (6.25a).

[11] The bound quoted here was obtained using the EW fit in Appendix B. It is slightly less stringent than the one given in Ref. [1], which read $|g_H/M| < 0.12\,\text{TeV}^{-1}$.

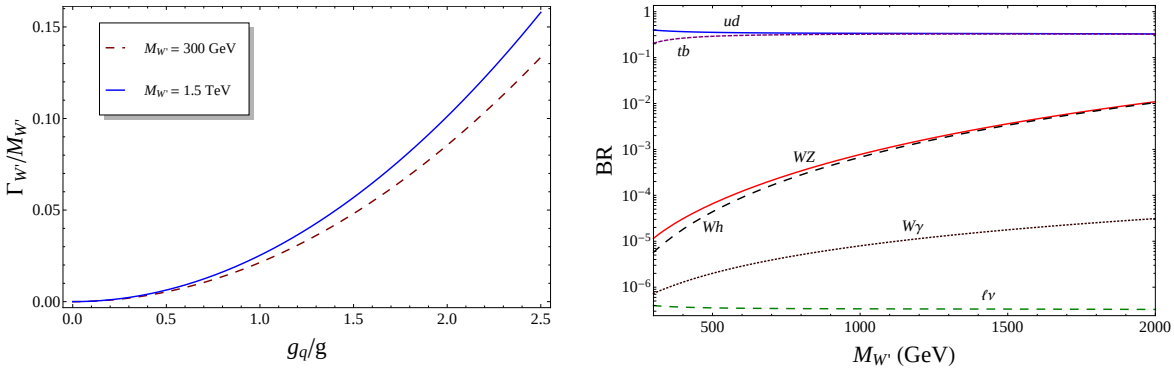

Figure 6.2: *(Left panel)* W' width over mass ratio as a function of g_q/g for negligible mixing, $\hat{\theta} \approx 0$, for $M_{W'} = 300\,\text{GeV}$ (dashed, red) and 1.5 TeV (blue). *(Right panel)* Branching ratios of the W' as a function of its mass, for the following choice of the remaining parameters: $g_q = g$, $\hat{\theta} = 10^{-3}$, $\delta_B = -2$, $g_4 = g$. From top to bottom: ud, tb, WZ, Wh, $W\gamma$, $\ell\nu$ (the latter includes all the three lepton families).

6.4.2 Tevatron bounds

Data collected by the CDF and D0 experiments at the Tevatron in the dijet and tb final states[12] can be used to set an upper limit on the coupling to quarks of the W' as a function of its mass. In this section, we assume negligible W-W' mixing, $\hat{\theta} \approx 0$, so the only relevant parameters are the W' mass and the coupling g_q, and we obtain an upper bound on g_q as a function of $M_{W'}$. If W-W' mixing happens to be sizable, then the branching ratio into quarks is reduced, and the upper bound on g_q gets relaxed accordingly. For instance, taking the relatively large value $\hat{\theta} = 10^{-2}$, the upper bound on g_q is relaxed by approximately 10% for $M_{W'} \gtrsim 1\,\text{TeV}$, and less for lighter W'. The dependence of the ratio $\Gamma_{W'}/M_{W'}$ on the coupling g_q is plotted in the left panel of Fig. 6.2, while the branching ratios as functions of $M_{W'}$ are shown in the right panel of the same figure, for representative values of the parameters.

- Searches for resonances in the invariant mass spectrum of dijet events at CDF and D0 are sensitive to the W' we are discussing, which decays into quarks with branching ratio close to unity. The most recent dijet search, based on 1.13 fb^{-1} of data, has been performed by the CDF Collaboration [155]. Since no discrepancy with the SM prediction was observed, upper limits on the product $\sigma(p\bar{p} \to W' \to jj) \times \mathcal{A}$, where $\mathcal{A}$ is the geometrical acceptance for having both jets with $|y| < 1$, have been set in Ref. [155] for several types of resonance, including a W'. Therefore, we can compute $\sigma(p\bar{p} \to W' \to jj) \times \mathcal{A}$ using our phenomenological Lagrangian, and extract an upper bound on g_q for each value of $M_{W'}$, which is reported in the left panel of Fig. 6.3. We compute cross sections at Leading Order (LO), using the CalcHEP matrix element generator [156], and make use of the CTEQ6L set of parton distribution functions [116].

  The acceptance $\mathcal{A}$ is 36% at $M_{W'} = 300\,\text{GeV}$, reaches a maximum of 51% for $M_{W'} \sim 800$ GeV, and decreases for larger masses, being 34% at 1.4 TeV. The decreasing behavior of the acceptance at high resonance masses is due to a threshold effect: for a W' mass around 1 TeV and above (that is, close to the kinematic limit of the Tevatron, which had a center of mass energy of 1.96 TeV), the probability that the on-shell production

[12] By tb we will always mean the sum $t\bar{b} + \bar{t}b$.

condition $x_1 x_2 \approx M_{W'}^2/s$ is satisfied is so small that the off-shell contribution to the $p\bar{p} \to W' \to jj$ cross section becomes relevant, making the acceptance behave differently from what we would naively expect for an on-shell production mechanism. As discussed in detail in Ref. [1], for $M_{W'} \gtrsim 800\,\text{GeV}$ the Narrow Width Approximation (NWA) is not reliable anymore, so we take into account off-shell effects when computing our limits at high masses.

The method we used to compute limits is valid for a resonance width smaller than the dijet energy resolution, which for the CDF experiment is of the order of 10% of the dijet mass. The W' we are studying has a width of $\sim 10\%$ of its mass for $g_q \sim 2g$; for larger couplings, the resonance width cannot be neglected, and the analysis would need to be corrected for this effect.

- Another final state which is relevant to our model is tb. The CDF and D0 Collaborations have searched for narrow resonances decaying into tb, with the W coming from the top decaying into a lepton and missing transverse energy. The most recent search is from D0, based on 2.3 fb^{-1} of data [157], and gives as result an upper limit on $\sigma(p\bar{p} \to W' \to tb)$. Therefore we compute the latter quantity using our phenomenological Lagrangian, and extract an upper bound on g_q for each value of the W' mass, which is shown in the left panel of Fig. 6.3. Similarly to what happened for the dijet final state, also in the tb channel threshold effects become relevant for $M_{W'} \gtrsim 800$ GeV, and correspondingly the NWA cannot be trusted.

6.5 LHC phenomenology

6.5.1 Dijet final state

Here we outline our strategy for estimating the reach of LHC dijet searches[13] on the W'. Following CMS [159], we assume kinematic cuts on the pseudorapidity $|\eta| < 2.5$ of each jet, and on the pseudorapidity difference $|\Delta\eta| < 1.3$. For values of $M_{W'}$ between 300 GeV and 2.6 TeV, in intervals of 100 GeV, we compute as a function of the coupling g_q the integral of the signal differential invariant mass distribution $d\sigma_S/dM_{jj}$ over the region $M_{jj} > M_{W'}(1-\epsilon/2)$, and compare the result with the integral of the background distribution over the same range, to obtain 95% CL exclusion contours in the $(M_{W'}, g_q/g)$ plane. Here ϵ is the dijet mass resolution, which following Ref. [159] we assume to vary from 8% at $M_{W'} = 500$ GeV to 5% at 2.5 TeV. We choose to compare the integrals over $M_{jj} > M_{W'}(1-\epsilon/2)$ of the signal and background differential dijet mass distributions rather than their integrals in a finite interval centered on the W' mass, because the former method is less sensitive to smearing effects generated by hadronization and jet reconstruction, which we cannot take into account in our parton-level analysis. In this way, we expect our parton-level estimate of the reach of the LHC to be closer to the actual experimental results than it would be if we compared signal and background in an interval centered around the W' mass. The results are shown in the left panel of Fig. 6.3 for two different integrated luminosities, namely 1 and 5 fb^{-1}, at LHC7. In the same figure we also show the exclusions obtained from the ATLAS and CMS dijet resonance searches based on 1 fb^{-1} [160]. Our estimate is found to be in fairly good

[13] In addition to those in the dijet final state, also LHC searches in the tb channel are relevant to the W' we are studying. We do not discuss them here, and refer the reader to the extensive analysis of Ref. [158].

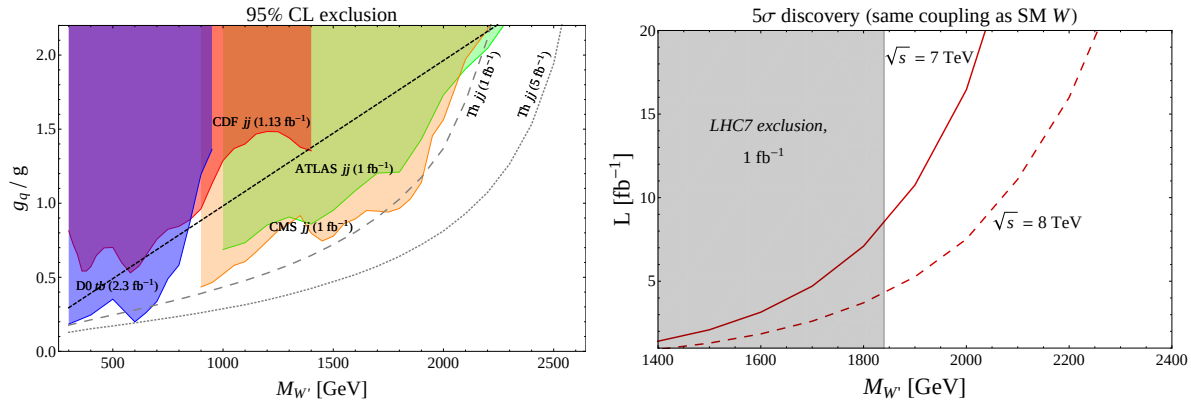

Figure 6.3: (*Left panel*) Current bounds in the plane $(M_{W'}, g_q/g)$ from Tevatron searches in the tb (blue) and dijet channel (red), from LHC searches for resonances decaying into dijets (green and pink), and from the CMS search for quark compositeness (dashed straight line). The exclusion expected from LHC dijet resonance searches after 1 and $5\,\text{fb}^{-1}$, computed in Ref. [1], are also shown as dashed lines. (*Right panel*) Discovery luminosity as a function of the W' mass, assuming a coupling $g_q = g$, at LHC7 and LHC8.

agreement with the exclusion bounds extracted from real data, confirming the reliability of our simple method.

In addition, we compute the bound coming from the CMS search for quark compositeness in dijet angular distributions [62]: by integrating out the W' and applying Fierz identities, we find the effective four-quark operator

$$\frac{g_q^2}{2M_{W'}^2}\overline{u}_R\gamma^\mu u_R\overline{d}_R\gamma_\mu d_R\,, \tag{6.33}$$

leading to the bound [63]

$$\frac{M_{W'}}{g_q} > \frac{2.2\ \text{TeV}}{\sqrt{2}}\,, \tag{6.34}$$

which is shown in the left panel of Fig. 6.3 as a dashed line. As expected, the bound from searches for contact interactions is more relevant for strongly coupled resonances.

In the right panel of Fig. 6.3, we show the integrated luminosity needed for $5\,\sigma$ discovery of a W' with coupling to quarks equal to that of the SM W ($g_q = g$), both for the 7 and 8 TeV LHC, as a function of $M_{W'}$. We see that after the bound from $1\,\text{fb}^{-1}$ of 7 TeV dijet data is taken into account, a discovery at 8 TeV would be possible only in the narrow range $1.8 \lesssim M_{W'} \lesssim 2.2$ TeV.

6.5.2 W + photon final state

We now move on to consider decay channels of the W' which have partial widths proportional to the W-W' mixing angle $\hat{\theta}$. These include WZ, Wh and $W\gamma$ final states. We will focus first on the last channel, which is of special interest since it is very suppressed if the W' is a gauge boson, as we will discuss. It follows that observation of $W' \to W\gamma$ would point to a composite nature of the W'. The partial width for decay into $W\gamma$ reads, for $M_{W'} \gg m_W$

$$\Gamma(W' \to W\gamma) \simeq \frac{e^2}{96\pi}\delta_B^2\,\hat{\theta}^2\,\frac{M_{W'}^3}{m_W^2}\,, \tag{6.35}$$

where $\hat{\theta} \simeq -\sqrt{2}\,(g_H/g)(m_W^2/M_{W'}^2)$.[14] Since the width for decay into this channel is controlled by $\hat{\theta}$ and δ_B, it is interesting to estimate which values of these parameters have been tested by the LHC in its first runs. To assess the discovery potential, we focus on one benchmark value for the W' mass[15], $M_{W'} = 800$ GeV, and we assume two representative values of the integrated luminosity, namely 1 and 5 fb^{-1}, at a center of mass energy of 7 TeV. As for the coupling to quarks, in Ref. [1] we had set it to $g_q = 0.84\,g$, which is however now excluded, the maximum allowed value being[16] $g_q \simeq 0.58\,g$, see Fig. 6.3. However we note that, since the total width of the resonance is dominated by the decay into light quarks, the scaling

$$\sigma(pp \to W' \to W\gamma) \sim g_q^2\,\frac{\Gamma(W' \to W\gamma)}{g_q^2} \tag{6.36}$$

holds, which implies that the analysis in the $W\gamma$ channel (and in any other rare channel as well, for example WZ) is only weakly sensitive to the value of g_q. As a consequence, we expect the results of Ref. [1] to hold also for the slightly smaller g_q we need to take to comply with current bounds.

We select decays of the W into an electron and a neutrino, and apply the following cuts on the $e\gamma\not{E}_T$ final state: $p_T^\gamma > 250$ GeV, $p_T^e > 50$ GeV, $\not{E}_T > 50$ GeV, $|\eta_{e,\gamma}| < 2.5$, and $|M(W\gamma) - M_{W'}| < 0.05\,M_{W'}$. We note that, even though the neutrino longitudinal momentum p_z^ν is not measured experimentally, it can be reconstructed by imposing that the lepton and neutrino come from an on-shell W: a quadratic equation for p_z^ν is thus obtained. It follows that a criterion must be chosen to unfold this ambiguity. The assessment of the effects of such choice on the cuts on $\not{E}_T$ and on the total invariant mass $M(W\gamma)$ goes beyond the scope of this exploratory study, and we leave it to the experimental collaborations. We neglect the interference between W and W', which is due to the $O(\hat{\theta})$ coupling of W' to left-handed quark currents. The main background process is the SM $W\gamma$ production, which we included in our analysis, while we left out the $W + j$ production with the jet misidentified as a photon. We have checked that applying the rejection factor for misidentification into a γ of very high-p_T jets, which is of the order of 5×10^3 if photon identification and isolation cuts are applied (see, *e.g.*, Ref. [161]), the $W + j$ background contribution is roughly one order of magnitude smaller than the irreducible $W\gamma$ process. This estimate suffers from the fact that we are not including NLO corrections to $W + j$, and from the fact that requiring photon identification and isolation has an efficiency of $\sim 80\%$ on 'real' photons [161], which would slightly reduce the number of signal events detected. Other possibly relevant instrumental backgrounds that we do not include in our study are $ee\not{E}_T$ with e misidentified as a photon, and QCD jets faking $e + \not{E}_T$. We leave the proper treatment of such detector-dependent backgrounds to the experimental analyses.

Our main results are shown in Fig. 6.4. As can be read from the left panel, assuming $\delta_B = 6$ the interval $5 \times 10^{-3} < \hat{\theta} < 1.25 \times 10^{-2}$ is accessible for a discovery with 5 fb^{-1}. For comparison, the bound from T reads $|\hat{\theta}| \lesssim 3 \times 10^{-3}$. This tension could be relaxed by extra new physics contributing positively to T (such as, for example, a heavy Z'). On the other hand, from the right panel of Fig. 6.4 we see that setting the mixing angle to the value $\hat{\theta} = 10^{-2}$, discovery of a W' with mass 800 GeV is possible with 5 fb^{-1} for $\delta_B \gtrsim 3$. For

[14] Notice that $\Gamma(W' \to W\gamma)$ is suppressed by a factor $m_W^2/M_{W'}^2$ compared to $\Gamma(W' \to WZ)$: the latter has an extra enhancement due to the longitudinal polarization of the Z.

[15] In Ref. [1] a second benchmark was also studied, with $M_{W'} = 1.2$ TeV.

[16] Notice that the upper limit on g_q from Tevatron searches in quark final states was computed for $\hat{\theta} = 0$; when the mixing is introduced, the bound on the coupling weakens, due to the smaller branching ratio of the resonance into quarks.

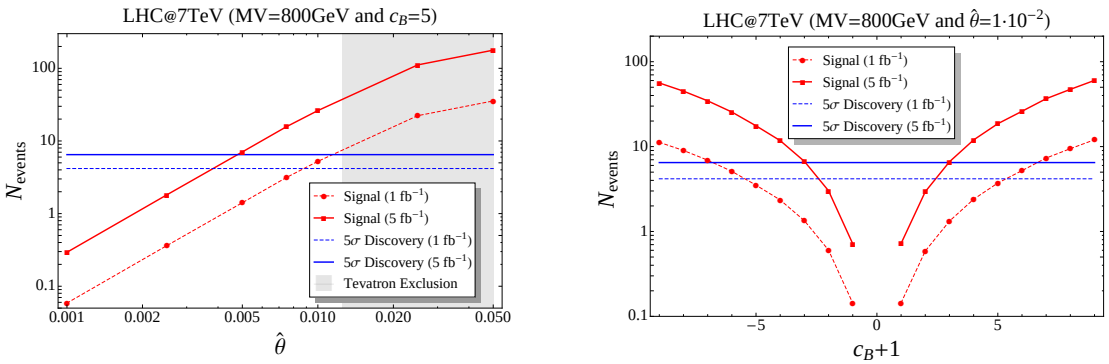

Figure 6.4: 5σ discovery prospects of the 7 TeV LHC for the $W' \to W\gamma \to e\nu\gamma$ process, for $M_{W'} = 800$ GeV. $N_{\rm events}$ is the number of signal events after applying the cuts described in the text. The red curves show the expected number of events as a function of the parameters of our phenomenological Lagrangian ($c_B + 1 \equiv \delta_B$), whereas the blue flat lines represent the number of events needed for a 5σ discovery, taking into account the SM background. The signal cross sections, after all cuts, are simply given by $\sigma_S = N_{\rm events}/L$; the background cross section after all cuts is $\sigma_B = 9.6 \times 10^{-2}$ fb. The region shaded in grey is excluded at 95% CL by Tevatron searches for resonances decaying into WZ, see Ref. [1].

δ_B	$N_{\rm s}$	$N_{\rm bckgr}$	N_σ
0.6	57	102	5.7
0.5	40	102	4.0
0.4	26	102	2.6

Table 6.1: Sensitivity on δ_B at the 14 TeV LHC with 300 fb^{-1}, for $M_{W'} = 800$ GeV and $\hat\theta = 10^{-2}$.

illustrative purposes, we also give in Table 6.1 an estimate of the sensitivity on δ_B of the 14 TeV LHC after 300 fb^{-1}. Background events are due to the irreducible SM $W\gamma$ process only. Cuts on the final state kinematics are the same as for the early LHC case discussed above.

Clearly, it is crucial to understand what are the predictions for the strength of the $W'W\gamma$ coupling in explicit theories described by our parameterization. To this extent, it is useful to write down the expression of the W'-W'-γ coupling

$$\mathcal{L}_{W'W'\gamma} = ie\left[A_\nu(W'^{+}_{\mu\nu}W'^{-\mu} - W'^{-}_{\mu\nu}W'^{+\mu}) + k'_\gamma F_{\mu\nu}W'^{+\mu}W'^{-\nu}\right] , \tag{6.37}$$

where $k'_\gamma = 1 - \cos^2\hat\theta\,\delta_B$. From Eq. (6.37) we can extract the expression of the magnetic dipole moment of the W'

$$\mu_{W'} = \frac{e}{2M_{W'}}\, g_{W'} , \qquad g_{W'} \equiv 1 + k'_\gamma = 2 - \cos^2\hat\theta\,\delta_B , \tag{6.38}$$

where $g_{W'}$ is the gyromagnetic ratio of the resonance. Now the g of any elementary particle of mass M (of any spin) coupled to the photon has to be equal to 2 at tree level in order for perturbative unitarity to be preserved up to energies $E \gg M/e$ [86]. As a consequence, in any theory where the W' is associated to a (spontaneously broken) gauge symmetry, at tree-level one finds $g_{W'} = 2$, since unitarity is preserved up to scales much larger than $M_{W'}$. From Eq. (6.38) it thus follows that if the vector is a gauge boson, $\delta_B = 0$ holds at tree

level. Indeed, in the 'minimal' gauge model containing an isosinglet W', namely a LR model, we find that $\delta_B = 0$ at tree level. Corrections to this equality will be loop-suppressed, so observation of the decay $W' \to W\gamma$ is likely to be out of the reach of the LHC.

On the other hand if the W' is a composite state, then significant departures from $\delta_B = 0$ can be envisaged. The only condition that needs to be satisfied even in the composite case is that the scale of violation of perturbative unitarity be sufficiently larger than the W' mass, in order to retain control on the theory at the scales $E \sim M_{W'}$ that are relevant for the LHC phenomenology. To verify that this is indeed the case, and since δ_B only appears in the BVV vertex (see Eq. (6.18)), where B is the hypercharge gauge boson and V is the extra vector, we compute the amplitude for $BB \to VV$ scattering. The two independent amplitudes that grow the most with energy are $B_+B_\pm \to V_LV_L$, where $B_\pm$ are the two transverse polarizations of the B, and V_L is the longitudinally polarized V. The leading term of these amplitudes in the high-energy limit reads

$$A_{++\to LL} \approx \delta_B(2-\delta_B)\frac{g'^2 s}{2M^2}\,, \qquad A_{+-\to LL} \approx \delta_B^2 \frac{g'^2 s}{4M^2}\,. \tag{6.39}$$

Notice that for $\delta_B \to 0$ the dangerous high-energy behavior is removed, as it was anticipated above. Requiring the amplitudes in Eq. (6.39) not to exceed $16\pi^2$, we find the cut-off Λ at which perturbative unitarity is lost, as a function of δ_B: taking the maximum value we used in the phenomenological analysis, namely $\delta_B \approx 10$, we find $\Lambda \approx 5M$; for smaller values of δ_B, the cut-off is obviously larger. This result guarantees that we can safely study the phenomenology at scale M with relatively large values of δ_B, without encountering any perturbative unitarity violation issues. We conclude that, since the size of the $W'W\gamma$ coupling is expected to be very small if the W' is a fundamental gauge boson, observation of $W' \to W\gamma$ at the LHC would be a hint of the composite nature of the W'. The situation is completely analogous for the other phenomenologically relevant type of W', the one belonging to a $(\mathbf{1},\mathbf{3})_0$: the $W'W\gamma$ coupling vanishes at tree level if the heavy vector is a gauge boson, but could be sizable for a composite state[17].

As a concluding remark, we wish to note that a similar situation could in principle have been faced in the early days of the SM, when trying to build a theory of the weak scale. In fact, in the 1950s or early 1960s, having established beyond any reasonable doubt the correctness of a gauge theory based on $U(1)_Q$ at low energies, one could have tried to couple new hypothetic heavy states to the known particles (the light fermions and the photon) by assuming only the electromagnetic gauge invariance. For a vector with electric charge $Q = 1$, the Lagrangian would have read[18]

$$\mathcal{L}_W = M_W^2 W_\mu^+ W^{-\,\mu} + D_\mu W_\nu^- D^\nu W^{+\,\mu} - D_\mu W_\nu^- D^\mu W^{+\,\nu} + ie(1-\delta_Q)F^{\mu\nu}W_\mu^+ W_\mu^- + \dots \tag{6.40}$$

with δ_Q a dimensionless parameter. $F^{\mu\nu}$ is the photon field-strength, and the covariant derivative has the standard expression $D_\mu = \partial_\mu - ieQA_\mu$. Equation (6.40) leads to $g_W = 2 - \delta_Q$: if the W is associated to a beyond-QED gauge symmetry, then $\delta_Q = 0$ and the g is equal to 2 (at tree level). One could thus have suggested to use the measurement of the gyromagnetic ratio of the W as a handle to infer whether the vector was a gauge boson or not, much in the same way we are now suggesting to search for the decay $W' \to W\gamma$ to

[17] Despite the close similarity, however, the results of our phenomenological study do not directly apply to the triplet W', because the constraints on the latter are different (and stronger) than those for the iso-singlet W'.

[18] The dots stand for couplings to fermions, which are not relevant for the goal of this discussion.

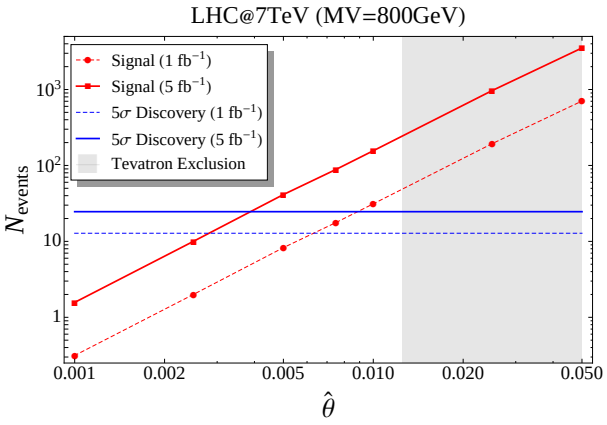

Figure 6.5: 5σ discovery prospects on the mixing angle $\hat{\theta}$ via the $W' \to WZ \to e\nu jj$ process at the 7 TeV LHC, for $M_{W'} = 800\,\text{GeV}$. The results are essentially independent of δ_B. The interpretation of the curves is analogous to Fig. 6.4; after all cuts, the background cross section is $\sigma_B = 3.5\,\text{fb}$. The region shaded in grey is excluded at 95% CL by Tevatron searches for resonances decaying into WZ.

uncover the true nature of a W'. While this is certainly not the path the history of the SM has followed, the analogy is nevertheless amusing.

6.5.3 $W + Z$ final state

We briefly discuss the $W' \to WZ$ decay, which is complementary to $W' \to W\gamma$ because its measurement would allow one to estimate the size of the mixing angle $\hat{\theta}$ (the rate for WZ production is only very weakly dependent on δ_B). Since we consider the early LHC reach, where the available luminosity is $\lesssim 5\ \text{fb}^{-1}$, the most promising final state is $WZ \to \ell \not{E}_T jj$, which has a larger rate with respect to the purely leptonic channel; on the contrary, selecting leptonic decays of the Z together with a hadronic W has been shown to be less promising [162]. Therefore, we implement simple cuts on the $e\nu jj$ final state (we only consider W decays into an electron, in analogy to what we did for the $W' \to W\gamma$ process) to enhance the ratio of signal over background, namely: $p_T^{e,j} > 50\,\text{GeV}$, $\not{E}_T > 50\,\text{GeV}$, $|\eta_{e,j}| < 2.5$, and in addition we require the invariant mass of the dijet system to reconstruct a Z, $|M(jj) - M_Z| < 20\,\text{GeV}$. Finally, we select events which have an invariant mass compatible with $M_{W'}$ as follows: $|M(e\nu jj) - M_{W'}| < 0.10 M_{W'}$. The background we consider is the SM $pp \to e\nu jj$, which includes a large contribution from $W + jj$. The $t\bar{t}$ background can be efficiently reduced to roughly one order of magnitude less than the QCD background by applying a central jet veto [162], and we do not consider it here.

Our results are shown in Fig. 6.5 for the same choices of the W' mass and couplings that we already discussed when studying $W' \to W\gamma$, so that a direct comparison between the two searches can be made. We can see that with $5\ \text{fb}^{-1}$, a mixing angle $|\hat{\theta}| \gtrsim 4 \times 10^{-3}$ is accessible for discovery; this result is to a very good approximation independent of the size of δ_B. We also notice that the number of signal events can be sizable, which is the main reason why this channel is more favorable than the purely leptonic one for limited LHC luminosity. We remark that the size of the cut on the total invariant mass of $e\nu jj$ agrees with Ref. [162], where it was chosen to retain most of the signal in the presence of jet energy smearing. In

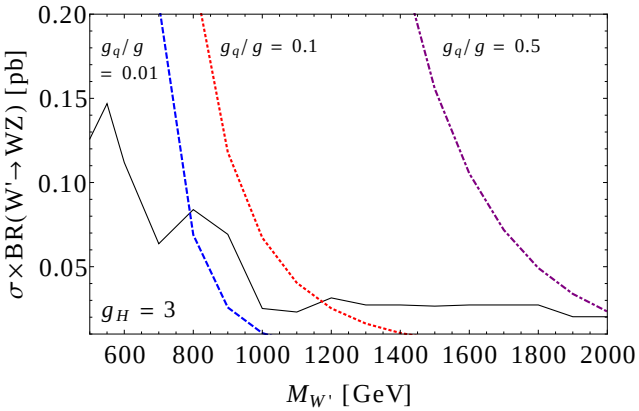

Figure 6.6: Comparison of the current experimental bound on $\sigma \times \mathrm{BR}(W' \to WZ)$ from $W' \to 3\ell + \nu$ searches [163] (black solid line) with the theoretical predictions for $g_H = 3$, representative of the partial compositeness scenario. The branching ratio $\mathrm{BR}(W' \to WZ)$ is $\sim 50\%$ for g_q/g in the range $0.01 \div 0.5$.

addition, the cut we set on the invariant mass of the jj system is even looser than the one adopted in Ref. [162]. Therefore we believe our results to be reasonably stable with respect to jet smearing, which was not included in our parton-level analysis.

The most recent search for resonances decaying to WZ is the one performed by the CMS Collaboration in the fully leptonic $(3\ell+\nu)$ final state, based on $\sim 20\,\mathrm{fb}$ of data at 8 TeV [163]. For our benchmark point, namely $M_{W'} = 800$ GeV and $g_q = 0.58\,g$, we obtain a bound on the mixing angle $|\hat{\theta}| \lesssim 3 \times 10^{-3}$. It is also interesting to consider a choice of parameters roughly representative of the partial compositeness scenario: in this case g_H is expected to be large, since both the W' and the Higgs are composites. Therefore we set $g_H = 3$, and vary g_q/g in the wide range $0.01 \div 0.5$. Notice that a large value of g_H can be compatible with constraints in this case: thanks to custodial symmetry, the contribution to the T parameter of the W' is automatically canceled by the associated Z', and the bound from the CKM matrix elements in Eq. (6.31) can be satisfied for small enough g_q. The comparison of the theoretical cross sections[19] with the CMS bound is shown in Fig. 6.6: for example, for $g_q = 0.5\,g \sim 0.3$, which could be realized in models with MFV, the lower bound on the mass of the W' is about 2 TeV.

Finally, we do not discuss the W' decay into Wh, and we refer the interested reader to Ref. [74].

[19]Notice that W' production via vector boson fusion, which is not considered here, can be relevant for very small g_q.

Chapter 7

Conclusions

The discovery of a new particle with mass $m_h \approx 125$ GeV and properties compatible with those of the Standard Model (SM) Higgs boson marked a milestone in the quest of the LHC to unveil the dynamics of electroweak symmetry breaking. If the electroweak scale is natural, then two broad scenarios can be envisaged for physics at the TeV: supersymmetry and compositeness. In this thesis we focused on the second possibility, and discussed several topics in the LHC phenomenology of theories where the Higgs is a composite state, bound by a new strong interaction. We studied possible signals from each sector of the theory, namely from scalars, fermions and vectors. In all cases, an approach as model-independent as possible was employed, as it is appropriate given our relatively limited knowledge of the strong dynamics.

In Chapter 2 we introduced models that concretely realize the Higgs as a composite state. A broad feature is that the Higgs emerges as the pseudo-Nambu Goldstone Boson associated to a spontaneously broken global symmetry of the strong sector, in analogy to the QCD pions. In addition, partial compositeness (which arises from *linear* mixings between elementary and composite states, and is automatically implemented in extra-dimensional 'holographic' models) leads to the so-called RS-GIM mechanism: effects from the light quarks are suppressed by the corresponding small mixings. Partial compositeness leads to a fairly satisfactory flavor picture in the quark sector, although some tension remains, as we briefly discussed. Another broad feature is that naturalness and the small observed value of the Higgs mass imply the presence of light ($\sim$ TeV) fermionic resonances. These colored states should be observed at the LHC in the upcoming 14 TeV run. We concluded the chapter by a short discussion of Little Higgs models, which realize the hierarchy $v \ll f$ in a natural way by means of the collective breaking mechanism, and commented on the compatibility of these models with the Electroweak Precision Tests (EWPT) of the SM.

We started Chapter 3 by presenting the electroweak chiral Lagrangian, where the SM gauge symmetry is nonlinearly realized, and we immediately applied it to discuss bounds from EWPT on composite Higgs models. Together with flavor, agreement with precision data is one of the long-standing issues of strongly coupled models. Indeed we found strong constraints: $\xi = v^2/f^2 \lesssim 0.08$ must be satisfied, corresponding to a tuning *at least* worse than 10% . This bound can however be relaxed, if a positive contribution to T is generated from UV physics. Motivated by early LHC data, which hinted at an enhancement of the hZZ coupling over the hWW one, we investigated the consequences of giving up custodial symmetry in the Higgs couplings. This has a dramatic effect on T, which now receives *quadratically* divergent corrections. We concluded that extra light degrees of freedom would be needed

to restore agreement with EWPT. We presented our methodology for taking into account custodial breaking when fitting to Higgs data, and discussed the current determinations by ATLAS and CMS of the parameter $\lambda_{WZ} = a/(a + a_{cb})$, which measures custodial breaking. The custodial-preserving point $\lambda_{WZ} = 1$ is currently within the 95% allowed region for both experiments. We concluded the chapter by presenting the Strongly Interacting Light Higgs (SILH) Lagrangian, where the physical Higgs is assumed to be part of a doublet together with the longitudinal W and Z. New physics effects are described by a set of dimension-6 operators, with coefficients dictated by a power-counting that takes into account the Goldstone nature of the Higgs.

Chapter 4 was entirely dedicated to several aspects of the LHC phenomenology of a composite Higgs. First we focused on the radiative couplings to gluons and photons, including by means of the Higgs Low-Energy Theorem (LET) the effects of fermionic resonances, the 'top partners', which are expected to be light by naturalness arguments and could thus give sizable effects. In most models, however, the effects of top partners are known to cancel out exactly in the amplitudes for $gg \to h$ and $h \to \gamma\gamma$. We reviewed the symmetry reason behind this result, and verified that the latter is not altered by corrections to the LET.

Then we extended the LET to double Higgs production, and found that the cancellation of the effects of resonances holds even in this case. However, comparison with the literature (in the case where only top loops are considered) showed that the LET approximation fails by up to 50% in double Higgs production. Thus we undertook an exact computation of $gg \to hh$, focusing for definiteness on the well-studied MCHM$_5$, where double Higgs production is enhanced compared to the SM. We found that the cross section does depend (altough not dramatically) on the spectrum of resonances. Therefore a measurement of double Higgs production could complement the information coming from other processes, notably from direct searches for vector-like quarks and from EWPT. We also briefly discussed the prospects for detecting hh production at LHC14.

Although the $ht\bar{t}$ coupling ($g_{ht\bar{t}}$) has not been directly measured yet by ATLAS and CMS, it can already be determined indirectly by means of a fit to Higgs data, thanks to the important contribution of the top to the 1-loop hgg and $h\gamma\gamma$ couplings. This determination is however plagued by an ambiguity in the *sign* of the coupling. We first discussed why Higgs fits in 'standard' channels cannot robustly lift the degeneracy. Then we argued that single top production in association with a Higgs is suitable for excluding the $g_{ht\bar{t}} < 0$ option, thanks to a striking enhancement of the cross section for nonstandard couplings (a factor ~ 13 for $g_{ht\bar{t}} = -1$). We performed a thorough phenomenological study of this process and of its main backgrounds at the LHC, selecting the decay of the Higgs into b quarks, and estimated the impact on the parameter space of Higgs couplings. We found that part of the 'negative sign' region could be excluded already with 8 TeV data. Following our proposal, the ATLAS Collaboration is currently performing a preliminary investigation of the $th \to tb\bar{b}$ process.

In Chapter 5 we discussed the phenomenology of top partners in the MCHM$_5$. We considered first EWPT, by including the three main effects that are expected in composite Higgs models: the IR divergences in S and T due to the σ model, the UV contribution to S from tree-level exchange of spin-1 resonances, and the radiative contributions of heavy fermions to T and to ϵ_b (to compute the latter one needs to specify some UV dynamics, represented by a 'two-site' version of the MCHM$_5$ in our case). We found that two types of resonance spectra are singled out as most viable. Region I features a relatively light $SO(4)$-singlet fermion, $\tilde{T}$, while the fermions in the **4** are heavy. This is not suprising: the singlet

gives a positive contribution to T, which as already said is welcome, since it helps to 'jump back' into the allowed ellipse in the (S,T) plane[1]. Region II has a light **4**, implying that the exotic $X_{5/3}$ is the lightest strong sector resonance.

With these results in the back of our mind we turned to study LHC searches for fermionic resonances. We discussed the bounds that ATLAS and CMS have placed with the full 8 TeV statistics, by performing only searches for pair-produced vector-like quarks. In region I the singlet $\tilde{T}$ is constrained to $m_{\tilde{T}} \gtrsim 700$ GeV, whereas in region II we find $m_{X_{5/3}} > 770$ GeV for the charge-5/3 exotic. These results imply that the exploration of a sizable region of the natural parameter space (which extends very roughly up to $\lesssim 1.5$ TeV) will be possible only at LHC14. Notice, however, that the current bounds could likely be improved (in particular for the singlet) if the *single* production mechanism were considered.

The last topic in our discussion was the phenomenology of heavy composite vectors, which we considered in Chapter 6. As an introduction we outlined, by means of a simplified 'two-sector' framework, the basic properties of spin-1 fields in partial compositeness. These states couple to light fermions with a strength $\sim g_{\rm SM}^2/g_\rho$, where g_ρ is the coupling in the strong sector; instead their couplings to longitudinal W, Z and to the Higgs is $\sim g_\rho$. On the other hand, EWPT suggest that $g_\rho \gg g_{\rm SM}$, which leads to a peculiar phenomenology: the Drell-Yan production is suppressed (with VBF being competitive), and the preferred decays are, for example, $Z' \to WW, Zh$ or $W' \to WZ$. Also decays into 3rd generation quarks can be important, due to the sizable degree of compositeness of the latter.

Then we focused on one specific type of resonance, an $SU(2)_L$-singlet electrically charged W'. A resonance with these quantum numbers is weakly constrained (in particular, it does not contribute to the S parameter), and could thus be relatively light. We studied the W' phenomenology, including EWPT, low-energy, Tevatron and LHC observables, by adopting a fully model-independent approach. We wrote down an effective Lagrangian which respects only the SM gauge symmetry, and did not assume the resonance to be associated with a spontaneously broken local invariance. We pointed out the particularly interesting role of one coupling (denoted δ_B), which controls deviations from the gauge-symmetric limit. We observed that for a generic resonance $\delta_B \neq 0$ can be realized. This opens up a novel subleading decay channel, $W' \to W\gamma$, which can thus be interpreted as a signal of compositeness. We performed an exploratory study of the LHC discovery reach in this final state. Deviations from the gauge-symmetric limit also lead to a faster growth of the $\gamma\gamma \to W'_L W'_L$ scattering amplitudes at high energies, which can cause a perturbative unitarity loss at a scale $E \sim M_{W'}$ and thus invalidate the theory in the energy range relevant to LHC phenomenology. We verified that this does not happen: the cutoff is $\Lambda \gtrsim 5\, M_{W'}$ in the entire range of parameters considered.

[1] The caveat is that the singlet also generates a positive ϵ_b, and the interplay of the two constraints is delicate [31, 32].

Appendix A

The one-loop effective potential

In this appendix we collect some useful formulas for the one-loop effective potential [11], which is used often in our discussion. The general expression of the potential is

$$V_1(H) = \frac{1}{2}\mathrm{STr}\int \frac{d^4p}{(2\pi)^4}\log\left[p^2 + m^2(H)\right] , \tag{A.1}$$

where $\mathrm{STr} \equiv (-1)^{2s}\mathrm{Tr}$, p is the Euclidean momentum, and $m^2(H)$ is the squared mass of each particle in the Higgs background H. Notice that the potential was derived assuming canonical kinetic terms for all fields in the loops (scalars, fermions and vectors). The counting of degrees of freedom in the trace goes as follows: $\mathrm{Tr} = 4N_c$ for a colored Dirac fermion, $\mathrm{Tr} = 3$ for a massive vector and $\mathrm{Tr} = 1$ for a real scalar. Cutting off the integral at $p^2 = \Lambda^2$ and neglecting terms that vanish for $\Lambda \to \infty$ we find

$$V_1(H) = \frac{1}{32\pi^2}\mathrm{STr}\left[m^2(H)\Lambda^2 + \frac{1}{2}m^4(H)\left(\log\frac{m^2(H)}{\Lambda^2} - \frac{1}{2}\right)\right] . \tag{A.2}$$

In the SM, writing the Higgs doublet as $H = (\,\pi_1 + i\pi_2,\, H + h + i\pi_0\,)^T/\sqrt{2}$ with H an arbitrary background, we find the masses (the background-dependence is understood)

$$m^2_{\pi_i} = m^2 + \lambda H^2 , \quad m^2_h = m^2 + 3\lambda H^2 , \quad m^2_W = \frac{g^2H^2}{4} , \quad m^2_Z = \frac{(g^2 + g'^2)H^2}{4} , \quad m^2_t = \frac{y_t H^2}{2} . \tag{A.3}$$

Appendix B

The electroweak fit

We present here the χ^2 test used to compute the constraints from EWPT on the parameters of the models discussed in the thesis. The best experimental determination of ϵ_1, ϵ_3 and ϵ_b still comes from the precision measurements at the Z pole mass performed at LEP [164]:

$$\begin{array}{rcl} \epsilon_1^{(exp)} &=& (5.4 \pm 1.0) \cdot 10^{-3}, \\ \epsilon_2^{(exp)} &=& (-8.9 \pm 1.2) \cdot 10^{-3}, \\ \epsilon_3^{(exp)} &=& (5.34 \pm 0.94) \cdot 10^{-3}, \\ \epsilon_b^{(exp)} &=& (-5.0 \pm 1.6) \cdot 10^{-3}, \end{array} \qquad \rho = \begin{pmatrix} 1 & 0.60 & 0.86 & 0.00 \\ 0.60 & 1 & 0.40 & -0.01 \\ 0.86 & 0.40 & 1 & 0.02 \\ 0.00 & -0.01 & 0.02 & 1 \end{pmatrix}. \tag{B.1}$$

Here ρ is the correlation matrix between the ϵ_i obtained from the App. E of Ref. [164], marginalizing over the three parameters m_Z, $\alpha_S(m_Z)$ and $\Delta\alpha^{(5)}_{had}(m_Z)$.[1] The status of electroweak precision observables did not change since then, except for the mass of the W boson. The latter was recently updated based on Tevatron results, and the current world average is [165]

$$m_W = 80.385 \pm 0.015 \text{ GeV}. \tag{B.2}$$

The parameter ϵ_2 is the only one depending on the mass of the W boson, through the term

$$\epsilon_2 = \frac{s_0^2}{1 - 2s_0^2}\, \Delta r_w + [\text{terms independent of } m_W] \ , \tag{B.3}$$

where $s_0^2 = 0.23098$, and the measurement of Δr_w is related to m_W through

$$\frac{\pi\, \alpha(0)}{\sqrt{2}\, m_Z^2\, G_F} \left(1 - \Delta\alpha - \Delta r_w\right)^{-1} = \frac{m_W^2}{m_Z^2} \left(1 - \frac{m_W^2}{m_Z^2}\right). \tag{B.4}$$

Here $\alpha(0)$ is the fine-structure constant and G_F the Fermi constant, both known to high accuracy. Furthermore, $\Delta\alpha$ accounts for the running of the electroweak coupling between the low energy limit and the Z-pole mass. The uncertainty associated to it is important, but the shift in Δr_w induced by the new value of m_W is independent of $\Delta\alpha$. The change of m_W and consequently ϵ_2 between the LEP data of 2006 and the present value is then

	2006	2012
m_W	80.425 ± 0.034 GeV	80.385 ± 0.015 GeV
ϵ_2	$(-8.9 \pm 1.2) \cdot 10^{-3}$	$(-7.9 \pm 0.9) \cdot 10^{-3}$

(B.5)

[1] Alternatively, we could set the three extra parameters to their experimental best values. This would give slightly more stringent constraints.

The experimental values for the ϵ_i used in this paper are therefore

$$\begin{array}{rcl} \epsilon_1^{(exp)} & = & (5.4 \pm 1.0) \cdot 10^{-3}, \\ \epsilon_2^{(exp)} & = & (-7.9 \pm 0.9) \cdot 10^{-3}, \\ \epsilon_3^{(exp)} & = & (5.34 \pm 0.94) \cdot 10^{-3}, \\ \epsilon_b^{(exp)} & = & (-5.0 \pm 1.6) \cdot 10^{-3}, \end{array} \qquad \rho = \begin{pmatrix} 1 & 0.80 & 0.86 & 0.00 \\ 0.80 & 1 & 0.53 & -0.01 \\ 0.86 & 0.53 & 1 & 0.02 \\ 0.00 & -0.01 & 0.02 & 1 \end{pmatrix}, \tag{B.6}$$

where we took into account the fact that $\epsilon_{1,3,b}$ and their covariances with ϵ_2 are not affected by the new measurement of the W mass. On the theoretical side, in the SM the ϵ_i are predicted to be[2]

$$\begin{array}{rcl} \epsilon_1^{(th)} & = & [+5.66 - 0.86 \log (m_h/m_Z)] \cdot 10^{-3}, \\ \epsilon_2^{(th)} & = & [-7.11 + 0.16 \log (m_h/m_Z)] \cdot 10^{-3}, \\ \epsilon_3^{(th)} & = & [+5.25 + 0.54 \log (m_h/m_Z)] \cdot 10^{-3}, \\ \epsilon_b^{(th)} & = & -6.48 \cdot 10^{-3}, \end{array} \tag{B.7}$$

where we used $m_t = 173.3$ GeV. The BSM contributions, which will be functions of a set of parameters $\mathbf{x}$, should be summed to the above expressions. The χ^2 is then defined as

$$\chi^2 (\mathbf{x}) = \sum_{i,j} \left(\epsilon_i^{(th)}(\mathbf{x}) - \epsilon_i^{(exp)} \right) C_{ij}^{-1} \left(\epsilon_j^{(th)}(\mathbf{x}) - \epsilon_j^{(exp)} \right), \tag{B.8}$$

where C^{-1} is the inverse of the covariance matrix

$$C_{ij} = \Delta\epsilon_i^{(exp)} \rho_{ij} \, \Delta\epsilon_j^{(exp)}. \tag{B.9}$$

[2]We thank A. Strumia for providing us with these values.

Appendix C

Derivation of the hgg, $hhgg$ and $h\gamma\gamma$ couplings in the SILH formalism

In this appendix we derive the expressions of the couplings hgg, $hhgg$ and $h\gamma\gamma$ in the SILH formalism.

C.1 The hgg and $hhgg$ couplings

Our starting point is Eq. (4.5). We also recall that since we chose to work in a general basis where $c_r \neq 0$, see Eq. (3.26), the relation between $\langle H \rangle$ and v is non-trivial, as can be read off the W boson mass term

$$m_W^2 = \frac{g^2 v^2}{4}\,, \quad \text{with} \quad v^2 = \langle H \rangle^2 \left(1 + \frac{c_r}{4}\frac{\langle H \rangle^2}{f^2}\right)\,. \tag{C.1}$$

We assume for definiteness the presence of one or more vector-like top partners, which upon integration contribute to c_g, and identify the light mass eigenstate of the heavy fermion mass matrix $\mathcal{M}$ with the top quark, whose mass reads

$$m_t(H) = \frac{y_t H}{\sqrt{2}}\left(1 - c_y^{(t)}\frac{H^2}{2f^2}\right)\,, \tag{C.2}$$

where $c_y^{(t)}$ parameterizes the correction to the SM top Yukawa coupling. The coefficients $A_{1,2}$ in Eq. (4.6) can be related to $c_y^{(t)}$ and c_g by separating the contribution (to the hgg and $hhgg$ coupling, respectively) of the top quark, which involves $c_y^{(t)}$, from that of top partners, which is parameterized by c_g. The results are

$$\langle H \rangle A_1 \;=\; \left(\frac{\partial}{\partial \log H}\log|\det \mathcal{M}(H)|\right)_{H=v} \;=\; 1 - c_y^{(t)}\frac{v^2}{f^2} + 3c_g\frac{y_t^2}{m_\rho^2}v^2\,, \tag{C.3}$$

$$\langle H \rangle^2 A_2 \;=\; \left(\left(\frac{\partial^2}{\partial(\log H)^2} - \frac{\partial}{\partial \log H}\right)\log|\det \mathcal{M}(H)|\right)_{H=v} \;=\; -1 - c_y^{(t)}\frac{v^2}{f^2} + 3c_g\frac{y_t^2}{m_\rho^2}v^2\,, \tag{C.4}$$

where we work at $\mathcal{O}(1/f^2)$.[1] Note that the 'implicit' expressions containing the determinant are in practice more useful than the explicit ones written in terms of $c_y^{(t)}$ and c_g, because

[1] In the second and third term of each of Eqs. (C.3) and (C.4) we have used the fact that the distinction between $\langle H \rangle$ and v expressed by Eq. (C.1) is higher order in ξ there.

using the former avoids diagonalizing the heavy fermion mass matrix, a rather complicated task in presence of multiple top partners.

In Eq. (4.5) we have assumed that h has a canonical kinetic term. However, in the SILH Lagrangian the operators proportional to c_H and c_r correct the Higgs kinetic term as follows

$$\Delta\mathcal{L}_{h\,kin} = \frac{1}{2f^2}\left(c_H + \frac{c_r}{4}\right)(\langle H\rangle + h)^2\partial_\mu h\partial^\mu h\,, \tag{C.5}$$

which also contains Higgs derivative interactions. At first order in ξ, these can be eliminated by the nonlinear redefinition [57]

$$h \to h - \frac{\xi}{2}\left(c_H + \frac{c_r}{4}\right)\left(h + \frac{h^2}{v} + \frac{h^3}{3v^2}\right)\,, \tag{C.6}$$

which leaves h canonically normalized. Notice that in a nonlinear σ-model, the Higgs is canonically normalized at all orders, which corresponds to the relation $c_H = -c_r/4$. Performing the transformation in Eq. (C.6), we arrive at the effective coupling of the Higgs to one and two gluons, Eqs. (4.8) and (4.9), respectively. The invariance of these expressions under the reparameterization in Eq. (3.27) can be easily verified by using Eqs. (C.3) and (C.4), respectively.

C.2 The $h\gamma\gamma$ coupling

Starting from Eq. (4.12), recalling the expression of the W boson mass in Eq. (C.1) and taking into account the rescaling needed to make the Higgs kinetic term canonical, see Eq. (C.6), it is straightforward to obtain Eq. (4.13). Similarly to Eq. (C.3), A_1 can be related to $c_y^{(t)}$ and c_γ (assuming that all contributions to c_γ come from the fermion sector)

$$\langle H\rangle\, A_1 = \left(\frac{\partial}{\partial \log H}\log|\det\mathcal{M}(H)|\right)_{H=v} = 1 - c_y^{(t)}\frac{v^2}{f^2} + c_\gamma\frac{g^2}{m_\rho^2}v^2\frac{1}{2Q_t^2}\,. \tag{C.7}$$

Plugging Eq. (C.7) into Eq. (4.13), the invariance under the reparameterization in Eq. (3.27) becomes explicit.

Appendix D

The Littlest Higgs

In this appendix we give a short description of the Littlest Higgs [71], and compute a subset of the SILH coefficients in the model. The Littlest Higgs model is based on the coset $SU(5)/SO(5)$. We consider here a variation where only one $U(1)$ group is gauged, as this eliminates one source of custodial breaking and thus relaxes the tension with EWPT suffered by the original model. In Ref. [72] it was shown that a scale as low as $f \sim 1.2\,\text{TeV}$ is allowed in this case. This, however, leaves an extra singlet Goldstone boson in the spectrum, whose effects will be ignored in the following.[1] The Σ field reads

$$\Sigma(x) = e^{2i\Pi/f}\Sigma_0\,, \qquad \Pi = \begin{pmatrix} \eta/(2\sqrt{5}) & H/\sqrt{2} & \varphi \\ H^\dagger/\sqrt{2} & -2\eta/\sqrt{5} & H^T/\sqrt{2} \\ \varphi^\dagger & H^*/\sqrt{2} & \eta/(2\sqrt{5}) \end{pmatrix}, \qquad \Sigma_0 = \begin{pmatrix} & & \mathbb{1}_2 \\ & 1 & \\ \mathbb{1}_2 & & \end{pmatrix}, \tag{D.1}$$

where H is the Higgs doublet, φ is a complex triplet and η is a singlet. An $SU(2)_1 \times SU(2)_2 \times U(1)_Y$ subgroup of the global symmetry is gauged and is spontaneously broken at the scale f to the diagonal $SU(2)_L \times U(1)_Y$. In Eq. (D.1) we omitted the GBs that get eaten by the heavy $SU(2)$ triplet of vectors. The two-derivative Lagrangian reads

$$\mathcal{L} = \frac{f^2}{8}\text{Tr}\left[(D_\mu\Sigma)^\dagger D^\mu\Sigma\right], \qquad D_\mu\Sigma = \partial_\mu\Sigma - i\sum_{j=1,2} g_j W_j^a (Q_j^a\Sigma + \Sigma Q_j^{a\,T}) - ig' B_\mu (Y\Sigma + \Sigma Y)\,, \tag{D.2}$$

with the gauged generators given by

$$Q_1^a = \begin{pmatrix} \sigma^a/2 & & \\ & & \\ & & \end{pmatrix}, \qquad Q_2^a = \begin{pmatrix} & & \\ & & \\ & & -\sigma^{a\,*}/2 \end{pmatrix}, \qquad Y = \text{diag}\left(1/2, 1/2, 0, -1/2, -1/2\right). \tag{D.3}$$

The SM fermions are taken to transform only under $SU(2)_1 \times U(1)_Y$.

The SILH coefficients c_H and c_r receive contributions of three different kinds. The first arises from the nonlinear σ model structure. Using

$$m_W^2 = \frac{1}{2}g^2 f^2 \sin^2\left(\frac{\langle H\rangle}{\sqrt{2}f}\right), \qquad g = \frac{g_1 g_2}{\sqrt{g_1^2 + g_2^2}}\,, \tag{D.4}$$

we find $c_H^\sigma = 1/6$ and $c_r^\sigma = -4\,c_H^\sigma = -2/3$.

[1] Additional sources of symmetry breaking are needed in order to give η a potential.

The second contribution comes from integrating out the heavy vector triplet. The procedure has been described in detail in Ref. [81], and we simply apply it to the case under study, obtaining $c_H^v = 1/4$ and $c_r^v = -1$, in agreement with Ref. [34].

The third and last contribution arises from integrating out heavy scalars. Since we also need to compute c_6, we write down the scalar potential up to order H^6. Neglecting g', the relevant terms are

$$\begin{aligned} V =& \lambda_+ \left\{ f^2 \left| \varphi_{ij} + \frac{i}{4f}(H_i H_j + H_j H_i) \right|^2 - \frac{1}{6f^2}|H|^6 + \frac{i}{2f}|H|^2 \left(\varphi_{ij} H_i^* H_j^* - \varphi_{ij}^* H_i H_j\right) - \frac{4}{3}|\varphi_{ij}|^2 |H|^2 \right\} \\ &+ \lambda_- \left\{ f^2 \left| \varphi_{ij} - \frac{i}{4f}(H_i H_j + H_j H_i) \right|^2 - \frac{1}{6f^2}|H|^6 - \frac{i}{2f}|H|^2 \left(\varphi_{ij} H_i^* H_j^* - \varphi_{ij}^* H_i H_j\right) - \frac{4}{3}|\varphi_{ij}|^2 |H|^2 \right\} , \end{aligned}$$

where the coefficient λ_+ receives contributions from g_1, whereas λ_- from g_2 and from the top Yukawa sector. In general, starting from a Lagrangian of the form

$$\mathcal{L}_\Phi = -\Phi^{a\,*} \Box \Phi^a - (M^2 - \beta_2 |H|^2) \Phi^{a\,*} \Phi^a + \left(\beta f \Phi^{a\,*} H^T \epsilon \frac{\sigma^a}{2} H + \text{h.c.} \right) + \left(\frac{\beta_4}{f} \Phi^{a\,*} H^T \epsilon \frac{\sigma^a}{2} H |H|^2 + \text{h.c.} \right) \tag{D.5}$$

($\epsilon = i\sigma^2$) and integrating out Φ one obtains $c_H^s = \beta^2 f^4/(2M^4)$ and $c_r^s = 2\beta^2 f^4/M^4$. In addition, there is a contribution to c_6,

$$c_6^\Phi = -\frac{1}{\lambda} \left(\frac{\beta \beta_4 f^2}{M^2} + \frac{\beta^2 \beta_2 f^4}{2M^4} \right) , \tag{D.6}$$

where λ is the Higgs quartic coupling (after the triplet has been integrated out). In the Littlest Higgs case we make the identifications

$$M^2 = (\lambda_+ + \lambda_-) f^2 , \qquad \beta = \frac{1}{\sqrt{2}}(\lambda_- - \lambda_+) , \qquad \beta_2 = \frac{4}{3}(\lambda_+ + \lambda_-) , \qquad \beta_4 = \frac{1}{\sqrt{2}}(\lambda_+ - \lambda_-) . \tag{D.7}$$

Therefore we find

$$c_H^s = \frac{1}{4} \left(\frac{\lambda_- - \lambda_+}{\lambda_- + \lambda_+} \right)^2 , \qquad c_r^s = \left(\frac{\lambda_- - \lambda_+}{\lambda_- + \lambda_+} \right)^2 . \tag{D.8}$$

On the other hand,

$$c_6 = -\frac{1}{\lambda} \left(\frac{\lambda_+ + \lambda_-}{6} \right) + c_6^\Phi = -\frac{2}{3} , \tag{D.9}$$

where we have used the expression of the quartic coupling $\lambda = \lambda_+ \lambda_- / (\lambda_+ + \lambda_-)$. Notice that in general the neutral component of φ gets a nonzero VEV, which is strongly constrained by EWPT. Small values of $f \sim 1\,\text{TeV}$ in fact require the approximate condition $\lambda_+ \simeq \lambda_-$ to be satisfied, which makes the triplet VEV very small[2] [72]. We assume this condition to be realized, and therefore neglect effects due to the triplet VEV in our discussion.

Concerning the top sector, in addition to the doublet $q_L = (\, t_L \,,\, b_L \,)^T$ and to the singlet t_R a pair of $SU(2)$-singlet fermions $\tilde{T}_L, \tilde{T}_R$ with electric charge $Q = Y = 2/3$ is introduced. The Yukawa Lagrangian then reads

$$-\mathcal{L}_Y = \frac{\lambda_1}{2} f\, \bar{t}_R \epsilon_{ijk} \epsilon_{ab} \chi_i \Sigma_{ja} \Sigma_{kb} + \lambda_2 f \overline{\tilde{T}}_R \tilde{T}_L + \text{h.c.} \tag{D.10}$$

[2] When $\lambda_+ = \lambda_-$ the potential does not contain any tadpole for φ.

$(i,j,k=1,2,3$ and $a,b=4,5)$. Here χ is an $SU(3)$ triplet, $\chi = (\, b_L\,,\, t_L\,,\, \tilde{T}_L\,)^T$. The fermion mass matrix in the Higgs background

$$H = \begin{pmatrix} 0 \\ H/\sqrt{2} \end{pmatrix} \tag{D.11}$$

reads

$$-\mathcal{L}_m = \begin{pmatrix} \bar{t}_R & \overline{\tilde{T}}_R \end{pmatrix} \mathcal{M} \begin{pmatrix} t_L \\ \tilde{T}_L \end{pmatrix} + \text{h.c.}\,, \qquad \mathcal{M} = \begin{pmatrix} -\frac{i}{\sqrt{2}}\lambda_1 f \sin\left(\frac{\sqrt{2}H}{f}\right) & \lambda_1 f \cos^2\left(\frac{H}{\sqrt{2}f}\right) \\ 0 & \lambda_2 f \end{pmatrix}, \tag{D.12}$$

implying

$$\det \mathcal{M}^\dagger \mathcal{M} = \frac{1}{2}\lambda_1^2\lambda_2^2 f^4 \sin^2\frac{\sqrt{2}H}{f}\,. \tag{D.13}$$

This allows us to write the amplitude for $gg \to hh$ in the Littlest Higgs, in the low-energy theorem limit as

$$C_{\text{LET}}^{\text{LH}}(\hat{s}) = \frac{3m_h^2}{\hat{s}-m_h^2}\left[1 - \frac{3}{4}\xi\left(\frac{7}{3} + \left(\frac{c_- - c_+}{c_- + c_+}\right)^2\right)\right] - 1 - \frac{\xi}{4}\left(1 + \left(\frac{c_- - c_+}{c_- + c_+}\right)^2\right). \tag{D.14}$$

We also note that in this case it is easy to diagonalize explicitly the fermion mass matrix at $\mathcal{O}(1/f^2)$, obtaining

$$-\mathcal{L}_m = m_t(H)\,\bar{t}_R t_L + m_T(H)\,\overline{T}_R T_L + \text{h.c.} \tag{D.15}$$

where

$$m_t(H) = \frac{y_t H}{\sqrt{2}}\left[1 + \frac{H^2}{f^2}\left(-\frac{1}{3} + \frac{y_t^2}{4\lambda_T^2}\right)\right], \tag{D.16}$$

$$m_T(H) = f\lambda_T\left(1 - \frac{H^2}{f^2}\frac{y_t^2}{4\lambda_T^2}\right), \tag{D.17}$$

with $y_t = \sqrt{2}\,\lambda_1\lambda_2/\sqrt{\lambda_1^2+\lambda_2^2}$ and $\lambda_T = \sqrt{\lambda_1^2+\lambda_2^2}$. In the notation of Eq. (4.28), we have

$$c_y^{(t)} = \frac{2}{3} - \frac{y_t^2}{2\lambda_T^2}\,, \qquad a_T = -\frac{y_t^2}{4\lambda_T^2}\,. \tag{D.18}$$

Thus $c_y^{(t)} - 2a_T = 2/3$ which is independent of the couplings, as it must be since the factorization in Eq. (4.24) holds.

Bibliography

[1] C. Grojean, E. Salvioni and R. Torre, *A weakly constrained W' at the early LHC*, JHEP **1107** (2011) 002 [arXiv:1103.2761 [hep-ph]].

[2] M. Farina, C. Grojean and E. Salvioni, *(Dys)Zphilia or a custodial breaking Higgs at the LHC*, JHEP **1207** (2012) 012 [arXiv:1205.0011 [hep-ph]].

[3] M. Gillioz, R. Gröber, C. Grojean, M. Mühlleitner and E. Salvioni, *Higgs Low-Energy Theorem (and its corrections) in Composite Models*, JHEP **1210** (2012) 004 [arXiv:1206.7120 [hep-ph]].

[4] M. Farina, C. Grojean, F. Maltoni, E. Salvioni and A. Thamm, *Lifting degeneracies in Higgs couplings using single top production in association with a Higgs boson*, JHEP **1305** (2013) 022 [arXiv:1211.3736 [hep-ph]].

[5] E. Salvioni, *Relevance of the decay $W' \to W\gamma$ at the early LHC*, Nuovo Cim. C **034N06** (2011) 195.

[6] E. Salvioni, *Some Z' and W' models facing current LHC searches*, to appear in the proceedings of DIS 2012, Bonn, March 2012.

[7] ATLAS Collaboration, Phys. Lett. B **716** (2012) 1 [arXiv:1207.7214 [hep-ex]].

[8] CMS Collaboration, Phys. Lett. B **716** (2012) 30 [arXiv:1207.7235 [hep-ex]].

[9] ATLAS Collaboration, ATLAS-CONF-2013-034, March 2013 [http://cds.cern.ch/record/1528170].

[10] CMS Collaboration, CMS-PAS-HIG-13-005, April 2013 [http://cds.cern.ch/record/1542387].

[11] S. R. Coleman and E. J. Weinberg, Phys. Rev. D **7** (1973) 1888.

[12] R. Barbieri and G. F. Giudice, Nucl. Phys. B **306** (1988) 63.

[13] S. P. Martin, in 'Perspectives on Supersymmetry II', Kane, G.L. (ed.), 1-153 [arXiv:hep-ph/9709356].

[14] S. Weinberg, Phys. Rev. Lett. **59** (1987) 2607.

[15] S. Dimopoulos and J. Preskill, Nucl. Phys. B **199** (1982) 206; D. B. Kaplan and H. Georgi, Phys. Lett. B **136** (1984) 183; D. B. Kaplan, H. Georgi and S. Dimopoulos, Phys. Lett. B **136** (1984) 187; T. Banks, Nucl. Phys. B **243** (1984) 125; H. Georgi,

D. B. Kaplan and P. Galison, Phys. Lett. B **143** (1984) 152; H. Georgi and D. B. Kaplan, Phys. Lett. B **145** (1984) 216; M. J. Dugan, H. Georgi and D. B. Kaplan, Nucl. Phys. B **254** (1985) 299.

[16] N. Arkani-Hamed, A. G. Cohen and H. Georgi, Phys. Lett. B **513** (2001) 232 [arXiv:hep-ph/0105239].

[17] R. Contino, Y. Nomura and A. Pomarol, Nucl. Phys. B **671** (2003) 148 [arXiv:hep-ph/0306259].

[18] K. Agashe, R. Contino and A. Pomarol, Nucl. Phys. B **719** (2005) 165 [arXiv:hep-ph/0412089].

[19] D. B. Kaplan, Nucl. Phys. B **365** (1991) 259.

[20] G. Panico and A. Wulzer, JHEP **1109** (2011) 135 [arXiv:1106.2719 [hep-ph]].

[21] S. De Curtis, M. Redi and A. Tesi, JHEP **1204** (2012) 042 [arXiv:1110.1613 [hep-ph]].

[22] O. Matsedonskyi, G. Panico and A. Wulzer, JHEP **1301** (2013) 164 [arXiv:1204.6333 [hep-ph]].

[23] M. Redi and A. Tesi, JHEP **1210** (2012) 166 [arXiv:1205.0232 [hep-ph]].

[24] D. Marzocca, M. Serone and J. Shu, JHEP **1208** (2012) 013 [arXiv:1205.0770 [hep-ph]].

[25] A. Pomarol and F. Riva, JHEP **1208** (2012) 135 [arXiv:1205.6434 [hep-ph]].

[26] G. Panico, M. Redi, A. Tesi and A. Wulzer, JHEP **1303** (2013) 051 [arXiv:1210.7114 [hep-ph]].

[27] M. Schmaltz, D. Stolarski and J. Thaler, JHEP **1009** (2010) 018 [arXiv:1006.1356 [hep-ph]].

[28] M. S. Carena, E. Ponton, J. Santiago and C. E. M. Wagner, Nucl. Phys. B **759** (2006) 202 [arXiv:hep-ph/0607106];

[29] M. S. Carena, E. Ponton, J. Santiago and C. E. M. Wagner, Phys. Rev. D **76** (2007) 035006 [arXiv:hep-ph/0701055].

[30] P. Lodone, JHEP **0812** (2008) 029 [arXiv:0806.1472 [hep-ph]].

[31] M. Gillioz, Phys. Rev. D **80** (2009) 055003 [arXiv:0806.3450 [hep-ph]].

[32] C. Anastasiou, E. Furlan and J. Santiago, Phys. Rev. D **79** (2009) 075003 [arXiv:0901.2117 [hep-ph]].

[33] A. Falkowski, Phys. Rev. D **77** (2008) 055018 [arXiv:0711.0828 [hep-ph]].

[34] I. Low and A. Vichi, Phys. Rev. D **84** (2011) 045019 [arXiv:1010.2753 [hep-ph]].

[35] A. Azatov and J. Galloway, Phys. Rev. D **85** (2012) 055013 [arXiv:1110.5646 [hep-ph]].

[36] M. Montull, F. Riva, E. Salvioni and R. Torre, to appear.

[37] J. R. Ellis, M. K. Gaillard and D. V. Nanopoulos, Nucl. Phys. B **106** (1976) 292; M. A. Shifman, A. I. Vainshtein, M. B. Voloshin and V. I. Zakharov, Sov. J. Nucl. Phys. **30** (1979) 711 [Yad. Fiz. **30** (1979) 1368].

[38] R. Gröber and M. Mühlleitner, JHEP **1106** (2011) 020 [arXiv:1012.1562 [hep-ph]].

[39] ATLAS Collaboration, ATLAS-CONF-2012-135, September 2012 [http://cdsweb.cern.ch/record/1478423].

[40] CMS Collaboration, JHEP **1305** (2013) 145 [arXiv:1303.0763 [hep-ex]].

[41] CMS Collaboration, CMS-PAS-HIG-13-015, May 2013 [http://cds.cern.ch/record/1547292?ln=en].

[42] M. E. Peskin, arXiv:1207.2516 [hep-ph].

[43] C. Degrande, J. M. Gerard, C. Grojean, F. Maltoni and G. Servant, JHEP **1207** (2012) 036 [Erratum-ibid. **1303** (2013) 032] [arXiv:1205.1065 [hep-ph]].

[44] S. Biswas, E. Gabrielli and B. Mele, JHEP **1301** (2013) 088 [arXiv:1211.0499 [hep-ph]].

[45] R. Contino, T. Kramer, M. Son and R. Sundrum, JHEP **0705** (2007) 074 [arXiv:hep-ph/0612180].

[46] M. A. Shifman, A. I. Vainshtein and V. I. Zakharov, Nucl. Phys. B **147** (1979) 385; Nucl. Phys. B **147** (1979) 448.

[47] G. 't Hooft, Nucl. Phys. B **72** (1974) 461; G. 't Hooft, Nucl. Phys. B **75** (1974) 461.

[48] E. Witten, Nucl. Phys. B **160** (1979) 57.

[49] S. Weinberg, Phys. Rev. Lett. **18** (1967) 507.

[50] T. Das, G. S. Guralnik, V. S. Mathur, F. E. Low and J. E. Young, Phys. Rev. Lett. **18** (1967) 759.

[51] R. Contino, arXiv:1005.4269 [hep-ph].

[52] R. Contino and A. Pomarol, JHEP **0411** (2004) 058 [arXiv:hep-th/0406257].

[53] J. Mrazek, A. Pomarol, R. Rattazzi, M. Redi, J. Serra and A. Wulzer, Nucl. Phys. B **853** (2011) 1 [arXiv:1105.5403 [hep-ph]].

[54] B. Gripaios, A. Pomarol, F. Riva and J. Serra, JHEP **0904** (2009) 070 [arXiv:0902.1483 [hep-ph]].

[55] M. Chala, JHEP **1301** (2013) 122 [arXiv:1210.6208 [hep-ph]].

[56] A. Manohar and H. Georgi, Nucl. Phys. B **234** (1984) 189.

[57] G. F. Giudice, C. Grojean, A. Pomarol and R. Rattazzi, JHEP **0706** (2007) 045 [arXiv:hep-ph/0703164].

[58] C. Csaki, A. Falkowski and A. Weiler, JHEP **0809** (2008) 008 [arXiv:0804.1954 [hep-ph]].

[59] M. Redi and A. Weiler, JHEP **1111** (2011) 108 [arXiv:1106.6357 [hep-ph]].

[60] B. Keren-Zur, P. Lodone, M. Nardecchia, D. Pappadopulo, R. Rattazzi and L. Vecchi, Nucl. Phys. B **867** (2013) 429 [arXiv:1205.5803 [hep-ph]].

[61] D. Pappadopulo, A. Thamm and R. Torre, arXiv:1303.3062 [hep-ph].

[62] CMS Collaboration, JHEP **1205** (2012) 055 [arXiv:1202.5535 [hep-ex]].

[63] O. Domenech, A. Pomarol and J. Serra, Phys. Rev. D **85** (2012) 074030 [arXiv:1201.6510 [hep-ph]].

[64] A. Atre, M. Carena, T. Han and J. Santiago, Phys. Rev. D **79** (2009) 054018 [arXiv:0806.3966 [hep-ph]]; A. Atre, G. Azuelos, M. Carena, T. Han, E. Ozcan, J. Santiago and G. Unel, JHEP **1108** (2011) 080 [arXiv:1102.1987 [hep-ph]]; A. Atre, M. Chala and J. Santiago, JHEP **1305** (2013) 099 [arXiv:1302.0270 [hep-ph]]; C. Delaunay, C. Grojean and G. Perez, arXiv:1303.5701 [hep-ph]; M. Redi, V. Sanz, M. de Vries and A. Weiler, arXiv:1305.3818 [hep-ph].

[65] M. Redi, Eur. Phys. J. C **72** (2012) 2030 [arXiv:1203.4220 [hep-ph]].

[66] R. Contino, L. Da Rold and A. Pomarol, Phys. Rev. D **75** (2007) 055014 [arXiv:hep-ph/0612048].

[67] K. Agashe, R. Contino, L. Da Rold and A. Pomarol, Phys. Lett. B **641** (2006) 62 [arXiv:hep-ph/0605341].

[68] S. R. Coleman, J. Wess and B. Zumino, Phys. Rev. **177** (1969) 2239; C. G. Callan, Jr., S. R. Coleman, J. Wess and B. Zumino, Phys. Rev. **177** (1969) 2247.

[69] C. Grojean, O. Matsedonskyi and G. Panico, arXiv:1306.4655 [hep-ph].

[70] M. Schmaltz and D. Tucker-Smith, Ann. Rev. Nucl. Part. Sci. **55** (2005) 229 [arXiv:hep-ph/0502182]; M. Perelstein, Prog. Part. Nucl. Phys. **58** (2007) 247 [arXiv:hep-ph/0512128].

[71] N. Arkani-Hamed, A. G. Cohen, E. Katz and A. E. Nelson, JHEP **0207** (2002) 034 [arXiv:hep-ph/0206021].

[72] C. Csaki, J. Hubisz, G. D. Kribs, P. Meade and J. Terning, Phys. Rev. D **68** (2003) 035009 [arXiv:hep-ph/0303236].

[73] M. Schmaltz and J. Thaler, JHEP **0903** (2009) 137 [arXiv:0812.2477 [hep-ph]].

[74] G. Azuelos *et al.*, Eur. Phys. J. C **39S2** (2005) 13 [arXiv:hep-ph/0402037].

[75] R. Contino, C. Grojean, M. Moretti, F. Piccinini and R. Rattazzi, JHEP **1005** (2010) 089 [arXiv:1002.1011 [hep-ph]].

[76] A. Azatov, R. Contino and J. Galloway, JHEP **1204** (2012) 127 [arXiv:1202.3415 [hep-ph]].

[77] R. Barbieri, B. Bellazzini, V. S. Rychkov and A. Varagnolo, Phys. Rev. D **76** (2007) 115008 [arXiv:0706.0432 [hep-ph]].

[78] R. Barbieri, Sc. Norm. Sup., Pisa, Italy (2007), 84 p [arXiv:0706.0684 [hep-ph]].

[79] A. Orgogozo and S. Rychkov, JHEP **1203** (2012) 046 [arXiv:1111.3534 [hep-ph]].

[80] A. Falkowski, S. Rychkov and A. Urbano, JHEP **1204** (2012) 073 [arXiv:1202.1532 [hep-ph]].

[81] I. Low, R. Rattazzi and A. Vichi, JHEP **1004** (2010) 126 [arXiv:0907.5413 [hep-ph]].

[82] R. Contino, M. Ghezzi, C. Grojean, M. Muhlleitner and M. Spira, arXiv:1303.3876 [hep-ph].

[83] P. H. Chankowski, S. Pokorski and J. Wagner, Eur. Phys. J. C **47** (2006) 187 [arXiv:hep-ph/0601097].

[84] M. -C. Chen, S. Dawson and T. Krupovnickas, Phys. Rev. D **74** (2006) 035001 [arXiv:hep-ph/0604102]; P. H. Chankowski, S. Pokorski and J. Wagner, Eur. Phys. J. C **50** (2007) 919 [arXiv:hep-ph/0605302].

[85] A. Carmona, E. Ponton and J. Santiago, JHEP **1110** (2011) 137 [arXiv:1107.1500 [hep-ph]].

[86] S. Ferrara, M. Porrati and V. L. Telegdi, Phys. Rev. D **46** (1992) 3529.

[87] B. A. Kniehl and M. Spira, Z. Phys. C **69** (1995) 77 [arXiv:hep-ph/9505225].

[88] A. Arvanitaki and G. Villadoro, JHEP **1202** (2012) 144 [arXiv:1112.4835 [hep-ph]].

[89] K. Hagiwara and H. Murayama, Phys. Rev. D **41** (1990) 1001.

[90] A. Pierce, J. Thaler and L. -T. Wang, JHEP **0705** (2007) 070 [arXiv:hep-ph/0609049].

[91] E. Furlan, JHEP **1110** (2011) 115 [arXiv:1106.4024 [hep-ph]].

[92] A. Djouadi, W. Kilian, M. Muhlleitner and P. M. Zerwas, Eur. Phys. J. C **10** (1999) 45 [arXiv:hep-ph/9904287].

[93] R. Contino, M. Ghezzi, M. Moretti, G. Panico, F. Piccinini and A. Wulzer, JHEP **1208** (2012) 154 [arXiv:1205.5444 [hep-ph]].

[94] A. D. Martin, W. J. Stirling, R. S. Thorne and G. Watt, Eur. Phys. J. C **63** (2009) 189 [arXiv:0901.0002 [hep-ph]].

[95] E. W. N. Glover and J. J. van der Bij, Nucl. Phys. B **309** (1988) 282.

[96] T. Plehn, M. Spira and P. M. Zerwas, Nucl. Phys. B **479** (1996) 46 [Erratum-ibid. B **531** (1998) 655] [arXiv:hep-ph/9603205].

[97] U. Baur, T. Plehn and D. L. Rainwater, Phys. Rev. Lett. **89** (2002) 151801 [arXiv:hep-ph/0206024].

[98] S. Dawson, S. Dittmaier and M. Spira, Phys. Rev. D **58** (1998) 115012 [arXiv:hep-ph/9805244].

[99] U. Baur, T. Plehn and D. L. Rainwater, Phys. Rev. D **67** (2003) 033003 [arXiv:hep-ph/0211224].

[100] U. Baur, T. Plehn and D. L. Rainwater, Phys. Rev. D **68** (2003) 033001 [arXiv:hep-ph/0304015].

[101] U. Baur, T. Plehn and D. L. Rainwater, Phys. Rev. D **69** (2004) 053004 [arXiv:hep-ph/0310056].

[102] M. J. Dolan, C. Englert and M. Spannowsky, JHEP **1210** (2012) 112 [arXiv:1206.5001 [hep-ph]].

[103] A. Papaefstathiou, L. L. Yang and J. Zurita, Phys. Rev. D **87** (2013) 011301 [arXiv:1209.1489 [hep-ph]].

[104] M. Gouzevitch, A. Oliveira, J. Rojo, R. Rosenfeld, G. Salam and V. Sanz, arXiv:1303.6636 [hep-ph].

[105] M. J. Dolan, C. Englert and M. Spannowsky, Phys. Rev. D **87** (2013) 055002 [arXiv:1210.8166 [hep-ph]].

[106] A. Azatov, R. Contino, D. Del Re, J. Galloway, M. Grassi and S. Rahatlou, JHEP **1206** (2012) 134 [arXiv:1204.4817 [hep-ph]].

[107] J. R. Espinosa, C. Grojean, M. Mühlleitner and M. Trott, JHEP **1205** (2012) 097 [arXiv:1202.3697 [hep-ph]].

[108] F. Maltoni, K. Paul, T. Stelzer and S. Willenbrock, Phys. Rev. D **64**, 094023 (2001) [arXiv:hep-ph/0106293].

[109] T. M. P. Tait and C. -P. Yuan, Phys. Rev. D **63**, 014018 (2000) [arXiv:hep-ph/0007298].

[110] V. Barger, M. McCaskey and G. Shaughnessy, Phys. Rev. D **81**, 034020 (2010) [arXiv:0911.1556 [hep-ph]].

[111] CMS Collaboration, CMS-PAS-HIG-12-025, September 2012 [http://cdsweb.cern.ch/record/1460423].

[112] S. Dawson, Nucl. Phys. B **249** (1985) 42; G. L. Kane, W. W. Repko and W. B. Rolnick, Phys. Lett. B **148** (1984) 367.

[113] T. Appelquist and M. S. Chanowitz, Phys. Rev. Lett. **59** (1987) 2405 [Erratum-ibid. **60** (1988) 1589].

[114] F. Maltoni, J. M. Niczyporuk and S. Willenbrock, Phys. Rev. D **65** (2002) 033004 [arXiv:hep-ph/0106281].

[115] J. Alwall, M. Herquet, F. Maltoni, O. Mattelaer and T. Stelzer, JHEP **1106**, 128 (2011) [arXiv:1106.0522 [hep-ph]].

[116] J. Pumplin, D. R. Stump, J. Huston, H. L. Lai, P. M. Nadolsky and W. K. Tung, JHEP **0207**, 012 (2002) [arXiv:hep-ph/0201195].

[117] R. Frederix, S. Frixione, F. Maltoni and T. Stelzer, JHEP **0910** (2009) 003 [arXiv:0908.4272 [hep-ph]].

[118] V. Hirschi, R. Frederix, S. Frixione, M. V. Garzelli, F. Maltoni and R. Pittau, JHEP **1105** (2011) 044 [arXiv:1103.0621 [hep-ph]].

[119] http://amcatnlo.cern.ch .

[120] ATLAS Collaboration, arXiv:1210.6210 [hep-ex].

[121] J. R. Espinosa, C. Grojean, M. Mühlleitner and M. Trott, JHEP **1212** (2012) 045 [arXiv:1207.1717 [hep-ph]].

[122] S. Biswas, E. Gabrielli, F. Margaroli and B. Mele, arXiv:1304.1822 [hep-ph].

[123] M. Carena, A. D. Medina, B. Panes, N. R. Shah and C. E. M. Wagner, Phys. Rev. D **77** (2008) 076003 [arXiv:0712.0095 [hep-ph]].

[124] R. Contino and G. Servant, JHEP **0806** (2008) 026 [arXiv:0801.1679 [hep-ph]]; J. A. Aguilar-Saavedra, JHEP **0911** (2009) 030 [arXiv:0907.3155 [hep-ph]]; G. Dissertori, E. Furlan, F. Moortgat and P. Nef, JHEP **1009** (2010) 019 [arXiv:1005.4414 [hep-ph]].

[125] J. Mrazek and A. Wulzer, Phys. Rev. D **81** (2010) 075006 [arXiv:0909.3977 [hep-ph]].

[126] G. Cacciapaglia, A. Deandrea, D. Harada and Y. Okada, JHEP **1011** (2010) 159 [arXiv:1007.2933 [hep-ph]]; M. Buchkremer, G. Cacciapaglia, A. Deandrea and L. Panizzi, arXiv:1305.4172 [hep-ph].

[127] N. Vignaroli, JHEP **1207** (2012) 158 [arXiv:1204.0468 [hep-ph]].

[128] A. De Simone, O. Matsedonskyi, R. Rattazzi and A. Wulzer, JHEP **1304** (2013) 004 [arXiv:1211.5663 [hep-ph]].

[129] R. Barcelo, A. Carmona, M. Chala, M. Masip and J. Santiago, Nucl. Phys. B **857** (2012) 172 [arXiv:1110.5914 [hep-ph]]; C. Bini, R. Contino and N. Vignaroli, JHEP **1201** (2012) 157 [arXiv:1110.6058 [hep-ph]]; A. Carmona, M. Chala and J. Santiago, JHEP **1207** (2012) 049 [arXiv:1205.2378 [hep-ph]]; M. Chala and J. Santiago, arXiv:1305.1940 [hep-ph].

[130] G. Altarelli and R. Barbieri, Phys. Lett. B **253** (1991) 161; G. Altarelli, R. Barbieri and S. Jadach, Nucl. Phys. B **369** (1992) 3 [Erratum-ibid. B **376** (1992) 444]; G. Altarelli, R. Barbieri and F. Caravaglios, Nucl. Phys. B **405** (1993) 3.

[131] K. Agashe and R. Contino, Nucl. Phys. B **742** (2006) 59 [arXiv:hep-ph/0510164].

[132] M. Aliev, H. Lacker, U. Langenfeld, S. Moch, P. Uwer and M. Wiedermann, Comput. Phys. Commun. **182** (2011) 1034 [arXiv:1007.1327 [hep-ph]].

[133] CMS Collaboration, CMS-PAS-B2G-12-015, June 2013 [http://cds.cern.ch/record/1557571].

[134] CMS Collaboration, CMS-PAS-B2G-12-012, March 2013 [http://cds.cern.ch/record/1524087].

[135] A. Falkowski, C. Grojean, A. Kaminska, S. Pokorski and A. Weiler, JHEP **1111** (2011) 028 [arXiv:1108.1183 [hep-ph]].

[136] K. Agashe, H. Davoudiasl, S. Gopalakrishna, T. Han, G. -Y. Huang, G. Perez, Z. -G. Si and A. Soni, Phys. Rev. D **76** (2007) 115015 [arXiv:0709.0007 [hep-ph]].

[137] K. Agashe, S. Gopalakrishna, T. Han, G. -Y. Huang and A. Soni, Phys. Rev. D **80** (2009) 075007 [arXiv:0810.1497 [hep-ph]].

[138] K. Agashe, A. Belyaev, T. Krupovnickas, G. Perez and J. Virzi, Phys. Rev. D **77** (2008) 015003 [arXiv:hep-ph/0612015].

[139] A. Altheimer *et al.*, J. Phys. G **39** (2012) 063001 [arXiv:1201.0008 [hep-ph]].

[140] C. W. Bauer, Z. Ligeti, M. Schmaltz, J. Thaler and D. G. E. Walker, Phys. Lett. B **690** (2010) 280 [arXiv:0909.5213 [hep-ph]]; R. Barbieri and R. Torre, Phys. Lett. B **695** (2011) 259 [arXiv:1008.5302 [hep-ph]]; T. Han, I. Lewis and Z. Liu, JHEP **1012** (2010) 085 [arXiv:1010.4309 [hep-ph]].

[141] F. del Aguila, J. de Blas and M. Perez-Victoria, JHEP **1009** (2010) 033 [arXiv:1005.3998 [hep-ph]].

[142] R. N. Mohapatra and J. C. Pati, Phys. Rev. D **11** (1975) 566; R. N. Mohapatra and J. C. Pati, Phys. Rev. D **11** (1975) 2558.

[143] M. Schmaltz and C. Spethmann, JHEP **1107** (2011) 046 [arXiv:1011.5918 [hep-ph]].

[144] K. Hsieh, K. Schmitz, J. -H. Yu and C. -P. Yuan, Phys. Rev. D **82** (2010) 035011 [arXiv:1003.3482 [hep-ph]].

[145] M. Frank, A. Hayreter and I. Turan, Phys. Rev. D **83** (2011) 035001 [arXiv:1010.5809 [hep-ph]].

[146] T. G. Rizzo, JHEP **0705** (2007) 037 [arXiv:0704.0235 [hep-ph]].

[147] M. Nemevsek, F. Nesti, G. Senjanovic and Y. Zhang, Phys. Rev. D **83** (2011) 115014 [arXiv:1103.1627 [hep-ph]].

[148] S. Jung, H. Murayama, A. Pierce and J. D. Wells, Phys. Rev. D **81** (2010) 015004 [arXiv:0907.4112 [hep-ph]].

[149] K. Cheung, W. -Y. Keung and T. -C. Yuan, Phys. Lett. B **682** (2009) 287 [arXiv:0908.2589 [hep-ph]]; K. Cheung and T. -C. Yuan, Phys. Rev. D **83** (2011) 074006 [arXiv:1101.1445 [hep-ph]].

[150] P. Langacker and S. U. Sankar, Phys. Rev. D **40** (1989) 1569.

[151] A. Maiezza, M. Nemevsek, F. Nesti and G. Senjanovic, Phys. Rev. D **82** (2010) 055022 [arXiv:1005.5160 [hep-ph]].

[152] A. J. Buras, K. Gemmler and G. Isidori, Nucl. Phys. B **843** (2011) 107 [arXiv:1007.1993 [hep-ph]].

[153] G. Gounaris *et al.*, in 'Physics at LEP2', vol. 1, 525-576, Geneva (1995) [arXiv:hep-ph/9601233].

[154] DELPHI Collaboration, Eur. Phys. J. C **66** (2010) 35 [arXiv:1002.0752 [hep-ex]].

[155] CDF Collaboration, Phys. Rev. D **79** (2009) 112002 [arXiv:0812.4036 [hep-ex]].

[156] A. Belyaev, N. D. Christensen and A. Pukhov, Comput. Phys. Commun. **184** (2013) 1729 [arXiv:1207.6082 [hep-ph]].

[157] D0 Collaboration, Phys. Lett. B **699** (2011) 145 [arXiv:1101.0806 [hep-ex]]. Supplemental material available at this web page.

[158] S. Gopalakrishna, T. Han, I. Lewis, Z. -g. Si and Y. -F. Zhou, Phys. Rev. D **82** (2010) 115020 [arXiv:1008.3508 [hep-ph]].

[159] CMS Collaboration, Phys. Rev. Lett. **105** (2010) 211801 [arXiv:1010.0203 [hep-ex]].

[160] R. Torre, arXiv:1109.0890 [hep-ph].

[161] ATLAS Collaboration, arXiv:0901.0512 [hep-ex].

[162] A. Alves, O. J. P. Eboli, D. Goncalves, M. C. Gonzalez-Garcia and J. K. Mizukoshi, Phys. Rev. D **80** (2009) 073011 [arXiv:0907.2915 [hep-ph]].

[163] CMS Collaboration, CMS-PAS-EXO-12-025, June 2013 [http://cds.cern.ch/record/1558197?ln=en].

[164] ALEPH, DELPHI, L3, OPAL, SLD, LEP Electroweak Working Group, SLD Electroweak Group, SLD Heavy Flavor Group Collaborations, Phys. Rept. **427** (2006) 257 [arXiv:hep-ex/0509008].

[165] Tevatron Electroweak Working Group, for the CDF and D0 Collaborations, arXiv:1204.0042 [hep-ex].